Controls on T-cell receptor phosphorylation and triggering

Ricardo A. Fernandes

Jesus College

Supervisor: Simon J. Davis

Thesis submitted for the degree of Doctor of Philosophy

Michaelmas Term, 2011

The work described in this Thesis was supported by a Doctoral Degree (BD) grant (SFRH / BD / 37806 / 2007) from Fundação para a Ciência e a Tecnologia, FCT, Portugal, co-financed by the FSE program integrated in POPH of QREN program. The BD grant was initiated on the 1st January of 2007 and finished on the 1st January 2012.

Abstract

Controls on T-cell receptor phosphorylation and triggering

Ricardo A. Fernandes, Jesus College

Thesis submitted for the degree of Doctor of Philosophy
Michaelmas Term, 2011

An effective immune response in mammalian cells relies on a network of molecular interactions to detect and respond to pathogens. The T-cell receptor (TCR) is one of the most important components of this system responsible for the outcome of the immunological response. Paramount to its role is its ability to efficiently signal a productive interaction with a peptide embedded in an MHC molecule. Important aspects of TCR structure and organization are unknown, limiting the current understanding of this process and rendering it highly controversial. The work described in this thesis seeks to define the valency, structural organization and signalling properties of the TCR in order to provide a better framework for thinking about the receptor-triggering problem. The results suggest that a largely monovalent complex diffuses at the surface of T cells, which is able to trigger intracellular signalling in the absence of large structural rearrangements of the extracellular subunits of the TCR. Moreover, a recently proposed mechanism involving conformational rearrangements of the cytoplasmic domains of the complex is shown to fail to explain the regulation of TCR phosphorylation. Steps are also taken toward investigating the role of more subtle conformational rearrangements at atomic resolution. Finally, an investigation of what controls tyrosine phosphorylation of the receptor in resting T lymphocytes led to the development of new approaches to address the role of specific phosphatases. The outcome of this analysis suggested how a finely-tuned balance between kinase and phosphatase activity, at both global and local levels, regulates TCR phosphorylation and T-cell activation.

Acknowledgements

In first place I would like to thank my supervisor for this thesis, Simon Davis. Thank you Simon, for the support, time, insightful discussions and for providing me with the best tools and environment to do challenging and enjoyable scientific research. Your active, incessant, search for outstanding scientific questions was a great stimulus and will not be forgotten. The great environment of the Davis lab stems, of course, from the collaborators in this group. I cannot be more grateful for all the friendship, help, the support and the relaxing moments inside, and outside, the lab. To present and past members of the Davis lab, an immense thank you, these four years could hardly have been any better. John, Claire, Jan, Heather, Mai, Ed, Sara, Dave and Xiaoxiao, thank you. I would also like to thank members of the Davis Klenerman group, in Cambridge, for the fruitful collaborations and for patiently introducing me to the world of single-molecules. The Davis lab is not isolated. It is in fact at the junction of two long corridors where, invariably, members of other groups were found. For the friendship, help, laughs, pubs and a bit of science, my sincere thank you.

And a final, brief (in the absence of time and skill) word to my friends who in some way, often quite different, helped me during this time. To my good brother-like friends Tiago and Daniel, simply thank you for everything we trust, do and share out there, I think that is enough to thank. To Carine and Telmo, thank you for coming all the way up here. For the talks, movies, walks, great diners, beautiful trips, tennis, coffees and teas, thank you. I could have not been luckier for meeting you and sharing my best time here with you. To Mafalda, for "treading softly" by my side at a charming and beloved "rhythm", thank you.

To mum and dad, who will always look puzzled at this thesis but also deeply proud, I know no words to say how much I thank you.

Contents

List of Figures

Abbreviations

APC	Antigen Presenting Cell
CD	Cluster of Differentiation
CDR	Complementarity Determining Region
cSMAC	Central Supramolecular Activation Cluster
Da	Dalton
E/GRE	Glucocorticoid Response Element
FACS	Fluorescently-activated Cell Sorting and Analysis
FCS	Foetal Calf Serum
FRET	Förster Resonance Energy Transfer
GPI	Glycosylphosphatidylinositol
HA	Hemagglutinin
IgSF	Immunoglobulin Superfamily
IgG	Immunoglobulin G
IP	Immunoprecipitation
IS	Immunological Synapse
Kd	Dissociation Constant
LAT	Linker for Activation of T Cells
Lck	Lymphocyte-specific Tyrosine Kinase
LFA-3	Lymphocyte Function-associated Antigen 3
MHC	Major Histocompatibility Complex
NF-κB	Nuclear Factor κB
NF-AT	Nuclear factor of activated T-cells
PBS	Phosphate-buffered Saline
PI-3K	Phosphoinositide 3-Kinase
pMHC	Peptide-complexed Major Histocompatibility Complex
PP2	Protein Phosphatase 2
PTP	Protein tyrosine phosphatase
pTyr	Tyrosine phosphorylation
RLU	Relative Luminescence Units
SFFV	Spleen Focus Forming Virus
SH2	Src Homology Domain 2
SLP-76	SH2 Domain-containing Leukocyte Protein, 76kDa
SMAC	Supramolecular Activation Cluster
TCR	T Cell Antigen Receptor
VSV-G	Vesicular Stomatitis Virus Envelope Protein G
ZAP-70	ζ-chain Associated Protein, 70kDa

Chapter 1

Introduction

1.1 The immune system

1.1.1 Overview of the immune system

The increasing levels of oxygen in the atmosphere, around 600 million years ago, led to a dramatic increase in development of multicellular organisms [1]. Development of complex metazoans is dependent on efficient cell-to-cell recognition and communication [2]. At the molecular level, the arrival of higher forms of metazoans is coupled to the development of: (1) adhesion molecules, which facilitate and promote cell-cell interactions; (2) apoptotic processes, responsible for maintaining homeostatic control of the organism; and finally, (3) an immune system, able to identify and respond to cells of different origin. These three basic constituents of a metazoan distinguish a unicellular/colonial organism from an integrated organism with complex cell-cell network interactions. The presence of these three basic properties can be traced back to the phylogenetically oldest metazoan organisms, sponges [3, 4].

The immune system is classically divided into two well-defined and overlapping parts, *i.e.* those controlling the innate and the adaptive immune responses. Sponges, and probably every single metazoan, possesses a simple, but fundamental, innate immune system which relies on genetically pre-encoded molecules that are constitutively expressed and able to recognize conserved patterns on different types of pathogens [5]. Later in evolution a new immunological response appeared, the adaptive response, relying upon the somatic diversification of antigen-receptor genes to generate an extremely large repertoire of cells, each one expressing a unique antigen receptor [6]. The adaptive response relies on lymphocytes, a new group of cells with highly specialized cell-

surface receptors for recognizing specific antigens. Activation of lymphocytes induces clonal expansion, cellular differentiation, and production of antibodies, specific to the agent that triggered the adaptive response [7].

1.1.2 The innate immune response

Innate immunity, also known as pattern recognition, is based on recognition of unique molecular structures. This response of the immune system relies on continuously expressed germline-encoded receptors that upon recognition of pathogenic markers can elicit an effective response on the time scale of minutes to hours. Most, if not all, of the metazoans found to date rely on some form of pattern recognition receptors to maintain integrity [8].

Pattern recognition receptors

Pattern recognition receptors (PRRs) belong to several distinct protein families and recognize conserved molecular patterns associated with microbial pathogens (PAMPs, for pathogen-associated molecular patterns). PAMP recognition triggers effector mechanisms such as expression of antimicrobial peptides, nitric oxide production by macrophages and induction of phagocytosis.

PRRs have broad specificity and can potentially bind to a wide range of molecules that share a common structural motif. Recognition of PAMPs is an efficient mode of immune recognition for three main reasons: (1) PAMPs are usually invariant in a given class of microorganisms; (2) they are products of pathways that are unique to microorganisms, and thereby allow discrimination between self and non-self; (3) they are usually present in molecules with essential roles in microbial physiology, and thus with limited evasion potential from innate immunity recognition through adaptive evolution [9]. PAMPs are present as components of the bacterial cell wall, such as peptidoglycans and lipopolysaccharide. Fungal cell-wall is also recognized by PAMPs in β-glucan. Viral infection, given that all viral components are synthesized in the intracellular compartment of the host cells, is recognized by PRRs that target specific chemical

modifications present in viral RNA and DNA, as well as the location where viral nucleic acids are found.

Recognition of such a wide range of different molecular structures is made possible by expression of distinct PRRs that can be broadly characterized according to structure into secreted, transmembrane and cytosolic protein classes. Soluble PRRs target the microbial cell surface, activate the complement system and thus opsonize pathogens for phagocytosis by macrophages and neutrophils [10].

The transmembrane PRRs include the Toll-like receptor (TLR) family and C-type lectins. Cell surface and endosomal TLRs recognize a wide range of structures such as lipopolysaccharide (LPS), dsRNA, flagellin and unmethylated CpG DNA [11, 12]. Expression of TLRs is usually cell specific, thereby explaining why different leukocytes play distinct roles in innate immune responses. C-type lectins, such as Dectin-1, detect components of the fungal cell wall [10]. Dectin-1 is of particular interest, from an evolutionary signalling perspective, as it contains an atypical immunoreceptor tyrosine-based activation motif (ITAM), responsible for recruitment of SYK tyrosine kinase to the cell membrane, thereby activating intracellular pathways through a similar signalling motif to that used by receptors of the adaptive immune system such as the TCR and BCR (discussed in more detail in §1.5.4).

Cytosolic PRRs include receptors like the retinoic acid-inducible gene I, (RIG-I)-like receptors (RLRs) and the nucleotide-binding domain and leucin rich repeat-containing receptors (NLRs). Whereas RLRs recognize viral RNA through a helicase domain and signal through a caspase recruitment domain, NLRs contain specific N-terminal domains able to signal the presence of degradation products of peptidoglycans, different forms of stress (such as ultraviolet irradiation) and microbial products [13]. Contrary to TLRs, most cells express at least one type of cytosolic PRR [10].

An important aspect of PRRs is that it does not differentiate between pathogenic and symbiotic microorganisms. Yet, despite the large number of symbiotic bacteria that colonize humans, a homeostatic balance is maintained

under normal conditions. It is now clear that innate immune recognition of symbiotic microorganisms is an important mechanism to control, for example, the intestinal flora [9]. The lack of a well-defined discrimination between host and foreign (pathogenic or symbiotic) microorganism can, however, under certain circumstances lead to autoimmune diseases [14, 15].

PAMP recognition by transmembrane or cytosolic PRRs triggers multiple pathways that usually converge on the activation of nuclear factors like NF-κB, IRF or NFAT. Depending on the cell type, the activation of nuclear factors will induce expression of specific cytokines which will initiate sites of inflammation by recruiting additional leukocytes and inducing secretion of antimicrobial peptides [16].

1.1.3 The adaptive immune response

Contrary to the innate immune response, adaptive, or acquired, immunity is present only in jawed vertebrates and is characterized by expression of highly variable receptors generated by somatic diversification. Adaptive immune recognition is mediated by two distinct antigen receptors: the T-cell receptor (TCR) and the B-cell receptor (BCR), expressed in T and B cells, respectively. A third element, the major histocompatibility complex (MHC), is also highly variable with such a vast number of possible somatic combinations that virtually allows the capture of any antigen. Antigens, small peptides of 8-20 residues bound to the MHC (pMHC) are then presented to T cells *via* interaction with the TCR. The MHC receptor is found on every nucleated cell of the body. The adaptive immune system also utilizes soluble proteins, antibodies, which display a similar structure to the BCR, to identify antigens in solution or at the cell surface.

1.1.3.1 Cells of the adaptive immune system

Both B and T cells share a common precursor in the bone marrow, the lymphoid progenitor cell. However, maturation of T cells occurs in the thymus whereas B cells reside in the bone marrow throughout their entire development. The extraordinary diversity found in receptors of the adaptive immune system

broadens significantly the range of pathogens jawed vertebrates can detect. However, this diversity also increases the potential of autoimmune responses or reaction to self. Maturation of B cells and T cells aims to eliminate potential self-reactive receptors by a selection process carried out in specialized organs [17].

Antigen recognition by the adaptive immune system

The advantage of adaptive immunity is its capacity to respond to an almost unlimited number of potential antigens, through the generation of a vast number of potential receptors either at the surface of or secreted by lymphocytes. It is usually estimated that 10^{12}-10^{18} different receptors can be generated in a process involving the random joining of small germline-encoded DNA sequences to produce receptors with the potential to bind almost any antigen. During development, T and B lymphocyte progenitors undergo a process where prototypic immunoglobulin (Ig), variable (V), diversity (D) and joining (J) DNA gene segments are randomly rearranged to generate specific binding regions of the TCR and BCR. During V(D)J recombination, receptor variability is further increased through the enzymatic addition of short, random nucleotide sequences to join the three sequences, V, D and J together. The nature of this process ensures that an almost unlimited number of receptors can be created. The V(D)J recombination relies on a lymphocyte specific enzyme, only found in jawed vertebrates and encoded by the recombination-activating genes, RAG-1 and RAG-2, which cleaves and joins, together with other enzymes, the germline-encoded DNA sequences thereby generating a completely novel gene [18, 19]. Addition of base pairs to join the V, D and J segments occurs randomly by another enzyme, terminal deoxynucleotidyl transferase (TdT). Whereas TCRβ is formed by V(D)J recombination, TCRα results from recombination of only V and J segments. An additional level of diversity for antigen receptors is generated upon pairing of two protein chains to form the final receptor structure.

Comparison of different TCR and BCR rearranged genes have identified hyper-variable regions, which correspond to the complementarity-determining regions (CDR) of the receptor. These structures usually form loops connecting

sequences that maintain the overall immunoglobulin superfamily (IgSF) domain. Three CDR regions have been identified, CDR1, CDR2 and CDR3, with CDR3 being formed from the junctional sequence of the V(D)J recombination, thus showing the highest degree of variability.

Gene rearrangement of the heavy- and light-chain of the BCR and of TCRαβ does not happen simultaneously: the heavy-chain and the TCRβ are made first. However, a tightly regulated process ensures that only paired receptors are expressed at the cell surface. In what initially seemed a paradox, TCRβ and the heavy-chain can be found at the cell surface during the early developmental stage of T or B cells without TCRα or the light-chain. It was later found that a precursor to TCRα, pre-TCRα, and for the light-chain, an invariant surrogate light-chain, could pair with TCRβ and the heavy-chain, respectively. This step-wise progress during the development of T and B cells has the advantage of selecting cells where the V(D)J gene rearrangements are successful, and eliminating all the other cells. Positively selected cells will enter the bloodstream and locate to lymphoid tissues where they scan for the presence of pathogens.

The role of B-cells and antibodies

The vast repertoire of BCR complexes formed during B cell development allows the adaptive immune system to recognize virtually any antigen and respond with antibody production. Remarkably, in spite of this vast repertoire of BCR, self-reactive complexes are mostly absent as self-reactive B cells are eliminated in the bone marrow by apoptosis. Cells expressing a self-reactive BCR can undergo a second round of gene rearrangement, termed receptor editing, which can change BCR specificity and thus rescue cell development. If the cells exhibit only weak reactivity towards self, they might not undergo apoptosis but instead enter an anergic state that precludes B-cell function. This selection mechanism ensures that only cells reactive to foreign antigens exit the bone marrow into the periphery where they will be able to function effectively.

The BCR complex consists of a bivalent antigen-binding membrane immunoglobulin (with an antibody-like structure), interacting with Igα/β (CD79a

and CD79b) proteins with cytoplasmic ITAMs responsible for initiation and transmission of intracellular signalling [20]. After leaving the bone marrow B lymphocytes target pathogens by secreting soluble antibodies recognizing a specific antigen, identical to the one that was initially identified by the BCR [21, 22]. Interaction between antigen and the BCR initiates a complex set of reactions that ultimately leads to B-cell activation [23, 24]. Following recognition of antigens by the BCR, B cells can differentiate to form either plasma cells, specialized in antibody production and secretion, or memory cells that provide long-lived protection and support a faster immunological response upon a subsequent encounter with a pathogen producing similar antigen. Together with antibody secretion, binding of the antigen to the BCR also contributes to T cell activation. Antigen capture by the BCR induces complex internalization and degradation, which leads to peptide fragments of the antigen being presented at the cell surface embedded in the MHC class-II complex. Previously activated T cells, recognizing a specific antigen presented by an MHC molecule at the B cell surface, can also "help" in B cell activation and induction of antibody secretion by secreting IL-4 and surface molecules (like CD40L) that together induce strong B cell activation. This dependence of B cell activation on previously activated T cells ensures that mainly B lymphocytes expressing a receptor specific for a pathogen-associated antigen are fully activated during an infection. The activated T cells are usually primed by the recognition of the same pathogen presented by professional antigen-presenting cells, such as dendritic cells. It is often the case that the BCR and the TCR respond to the same pathogen, but through different epitopes. The ability to target different epitopes from a specific pathogen is an advantage of the immune response and guarantees that specific B cell and T cell clones can act in concert, with mutual benefit, to successfully eliminate a pathogen.

Activation of the B cells generally occurs in the lymph node. Cells, lymphatic and interstitial fluid, and foreign molecules constantly circulate through these specialized structures, which effectively increase local concentration of molecules, promote cell-cell interactions and in this way provide an optimized environment to initiate an effective immune response. In the periphery, contrary

to the lymph node, the likelihood of a cognate B cell-T cell interaction is negligible.

T cells, B cells and dendritic cells act together to form a primary focus for activation that leads to germinal centre formation [25]. Within the germinal centre, B cell activation results in clonal expansion and antibody secretion. During this stage the B cell optimizes the affinity of the secreted antibodies to the specific antigen *via* somatic hypermutation [26]. This process is termed affinity maturation, and is the result of mutation of the CDR loops of the BCR. B cell clones are gradually selected and enriched for BCR molecules with increasing affinity for the initial antigen. During this stage the BCR structure is altered in order to eliminate the transmembrane domain and allow antibody secretion, in a process termed class switching.

In the plasma environment, antibodies function in similar fashion to molecules found in innate immunity. Antibodies are bivalent and can thus cross-link antigens, exhibit remarkable affinity and specificity and recognize both soluble and surface bound antigens. Furthermore, antibodies can opsonize pathogens and readily activate the complement cascade. Cells expressing Fc receptors, surface proteins that bind to the constant region of antibodies, can also recognize antibodies bound to antigens and promote phagocytosis [27].

In contrast to the innate response, antibodies can target any exposed part of the pathogen, which often includes regions or structures that are crucial for cell binding, invasion or pathogen proliferation. And, due to the constant development and selection process of B cells, even if the pathogen evades the initial immunological response by a specific mutation on a particular antigen, in theory, it will never completely escape recognition by other B cells.

1.1.4 The interface between innate and adaptive immunity

After the discovery of TLRs, which led to a much better understanding of the innate immune response, the connections between innate and adaptive immunity became clearer [28]. In fact, it is now well acknowledged that full activation of adaptive immunity benefits from innate responses to pathogen infection. First of

all, T cells rely on antigen presentation to become activated and particularly on professional antigen presenting cells, like dendritic cells that express ligands for the costimulatory molecules. The initial identification, uptake and processing of pathogens is facilitated by receptor-mediated recognition of microbial molecules, such as scavenger receptors and the complement system. Recognition of pathogens by dendritic cells, through mechanisms of the innate immune system, up-regulates MHC molecules, costimulatory ligands like CD80 and CD86 and cytokines which together will be capable of efficiently activating a naïve CD4 and CD8 T cell in an antigen-specific manner [9, 16, 29]. Increased secretion of type I interferon, mediated by TLR signalling pathway activation, is also known to augment and sustain T cell responses.

The mammalian immune system is also equipped with two cell types that contribute to both innate and adaptive immune response: natural killer cells (NKs) and γδ T cells. NK cells do not require prior activation to target and eliminate potential cellular threats to the host, such as virus-infected cells or tumour cells. NK cells have the ability to detect and respond to the absence of "self" MHC molecules at the cell surface. In the absence, or upon reduced expression, of MHC class I, NK cells can directly kill cellular targets and produce cytokines to initiate and support other immune defence mechanisms [8, 30].

At the border between the innate and the adaptive immune system are γδ T cells [31]. These cells express a different form of TCR complex, where the γδ chains, like TCRαβ, undergo DNA rearrangements producing junctional diversity. however these TCRγδ seem capable of responding to antigens independently of MHC presentation, in a way that resembles the recognition by PRRs [32]. More recently γδ T cells were also found to be capable of phagocytosis, a function not found in B or T lymphocytes.

1.2 Antigen recognition by T cells

The defining characteristic of T cells is the expression of the TCR complex, a receptor able to scan small peptides embedded in an MHC molecule and respond

with extremely high sensitivity to agonistic antigens.

1.2.1 Maturation of T cells

T cell precursors, prothymocytes, leave the bone marrow for the thymus, attracted by a chemotactic factor, thymotaxin, secreted by thymic epithelial cells. Once in the thymus, T cells initiate rearrangement of the TCRαβ genes, starting with rearrangement of the TCRβ which is expressed at the cell surface after pairing with an invariant, germline-encoded, pre-TCRα, forming the pre-TCR. Once the pre-TCR reaches the cell surface, the cell initiates TCRα rearrangement and expresses coreceptors CD4 and CD8, entering the "double-positive" stage of T cell maturation. Through a mechanism of allelic exclusion, each T cell only expresses TCR complexes with identical TCRαβ sequence and, unlike B cells, there is no further rearrangement or "affinity maturation" of the TCR. T cells that fail to successfully rearrange TCRα or β genes are eliminated by apoptosis. Throughout these developmental stages T cells migrate to different regions of the thymus. Once the TCRα gene has been successfully rearranged a fully assembled TCRαβ complex is expressed at the cell surface and T cells migrate to the deep cortex of the thymus, where they interact with cells expressing both class I and class II MHC molecules. These initial interactions between a newly formed TCR and the MHC molecule are crucial for the outcome of T-cell maturation. Importantly, cells that fail to recognize and signal to the MHC present in the thymus at this stage will die by apoptosis. Only cells that can sense the presence of host MHC survive, and thus this maturation stage is known as positive selection. The class of the MHC molecule recognized by the TCR determines which coreceptor is eliminated from the cell surface. Interaction between the TCR and MHC class I will preserve CD8 expression, whereas interaction between the TCR and an MHC class II will eliminate CD8 and maintain CD4 expression, giving rise to single-positive T cells.

Cells that survive positive selection migrate from the cortex to the medulla. At this stage only cells that recognize "self" MHC are present. However, due to the random nature of TCRαβ gene rearrangement and the extraordinary diversity

that is generated, some of these cells will become activated upon interaction with an MHC molecule presenting an endogenous, self-derived, peptide. Failure to eliminate these cells could potentially lead to autoimmune responses with severe consequences. In the medulla, positively selected cells interact with bone-marrow derived dendritic cells and macrophages presenting a wide variety of self-peptides, in an attempt to represent the vast majority of self-antigens found in the periphery. Auto-reactive T cells, those that become activated upon interaction with self-peptide MHC are "negatively selected", *i.e.*, they are eliminated by apoptosis. The combination of positive and negative selection ensures that (1) T cells recognize self-MHC but (2) are not reactive to self.

1.2.2 The TCR complex

The discovery of the TCR complex was initiated with the development of monoclonal antibodies able to immunoprecipitate a glycoprotein composed of two disulphide-bonded subunits that had recognized CD3 proteins [33-35]. From antibody immunoprecipitation to identification of the cDNA sequences encoding the T cell receptor subunits was not a trivial task in the early 1980s. A combination of advanced cellular immunology, using a novel subtraction hybridization technique [36, 37], molecular biology and elegant experimental design allowed M. Davis and S. Hedrick *et al.* to isolate and sequence the mouse TCRβ [38, 39] and TCRα [40] cDNA. At the same time and with a similar approach, Tak Mak and co-workers managed to identify human TCRβ cDNA [41].

The vast majority, around 90-95%, of T cells express a surface complex composed of a disulphide-linked heterodimer TCRα and TCRβ chains, non-covalently associated with a CD3δε and CD3γε heterodimers and the homodimer CD3ζζ (Fig. 1.1). Both TCRαβ chains consist of two IgSF domains: one constant region, closer to the membrane that includes the transmembrane and a short cytoplasmic tail; and a variable domain resulting from the V(D)J recombination [42, 43].

Only fully assembled complexes are expressed at the cell surface [44, 45] with CD3ζζ homodimer being the last chain to be added to the complex [46, 47]. In fact, the absence of CD3ζζ can still lead to a minimal expression of the TCR complex [46].

Assembly of the complex is guided by electrostatic charge interactions within the transmembrane, which stabilize interactions between different chains (Fig. 1.1c; [48-50]). Superimposed upon these interactions are likely non-covalent contacts between the extracellular regions of the TCR subunits, involving both the "connecting peptides" [51] and the immunoglobulin superfamily domains [52, 53]. Initial mutational data suggest that the DE loop of the constant (Cα) region of TCRα contacts CD3εδ and that CD3εγ contacts the TCR via the CC' loop of Cβ [52, 54], ruling out the "bunch of balloons"-like arrangement of non-associated extracellular domains implied by a lack of detectable interactions in solution [47, 53, 55, 56]. There is structural information, obtained by X-ray crystallography or NMR, for the extracellular dimers: αβ antigen receptors [43, 57-59], CD3δε [55, 60], CD3γε [61], and for the transmembrane domain of CD3ζζ [62]. However, no complete structure is available for the overall complex and relatively little is known about any extracellular interactions established between the TCRαβ and the CD3 chains (Fig. 1.1; [53, 63]). Probing the extracellular interactions between TCR subunits and the development of an approach to determine the overall quaternary structure of this signalling receptor will be discussed later in more detail (§4 and §7).

The pMHC is recognized by TCRαβ chains, however, these subunits have no intracellular signalling motifs. Signalling from the TCR is initiated from ITAMs, consisting of the protein sequence [DE]xxYxx[LI]$_{6-12}$Yxx[LI] [64], which are present in the CD3 chains associated with the TCRαβ heterodimer. The two Tyr residues present in the ITAMs are targets for Src kinases, which phosphorylate these residues, creating a signalling motif that is recognized by SH2 domains, usually present in Tyr kinases and "scaffold" proteins [65-69]. The TCR complex contains a total of ten ITAMs, one in each CD3ε, γ and δ and three in each CD3ζ. The high number of ITAMs found in the TCR is not found in any

other receptor. Both qualitative and quantitative differences in T cell development and activation have been found upon elimination of specific ITAMs, which suggest that although the ITAMs share a common organization and have a high degree of sequence similarity they do not play identical roles in signalling transduction [70].

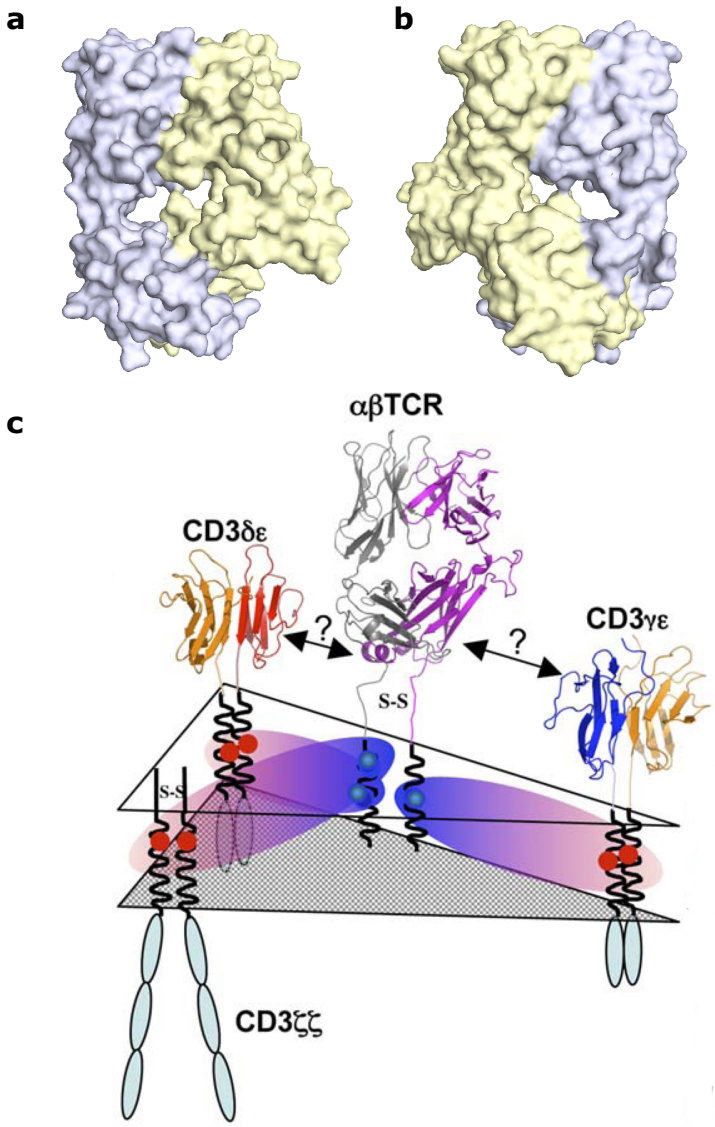

Figure 1.1: The overall quaternary structure of the TCR complex is not known. **(a, b)** The structure of TCRαβ extracellular region has been determined by X-ray crystallography (TCRα is depicted in blue and TCRβ in yellow; in (b) TCRαβ is rotated 180° along y axis; PDB 1OGA). **(c)** Assembly of the complex is guided by charge-charge interactions between basic residues present in the transmembrane of TCRαβ (collared blue) and acidic residues (collared red) in the transmembrane of the CD3 subunits. The extracellular interactions established between TCR-CD3 subunits are not known. Image adapted from Kuhns et al. [53].

1.2.3 Antigen presentation to the TCR complex

Unlike the BCR and antibodies, that directly recognize folded intact antigens, the TCR only recognizes small peptides presented by an MHC class-I or class-II molecules [71, 72]. This strict dependence on pMHC recognition for T cell selection is somehow linked to CD4 and CD8 expression [73] as knocking-down these coreceptors in mice leads to MHC-independent antigen recognition by the TCR [74].

Although structurally similar, MHC class-I and class-II have important differences. All nucleated cells express MHC class-I, whereas the MHC class-II is only present in professional antigen presenting cells (APCs). In both class-I and class-II, the peptide binding groove is formed by a β-sheet flanked by two α-helices [75]. However, the size of the peptides these molecules bind is not the same, with MHC class-I presenting shorter peptides of 8-10 residues and the class-II binding peptides of at least 13 residues [75-77]. Overall MHC molecule stability is dependent upon peptide binding, so the majority of MHC molecules found at the cell surface have an embedded peptide in the binding groove.

More importantly, MHC class-I and class-II have distinct roles in the immune response, mainly reflecting the origin of the peptides being presented. There are two major intracellular compartments that can contain pathogens or antigens derived from microorganisms: the cytosol, where most proteins are synthesized, including host proteins, and importantly where viral proteins are produced and some pathogenic bacteria replicate; and the endosomal-lysosomal system, where extracellular microorganisms enter through phagocytosis or endocytosis. Each one of these two compartments generates a vast number of small peptides that are monitored and presented by the two different classes of MHC molecules. MHC class-I molecules present peptides from the cytoplasmic pool, and MHC class-II molecule is specialized in the presentation of peptides from the endosomal-lysosomal pathway. Distinguishing the origin of the peptide presented to the TCR is valuable information to decide the most appropriate response by T cells.

Structurally, the MHC class-I is composed by an α-chain, that has a short cytoplasmic tail, a transmembrane domain, one membrane proximal domain and two membrane distal domains, which together form the peptide-binding groove region, and a single domain, β_2-microglobulin, that has no transmembrane domain [78, 79]. The MHC Class-II molecules are composed by an α- and a β-chain, both comprising short cytoplasmic tails, a transmembrane domain, one membrane proximal and a membrane distal domain. The peptide-binding groove is jointly formed by the α- and β-chain. The MHC molecule itself is therefore a dimer, but in fact the final molecule is a trimer, composed by the α- and β-chain stabilized by a small peptide.

The peptide-binding region of the α-chain is never exposed to the cytosol. Peptide loading of the MHC class-I molecule occurs in the lumen of the endoplasmic reticulum (ER), where small peptides are imported by a specialized membrane transporter, the transporter associated with antigen processing (TAP), present in the ER membrane [80, 81]. Once in the ER lumen peptides are cleaved by the ER aminopeptidase1 (ERAP1). The assembly of the final MHC trimer, α-chain, β_2-microglobulin and peptide is a complex process mediated by several chaperones [82]. At the cellular level, presentation of a foreign, pathogenic-derived, peptide by an MHC class-I molecule is perceived by the immune system as an indication that the cell has been infected or is expressing an unknown form of a protein. These cells will be destroyed by CD8 T cells which recognize agonist pMHC class-I molecules [83, 84].

The MHC class-II molecules monitor specialized compartments and are usually expressed by a restricted group of cells which includes phagocytes, dendritic cells and B cells which have evolved mechanisms to efficiently internalize antigens to be presented to CD4 T cells [85, 86]. Peptide loading of the MHC class-II molecule involves the incorporation of the products of protein cleavage that occur in the acidic and reducing environment of the endosomal-lysosomal system. A large group of cysteine and aspartyl enzymes, cathepsins, are expressed in this system by most cells. However, phagocytes, dendritic cells and B cells, express a wider range of these proteases with many of them being induced

upon activation of the immunological response in an attempt to ensure that a maximal range of peptides is generated [87]. Like the MHC class-I molecule, newly synthesized MHC class-II molecules are unstable if a peptide is not bound to the peptide-binding groove. To stabilize the protein and ensure that the binding groove does not bind cytosolic peptides, or those present in the ER lumen, a specialized chaperone, the invariant chain (I chain or Ii) binds transiently to the peptide-binding groove, until the complex reaches the correct cellular compartment for peptide loading [88]. Ii not only stabilizes the complex but it is also responsible for directing the MHC complex into the endosomal pathway [88]. Once in the endosomes, the Ii protein is degraded leaving a small peptide bound to the peptide-binding groove, the class II-associated invariant chain peptide, CLIP [89]. In a process that is still not fully understood it is thought that CLIP is kept bound to the MHC molecule until being replaced by a peptide with higher affinity.

1.2.4 γδ T cells

In humans, around 5% of T cells express CD3 proteins but no TCRαβ is found at the cell surface. Instead of the αβ chains these cells express a TCR complex composed by γδ subunits [90] and are known as γδ T cells. Like other lymphocytes these cells can be found in blood and lymphoid tissues but also in the skin, and in the intestinal and pulmonary epithelium. In general, γδ T cells do not express CD4 and CD8 coreceptors and are not MHC-restricted. Although γδ T cells also undergo somatic recombination and the potential of the γ and δ TCR loci to generate diversity is equal if not higher than that of α and β TCR, the cells often express a limited set of antigen receptors derived from a restricted set of variable gene segments. Much is still unknown about the selection and the antigens recognized by these cells [91]. It is likely that some bacterial molecular patterns, including lipids, or MHC related molecules, such as MICA/B, can be recognized by γδ TCR [92]. These properties, gene rearrangement, limited receptor variability, recognition of molecular patterns and rapid reactivity suggest these cells play an important role connecting innate and adaptive immune

responses (discussed in §1.1.4). The ability to recognize antigens independently of MHC molecules also raises the possibility that γδ T cells can act as antigen presenting cells to αβ T cells.

1.3 T lymphocyte activation

1.3.1 Overview of T cell-APC interaction

Antigen recognition by naïve T cells induces several responses: proliferation of antigen specific lymphocytes (clonal expansion), cytokine secretion and differentiation of the naïve T cells into effector or memory T cells. The encounter between T cells and professional APCs, such as dendritic cells, occurs in the lymph node [93]. Dendritic cells constantly cross epithelial barriers, capture antigens and then return to the lymph node where they interact with T cells. The initial interaction between a T cell and a dendritic cell is not antigen dependent, in fact, regular interaction with dendritic cells expressing self-pMHC is thought to promote T cell viability. This interaction is mediated by adhesion molecules expressed at the surface of both cells. Adhesion molecules have a specific, but weak, interaction which is ideal for brief cell-cell interactions. In this particular case, adhesion molecules allow the T cell to rapidly scan the surface of several DCs in search of an agonist pMHC. Upon cognate TCR-pMHC interaction the T cell becomes activated. Full activation, however, relies on a secondary signal induced by costimulatory ligands [94, 95]. Activated dendritic cells express CD80 and CD86 proteins, which bind to CD28 expressed by T cells. The two signals generated, cognate TCR-pMHC together with CD28-CD80/CD86, induce strong activation of the T cell leading to a wide range of responses. Ultimately, the main goal of the adaptive immunity is to expand a specific clone of T lymphocytes that will be able to mount an effective immune response to eliminate the microorganism or malignant cell.

There are several types of differentiated effector T lymphocytes. One of the key differences is controlled by the coreceptor expressed, CD4 or CD8. Activated CD8 T cells differentiate into a cytotoxic effector T cell, T_C, whereas naïve CD4 T

cells differentiate into a wider range of "helper" T cells, T_H. The main function of T_C cells is to directly eliminate infected cells upon cognate TCR-pMHC interaction through the release of lytic granules, which induce apoptosis, similar to the action of NK cells. Helper T cells are involved in a wider range of effector functions and are usually subdivided into at least two different subsets: T_H1 cells that control cell-mediated immunity by recruiting and activating phagocytic cells to the sites of infection and T_H2 cells that recruit eosinophils, basophils, mast cells and macrophages to protect epithelial barriers. More recently, a third helper T cell subset has been defined T_H17, which seems to boost the phagocytic activity of the adaptive immune response. Follicular helper T cells, T_{FH}, formed from the T_H1 and T_H2 subsets, are a specialized group of helper T cells that induce the production of antibodies by B cells.

At the final stage of the immune response, the expanded number of cells of a specific clone of T lymphocytes returns to basal levels, leaving a legacy of antigen-specific, memory T cells that provide a faster adaptive response upon reinfection. The differentiation and survival of T lymphocytes is controlled by cytokines, especially those that signal through a group of trimeric receptors that share a common subunit, the γ_C. T cells constitutively express the γ_C chain, but the expression of the other two chains of the cytokine receptor, α and β, controls the cytokine specificity of the response, and varies in T cells of different subsets and at different stages of the adaptive immune response. In this way, the same cytokine can induce different signals in different cells. The combination of cytokines and $\alpha\beta$ chains can dynamically control the course of T cell survival, proliferation and effector responses.

1.3.2 Early biochemical events following TCR-pMHC interaction

Soon after the discovery of the TCR complex attention was given to the early events occurring inside the T cell responsible for initiating the signalling cascade following cognate TCR-pMHC interaction. The TCR ITAMs were found to become highly phosphorylated upon TCR triggering. In T cells, two members of the Src kinase family, Lck and Fyn, are responsible for phosphorylation of these

motifs [96, 97]. Phosphorylated ITAMs function as docking sites for the SH2 domains of ZAP-70, a cytosolic kinase [65, 98]. Binding of both ZAP-70 SH2 domains to phosphorylated TCR ITAMs coupled with tyrosine phosphorylation of a specific ZAP-70 residue by Lck, activates ZAP-70 kinase activity and initiates a signalling cascade inside the T cell [67]. The major substrates of ZAP-70 are the transmembrane adaptor protein LAT and the cytosolic adapter protein SLP-76 [67, 99]. LAT contains nine tyrosine residues that upon phosphorylation become docking sites for a group of signalling proteins that include: PLCγ1, the p85 subunit of phosphoinositide 3-kinase (PI3K), GRB2, Gads and SLP76 which is indirectly recruited to LAT through binding to Gads [100, 101]. Assembly of this large signalling complex leads to activation of multiple pathways giving rise to an increase in cytosolic calcium, initiation of MAPK signalling pathway, activation of NF-kB and NF-AT transcription factors that combined together induce changes in gene expression, cytoskeleton rearrangement and cell adhesion/motility (Fig. 1.2; [101, 102]). The combined outcome of these pathways determines the fate of the activated T cell.

Recent results have shown that these signalling cascades are not completely linear. An intricate balance between feedback loops at key steps in the signalling pathway allows the T cell to efficiently respond to agonist, non-agonist or antagonist peptides [103-105].

1.3.3 The immunological synapse

The productive interaction between a T cell and an APC is accompanied by dynamic changes in the actin cytoskeleton that lead to a significant rearrangement in the distribution of cell membrane proteins. The contact that is formed between the T cell and the APC was termed as the immunological synapse (IS; [106, 107]), by analogy with the neuronal synapse.

Upon activation, proteins segregate into two well defined areas. At the centre of the cell-cell interaction a central supramolecular activation complex, c-SMAC, is formed, where the TCR, the coreceptors CD4 and CD8, the costimulatory receptor CD28 and the adhesion molecule CD2 can be found,

associated with various other molecules. Surrounding this area, a peripheral and a distal supramolecular activation complex, p-SMAC and d-SMAC, contain integrins such as LFA-1 and tyrosine phosphatases like CD45.

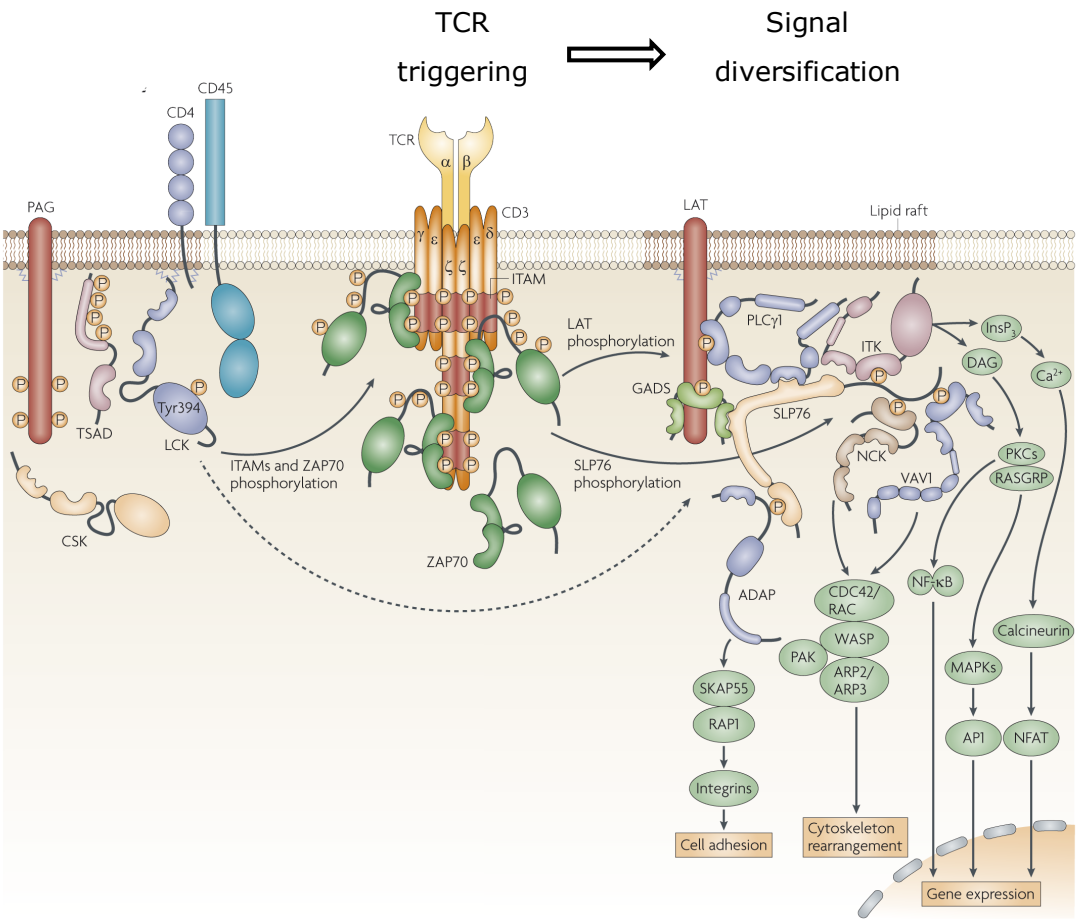

Figure 1.2: TCR signalling cascade. TCR engagement by an agonist pMHC is signalled across the membrane by an increase in stably phosphorylated CD3 ITAMs. Lck is responsible for ITAM phosphorylation, which leads to ZAP-70 recruitment to the cell membrane. ZAP-70 then phosphorylates LAT and SLP-76. Different proteins can then bind to tyrosine phosphorylated LAT residues and form a signalling complex that activates multiple pathways (signal diversification). More details are given in the main text. AP1, activator protein 1; ARP, actin-related protein homologue; CDC42, cell-division cycle 42; GADS, growth-factor-receptor-bound-protein-2-related adaptor protein; $InsP_3$, inositol-1,4,5-trisphosphate; MAPK, mitogen-activated protein kinase; PAK, p21-activated kinase; PKC, protein kinase C; SHP1, SH2-domain-containing protein tyrosine phosphatase 1; SKAP55, SRC-kinase-associated phosphoprotein of 55 kDa; WASP, Wiskott–Aldrich syndrome protein. Image adapted from [102].

This rearrangement in protein distribution occurs minutes after TCR activation and is thus a cellular response to TCR triggering [108]. This coordinated protein distribution is a process driven by actin that directly or indirectly attaches to proteins and induces a centripetal movement towards the centre of the immune synapse [109]. In the case of the TCR, soon after TCR triggering, clusters of up to 100 TCR complexes, *i.e.* TCR microclusters, are pulled together and directed to the c-SMAC [110, 111]. Signalling through the receptor occurs only in the small clusters present at the periphery of the SMAC [112]. Once in the c-SMAC signalling through the TCR is attenuated and the active internalization for lysosomal degradation of these and other signalling receptors is initiated. The c-SMAC also seems to be the place where targeted secretion of cytokines takes place [113].

1.3.4 The role of costimulatory molecules

The productive activation of naïve T cells requires the action of costimulatory signals from CD80 and CD86 molecules, expressed at the cell surface of professional APCs that bind CD28 molecules. Signalling through CD28 is thought to augment and sustain the initial signalling induced by the cognate TCR-pMHC interaction [94, 95]. As with other receptors, signalling through the CD28 molecule follows tyrosine phosphorylation of specific motifs present in the cytoplasmic tail of this receptor. Once phosphorylated, these motifs recruit SH2-domain containing proteins that will drive intracellular signalling. One of the molecules that play an important role in CD28 signalling is the phosphoinositide-3-kinase, PI3 kinase, which is recruited to CD28 and activates other kinases, such as Itk and PLC-γ1 [114-117]. Although TCR signalling also induces PI3 kinase activity, CD28 boosts this signalling to higher levels, leading to stronger T cell activation. Expression of cytokines like IL-2, which plays an important role in inducing lymphocyte proliferation, is dependent on TCR and CD28 stimulation.

The crucial role played by molecules like CD28 led to the search for structurally and functionally similar molecules. Surprisingly, it was found that other members of this family of receptors played an inhibitory role in T cell

activation. CTLA-4 and PD-1 are membrane receptors [118, 119], expressed at different stages during T cell activation, that share homology with the costimulatory molecule CD28, but have inhibitory roles, that is, activation of CTLA-4 and PD-1 attenuates T cell activation [120, 121]. These proteins are not expressed at the surface of resting or naïve T cells. Upon T cell activation intracellular vesicles containing CTLA-4 are fused with the cell membrane [122]. Once at the surface, CTLA-4 interacts strongly with CD80, effectively sequestering this protein from binding CD28, and attenuating the activation signal induced by this receptor. The molecular mechanism behind CTLA-4 inhibition of T cell activation is not fully understood, but together with the competition with CD28 for the CD80 ligand it also seems to promote cell motility [123, 124]. Recently it has been suggested that the strong interaction between CTLA-4 and CD80 might even lead to removal of CD80 from the cell membrane [125]. PD-1 is expressed at the cell surface of an activated T lymphocyte hours after productive TCR-pMHC interaction. PD-1 binding to PDL-1 leads to inhibitory signals that dampen the effector function of activated T cells. These three T cell receptors, *i.e.* CD28, CTLA-4 and PD-1, are major therapeutic targets.

1.4 T cell receptor triggering: an unsolved problem

Despite an improving understanding of the signalling pathways and the final outcome at both the molecular and cellular level following cognate TCR-pMHC interaction the molecular mechanism leading to TCR triggering remains poorly understood.

1.4.1 Signalling properties of the T cell receptor

The mechanisms responsible for cell surface expression of pMHC do not distinguish between self or foreign peptides, *i.e.* the TCR complex is repeatedly being exposed to self pMHC ligands which largely dominate in terms of density over agonist-pMHC. This implies that an extraordinarily sensitive mechanism allows recognition of and responses to the presence of very few agonist-pMHC

while remaining unresponsive to the multiple interactions with non-agonist pMHC [126, 127]. Like other membrane protein receptor-ligand interactions, the TCR-pMHC has a low affinity, with 3D KD values in the 1-100 μM range [128, 129]. This low affinity is probably important to allow reversible ligand-receptor association [130, 131], and is compensated for by a high specificity driven by electrostatic surface-complementarity interactions [132]. The different affinities of TCR-pMHC interaction lead to another property of the TCR molecule, versatility. The TCR recognizes both high- and low-affinity pMHC during the development in the thymus and is able to respond appropriately to both. In the periphery, low-affinity TCR-pMHC interactions are thought to sustain T cell viability. These observations indicate that the TCR is capable of producing adequate signals according to the stimuli provided by the pMHC. Furthermore, despite the low affinity range of TCR-pMHC interactions, the TCR shows single-molecule sensitivity insofar as it is able to respond to as few as 1-10 pMHC [133-135]. Another important feature of TCR triggering is the ability to induce signalling even though the TCR-pMHC structural interactions are extraordinarily diverse [136]. In fact, in the TCR-pMHC complex structures that have been solved to date, no conserved contacts or conformational changes at the binding interface have been identified [63].

Before presenting some of the models proposed to explain the molecular mechanism of TCR triggering, the membrane environment, the evolution of SH2 signalling cascades and molecules involved in controlling TCR tyrosine phosphorylation level, namely Src kinases and CD45, will be discussed in more detail.

1.4.2 The cell membrane: a specialized structure in signal transduction

From being just a major barrier between the cell and its surroundings the cell membrane has evolved as a specialized structure for protein-protein interactions. Simple features combined together make this structure unique in the cell environment. Membrane proteins are reduced in their mobility by one dimension when compared with soluble molecules. This implies that affinities measured at

cell surface are correctly defined not by classic 3D K_D measurements but by 2D K_D affinities [137, 138]. Not only diffusion is limited, however, since the orientation of membrane proteins are also restricted. Proteins can both "tilt" by 10 degrees and move within the axial plane of the membrane by 5Å [139]. These properties, however, imply that orientation of the proteins is largely maintained in a well-defined manner. Multiple copies of the same protein are present at the membrane; this can lead to *avidity* effects in proteins interacting with given 2D K_D *affinities* [140, 141]. Lastly, given the restraints in diffusion, the membrane environment promotes a constant high level of non-specific interaction between proteins [142, 143], which is likely to have a crucial role in signal transduction.

Protein diffusion and organization at the cell membrane

The restriction of membrane proteins to 2D diffusion has profound implications for protein-protein interactions. Lateral diffusion at the cell membrane is constrained by surface crowding (protein density), lipid viscosity, intracellular interactions with cytoplasmic structures and also the external volume above the lipid bilayer. All these effects reduce membrane protein diffusion by 10 to 100 fold, when compared with molecules in solution [144]. As just mentioned above, the restriction to a 2D plane alters the thermodynamics of ligand-receptor binding. The classically determined 3D K_d values for protein-protein interactions cannot be easily correlated with the biologically relevant 2D K_d affinities. It is also becoming clear that weak 3D affinities, in the 10-200 μM range, can be extremely relevant and surprisingly stable, once proteins are restricted to a 2D plane.

Protein mobility at the cell membrane is also affected by the underlying actin meshwork that shapes the cell surface and connects it with the cytoskeleton. The cytoplasmic domain of several membrane proteins have docking sites for intracellular proteins that bind to actin. This indirect attachment of membrane proteins to actin constricts protein diffusion and can lead to significant rearrangement of protein distribution at the cell membrane and alter the random distribution of these proteins. In the case of T cells, formation of the IS is an example of an actin-driven process with important consequences for cell

signalling. In T cells the simple interaction with a glass surface is enough to trigger changes in TCR mobility [145]. This process can be caused by surface molecules that recognize and respond to mechanical stimulus, like focal adhesion macromolecular structures. Single-particle tracking of surface proteins has revealed how actin limits the Brownian diffusion of proteins over large distances. Proteins have been found to migrate along actin structures or to have their diffusion restricted by the underlying actin network [146, 147]. Surprisingly this restriction has also been found for GPI-anchored proteins and outer leaflet lipids [148, 149]. Whether these observations are a consequence of indirect actin control of adjacent proteins is not known, but the influence of actin and protein-protein interactions in the random distribution and diffusion of membrane proteins is increasingly evident.

As mentioned above, lipid viscosity also affects protein diffusion. Molecules like cholesterol have a distinct structure that alters significantly the lipid fluidity. In a highly influential model Simons and van Meer proposed the existence of lipid-ordered and disordered phases of the cell membrane, the basis of the lipid raft model [150, 151]. Surface molecules would partition between these two structures, according to specific properties (such as the mode of membrane attachment or the amino acids present in the transmembrane domains) and would thus induce a basal organization and distribution of the membrane proteins, with significant implications for receptor triggering [152]. Proteins resistant to plasma membrane solubilization with Triton X-100, at 4°C, are generally considered to be associated with lipid rafts. However, using *in situ* stimulated emission depletion far-field fluorescence microscopy combined with fluctuation correlation spectroscopy, it became possible to study the "nano-scale" organization of lipids at the cell surface [153]. This showed that domains containing sphingolipids and glycosylphosphatidylinositol-anchored proteins, *i.e.* lipid rafts, are, at best, very small (<20 nm diameter) and extremely short-lived (~10-20 ms) [153]. The functional significance of such dynamic and transient structures for receptor signalling has not been determined yet but it is possible that lipid rafts are not able to efficiently promote or impede protein-protein

interactions [154]. Lipid rafts have been suggested to induce TCR oligomerization in a resting state or upon interaction with cognate pMHC [155-157]. It has, however, been shown that classically considered markers of lipid rafts are randomly distributed *in vivo* [158, 159] and in an elegant study Douglass and Vale showed how protein-protein interactions, rather than lipid rafts, can lead to protein clustering [160]. The valency of the TCR in a resting T cell will be discussed in more detail in Chapter 3.

1.4.3 The role of Src kinases and tyrosine phosphatases in TCR signalling

T cell activation is initiated with an increase in the number and/or half-life of phosphorylated tyrosine residues present in TCR ITAMs. Understanding the regulatory mechanisms of kinases and phosphatases that control TCR tyrosine phosphorylation will likely contribute to elucidate the TCR triggering mechanism. The Src family kinases, especially Lck, are known to phosphorylate the TCR ITAMs, however, these tyrosine kinases have evolved complex mechanisms to regulate their activity, which will now be discussed in more detail.

Evolution of a tyrosine phosphorylation-based signalling system

In metazoans, the interplay between three components: a tyrosine kinase (TyrK), a phosphotyrosine phosphatase (PTP) and a target tyrosine residue in a specific sequence give rise to a simple readout. Inclusion of a fourth component, SH2 domains, attached to other proteins, like TyrK, dramatically increases the possible outcomes for such a signalling system.

How did this four component system appear during evolution? Sequencing of the budding yeast *Saccharomyces cerevisiae*, revealed that this single-cell organism has no TyrK, one proto-SH2 domain [161]) and around 5 PTPs [162]. This suggests that PTPs were the first component of this system to evolve. The functional advantage of PTPs in a cell without TyrK might come from a rare and inefficient, but functionally important, event: tyrosine phosphorylation by Ser/Thr kinases [163]. PTPs probably arose from dual specificity phosphatase enzymes, able to dephosphorylate both Ser/Thr and Tyr residues [164, 165]. With

PTPs in place, SH2 domains evolved to generate a complex system for responding to tyrosine phosphorylated residues. The slime mold *Dictyostelium discoideum* has no TyrK, but already expresses 13 SH2 domains and, like the *Saccharomyces cerevisiae*, around 5 PTPs. The most ancient organisms where TyrK have been found are the choanoflagellates, the closest single-cell relatives of metazoans [162]. In metazoans, between 50 to 100 TyrK, 100 SH2 and around 40 PTPs, give rise to a complex signalling network involved in a wide range of cellular responses. Of these, members of the Src family and phosphatases like CD45 probably evolved to play a crucial role in TCR triggering.

Lck and CD45: setting the stage for TCR triggering

The key Src kinase involved in TCR triggering is Lck [101, 166]. All members of the Src kinase family, *i.e.* Src, Hck, Fyn, Blk, Lyn, Fgr, Yes, Yrk and Lck, share a similar architecture consisting of five functional domains, which are, from N- to C-terminus: an SH4 domain, a region which is modified by the addition of lipids and targets Src kinases to the cell membrane; a unique domain, which in Lck is responsible for its interaction with CD4 and CD8 *via* a zinc-clasp structure [167-169]; followed by an SH3 domain, an SH2 domain and the catalytic SH1 domain. The present view of Lck regulation is based on biochemical analysis and crystal structures of Src family kinases, including Lck (Fig. 1.3; [102, 170]). Classically, phosphorylation of the C-terminal Tyr505 residue by Csk is considered to inhibit the kinase whereas trans auto-phosphorylation of activation-loop Tyr394 promotes its activity. CD45 dephosphorylates both Tyr sites, somewhat complicating the interpretation of its role during TCR triggering. The crystal structure of Src and Hck in the autoinhibited form, Tyr505-phosphorylated state, suggests how Src kinases are inactivated [171-173]. Tyr505 phosphorylation promotes binding of the SH2 to the C-terminal tail and stabilizes an association of the SH3 domain with a PxxP motif present in the linker segment that connects the SH2 and kinase domain. These interactions do not directly occlude the catalytic clef, instead they promote the displacement of the kinase domain C-helix to a configuration that (1) does not favor efficient substrate binding, (3) sterically

occludes Tyr394 phosphorylation and (3) removes a catalytically important glutamate residue from the kinase active site [171, 172]. Phosphorylation of Tyr394 reverses these effects and stabilizes the conformation of the C-helix in the catalytic site of the enzyme in a way that promotes both ATP binding and substrate recognition. Importantly, the effects of Tyr394 phosphorylation are dominant over those of Tyr505 [170, 174].

The signalling unit formed by Lck and the TCR is intimately connected with the PTP CD45. In T cells, CD45 can account for 10% of the total cell surface expressed proteins, it is also a PTP with broad specificity and high catalytic activity [175-177]. CD45 is expressed in T and B cells and in many other cells of hematopoietic origin [178].

The cytoplasmic region of CD45 is formed by two tandem PTP domains (D1 and D2) that share a high degree (95%) of homology among the mammalian species analysed. Of these two PTP domains only the membrane proximal (D1) is catalytically active even though both domains are required for efficient phosphatase activity. However the precise function of D2 is still not known. Dimerization of CD45 has been proposed to influence its catalytic activity [179] however, CD45 appears to be largely monomeric at the cell surface of T cells [145]. In contrast to the cytoplasmic region, the sequence of the extracellular region varies significantly across different mammalian species (35% sequence homology) although the general domain organization is conserved. The extracellular region of CD45 is highly glycosylated with both *N*-glycosylation and *O*-glycosylation that vary according to cell type, developmental stage and activation state of the cell. The first four membrane proximal domains of CD45 form the core of the extracellular domain that is present in all different isoforms of this protein. This region is composed of three contiguous fibronectin-like domains followed by a cysteine-rich domain, with all four domains being *N*-glycosylated. Alternative splicing of three exons, N-terminal to the cysteine-rich domain, can generate eight different isoforms and there is evidence of expression at the protein level for at least five of these isoforms [180]. The three exons have multiple sites of *O*-glycosylation and can be further modified by sialic acid.

Attribution of specific roles to each isoform has not been possible so far. Primary naïve T cells express mainly the longer isoforms of CD45 whereas memory and helper T cells have a tendency to express the shortest isoform. This change in isotype expression is dependent on T cell activation and has been linked to increases in expression of the heterogeneous ribonucleoprotein L-like, a key regulator of alternative splicing in activated T cells [178, 181].

CD45 has a crucial role in T cell development and activation. CD45 deficient humans or mice [182-185] develop a severe-combined immunodeficiency phenotype. However, the CD45 contribution to TCR signalling is controversial with several reports showing a positive, a negative or even a dual contribution [178, 186-190]. CD45 dephosphorylates C-terminal Tyr505 of Lck, and thus has a positive contribution to Lck kinase activity but it is also capable of dephosphorylating Tyr394, required for Lck catalytic activity [186, 188]. Furthermore, CD45 has been shown to also dephosphorylate CD3ζ ITAMs [191]. The combination of these observations has made it difficult to dissect the global contribution of CD45 during the early events of TCR signalling. The role of CD45 will be discussed in more detail in Chapters 5 and 6.

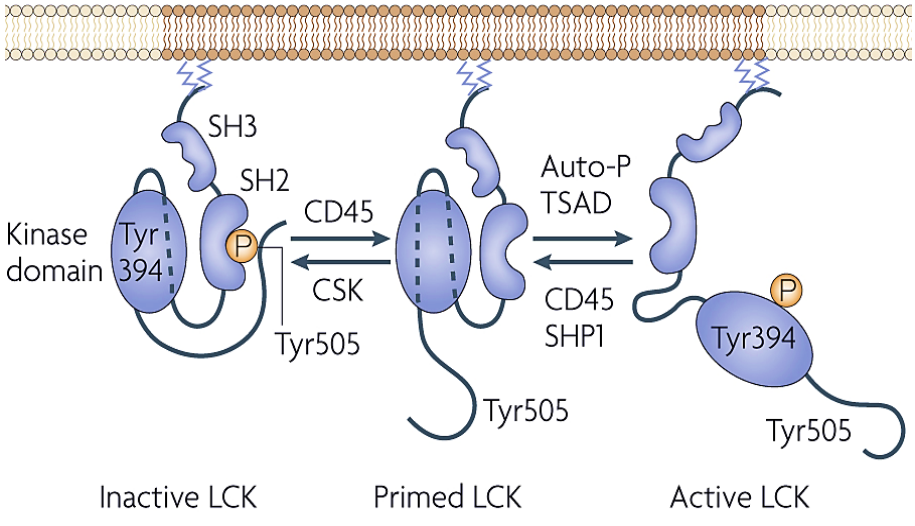

Figure 1.3: Regulation of Lck catalytic activity. Phosphorylation of C-terminal Tyr505 by Csk promotes an inactive conformation of the enzyme (*left structure*). Dephosphorylation of Tyr505 by CD45 and trans auto-phosphorylation of Tyr394 fully activates Lck kinase (*right structure*). Unphosphorylated Lck is considered to be in a "primed" state (*middle structure*). Image adapted from [102].

1.5 Models of TCR triggering

As discussed above, in the almost 30 years after TCR discovery, much has been learnt about the signalling pathways that lead to intracellular Ca^{2+} increase, changes in gene expression and T cell differentiation. However, the central question in TCR signalling remains to be solved: how TCR binding to a cognate pMHC results in the tyrosine phosphorylation of the CD3 subunits cytoplasmic domains. Models of TCR triggering are usually based on three distinct molecular mechanisms: aggregation, conformational change and molecular segregation.

1.5.1 Aggregation

Several models for TCR triggering have been proposed based on aggregation of the receptor [101, 192]. The classical example of a receptor that is triggered by dimerization is the epidermal growth factor receptor (EGFR). Upon ligand-binding the dimeric form of the receptor is stabilized and the covalently associated TyrK present in the cytoplasmic tail of the EGFR can trans auto-phosphorylate and become activated [193-197]. However, the TCR has no intrinsic kinase activity and the native TCR ligand, pMHC, is neither a dimer nor bivalent and so is not expected to induce TCR crosslinking. Furthermore, recent observations challenge the classic view on EGFR triggering by showing that these receptors are present at the cell surface in an equilibrium between monomeric and dimeric forms [198-200].

Aggregation of the TCR could lead to triggering by inducing changes in the conformation of cytoplasmic tails of TCR chains or by locally increasing the concentration of TCR-associated Lck molecules. However, as discussed above, the surface of the APC contains very few agonist pMHC and no evidence has been found for the existence of clusters of these molecules. The low affinity of the TCR-pMHC interaction together with the low abundance of agonist-pMHC ligand also implies that the TCR, either monovalent or in clusters, will likely dissociate before encountering another agonist-pMHC. Adding to these results no apparent dimer was ever found present in the several crystal structures of TCR-pMHC produced so far [201]. And, more importantly, other studies have

demonstrated that T cells can respond to a single agonist pMHC [133, 134]. In the case of the pre-TCR, results obtained from the crystal structure of the pre-TCRαβ suggested that spontaneous dimerization of these receptors could be responsible for inducing basal signalling in double positive T cells [202, 203]. These results, however, are difficult to reconcile with studies where the extracellular domain of the pre-TCRα was found to have no effect on thymocyte development *in vivo* [204, 205].

The valency of the TCR at the cell surface is still controversial. Some studies report that some fraction of the TCR is present in clusters, or "protein islands" [206-208] with other studies indicating that it is a monomeric receptor [142, 209]. In Chapter 3 the TCR valency in a resting T cell will be investigated further [142]. It is, however, quite clear that upon TCR-pMHC interaction the TCR aggregates in clusters containing 10-100 TCRs [111, 112], as discussed in §1.1.5. This induced aggregation seems to be the result of an active process, controlled by actin, although other mechanisms could also be involved.

Other aggregation models are dependent on the binding of coreceptors, CD4 or CD8, to pMHC, which could thus form a ternary complex of a coreceptor bound to a TCR-pMHC. Binding of the coreceptor to the cognate, TCR-bound, pMHC or to the more abundant self-pMHC would favor dimerization of the TCR. The increase in the concentration of the Lck molecule, which is bound to the coreceptor, in the vicinity of the TCR complex could then lead to an increase in TCR phosphorylation. These models have been supported by experiments where blocking of CD4 or CD8 binding to pMHC reduced TCR sensitivity. However, these studies also show that inhibiting coreceptor binding to MHC molecule does not completely block TCR triggering, in agreement with other observations demonstrating that TCR triggering can occur in the complete absence of CD4 or CD8 molecules [74, 210] . Moreover, the affinity of CD8 and especially CD4 for MHC molecules is extremely low, almost undetectable. Recently, it has also been shown that binding of the CD8 coreceptor to the MHC molecule is, initially, driven by the SH2 domain of Lck, that is, it is dependent on prior phosphorylation of TCR ITAMs of a complex that is interacting with a

specific pMHC [211]. These recent observations fit very well with much earlier data in which the Lck-dependence of thymic selection was affected more by mutations that destroyed SH2 domain binding than those that blocked kinase activity [212].

1.5.2 Conformational change models

Several TCR triggering models are based on a conformational change. The structural complexity of the TCR has provided the framework to propose triggering models where the cognate pMHC interaction is transduced across the cell membrane *via* intra- or inter-subunit changes. Models of TCR triggering invoking conformational changes are of two types: those involving the TCR or CD3 ectodomains and those dependent on the CD3 cytoplasmic domains.

TCR ectodomains

Crystallographic studies have not found conserved differences between free, unliganded, TCRαβ or bound to MHC with agonist or antagonist peptides [42, 43, 57]. The growing set of TCR-pMHC crystal structures is also showing a remarkable diversity of both the variable region of αβ chains and its mode of interaction with the pMHC, which challenges identification of a common conformational change that could be transmitted across the membrane [63, 136]. However, a close analysis of the LC13 TCR structure upon binding to pMHC (HLA-B8-FLRGRAYGL) identified a subtle rearrangement in the AB loop of Cα [213]. Mutation of this loop impaired TCR triggering, yet it remains to be understood how the subtle rearrangement identified could be transmitted across the membrane. Moreover, in the case of the TCR it is difficult to dissect complex structural stability from functional efficiency, *i.e.*, mutation of residues might lead to a decreased complex stability (such as surface expression or subunit pairing) which affects signal transduction. It has also been proposed that the mutations in the AB loop affected TCR dimerization [206], and several models have been proposed based on conformational changes that can induce receptor clustering

[214, 215]. At present there is no definitive experimental support for these models.

CD3 ectodomains

Although there is no quaternary structure available for the entire TCR complex, information from the transmembrane interactions between the TCR-CD3 chains suggest some degree of interaction between the different subunits. Different models have been proposed where binding of a pMHC to TCRαβ induces large inter-subunit rearrangements able to initiate TCR triggering (Fig. 1.4; [53]). Similar proposals have been suggested to explain TCR triggering with anti-CD3 antibodies [60]. A common feature of these models is the formation of new contact interfaces between different TCR-CD3 subunits during TCR triggering. An approach to probe the dependence of TCR triggering on formation of new interfaces will be discussed in detail in Chapter 4.

CD3 cytoplasmic domains

A conformational change in CD3ε has been proposed to initiate TCR signalling by inducing recruitment of the Nck adaptor protein to the CD3ε cytoplasmic domain [216-218]. *In vitro*, Nck is recruited in response to anti-CD3 Fab ligation in the absence of TCR aggregation, prompting the conclusion that conformational adjustments in CD3ε expose the proline-rich sequence (PRS) Nck binding site of CD3ε [216]. Despite these observations the importance of the PRS for TCR triggering remains controversial. More recent reports have shown that in mice lacking the PRS neither T cell development and function nor mature T cell responsiveness is affected, thereby suggesting that the interaction between CD3ε PRS and Nck is not required for TCR signalling [219-221].

Building on early observations made by Stern and colleagues where CD3ζ cytoplasmic domain was found to undergo a conformational change upon lipid binding [222, 223], Xu *et al.* recently investigated the effect of cell membrane association on the CD3ε cytoplasmic domain. In this study it was shown that a basic residue-rich region in CD3ε mediates a surprising interaction between the

cytoplasmic tail of this subunit and the inner leaflet of the cell membrane [224]. This observation has now been extended to CD3ζ [225]. In an elegant NMR study, Wucherpfennig and colleagues showed that the tyrosine residue of the ITAM sequence was buried within lipid bicelles used to mimic the cell membrane [224]. These results, however, must be interpreted with caution as the interactions between CD3 cytoplasmic domains and the lipid bicelles were found to be extremely dependent on the lipid environment created [226-228].

What could be the functional significance of this interaction? The ITAM-phospholipid interaction was proposed to be a safety mechanism to prevent random ITAM phosphorylation (Fig. 1.5; [224, 229, 230]) implying that triggering is dependent on an unknown mechanism to dislodge the ITAM from the inner leaflet of the T-cell membrane prior to its phosphorylation by Src kinases [224]. In a follow up to these studies, it has been argued that clustering of the TCR, upon pMHC engagement, would induce translocation of the TCR oligomers to specific lipid domains unable to interact with the CD3ε ITAMs thereby "releasing" these motifs and initiating signalling [230]. The role, if any, of the association of the CD3ε cytoplasmic domain with the cell membrane will be investigated further in Chapter 5.

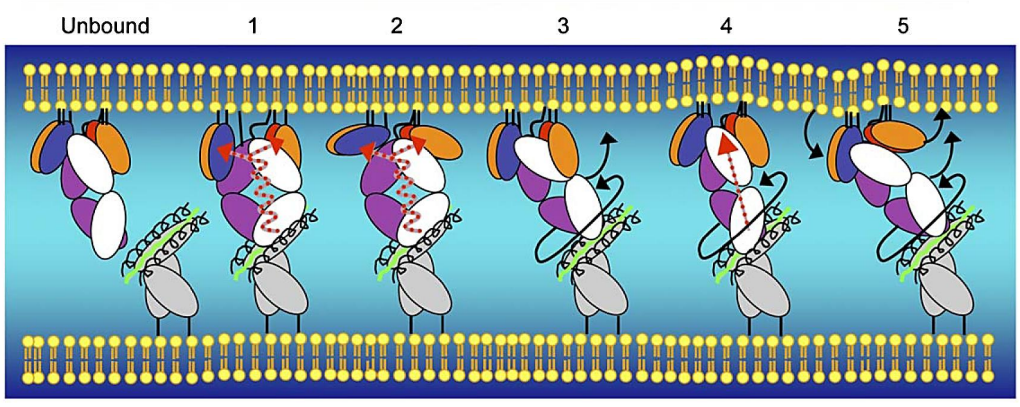

Figure 1.4: Possibilities for large inter-subunit conformational changes that could drive TCR signalling. The common feature in these models (1 to 5) is the large-scale reorganization of the positions of CD3 subunits (collared in orange and blue) relative to the TCR αβ chains (cooler in purple and white), creating new interfaces. Image adapted from [52].

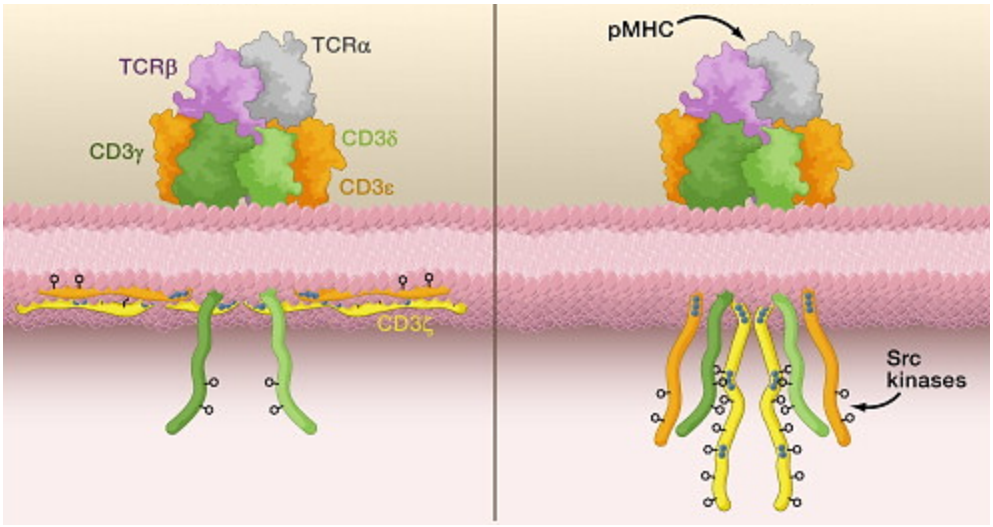

Figure 1.5: Following the work of Xu *et al.* (discussed in the main text) it has been proposed that in a resting T cell (left panel) the CD3 ITAMs are not accessible to Tyr phosphorylation by Lck. Following binding to cognate pMHC, CD3 ITAMs are somehow released from the membrane and become phosphorylated. Image adapted from [229].

1.5.3 Segregation models

The kinetic-segregation (KS) model introduced a new concept in TCR triggering: that passive spatial reorganization of cell surface molecules could initiate local changes in receptor phosphorylation. Several observations contributed to the formulation of this model [231, 232]. It was initially noticed that the distance formed between the T cell and the APC, upon contact formation between the TCR and pMHC, around 15 nm, is considerably smaller than the extracellular size of heavily-glycosylated PTPs, like CD45 [140]. To date, no PTP expressed at the cell membrane with an extracellular domain smaller than 15 nm has been found, with the exception of RPTPα and RPTPε. Interestingly, whereas CD45 and other tyrosine phosphatases are extremely promiscuous regarding substrate selectivity, RPTPα and RPTPε display reduced peptide recognition capacity [233]. Later on, blocking PTP activity by treating T cells with pervanadate indicated that there is a continuous tyrosine phosphorylation of a large number of proteins, including CD3 subunits of the TCR [234]. It was thus hypothesized that tyrosine phosphorylation was low, almost absent, in resting T cells because of the action of

PTPs. CD45 appeared as an obvious candidate to perform this crucial task. These findings implied that the overall phosphorylation level of the TCR could be dependent on the local balance between Src kinases and PTPs, such as CD45. Combined together, these observations led to formulation of the kinetic-segregation model (Fig. 1.6; [231]). This proposes that, upon close contact formation between the T cell and the APC, phosphatases, because of their large extracellular domains, are passively excluded thus creating phosphatase-free areas. In these regions the balance between phosphatases and kinases is disrupted leading to an increase in the half-life of phosphorylated TCR complexes, or new increased phosphorylation events, *i.e.* TCR triggering. TCR complexes with low affinity for the pMHC being presented by the APC diffuse away from the contact region to be dephosphorylated by PTPs, providing specificity to the mechanism. Several results support predictions made by this model, namely: increasing the dimensions of the TCR-pMHC or reducing the size of CD45 and CD148 PTPs reduces the extent of TCR triggering [235-237]; surface bound TCR ligands are more effective in inducing triggering than their counterparts [135, 238]; TCR triggering driven by engineered TCRs is stronger when the epitope is positioned close to the plasma membrane of the target cell [239]. Despite these results, a key assumption of this model still remains to be demonstrated: is CD45 passively excluded from the initial contacts between the T cell and APC? It has been shown that in the course of IS formation the majority of CD45 relocates to the p-SMAC [240] with a small fraction residing in the c-SMAC [241]. However, these translocations are actin-dependent thereby implying they occur as a consequence of triggering. CD45 is also excluded from initial TCR microclusters formed at the periphery of the T cell [112]. Although microclusters precede SMAC formation this is again an active, actin-driven response to triggering [110, 111, 242]. Observing the movement of CD45 in live cells during the initial contacts between a resting T cell and an APC is a technically challenging but necessary experiment to test the validity of the KS model.

In Chapter 6, the global homeostatic balance between Src and PTP activity in T cells will be perturbed in an attempt to gain a better insight on the molecular mechanisms controlling TCR phosphorylation.

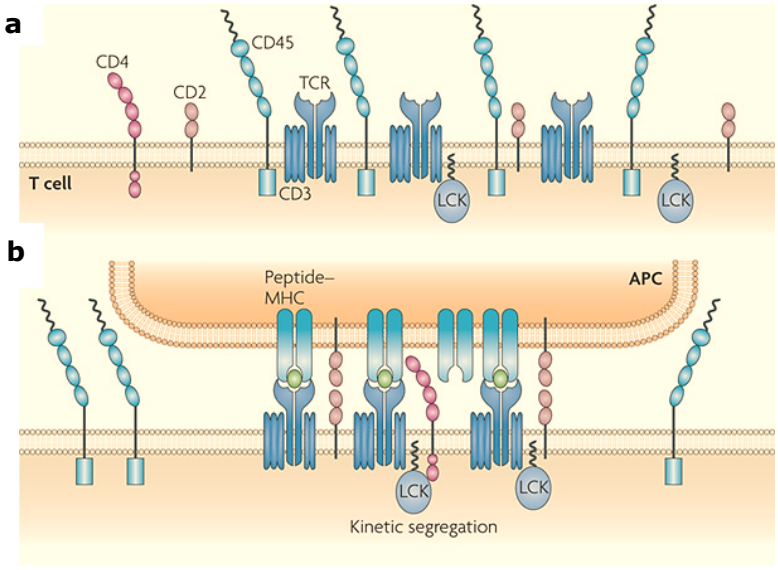

Figure 1.6: The kinetic-segregation model proposes that in a resting cell **(a)** the local balance between kinase (Lck) and phosphatase (CD45) activity determines overall TCR phosphorylation levels. **(b)** Close contact formation between a T cell and an APC induces passive, size-driven reorganization of signalling molecules. Exclusion of CD45 from the close contact region shifts the equilibrium and promotes the phosphorylation of TCRs stably bound to pMHC. Image adapted from [242].

1.6 Aims of this thesis

The key objective of this thesis is to extend the current knowledge on specific properties of the TCR receptor to provide a better framework for thinking about the receptor-triggering problem. The initial focus will be in addressing the aggregation level of the TCR in a resting, pre-triggered, T cell using a new quantitative form of single-molecule tracking video microscopy. Secondly, it will be determined whether or not extracellular inter-subunit large-scale

conformational changes play a part in the triggering mechanism. A similar question will be addressed for the contribution of intracellular conformational changes to TCR triggering. Probing the contribution of these structural rearrangements to TCR triggering will be made alongside an attempt to produce the TCR in such a way that small scale structural rearrangements could eventually also be ruled in or out. Finally, in the presence of an apparently monovalent and static complex, the possibility that a fine-tuned interplay of tyrosine kinases and phosphatases regulates TCR phosphorylation at global and local levels is considered.

Chapter 2

General methods

2.1 Molecular cloning and vector design

2.1.1 Overview of cloning method

Standard molecular cloning techniques were used to express the proteins of interest in suitable cell lines. Genes were amplified from vector templates or appropriate cDNA using oligonucleotide primers that incorporated suitable restriction enzymes sites at both the 5' - and 3'-ends. Following polymerase chain reaction (PCR) amplification, the gene of interest and the destination vector were digested with the appropriate enzymes. After purification of the correct DNA fragments, a ligase reaction was performed in order to obtain a contiguous plasmid. The product of the ligase reaction was used to transform bacteria that were grown in culture plates with the appropriate antibiotics. After confirming the size and orientation of the DNA insert larger preparations of DNA plasmid was made and sent for sequencing to confirm sequence integrity.

Vectors used for gene expression

pHR-SIN-CSGW

The lentiviral pHR vectors are derived from the HIV genome to allow self-inactivating viral particles to be packaged, expressed to the extracellular medium, and used to stably infect target cells. The gene of interest is expressed under control of an SFFV viral promoter and includes an additional WPRE enhancer activity at the 3'-end. The vector confers resistance to ampicillin in bacterial cells.

pHR-I

The pHRI is derived from the pHR-SIN-CSGW after changing the SFFV for an E/GRE promoter. The E/GRE promoter is an ecdysone inducible promoter that requires the combined activity of the nuclear factors RXR and FB-ERV to induce optimal expression levels. In the experiments described in this thesis RXR and FB-ERV were not present in target cells and thus the expression levels of the desired protein were only residual.

2.1.2 Molecular cloning methods

Genes of interest were amplified by PCR using the following reaction mixture:

	Company	Conc.	Volume / µl
Polymerase Buffer	NEB	10 x	8.0
dNTP	Bioline	10 mM	2.0
5'-oligo	Sigma-Aldrich	10 µM	2.0
3'-oligo	Sigma-Aldrich	10 µM	2.0
Template	-	100 ng/µl	1.0
DNA Polymerase	NEB	5 U/µl	0.5
ddH_2O			24.5

For most cloning procedures, oligonucleotide primers with appropriate restriction sites at the 5'- and 3'-ends were used. To ensure sequence integrity for cloning, a Taq DNA polymerase (New England Biolabs, UK) with a robust proofreading protein was used to ensure the correct sequence was amplified. The amplification process was made on a DNA Engine Tetrad (MJ Research), using the following reaction scheme:

	Step	Temp. (°C)	Time
1	Enzyme Activation	95	2 min
2	Denaturing	94	30 s
3	Annealing	58	30 s
4	Extension	72	35 s/kb
5	Repeat 2-4		28 x
6	Final Extension	72	8 min
7	Cooling	4	∞

Screening of bacterial colonies to detect presence of inserted DNA sequence and correct plasmid, a different PCR reaction mixture was used:

	Company	Conc.	Volume / µl
Polymerase Buffer	Bioline	10 x	3.0
dNTP	Bioline	10 mM	1.0
5'-oligo	Sigma-Aldrich	10 µM	1.5
3'-oligo	Sigma-Aldrich	10 µM	1.5
Colony Stab	-	-	-
DNA Polymerase	Bioline	10 U/µl	0.2
ddH_2O			21.8

The PCR reaction cycle was also modified to ensure lysis of bacterial cells prior to amplification:

	Step	Temp. (°C)	Time
1	Lyse Bacteria	95	7 min
2	Denaturing	95	30 s
3	Annealing	58	30 s
4	Extension	72	70 s/kb
5	Repeat 2-4		30 x
6	Final Extension	72	75 s
7	Cooling	4	∞

For the creation of chimeric or genes or introduction of mutations, a two-step PCR protocol was used. Oligonucleotide primers were designed to incorporate overlapping (around 20 nucleotides) internal DNA sequences at the point of junction or mutation and two separate PCR products were amplified using the standard reaction protocol. The two overlapped products of the correct size were purified and used as templates in a second round of PCR according to the original protocol, except that the number of cycles (step 4) was reduced to 15.

Agarose gel separation of DNA

Agarose gels were used to resolve size and purity of plasmids or PCR products. High-quality agarose (SeaKem LE agarose, BioWhitakker) was dissolved in Tris-

borate EDTA (TBE) buffer (Sigma-Aldrich) at 1% (w/v) for most of the separations. If greater resolution was required 1.5% (w/v) agarose gels were used. The gel was melted using a microwave for 70s, followed by addition of ethidium bromide at a final concentration of 0.5 μg/ml before the gel was cast with appropriate combs. Loading buffer (40% (w/v) sucrose, bromophenol blue, xylene cyanol) was added to the DNA sample before loading in the gel and electrophoresed at 70 mA for 60 minutes or until deemed necessary, using a PowerPac 300 (BioRad). DNA was detected using a ultra-violet (UV) irradiation in a GelDoc (BioRad) and, if excision of specific bands was necessary, a clean scalpel blade was used to cut the DNA-embedded gel slice under low power UV light. DNA was extracted and purified from agarose using a Gel Extraction Kit (Qiagen) according to the manufacturer's instructions.

DNA digestion by restriction enzymes

Enzymatic cleavage of DNA at defined restriction sites was made by incubating purified DNA samples with the appropriate restriction enzymes (NEB), usually at 10 U/μl, in a reaction mixture as follows:

	Company	Conc.	Volume / μl
Digestion Buffer	NEB	10 x	10.0
BSA	NEB	100 x	1.0
DNA sample	-	-	50.0
Restriction Enzyme(s)	Sigma-Aldrich	10 U/μl	5.0
ddH_2O			34.0

If two restriction enzymes were needed to be used simultaneously, 2.5 μl of each enzyme was used to ensure glycerol concentration of the reaction mixture was kept at a minimum in order to avoid any possible interference with enzyme activity. If no compatible buffer could be used for simultaneous digestion with both enzymes, the digestion was performed sequentially. To purify DNA between each digestion a PCR Purification Kit (Qiagen) was used. Samples were digested at appropriate temperature for at least 60 minutes.

Alkaline phosphatase treatment of vectors

In preparation for ligating inserts, digested vector DNA was subjected to alkaline phosphatase treatment to remove the 5' phosphatase groups in order to minimize vector self-ligation and increase overall ligase reaction efficiency. Following the digest reaction the following mixture was prepared:

	Company	Conc.	Volume / µl
Phosphatase Buffer	Roche	10 x	20.0
Digested DNA	-	-	100.0
Alkaline Phosphatase	Roche	10 U/µl	1.0
ddH_2O		-	79.0

After digestion and phosphatase treatments, plasmid DNA was resolved on appropriate agarose gel (usually 1%) to access efficiency of digestion and remove any possible contamination from uncut vector in subsequent cloning steps.

Insert ligation into vectors

Digested PCR or DNA products were cloned into the desired plasmid using the following reaction mix:

	Company	Conc.	Volume / µl
T4 Ligase Buffer	NEB	10 x	2.0
Insert DNA	-	Various	10.0
Vector DNA	-	100 ng	5.0
T4 DNA Ligase	NEB	400 U/µl	1.0
ddH_2O		-	2.0

To control for complete plasmid digestion, ligations without the insert of the T4 DNA ligase were also made. Cohesive and occasionally blunt-ended ligations were incubated at room temperature overnight.

Transformation of competent bacterial cells

Transformation of ligation products and supercoiled purified plasmids into bacterial cells was made using competent cells. One ml of an overnight culture of

E.coli grown at 37°C was used to inoculate 30ml Luria-Bertani (LB) Broth in a 75cm^2 sterile tissue culture flask and incubated at 37°C with orbital shaking at 200rpm until the optical density at 600nm was found to be 0.3-0.6. The bacterial cells were then centrifuged at 2000*g* for 13 minutes and the pellet resuspended in ice-cold 2.5ml TSS buffer, prepared as follows:

	Company	Conc.	Volume / µl
DMSO	Sigma-Aldrich	100%	5.0 ml
Polyethylene Glycol 600	Sigma-Aldrich	-	10.0 g
$MgCl_2$	Sigma-Aldrich	1 M	5.0 ml
LB Broth	Sigma-Aldrich	-	90.0 ml

For transformation, 10µ or 10ng of supercoiled DNA plasmids was added to 100µl of competent cells. Cells were then incubated on ice for 15 minutes. Cells were heatshocked at 37°C for 4 minutes and 30 seconds before putting the aliquots back on ice for 30 seconds. 400µl of LB Broth 400 was added to the bacteria cells before incubating at 37°C for 1 hour.

Agar was made using LB agar tablets (Sigma-Aldrich) and autoclaved. Antibiotics at the appropriate concentration were added to the agar while still molten and poured in 90mm petri dishes (Sterilin) and allowed to cool, set and dry. The transformed bacteria (300-400µl) were pipetted onto the plates and spread using an ethanol-sterilized glass spreader. Agar plates were then incubated overnight at 37°C and colonies were later checked for correct insert and orientation where necessary by colony PCR.

Vector preparation

To prepare enough quantities of plasmid DNA suitable for sequencing and downstream applications, DNA was extracted from overnight transformed bacterial cultures of 5-10ml, grown at 37°C with appropriate antibiotics. PureLink™ HiPure Miniprep kit (Invitrogen) was used according to manufacturers' instructions. For larger stocks of plasmid DNA, Qiafilter™ Midi kits (Qiagen) were used with 100ml of bacterial cell culture. Following DNA purification *via* alkaline lysis of bacterial cell and adsorption of plasmid DNA onto

silica in the presence of low salt and extensive washed prior to elution under high salt conditions, plasmid DNA was precipitated with propan-2-ol (Sigma) and washed with 70% ethanol (Sigma) in order to remove excess salt from preparation. All DNA pellets were resuspended to an appropriate concentration with TE buffer (10mM Tris-HCL, 1mM EDTA, pH 8.0). DNA concentration was determined spectrophotometrically at 260nm and purity was accessed by ensuring the 260nm/280nm ratio was >1.8.

DNA sequencing and analysis

DNA sequencing was performed by the dideoxy termination method in house (WIMM) or at the Biochemistry Department Sequencing Facility (University of Oxford). To confirm sequence identity and integrity, automatically called base pairs from sequencing traces were analysed with the online software available at:
(1) http://www.ncbi.nlm.nih.gov/projects/gorf/
(2) http://blast.ncbi.nlm.nih.gov/Blast.cgi?PAGE_TYPE=BlastSearch&PROG_DED=blastn&BLAST_PROG_DEF=megaBlast&BLAST_SPEC=blas2seq

Glycerol stocks of transformed bacteria

To store transformed bacteria with the desired plasmid DNA vector, 100µl 80% (v/v) filter-sterilised glycerol was added to 500µl of an overnight bacterial culture and frozen at -80°C. To grow bacteria from glycerol stocks, a small portion of the frozen bacteria culture was removed with a pipette tip that was used to inoculate 5ml LB Broth with the appropriate selective antibiotic at an appropriate concentration. Bacterial culture was then incubated overnight at 37°C with orbital shaking at 200rpm.

2.2 Cell culture

2.2.1 General techniques

Work with eukaryotic cells was performed in HEPA-filter microbiology safety cabinets in order to maintain sterility. Cells were grown in 37°C incubators with 5% CO2.

Freezing and thawing of cells

To freeze cells for long-term storage, 6-10x10^5 cells in growth phase were harvested, centrifuged at 1300rpm for 3 minutes and resuspended in 1ml of freezing solution (10% (v/v) dimethyl sulfoxide in foetal calf serum). Cells were transferred to a cryovial (Nunc) and placed in a -80°C freezer in a suitable freezer chamber to allow gradual decrease in temperature necessary to ensure adequate cell viability on thawing. Cells were thawed by immersing the cryovials in at 37°C water bath and then diluted in 30ml of pre-warmed appropriate medium. Cells were centrifuged at 1300rpm for 3 minutes and resuspended in fresh growth medium. Cell viability was monitored assessed microscopically every 24 hours.

Cell counting

Cell density and viability of growing cultures was made by mixing equal volumes of trypan blue and cells. To count cells, the mixture was placed in a haemocytometer and examined by light microscopy. Trypan blue staining gives a measure of the number of cells with compromised cell membranes thus allowing quantification of cell viability.

Subculturing of cells

For suspension cells, such as Jurkat T-cells and all the cell lines derived from them, cell density was measured and used to determine adequate dilution. Cells were kept between 1-9x10^5/ml and growing in RPMI-1640 (Gibco), 10% (v/v) Foetal Calf serum (Gibco), 10mM Hepes (Sigma), 1mM Sodium Pyruvate (Gibco) and antibiotics (Pen/Strep/Neo; Sigma).

For the adherent HEK-293T cell line medium was removed and cells were washed in sterile cold phosphate-buffered saline (PBS) solution. Five ml of trypsin diluted in PBS was added to the cell flask and returned to the incubator for 5 minutes. Gentle shaking caused all cells to detach completely. Trypsin activity was inactivated by adding equal volume of fresh medium. The cell suspension was harvested, centrifuged at 1300rpm for 3 min and resuspended in the appropriate volume. Cells density was counted and used to determine the appropriate volume of cell suspension to add to a new flask to maintain cell growth. For HEK-293Ts a medium composed by DMEM (Sigma), 10% (v/v) of Foetal calf serum (Gibco), Glutamine (Sigma) and antibiotics (Pen/Strep; Sigma) was used.

Plating of cells for production of lentivirus or transient transfection

To plate out adherent cells for transfection in 6-well (Nunc) or 10cm plates, cells were detached from flask and resuspended in medium as described above. After counting cells an appropriate density was prepared and added to desired plates. These were then left in the incubator overnight to allow re-adhesion. Cells were plated at a density that would lead to a 60-80% confluence on the day of transfection.

2.3 Phenotypic analysis

2.3.1 Fluorescently-activated cell sorting and analysis

To quantify cell surface expression fluorescently-activated cell analysis (FACS) was used. A 5-10x10^5 aliquot of sample cells was harvested and centrifuged at 1300rpm for 3 minutes in appropriate polypropylene tubes. Pellet was resuspended in 100µl ice-cold FACS buffer (2% FCS, 0.05% azide in PBS). To specifically label cell surface proteins specific antibodies were used. Antibodies could either be directly conjugated to fluorochromes or indirectly by secondary reagents, which included antibodies or streptavidin. Antibodies targeting cell surface proteins were incubated with the resuspended cells at a working concentration of 10µg/ml unless otherwise indicated by the manufacturers'

protocol. Whenever the cells expressed GFP or a variant of GFP, either directly attached to the protein of interest of on the cytoplasm, appropriate choice of the fluorochrome was required in order to ensure minimal overlap of fluorescence between the two molecules. After surface labelling cells were washed twice with 4 ml FACS buffer and resuspended to either 500µl for FACS analysis or to 100µl for incubation with secondary fluorescently-labelled reagent when this was required. After the second incubation cells were washed as before. Cells were maintained on ice at all times and upon labelling with fluorescently-labelled proteins were kept in the dark. The labelled cells were analysed on a Cyan ADP® (Dako) FACS cytometer using the appropriate lases. Viable cells were gated based on forward and side scatter and fluorescence emission was collected after compensating channels when necessary using singly-labelled controls.

2.3.2 Confocal microscopy

Cellular localisation of fluorophore-tagged proteins was made by confocal microscopy. Cells were attached to coverslips and excited with the appropriate laser line, usually 488nm, and examined using a BioRad Radiance 2000 confocal microscope under an oil immersed 60x objective with light filtered in the green channel from 515±15nm. Fluorescence images were collected at the midpoint of the cell and minimally manipulated, at the time of acquisition, to optimise and adjust signal:noise ratio.

2.4 Protein analysis

Polyacrylamide gel separation and Western blotting

Proteins were separated by 10-12% SDS-PAGE as deemed appropriate under reducing or non-reducing conditions and then transferred to Hybond-C-extra membranes by electroblotting with ice-cold transfer buffer. Membranes were blocked in TBS, 0.1% (v/v) Tween 20 (TBS-T), containing 5% (w/v) BSA (Sigma), probed with unconjugated primary antibody for 1 hour and revealed with HRP-conjugated goat anti-mouse or goat anti-rabbit IgG (both from Sigma), or strep-HRP (Cell signalling) at appropriate dilutions. Membranes were washed

thoroughly with TBS-Tween, with or without 0.005% SDS. For some incubations, primary antibody was left in falcons rotating overnight at 4°C. Immunoblots were developed using ECL or ECL– plus (Amersham Biosciences) and exposed to CL-XPosure films (Pierce).

Chapter 3

Valency of the TCR complex at the cell membrane[1]

3.1 Introduction

3.1.1 Current understanding of the TCR complex valency at the cell membrane

It is now well accepted that the TCR is composed of disulphide-linked TCRα and β chains, which are associated with CD3δ, γ and ζ subunits, but a question still remains concerning what is the TCR valency at the cell surface of a resting T-cell [53, 63]. Understanding both the stoichiometry and the valency of the TCR is challenging due to the intrinsic complexity of this receptor and to the general technical limitations that exist to study, in a native form, complexes present at the cell membrane. The apparent imbalance between the charged transmembrane domains of the TCR [48, 50] prompted the idea that dimerization, or oligomerization, between non-covalent pairing of the αβ heterodimers was required. Results arising from immunoprecipitation [192, 208, 243] and fractionation studies [244] suggested that this could indeed be the case. These results, however, proved to be highly dependent on the detergents used for TCR extraction and solubilization from the cell membrane [49, 208, 245]. *In situ* fluorescence resonance energy transfer studies made so far have relied on bivalent antibodies to label the TCR complex and determine its valency [246].

[1] The work described in this chapter was done in collaboration with Paul Dunne and James T. McColl of the Klenerman Group, Dept. Chemistry, Cambridge University. This study has been published in [209]

3.1.2 Current tools available to probe the oligomerization state of proteins at the cell surface

It becomes clear from the detergent solubilization studies that an approach able to probe TCR complex valency, *in situ*, at the cell membrane, with minimal perturbation, would be the preferred method of choice. Transmission electron microscopy has been used to image gold-labelled, bivalent, antibodies targeting receptors present in fixed cell membrane "sheets", including the TCR [247-249]. However, there is now evidence that fixation protocols do not impede protein movement and can thus lead to artefactual protein behaviour [250].

A different approach takes advantage of recent developments in cell imaging, like TIRF microscopy, to track single molecules on the cell membrane of live cells [251]. To probe the oligomerization state of proteins at the cell surface, single-colour fluorophores, directly attached to the receptor or to a receptor-specific Fab, can be tracked and the amount of fluorescence quantified [252, 253]. A natural extension of this approach is the dual-colour imaging of individual molecules to identify proteins that can form transient or constitutively-associated oligomers [254]. In the work described here, this approach has now been extended to include a quantification of the extent of association. Previously, the Klenerman Group, University of Cambridge, in collaboration with the T-cell biology Group had also developed the Two Colour Coincidence Detection (TCCD) method, in which two overlapped confocal beams independently excited single diffusing membrane proteins labelled with a specific red- or blue-tagged antibody fragment [142]. Association was quantified by calculating the number of coincident fluorescence events that occurred above the level expected by chance. Here, the method described extends the TCCD concept by allowing a time course analysis of protein diffusion. Dynamic Single-Molecule Colocalization, or DySCo, thus relies on detection and quantitative video analysis of two distinct fluorophores diffusing at the cell surface using TIRF microscopy, and has now been applied to the TCR complex to probe its valency at the cell membrane.

3.2 Materials and methods

3.2.1 Preparation of proteins and cell lines for imaging

Constructs

The sequences of all genes were amplified using PCR from cDNA, IMAGE sequences or previously cloned vectors. For CD28, CD86 and TCRβ the stop codons were mutated for an appropriate restriction enzyme and the genes then inserted, in frame at the N-terminus of three in frame copies of (3x) Citrine or 3x mCherry proteins. All genes were sequenced to confirm both the reading frame and integrity. The SFFV promoter on the pHR lentiviral vector (kindly provided by Yasuhiro Ikeda, Mary Collins laboratory, UCL) was changed to an ecdysone-inducible promoter, producing the pHR Inducible vector, pHRI. In the absence of ecdysone or any other analogue the genes encoded by the pHRI vector are transcribed at low levels.

Cell culture and lentivirus infections

Lentivirus infections were used to generate stably transfected cell lines expressing the desired genes. HEK-293T cells, grown in DMEM supplemented with 10% FCS, 1% HEPES buffer, 1% sodium pyruvate and 1% antibiotics, were plated in six well plates, $6x10^5$ cells/plate (all reagents from Sigma Aldrich, Dorset, UK). After 24 hours cells were transfected with equal amounts of pHRI vector (encoding the gene of interest), p8.91 and pMDG (kindly provided by Yasuhiro Ikeda, Mary Collins lab, UCL) using Genejuice (Novagen Merck, Hull, UK) [255]. 48 hours later the supernatant from two six well plates was removed and added to $1x10^6$ Jurkat (for CD86) or J.RT3 cells (for CD28 and TCRβ since these are $CD28^-$ and $TCR\beta^-$). These cells were grown in phenol red free RPMI supplemented with 10% FCS, 1% HEPES buffer, 1% sodium pyruvate and 1% antibiotics. Cells were analysed using FACS after 5 days of lentiviral infection to confirm expression of the desired proteins.

Latrunculin treatment of cells

Latrunculin B (Biomol International, Exeter, UK) was dissolved in dimethyl sulfoxide (DMSO from Alfa Aesar, Heysham, UK) to a concentration of 2.5 mM. Cells were incubated at 37°C in supplemented RPMI media containing 2.5 μM latrunculin B for 20 minutes to disrupt actin formation. Following re-suspension in phosphate buffered saline (PBS- 150 mM NaCl, 10 mM $HNaPO_4$ (Sigma Aldrich Dorset, UK) in ultrapure water (MilliQ 18.2 MΩ, pH 7.2) the cells were imaged using the same protocol as for untreated cells.

Sample preparation for microscopy

Microscope coverslips were cleaned for 1 hour in Piranha solution (3:1 sulfuric acid:hydrogen peroxide) and thoroughly rinsed with ultrapure water (MilliQ 18.2 MΩ) before incubating with 100 μl of 20 μg/ml donkey anti-mouse, non-specific IgG antibody (Jackson Immunoresearch Europe, UK) at 37°C for 1 hour. Cells were centrifuged at 600*g* for 2 minutes and the supernatant removed, before resuspending in 37°C phosphate buffered saline (PBS) solution for imaging (150 mM NaCl, 10 mM $HNaPO_4$ in ultrapure water). Slides were rinsed again to remove non-adsorbed antibody and transferred to a heated microscope stage. Cells were added and allowed to settle for 5 minutes and imaged within the subsequent 15 minutes.

3.2.2 Dynamic Single-Molecule Colocalization

TIRFM experimental setup

Imaging was performed using total internal reflection fluorescence microscopy (TIRFM), restricting detectable fluorescence signal to within ~100 nm from the sample slide [256]. Briefly, the output from a dual line Kr/Ar laser operating at 488 and 568 nm (353-LDL-840-240, Melles Griot) was directed down the edge of a 1.45 NA TIRF objective (60x Plan Apo TIRF, NA 1.45, Nikon) mounted on a Nikon TE2000-U microscope. Fluorescence collected by the same objective was separated from the returning TIR beam by a dichroic (490575DBDR, Omega

Optical), split into yellow and red components (585 DXLR, Omega Optical) and filtered using Dual-View™ (Optical Insights) mounted filters. The images were simultaneously recorded on an EMCCD (Cascade II: 512 Princeton instruments,) whereby the EMCCD was split so that each colour was recorded on one half of the EMCCD, operating at minus 70°C. Data were acquired at 17.8 frames s^{-1} using IPlab 4.0.2 software.

The blue beam was attenuated by 64 % using filters (Comar, Cambridge, UK). The laser power used for taking measurements being 1.2 mW for the 568 channel and 0.35 mW for the 488 channel (as measured by epifluorescence at the sample plane) over an area of ~45 μm diameter. Images were taken for 30 frames and data only captured during the first 20 minutes after cells began to attach to the surface.

To achieve good image registration, a grid consisting of regularly spaced ion-beam etched holes in gold-on-glass was utilised. Dual-View™ optics were adjusted so as to maximize the overlap between red and green images of the grid under white-light illumination, resulting in measured image registrations in the range of ~75 nm.

3.2.3 Data acquisition and analysis

Bayesian tracking approach

Tracking was carried out using custom software implemented in MATLAB (The MathWorks, Natick, MA). The Bayesian based algorithm is an extension of work by Oh *et al.* [257] and similar to the published Bayesian method [258].

After detecting centroid positions of potential targets above a user defined threshold [259] (five standard deviations above the image mean pixel count for this work), the program links spots using a Markov Chain Monte Carlo (MCMC) algorithm programmed within a Bayesian framework (for details of Bayesian formulation see Yoon *et al.* [258]). Detected spots are initially linked at random over the entire image sequence and this configuration is assigned a possible

likelihood according to its statistical fit to Brownian behaviour. The program then iterates the configuration, with several possible outcomes at each iteration:

- Birth (new track is proposed)
- Death (track is removed)
- Split (track splits into smaller tracks)
- Merge (smaller tracks are merged)
- Update (track configuration is altered)
- Increase (track increases in length)
- Decrease (track decreases in length).

With increasing iterations the program approaches the most likely configuration, which may not always give the same result as those from traditional deterministic tracking (as found in the previously used algorithm [258]). Very few initial parameters are specified by the user - thus the contribution of error introduced by poor parameter initialization is minimized.

This method differs from other published methods [258] in two important ways that decrease the computational complexity significantly. In the initial implementation, particle detection was incorporated into the Bayesian framework, but for the analysis in this work we identify objects as peaks above a user defined threshold, using an established method [259]. This means that we did not need to consider every pixel in the image when it comes to the tracking step. The tracking for the previous implementation used a Sequential Monte Carlo (SMC) algorithm, with tracks being updated at each frame based on their previous history. That is to say, after the n^{th} frame is processed, the result is inputted into the calculation for the $(n+1)^{th}$ frame, and is not considered again. Tracking was carried out using a MCMC method, whereby the whole video sequence is considered for each iteration.

MSD calculation and positional accuracy

We performed mean-square displacement (MSD) calculations on the data and fitted the first three points of the MSD curve to a linear equation,

$$MSD = 4Dt + A_0 \qquad (1)$$

where D is the diffusion coefficient. The median and upper and lower quartiles are chosen to represent the overall distribution of D and A_0 for this work as the diffusion coefficients and A_0 have skewed distributions.

To estimate the inherent uncertainty, σ, in the assignment of particle positions, we use [260],

$$A_0 = 2\sigma^2 . \qquad (2)$$

The mean positional accuracy across the six different datasets was found to be 67.3 ± 5.4 nm for the yellow channel, and 75.8 ± 3.2 nm for the red.

Colocalization distance criterion

The colocalization criterion was obtained from the root mean-square (RMS) deviations in the positional accuracies for yellow and red molecules using,

$$\sigma_t = (\sigma x^2 + \sigma y^2)^{1/2} \qquad (3)$$

Using equation 3 with the positional accuracies calculated above gives a value of 101.4 nm. Hence, iin order to obtain a 90% probability of colocalization the distance threshold is $1.65\sigma_t$, corresponding to 167.3 nm. Adding the image registration and distance threshold values, gives a colocalization distance value of 242.3 nm. For this work the colocalization distance of 300 nm was chosen to minimise the chance of missing associated molecules.

Calculation of degree of association (% coincidence)

After tracks were identified, we examined association by applying a nearest-neighbour distance approach [254, 261]. Distances between red and yellow tracks were calculated for each video frame, and a track was determined to be associated if it remained within the 300 nm colocalization distance for 3 or more frames. The overall coincidence is taken to be

$$\%Coincidence = 100 \times \frac{number\ of\ colocalized\ tracks\ in\ red\ channel}{total\ number\ of\ tracks\ in\ red\ channel} \quad (4)$$

with the red channel chosen due to the lower detection efficiency of events. The coincidence is calculated for each video and the overall coincidence for an experiment is taken as the mean across individual files. To examine the contribution of chance coincidence, the colocalization analysis was repeated for all combinations of non-coupled red and yellow file pairs.

3.3 Results

3.3.1 Setup of the DySCo microscope

Dynamic single-molecule colocalization (DySCo) relies on the simultaneous excitation and single-molecule tracking of two different fluorophores fused to the molecules of interest diffusing on the basal surface of the cell. To excite the fluorophores two overlapped 488 and 568nm laser beams in total internal reflection (TIRF) geometry were used (Fig. 3.1a). The output from the dual laser was directed down to a single objective and split into yellow and red components which were separately recorded by an Electron Multiplying CCD camera. Detection of single-molecules was made possible by combining TIRF microscopy, which dramatically reduces the background fluorescence of cells by restricting detectable fluorescence signal to within ~100 nm from the sample slide, with a low expression of the molecules of interest in order to allow identification of single molecules. By tracking single-molecules diffusing at the cell surface it was expected to be possible to distinguish a protein-protein dimer, which in theory will show correlated motion over time, from a monomeric protein behaviour of proteins that may track together by chance over a short period of time but which eventually dissociate (Figure 3.1b).

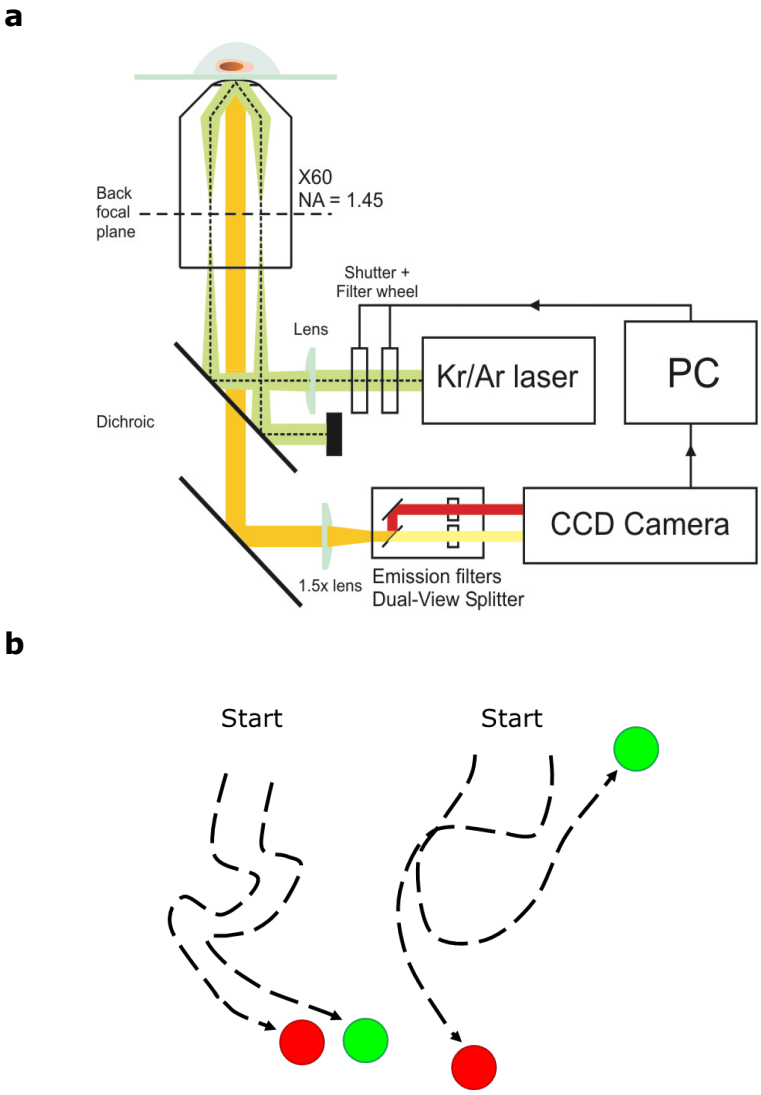

Figure 3.2: Dynamic single-molecule colocalization setup. **(a)** Single proteins are tracked after simultaneously exciting cells with overlapped 488 and 568 nm laser beams. TIRF microscopy penetrates up to a depth of 100 nm on the cell surface contacting with glass. **(b)** Principle of DySCo method. Tracking protein diffusion during multiple frames increases probability to correctly distinguish dimers, which are associated for long periods, from monomers, which are transiently and randomly associated over shorter periods of time.

3.2.2 Establishing cell lines expressing the proteins for single-molecule imaging

Two fluorescent proteins, designed by the Roger Tsien Lab, Citrine and mCherry, monomeric YFP and RFP variants respectively, were fused to the C-terminus of CD28, a covalent dimer, and CD86, a monomer [143, 262], and TCRβ. Preliminary results showed that the signal-to-noise ratio was very low making it almost impossible to detect single-molecules. It was therefore decided to fuse three copies of Citrine or mCherry (3xFP) to the proteins under analysis (Fig. 3.2). To achieve low protein expression the pHR-SIN vector was modified by replacing the SFFV promoter with a E/GRE promoter, named pHRI plasmid [263]. The E/GRE promoter relies on co-expression of the transcription factors RXR and VgEcR together with ponasterone in the cell line of interest to achieve high levels of protein expression. In the absence of these transcription factors, protein expression levels were found to be low and therefore suitable for the DySCo analysis. The cytoplasmic domain of the three proteins was not included in the final constructs and the three tandem copies of the fluorescent proteins were therefore attached immediately after the transmembrane domain of CD86, CD28 and TCRβ. The cytoplasmic domains were not included in order to avoid as much as possible the interference of actin in protein diffusion. Protein expression of the chimeric proteins was confirmed by FACS (Fig. 3.2) and confocal microscopy (Fig. 3.3) in J.RT3 cells stably expressing these proteins after lentiviral infection with the appropriate plasmids. Quantitative FACS analysis revealed that the pHRI plasmid induced around 1,500-2,500 proteins per cell for the three chimeric proteins (Fig. 3.4). The expression of TCRβ-3xFP is thus 5-7 fold lower than that found on wild-type Jurkat cells (Fig. 3.4).

3.3.3 The TCRβ-3xFP can be triggered in T-cells

Before proceeding with the single-molecule analysis it was necessary to determine if the chimeric protein TCRβ-3xFP was able to trigger T-cell activation as the wild type form of TCRβ does. TCR complex expression was stably reconstituted in

J.RT3 cells, which lack the TCRβ chain, with TCRβ-3xFP expressed at either low level, using the E/GRE promoter, or at the wild-type level, using the SFFV promoter. Cells were also infected with lentivirus carrying a reporter plasmid which drives the expression of *Renilla Luciferase* under the control of three copies of the IL-2/NF-AT promoter. A quantification of *Renilla Luciferase* activity was later used to measure T-cell activation. J.RT3 TCRβ-3xFP cells were stimulated with plate-bound anti-CD3ε antibody (OKT3) or a control antibody, anti-rat Thy1 (OX7), for six hours. Addition of the 3xFP to the C-terminus of TCRβ protein allowed normal T-cell activation, as the IL-2/NF-AT promoter activity was found to be similar between J.RT3 cells expressing wild-type TCRβ or TCRβ-3xFP, following treatment of the cells with OKT3 antibody (Fig. 3.3).

3.3.4 Two colour single-molecules can be simultaneously observed at the cell surface of live cells

In the setting described here the signal-to-noise ratio was a major limiting factor which, coupled with ordinary fluorophore blinking and photobleaching, made it difficult to distinguish single-molecules from random fluorescent particles. However, the combined usage of TIRF microscopy and the coupling of three fluorescent proteins to the proteins under analysis, together with the low surface expression levels, achieved the required signal-to-noise ratio in order to use an optimized Bayesian-based tracking algorithm to identify single-molecules. The algorithm used relies on spatial and temporal information present in individual frames to identify single-molecules [258]. With this approach, single-molecules could be detected diffusing at the cell surface of live cells (Fig. 3.6).

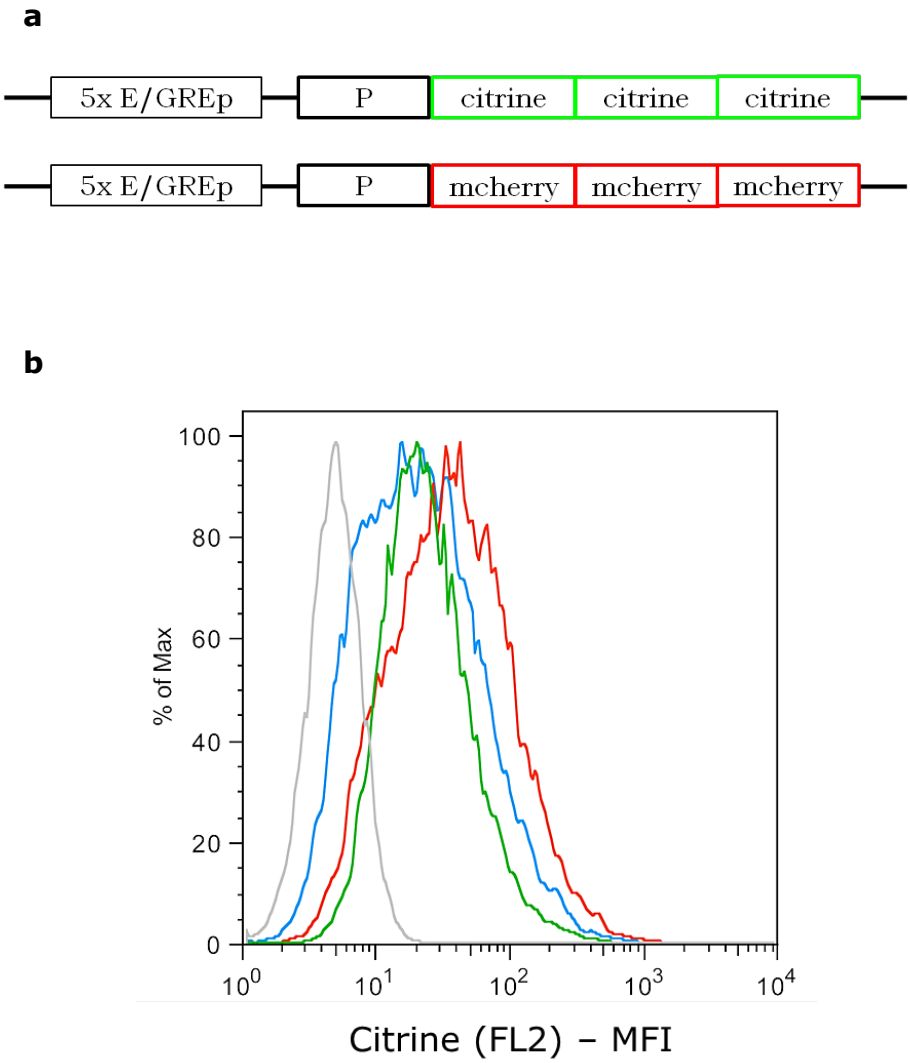

Figure 3.2: In order to increase signal-to-noise ratio, **(a)** three copies of Citrine or mCherry were fused to the C-terminus of the proteins under analysis and cloned into pHRI plasmid. **(b)** Lentiviral mediated delivery of the pHRI plasmid was used to drive expression of CD28-3xFP (red), CD86-3xFP (blue) and TCRβ-3xFP (green). Expression of these proteins was confirmed by FACS using emission from the 3xFP as readout.

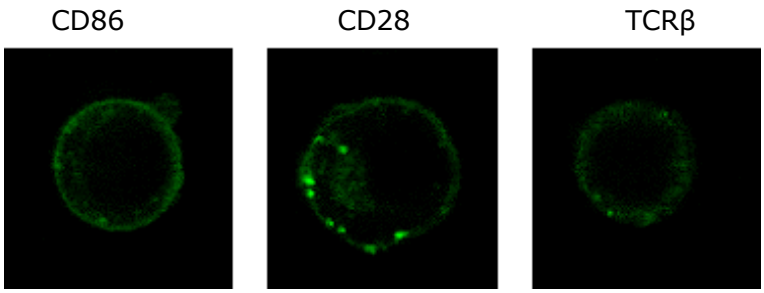

Figure 3.3: Expression of the chimeric proteins at the cell surface fused to 3xFP was detected by confocal microscopy. Proteins were mainly found at the cell membrane.

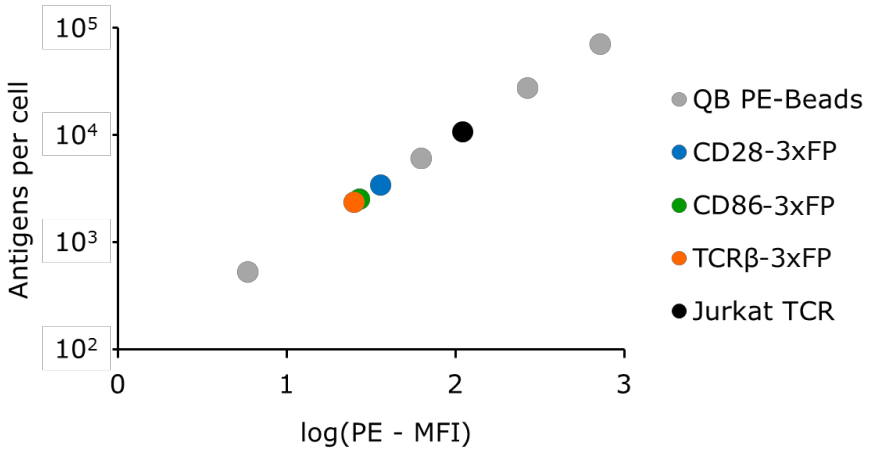

Figure 3.4: Quantitative FACS analysis of cells expressing CD28, CD86 or TCRβ -3xFP. QuantiBrite-PE beads, with known amount of Phycoerythrin (PE) labels per bead were used to calibrate the relative fluorescence intensity from antibody-labelled PE, directed against target proteins, to the number of binding sites per cell. Cells expressed between 1500 to 2500 cell surface receptors for each of the three proteins under analysis.

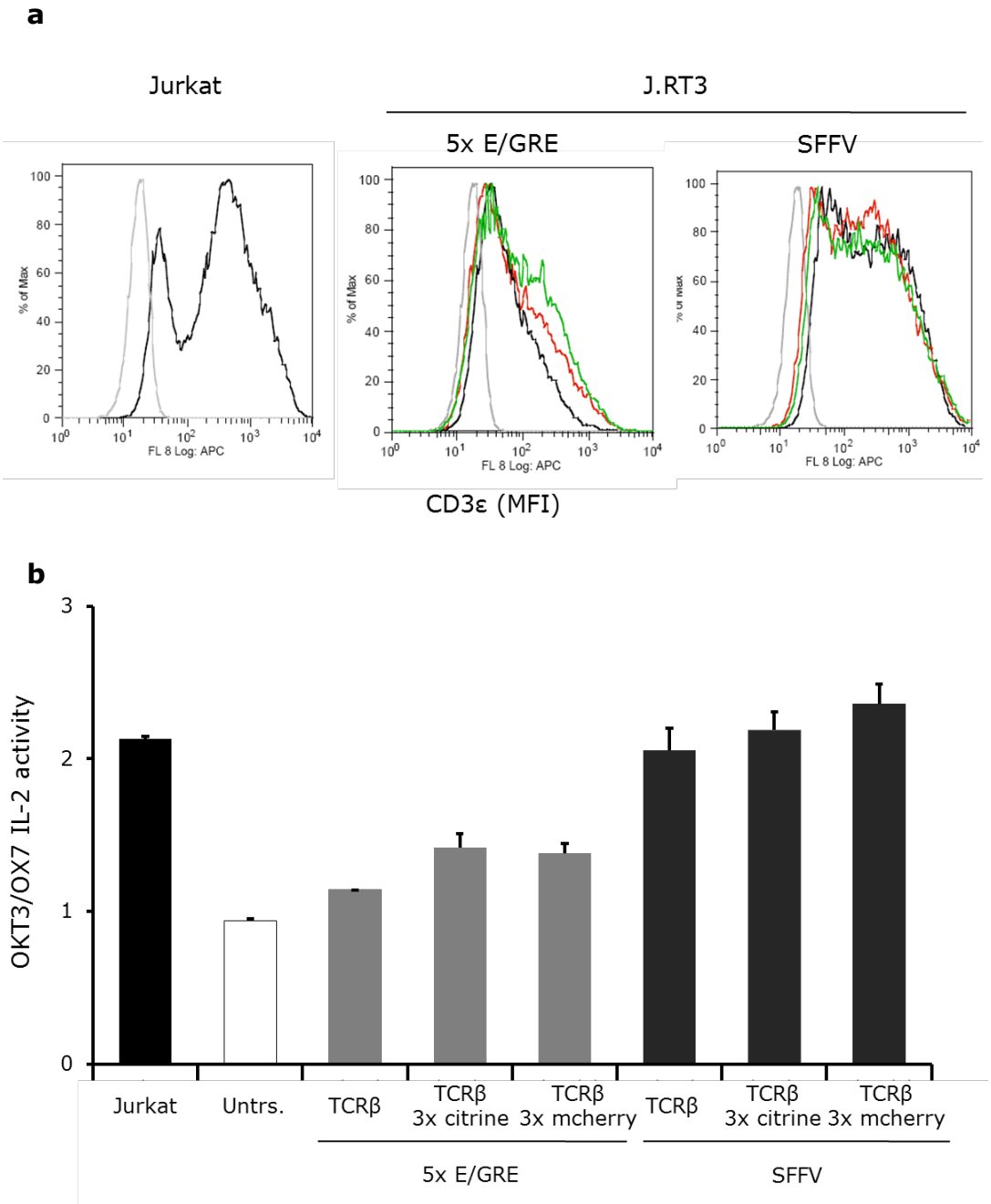

Figure 3.5: Fluorescently labelled TCRβ is functional. **(a)** Surface expression levels of TCR in J.RT3 cells (negative for TCR expression; grey line) were quantified by FACS. Expression of wild type (black line) or fluorescently labelled TCRβ under control of SFFV promoter (right panel; mCherry, red line; Citrine, green line) is comparable to native TCR surface expression in Jurkats (left panel, black line). Expressing TCRβ under E/GRE promoter (middle panel) significantly reduces surface expression. Wild-type (black line) or fluorescently labelled TCRβ are expressed at similar levels. **(b)** T-cell activation with OKT3 correlates with TCR surface expression. Fluorescently labelled TCRβ activates cells to similar levels as wild-type. Mean of triplicates with ± SE are shown.

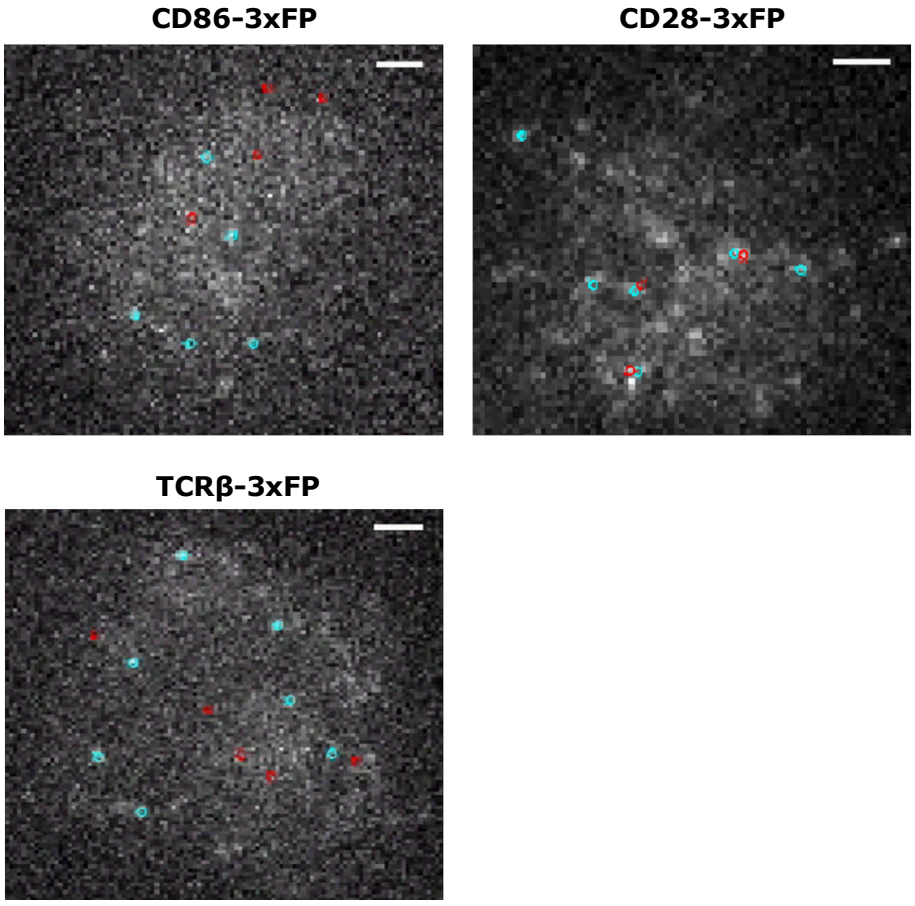

Figure 3.6: Detection of single-molecules at the cell surface of live cells. Proteins of interest labelled with three copies of Citrine or mCherry could be detected at single-molecule level diffusing at the cell surface of Jurkat T-cells. The first frame images for CD28-3xFP are shown. The background fluorescence, however, perturbs direct single molecule identification. An optimized Bayesian-based tracking algorithm was used to identify single-molecules. Blue (Citrine) and red (mCherry) circles identify location of single-molecules.

3.3.5 Analysis of protein diffusion at the cell surface

Before attempting to determine the degree of association for the molecules under study, CD28, CD86 and the TCR, it was important to determine if the three tandem fluorescent proteins were changing the normal diffusion behaviour of the proteins under analysis. To probe this, fluorescently labelled Fab fragments from antibodies directed against CD28TM, CD86TM and TCRβTM, expressed without FPs, were used to measure the diffusion coefficient of these proteins. The comparison between the diffusion coefficient of CD28TM, CD86TM and TCRβTM imaged through the fluorescently labelled Fab, with that from the same proteins expressed with 3x mCherry or Citrine, revealed that addition of the 3xFP did not alter the diffusion coefficients considerably (Fig. 3.7). In particular, for TCRβTM and TCRβTM-3xFP the diffusion coefficient was almost identical, and in good agreement with previous studies [264].

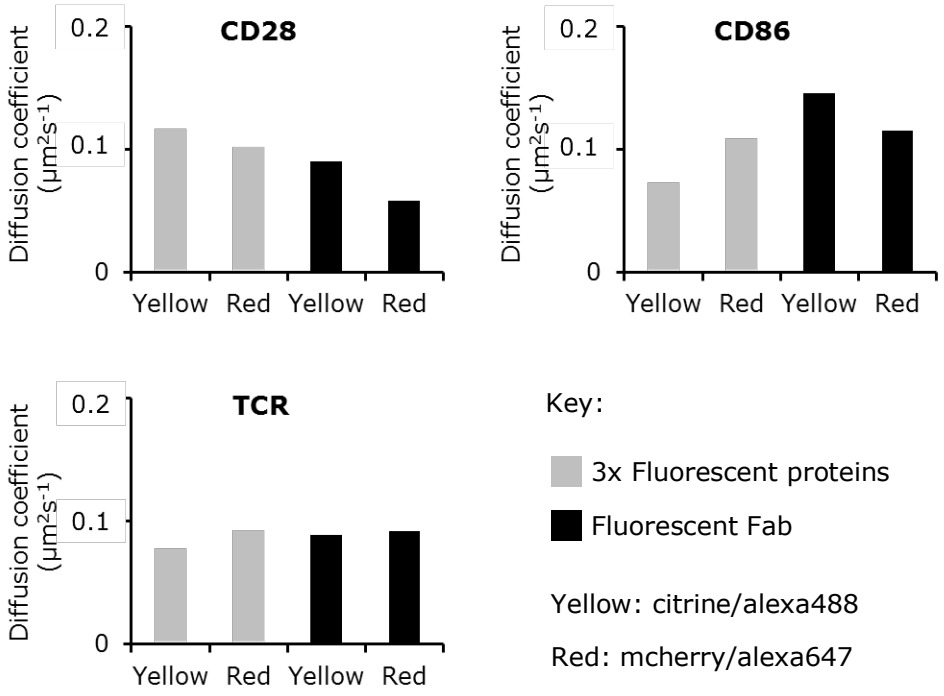

Figure 3.7: Addition of three fluorescent proteins to C-terminus of CD28, CD86 and TCRβ did not affected protein diffusion. Proteins were detected through the 3xmCherry or 3xCitrine present at the C-terminus or through fluorescently labelled, alexa488 or alexa647 Fabs targeting CD28, CD86 or TCRβ. In the latter case, protein expression was terminated after the transmembrane domain, and no fluorescent proteins were present.

3.3.6 Tracking single-molecules at the cell surface

To quantify the degree of association between proteins, the distances between red and yellow tracks were determined for each video frame, similar to the approach used by Lachmanovich *et al,* [261]. Tracks of Citrine- and mCherry-labelled proteins were defined as being associated when proteins remained within 300 nm for three consecutive frames, recorded at 17.8 frames s^{-1} (Fig. 3.8). The degree of association was determined by calculating the total number of coincident tracks, divided by the total number of tracks found, for a given colour, and expressing this value as a percentage. Measurements were made relative to the red tracks, since these were detected the least efficiently. The degree of association found for CD28, 22.7 ± 5.9%, was significantly higher than that found for CD86, 10.2 ± 3% (Fig. 3.9a). These values were thus used as a reference for the degree of association expected to be found for dimeric or monomeric proteins. After standardizing the assay with a dimeric and a monomeric protein the degree of association for the TCR complex was determined and found to be 4.8 ± 2.3%, significantly lower even than that obtained for CD86 (Fig. 3.9a). These results were not strongly dependent on the distance used to identify associated molecules, within 100-500 nm range (Fig. 3.9b). The degree of association due to random association of molecules expressed at a given cell surface density was also determined. This was made by shuffling the red and yellow videos relative to one another, and re-running the data analysis for non-matched file pairs. Random colocalization was determined to account for 0.6% of the degree of association, indicating that the values obtained for CD86 and the TCR cannot be solely explained by random interactions. It was thus hypothesized, based on previous reports [143, 265], that the cytoskeleton could be playing a role in confining diffusion of CD86 and TCR thereby causing an increase in the degree of association. This hypothesis was tested by repeating the quantification of the degree of association in cells treated with the actin depolymerizing agent, latrunculin. A significant reduction in the degree of association was observed for CD86 and TCR upon latrunculin treatment (Fig. 3.9a).

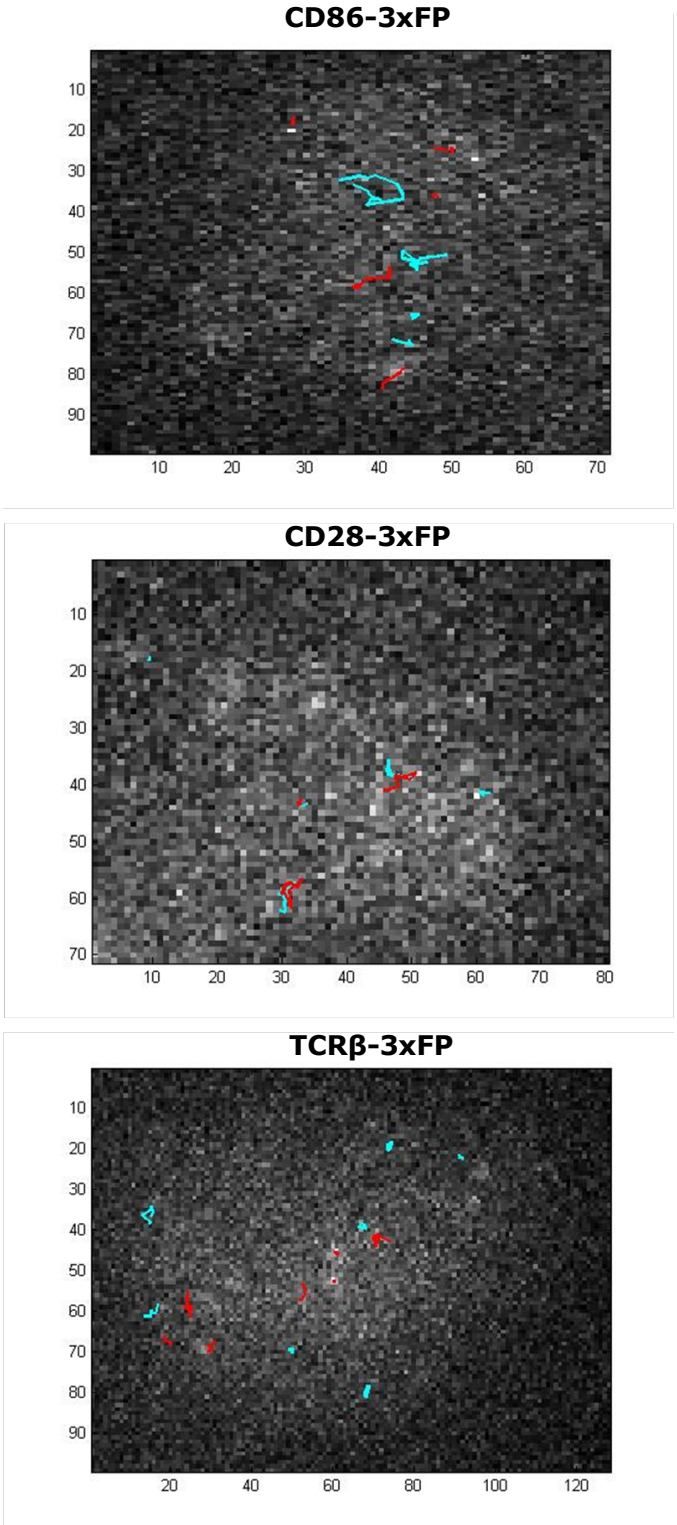

Figure 3.8: Tracking single-molecules at the cell surface of live cells. The trajectories of fluorescently labelled proteins identified using the described Bayesian-based tracking algorithm (see §3.3.4) is shown for each of the three proteins under analysis. Blue (Citrine) and red (mCherry) lines identify trajectories of single-molecules over the course of three consecutive frames, at 17.8 frames s^{-1}.

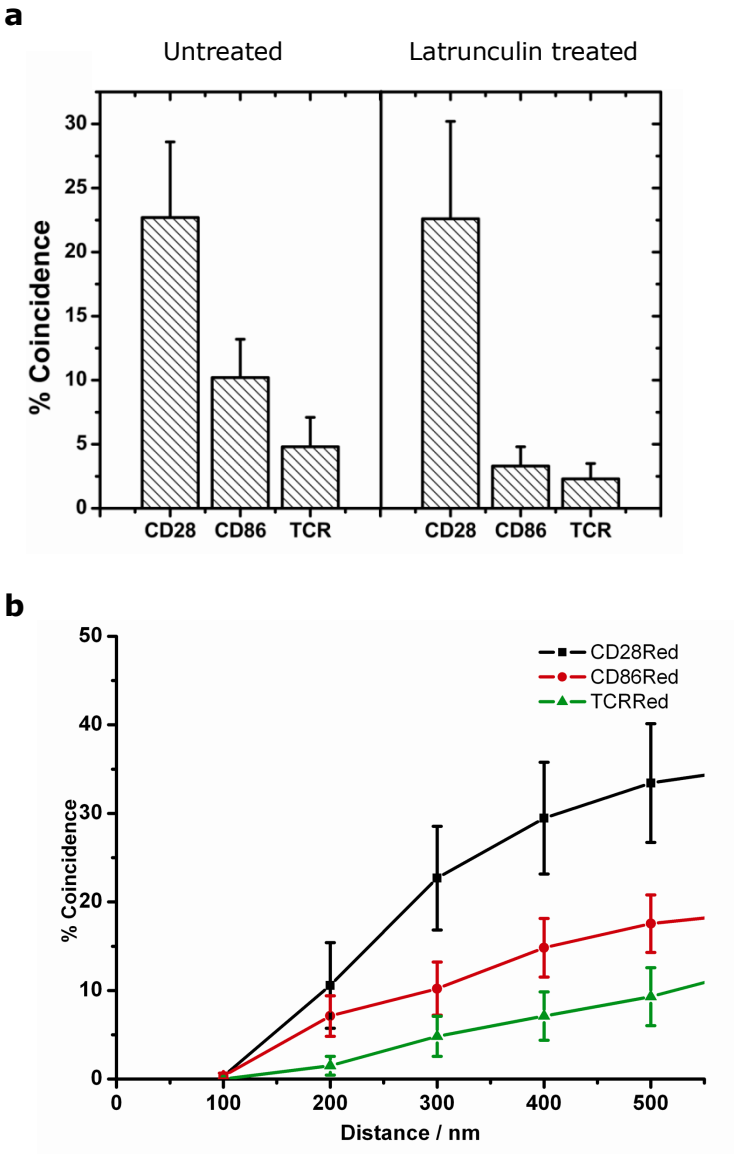

Figure 3.9: The TCR is present as a monovalent complex at the surface of T cells. **(a)** Coincidence levels quantified by DySCo allowed discrimination between dimeric (CD28) and monomeric (CD86) proteins. The TCR complex shows a lower coincidence value than CD86. Actin affects coincidence levels detected for monomeric proteins by possibly restricting protein diffusion, as implied by the effects of latrunculin. **(b)** The determined coincidence level changed according to the colocalization distance threshold but the overall behaviour was not dependent on the 300 nm limit used in the present analysis. Data points shown are mean ± SE.

3.4 Discussion

3.4.1 DySCo analysis identifies monomeric and dimeric proteins

Tracking single molecules at the surface of live cells with the approach described here allowed the stoichiometry of dimeric CD28 and monomeric CD86 to be distinguished. The theoretical degree of association for a dimeric protein would be 50%, however for CD28 the value obtained was considerably lower, 22.7 ± 5.9%. Calculation of the degree of association is dependent on the fluorophores used. Both the photophysics, *e.g.* photobleaching and photoblinking, and the slow fluorophore maturation rate of the FPs used in this assay limited the experimental maximum of the degree of association.

In the case of CD86, the degree of association of 10.2 ± 3% is significantly lower than what was obtained for CD28 but still higher than anticipated. In fact, a completely random association of proteins would lead to an estimated degree of association of 0.6% (taking into account the surface density of the molecules used in this analysis). This observation highlighted the importance of standardizing and validating the experimental method with known monomeric and dimeric control proteins. Comparing with the calculated degree of association for a randomly diffusing protein, if nothing was known about the valency of CD86, it could be argued that CD86 was forming protein-protein dimers at the cell surface, which is known not to be the case [143]. In agreement with previous results [264], it was found that the actin cytoskeleton is restricting diffusion of molecules at the cell surface and confining their movement thus causing an increase in the degree of association. This result, as suggested by others, also indicates that there is a non-random organization of the proteins present at the cell membrane [143, 160].

3.4.2 The TCR is a monovalent complex

The degree of association of the TCR complex was directly compared with that of CD28 and CD86. This direct comparison avoids the use of *in silico* simulations of what would be a random distribution of proteins at the cell surface, especially

when there is evidence indicating that the cell surface is not randomly organized, as we have just discussed. The TCR complex was found to have a degree of association of 4.8 ± 2.3 %, approximately 50% lower than that determined for CD86, thus indicating that in a resting T-cell the TCR receptor is a monovalent complex. As with CD86, depolymerization of actin led to a significant decrease in the degree of association of the TCR.

It is important to note that the TCR expression levels present in J.RT3 during the DySCo analysis were ~5 to 7-fold lower than what is found in Jurkat cells. This lower level of expression likely reduces the concentration of dynamically associated molecules. However, the degree of association obtained for the TCR was directly compared to that found for the CD86 and CD28 proteins, which were also expressed at the same surface density as that of the TCR. It can thus be reasoned that even if the low level of expression caused a reduction in weak TCR-TCR transient dimer interaction, the TCR is not an obligate dimer or oligomer. In fact, since the coincidence level for CD28 was 22.7% and that for the TCR expressed in latrunculin-treated cells was 2.3%, at most, only ~10% of the TCR is associated, a value lower than that found for the well-defined monomer CD86. Importantly, even at these low levels of expression and following its labelling with three fluorescent proteins, the TCR was functional as cells responded to anti-CD3ε stimulation. This observation is consistent with studies of mouse T-cells engineered to express ~1000 copies of the TCR per cell which, were found to respond to cognate pMHC with Ca^{2+} elevation and cytokine secretion, *in vivo* [266].

3.4.4 Advantages, caveats and future applications of the DySCo analysis

The ability to track two different fluorophores at the single-molecule level, over a period of time, allowing quantification of homo- and hetero-interactions, from constitutive dimers to much weaker and transient protein-protein interactions, is the key advantage of DySCo. Especially, considering that weak protein-protein interactions are likely to have important biological functions and underpin signal

transduction at the cell surface [267, 268]. Another advantage of single-particle tracking is that there is no need to correct the data for chance coincidence events, since the probability of two non-associated molecules diffusing within a short distance of one another for a number of frames is very low. In addition, immobile or slowly diffusing molecules that are unobservable using techniques such as TCCD can be detected by DySCo. It has also the potential to be a minimally perturbative approach, as it is not, for example, reliant on the prior crosslinking of molecules [269] and, like TCCD, it provides an opportunity to analyse natively expressed proteins tagged with labelled Fab fragments [142]. Finally, DySCo has been developed to detect very low levels of surface proteins, which, for example, could be useful to study weakly expressed membrane proteins, such as G-protein coupled receptors. This requirement for low levels of protein expression is, however, an important limitation of the DySCo technique. The problem of having a high fluorophore density in the sample under analysis is the difficulty that arises in determining the exact position of a centroid of the point spread function of the individual emitters present in close proximity beyond the diffraction limit (250 nm). Recently developed techniques, like PALM and STORM, use different approaches to overcome the problem created by high fluorophore density and can achieve super-high resolution (as low as 10 nm). These imaging techniques, however, cannot track diffusion of single-molecules over time [270-272] which makes DySCo a complementary approach to the current super-resolution techniques available.

Chapter 4

A relatively rigid TCR is capable of initiating signalling[2]

4.1 Introduction

4.1.1 The role of conformational changes during TCR triggering

Ligands of the TCR have been proposed to induce triggering *via* intra- or inter-subunit conformational rearrangements within the extracellular regions of TCR complexes [53, 213, 216-218, 243, 273, 274]. Comparison of the crystal structure of free, unligated, TCRαβ with the same complex bound to pMHC has not revealed any major conformational change [57, 77, 275], except in the CDR3 loop, which has an inherent flexibility to allow binding to the pMHC [276]. Recently, the crystal structure of a CD3ε-antibody complex for which the apo (*i.e.* unliganded) CD3ε structures are already known [55, 61] was determined and comparison of these structures indicates that no large-scale changes in CD3ε structure accompany mitogenic antibody binding (S. J. Davis, personal communication).

Despite the lack of conserved or significant intra-subunit conformational changes, triggering through pMHC or antibody binding could be due to an inter-subunit conformational rearrangement of the extracellular domains of the TCR complex, *i.e.* triggering could be dependent on the formation of new interfaces by the extracellular TCR subunits. Testing this hypothesis is, however, challenging

[2] Parts of the work described in this chapter have been done in collaboration with Mai Vuong, Selma P. P. Lopes, Janet A. Fennelly, Heather Brouwer and Edward J. Evans and have been submitted for publication.

given there is limited information regarding the interfaces established between the TCRαβ and the CD3 chains [53]. The work described in this chapter addresses this problem by probing whether the interactions of the TCRαβ and CD3ε with the rest of the complex change substantially during triggering using a saturation mutagenesis-based approach.

4.1.2 Saturation mutagenesis-based subunit interface mapping

Assuming an intimately assembled complex that allows the transmission of structural changes between subunits [53], such rearrangements would be predicted to bury surfaces previously exposed in the assembled complex. Mutations that prevent these surfaces from becoming buried would be expected to block signalling. How can the subunit interfaces that are formed in the TCR complex be identified? A definitive answer to this question could arise from a crystal structure of the entire complex or from cryo-electron microscopy analysis of isolated and purified complexes. These approaches, however, rely on the extraction and purification of the complex from the cell membrane, which, to date, remains a major technical challenge for the TCR just as it does for most membrane-bound protein complexes. To identify residues that are exposed in the assembled TCR complex prior to triggering, it was decided to make use of the fact that the TCR complex is an obligate hetero-oligomer, that is, surface expression is dependent on the assembly of the entire complex [277, 278]. Thus, drastic mutations of residues lining subunit interfaces, but not residues exposed in the fully assembled complex, should prevent assembly and expression of the complex at the cell surface, allowing the exposed and buried surfaces of the subunit to be mapped. The types of mutations are referred to as "drastic" because they alter both side-chain size and charge. The aim of these mutations was to disrupt any interaction that buries the residue being mutated. Alanine-scanning mutagenesis is a widely used strategy to identify binding sites on proteins, however, this strategy was shown to identify residues that contribute to the binding energy of the protein-protein interface and not the larger structural binding site that is formed in stable

protein-protein interactions [279-281]. Therefore, mutations that increase (rather than remove or decrease) side-chain size were desirable. The introduction or reversal of charge would also be disruptive. Addition of hydrophobic side chains, however, was not deemed desirable as this may decrease the solubility of recombinant protein and lead to increased aggregation or non-specific association. This strategy was therefore used to map the exposed surfaces of the TCR complex subunits, in a resting state and during TCR triggering.

4.2 Materials and methods

4.2.1 Cloning, expression and surface detection of TCR mutants

Constructs

A cassette encoding a standard signal peptide (derived from human RPTP) followed by an HA tag (as defined by Sigma-Aldrich, UK) was cloned into a lentiviral expression vector based on pHR-SIN [282] already encoding an IRES sequence and GFP downstream of the insertion site, *via BglII* (5') and *BamHI* (3'). This vector allows for the expression of GFP in addition to the desired construct to act as a control for transfection efficiency and a normalization factor for comparison between different mutant expression levels. Human TCR and CD3 genes were amplified from plasmid templates and cloned into this vector using the *BamHI* and *XhoI* restriction sites (using compatible enzymes where necessary). Constructs comprised the codon encoding the first amino acid of the mature protein and continued through the stop codon. Mutations were introduced by PCR and final constructs were checked by dideoxy sequencing.

Table 4.1: List of mutations made for CD3ε, TCRα and TCRβ. Each mutant was made by site-directed mutagenesis with appropriate primers and cloned into the pHR-SIN-IRES-GFP lentiviral vector.

	CD3ε	TCRα	TCRβ
1	I19R	N112R	E115R
2	S20R	Q114R	D116R
3	I25K	N115R	N118R
4	Q30R	P116R	K119E
5	W38R	D117R	F121R
6	K43D	Q122R	P122R
7	D48R	R124E	E124R
8	E58R	K127E	A126R
9	H60E	S128R	E132R
10	K64E	S129R	A133R
11	E65F	D130R	I135R
12	E70R	K131E	S136R
13	F89E	D140R	Q139R
14	Y92R	Q142R	T148R
15	R94E	N144R	G149R
16	D2K	S146R	E156R
17	E6R	Q147R	S158R
18	I10E	K149E	N162R
19	Q12R	D150R	G163R
20	T13R	S151R	K164E
21	P14R	R164E	E165R
22	K16E	S165R	V166R
23	V17R	M166R	H167R
24	S18R	D167R	S168R
25	G21E	N178R	E179R
26	T22R	K179E	Q180R
27	T23R	S180R	P181R
28	T27R	D181R	A182R
29	Y31D	A183R	L183R
30	P32R	A185R	N184R
31	H40E	N186R	S197R
32	N41R	N189R	T199R
33	D42K	N190R	F200R
34	I45E	I192R	Q202R
35	D50K	P194R	N203R
36	D51K	E195R	P204R
37	N53R	D196R	R205E
38	I54E	F198K	H207E

	CD3ε	TCRα	TCRβ
39	G55E	F199K	R209E
40	D59K	S201R	Y215F
41	S62R	-	S218R
42	S67R	-	E219R
43	E68R	-	N220R
44	L69R	-	E222R
45	Q71R	-	T224R
46	S72R	-	D226R
47	G73E	-	A228R
48	Y74D	-	K229E
49	P79R	-	V231R
50	N88R	-	T232R
51	Y90D	-	I234R
52	L91E	-	S236R
53	L93E	-	A237R
54	R96E	-	E238R
55	V97R	-	W240R
56	C98S+C101S	-	R242E
57	-	-	A243R
58	-	-	D244R

Lentiviral transduction of cell lines

HEK-293T cells were transiently transfected with pHR-SIN vector constructs, together with pMD.G and p8.91 lentiviral vectors [255] in 6-well plates using Genejuice™ (Merck, Darmstadt, Germany) according to the manufacturer's instructions. Supernatant was harvested at 48-72 hours after transfection and centrifuged at 3000 rpm for 5 minutes at RT to remove cell debris. $1x10^6$ cells in 0.5 ml JMEM (10% FCS 2% L-glutamine, 1% Pen/Strep/Neo, 1% Hepes and 1% Sodium Pyruvate in RPMI 1640) were transduced with this supernatant overnight.

FACS analysis

Samples were stained on ice in the dark in PBS, 0.05% sodium azide using monoclonal antibodies specific for HA (HA-7, Sigma, Gillingham, UK) and

hTCRαβ (Caltag, Burlingame, CA; directly conjugated to R-Phycoerythrin) for 30 minutes. After washing, they were then stained with zenon anti-mouse IgG1 Alexa 647 (Invitrogen, Paisley, UK) for 30 mins. Cells were fixed in 2% PFA 0.05% sodium azide in PBS for 30 mins. Fluorescence for 10,000 live cells was collected on a CyAn FACS machine (Dakocytomation, Glostrup, Denmark) and the data was analysed using FlowJo software version 8.7.3 (Treestar, Ashland, OR). After compensation for overlap between fluorescence channels, live, hTCRαβ positive populations were selected. Pseudo-colour dot plots of GFP expression versus HA-7 staining of these cells were produced and their median fluorescence in each channel was used for data analysis.

4.2.2 T-cell activation and NFAT/IL-2 promoter reporter assay

Jurkat T-cells stably expressing wild-type or mutated HA-tagged proteins were transduced with an IL-2 Renilla Luciferase reporter construct using lentivirus. Forty-eight hours after infection cells were plated at $1x10^5$ per well in 100 µl of JMEM in 96-well flat bottomed tissue culture plates previously treated with a 25 mg/ml solution of donkey anti-mouse IgG (Jackon ImmunoResearch, West Grove, PA) overnight at 4°C followed by a second overnight incubation at 4°C with anti-CD2 (Miltenyi Biotech, Bergisch Gladbach, Germany) and anti-CD28 (7.3b) plus either anti-CD3 (OKT3), anti-HA (HA-7, Sigma) or anti-Thy1 (OX7) antibody at 10 µg/ml each. After 6 hours of antibody stimulation, luciferase activity was measured by adding coelenterazine-h (Lux Biotechnology, UK) at a final concentration of 10 µM to cells before reading total emission on a microplate analyser. Results were plotted as a ratio of luminescence induced by anti-HA antibody over that induced by OKT3 antibody stimulation after background subtraction. During the 6 hour stimulation, cell surface expression of HA-tagged proteins and GFP levels expressed under IRES regulator were quantified by FACS.

4.3 Results

4.3.1 CD3ε is fully exposed in the TCR complex

Mapping of the TCR/CD3 subunit interactions was initiated with an assay for CD3ε incorporation in the complex. J.RT3-T3.5 cells, which lack a functional TCRβ-chain [278], fail to detectably express lentivirally-transduced HA-tagged human CD3ε (Fig. 4.1b, *left panel*). J.RT3-T3.5 cells stably expressing a TCRβ/luciferase chimera, however, do express HA-tagged CD3ε at the cell surface (Figure 4.1b, *middle and right panel*). Surface expression of HA-tagged CD3ε, quantified by FACS, was used as a proxy for CD3ε incorporation into the TCR complex (Fig. 4.1c). To identify the exposed surface of CD3ε an extensive mutagenesis approach was undertaken. Using the CD3εδ and CD3εγ crystal structures as a guide [55, 61], surface-exposed residues of CD3ε were drastically mutated. The bulkiest charged side chain available is that of arginine, so all residues were mutated to arginine except those that were already positively charged (Arg, Lys, His), which were mutated to glutamic acid. For completeness, any residue whose side chain contained an atom whose solvent exposed surface area was >5 $Å^2$ according to NACCESS (54 HA-tagged CD3ε mutants in total; [283]) was mutated. However, the known UCHT1 [284] and OKT3 [285] antibody epitopes exposed in the complex were not mutated. W38 and I45 buried in the core of the domain were mutated as misfolding controls. The site-directed mutagenesis and sub-cloning of the mutants into the pHR-SIN-IRES-Emerald plasmid was done by Mai Vuong, Selma P. P. Lopes, Janet A. Fennelly and Heather Brouwer.

The majority of mutant CD3ε proteins were detectable at the cell surface with anti-HA antibody at levels similar to wild-type HA-tagged CD3ε (Fig. 4.2; the W38R and I45R misfolding controls were not expressed). Residues mutated in 12 of the 13 other non-expressing mutants (V17, I19, E68, G73, Y74, Y90, L91, Y92, L93, R94, R96, V97) form a contiguous surface (Fig. 4.2b; residues coloured in red) exhibiting remarkable overlap with the shared interface that CD3ε forms with CD3δ or CD3γ (Fig. 4.2c; [284, 285]). Mutation of H40, which lies immediately

"behind" the interface, prevents expression, presumably by perturbing neighbouring residues S72, G73 and Y74 at the interface with CD3δ and CD3γ. Smaller effects were observed for residues at the edges of the interface (Fig. 4.2a, b). These results suggest that, apart from the surface buried with CD3δ and CD3γ, CD3ε is completely exposed in the TCR complex.

4.3.2 Subunit interface mapping of TCRαβ, CD3δ and CD3γ

The analysis done for CD3ε was then extended to the rest of the complex. All of the residues whose side chains were >5 $Å^2$ solvent exposed in the TCR-α and -β constant domains and in CD3δ and CD3γ according to NACCESS (apart from those buried by CD3ε) were mutated and tested for expression. The site-directed mutagenesis and sub-cloning of these mutants was done by Mai Vuong, Selma P. P. Lopes, Janet A. Fennelly and Heather Brouwer. Most mutations of TCR-α and -β were without effect, indicating that large regions of the αβ heterodimer are exposed in the TCR complex (Fig. 4.3). Unclustered mutations that reduced anti-HA-detectable expression were attributed to folding effects; these included one residue in Cβ (K229 in the FG loop) and five others scattered throughout Cα (R124, K131, D140, Q147, K179; Fig. 4.3). Other mutations with large effects on surface expression clustered in a single, relatively small contiguous surface comprised of two Cα DE loop residues (S165, D167), and six Cβ CD (S168, V166, N162) and EF (F200, N203, R205) loop residues. Mutations of six other residues surrounding this region, *i.e.* αM166, βG163, βK164, βT199, βH207 and βR209, had weaker effects.

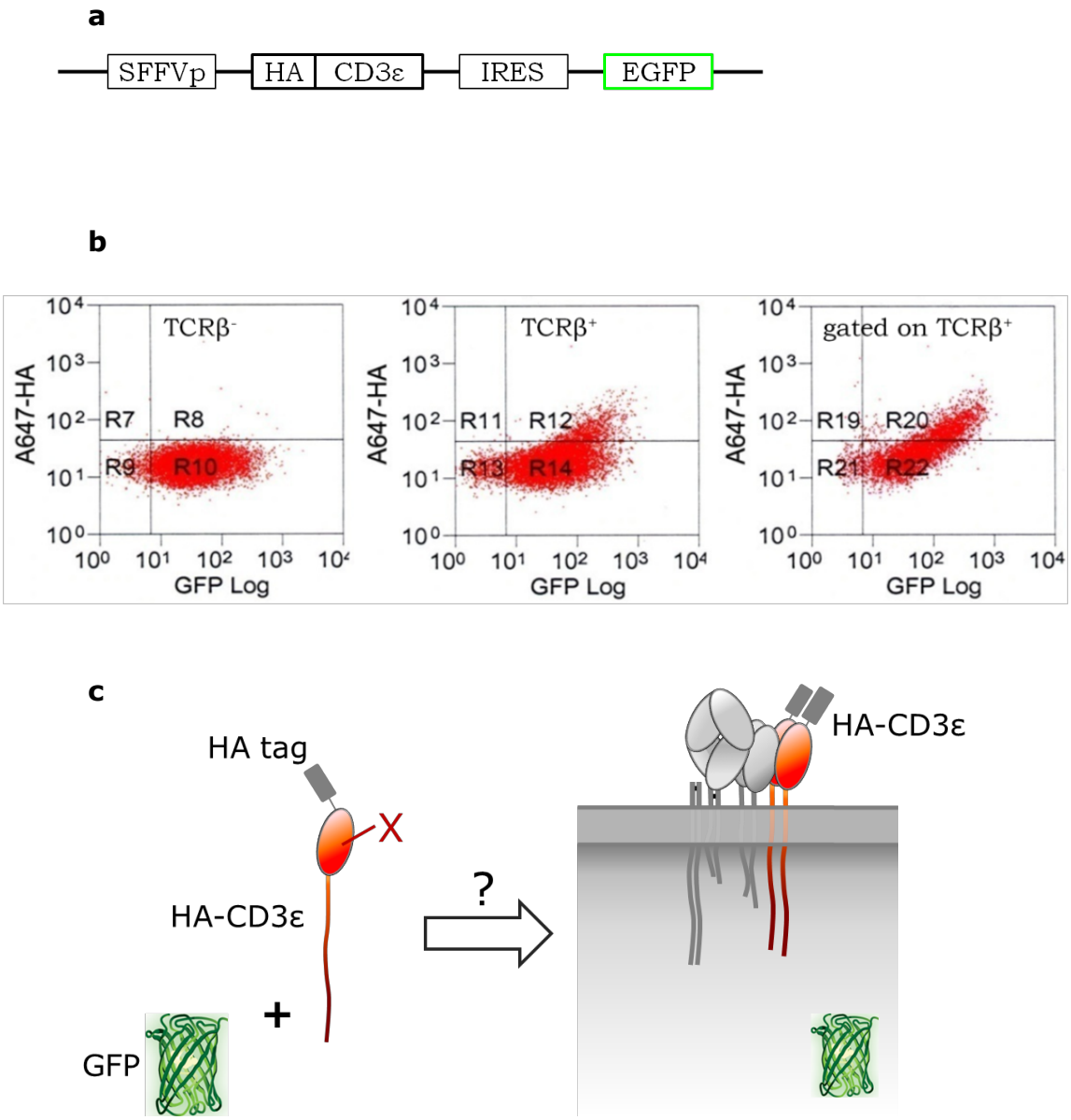

Figure 4.1: Protein complex interface analysis. **(a)** CD3ε fused with an HA tag was expressed using a lentiviral-mediated delivery system. **(b)** Only fully assembled TCR complexes are expressed at the cell surface. Mutant CD3ε fused with an HA tag is not expressed at the cell surface of the TCRβ$^-$ Jurkat-derived T-cell line. **(c)** Complex interface analysis relies on incorporation of a specific mutant subunit, fused to an HA-tag, into the TCR complex. Surface expression is detected by FACS analysis of anti-HA antibody staining.

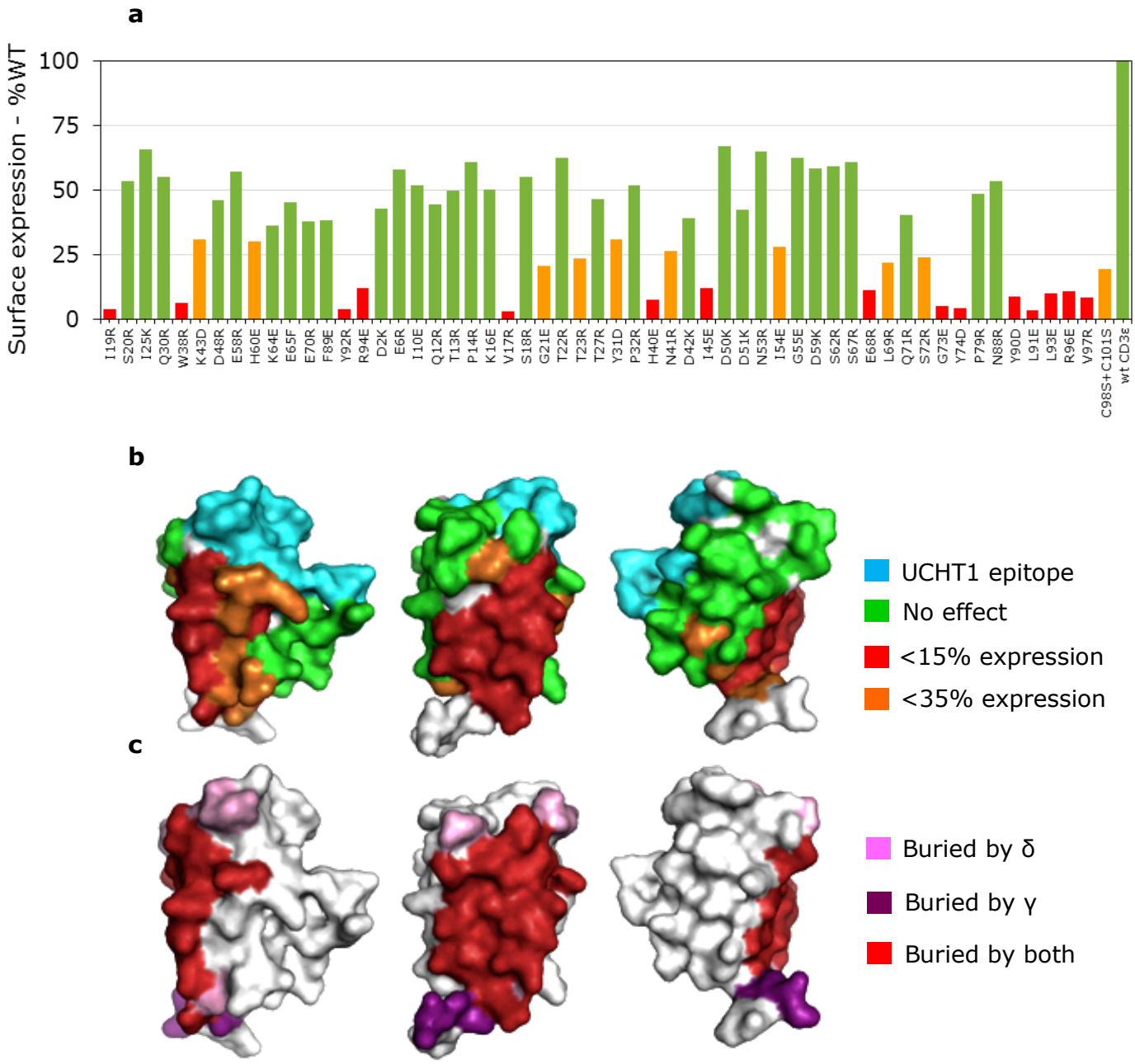

Figure 4.2: Identification of CD3ε interface interactions. **(a)** Surface expression of HA-tagged wild-type and mutant CD3ε proteins was evaluated by FACS and normalized to wild-type HA-CD3ε expression. Similar infection levels were obtained for all mutants (as detected by EGFP expression). **(b)** Drastic mutations of surface residues on CD3ε identified crucial amino acids (red) for protein expression at cell surface. **(c)** These regions correlated well with known residues involved in the interface between CD3εδ and CD3γε. No other interface was detected for CD3ε.

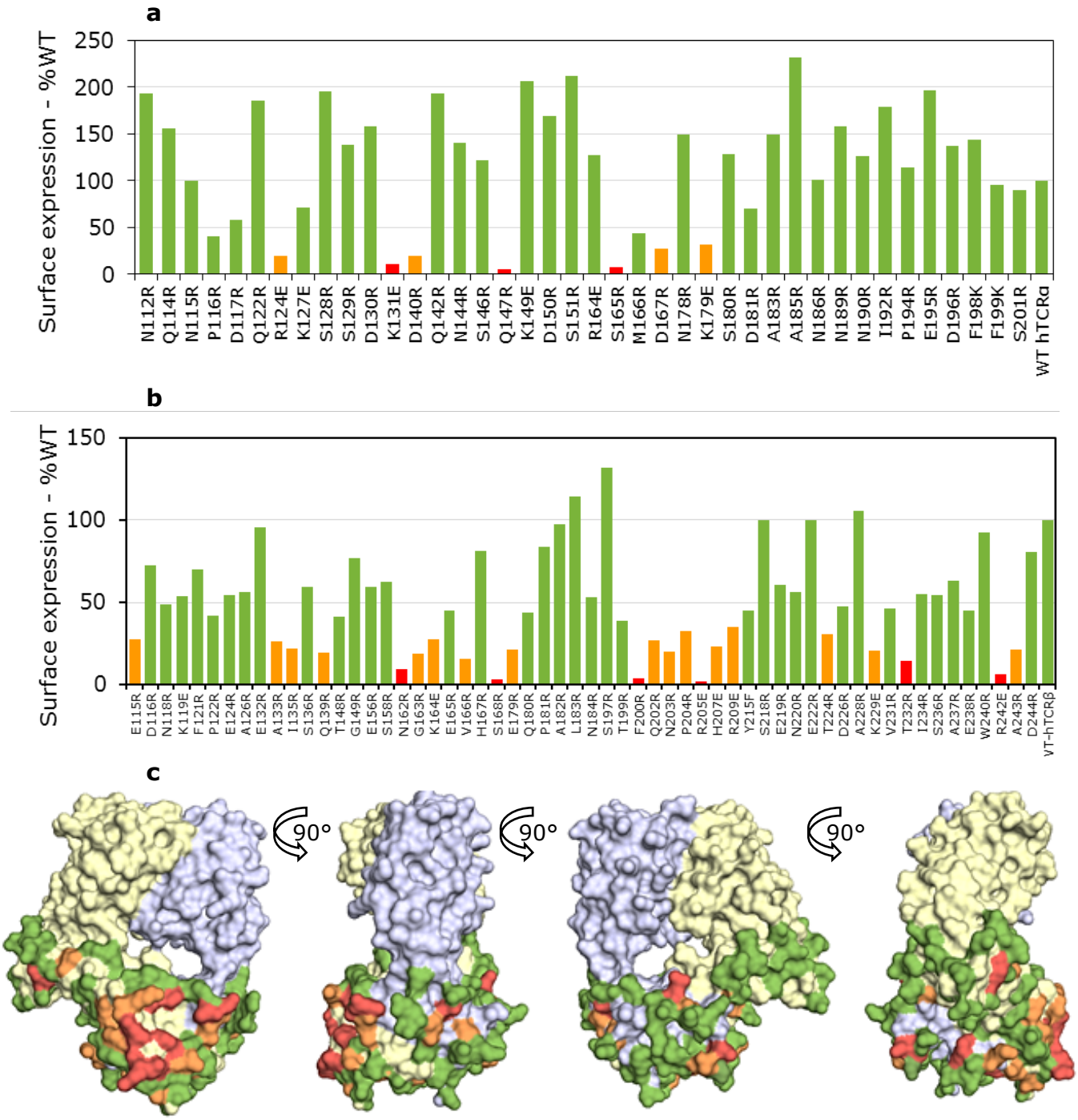

Figure 4.3: Complex interface analysis of the TCRαβ. **(a, b)** Surface expression of HA-tagged wild-type and mutant TCRα **(a)** and TCRβ **(b)** was quantified by FACS and normalized to wild-type expression. **(c)** Views of the TCRαβ heterodimer (from pdb 1OGA) with the α chain coloured blue and the β chain yellow. Mutated residues are coloured according to whether their mutation reduces TCR expression by more than 85% (red), by 60-85% (orange) or by less than 60% (green) versus wild-type TCR expression.

For CD3δ and CD3γ, the analysis was less clear-cut. Incorporation of HA-tagged CD3δ and CD3γ into the TCR complex was less efficient than for CD3ε and only the most highly transfected cells could be analysed. In contrast to CD3ε and TCRαβ, the majority of surface mutants of CD3δ and about half those of CD3γ failed to reach the cell surface (Fig. 4.4). The few expressed mutants nevertheless identify a contiguous surface at a membrane distal position apparently exposed at the "top" of the subunits (Fig. 4.4).

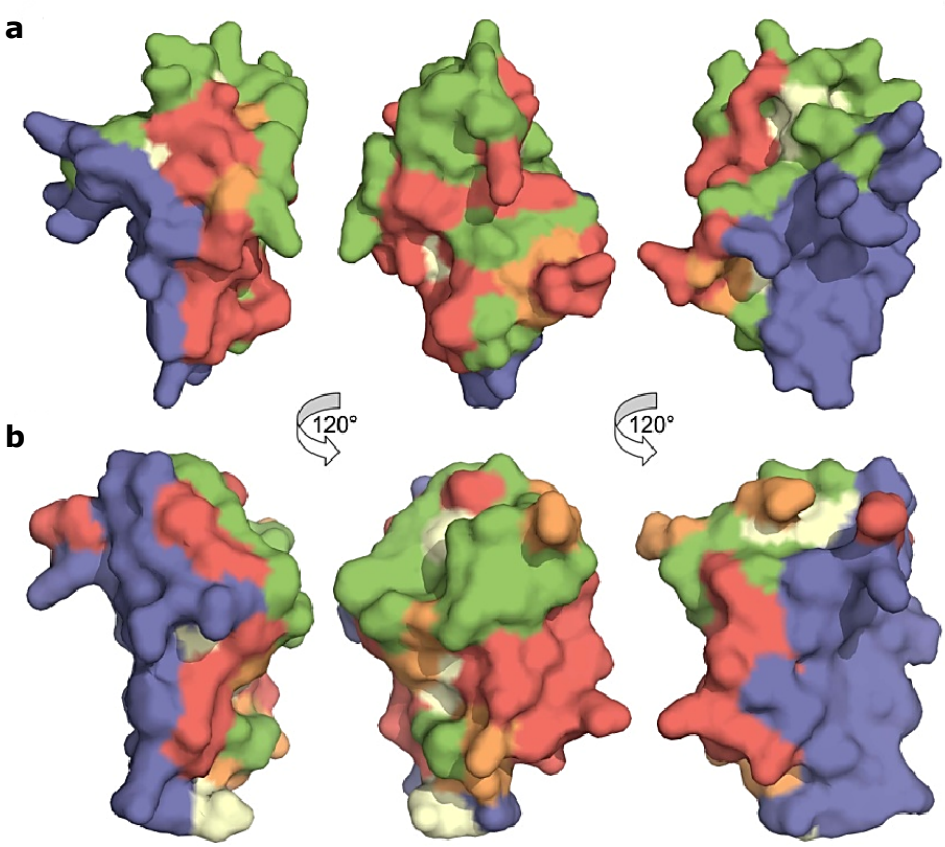

Figure 4.4: Complex interface analysis of CD3γ and δ. **(a, b)** Three views of the surface of CD3γ (**a**; from pdb 1SY6) and of CD3δ (**b**; from pdb 1XIW) related by 120° rotations about the vertical axis. In **(a)** and **(b)**, residues coloured blue are buried in interactions with CD3ε. Mutated residues are coloured according to whether their mutation reduces CD3 expression by more than 85% (red), by 60-85% (orange) or by less than 60% (green) versus wild-type expression.

4.3.3 Quaternary structure of the TCR

The mutational data suggest a new interpretation for the configuration of the quaternary structure of the TCR complex (Fig. 4.5), wherein CD3ε is fully exposed and the αβ heterodimer associates asymmetrically via contacts with CD3γ and CD3δ only. The apparent "sidedness" of the TCR complex, wherein CD3γδ interacts with one side of the TCRαβ, has been noted previously [206].

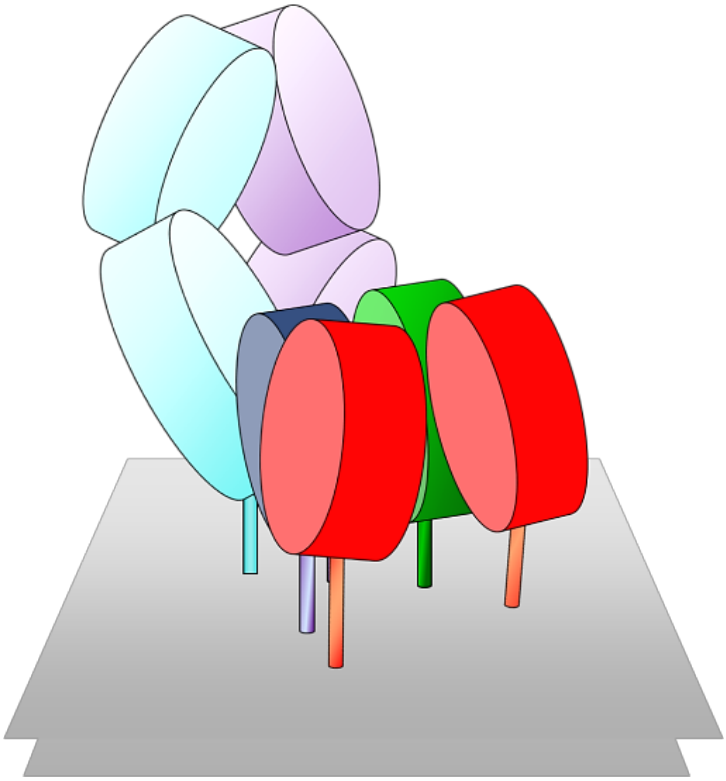

Figure 4.5: Cartoon illustration of the suggested quaternary arrangement of extracellular domains within the TCR-CD3 complex based on all of the mutagenesis data presented here. It remains unclear whether both CD3γ and δ (coloured green and dark blue) contact the TCRαβ heterodimer or whether one forms the major contact and stabilises the association of the other in the complex in the absence of direct contacts with TCRαβ.

4.3.4 Mutations of exposed CD3ε, TCRα and TCRβ surface residues do not block triggering

Triggering models that rely on large conformational changes of CD3ε relative to the complex are dependent on burial of previously exposed protein surfaces during TCR triggering. Therefore, with the saturation-mutagenesis analysis used to identify buried surfaces in resting complexes it should also be possible to identify new buried surfaces that form in the course of receptor triggering. Importantly, systematic mutation of exposed residues in the resting complex should impair, to some extent, triggering if these residues need to become buried during triggering. To specifically target mutated TCR subunits, cells were stimulated with an anti-HA antibody. OKT3 antibody [286, 287] was used as a positive control (to stimulate all complexes expressed at the cell surface) and OX7, an anti-rat Thy-1 antibody, was used to correct for non-specific activation.
Activation levels were measured with a reporter assay for IL-2/NF-AT promoter activity. During TCR triggering, the increase in cytoplasmic calcium triggers activation of the phosphatase calcineurin, which is responsible for dephosphorylating cytoplasmic NF-AT (NF-ATc) resulting in its import into the nucleus. NF-ATc is subjected to constant export from the nucleus unless high calcium levels are maintained. This prerequisite for a strong long-lasting, cytoplasmic, calcium increase is complemented by the requirement of activation of other pathways, like PKC, that allow NF-ATc to interact with NF-AT nuclear partners forming a complex with strong affinity for well-defined DNA sequences [288, 289]. Altogether, this makes IL-2/NF-AT promoter activity a robust and sensitive readout for TCR triggering. For this purpose, cells were stably infected with a lentiviral plasmid encoding three copies of the IL-2 promoter upstream of the *Renilla luciferase* gene. With this approach, it becomes possible to quantify the activation induced by antibody stimulation on cells expressing TCR subunit mutants by measuring luminescence from *Renilla luciferase* (Fig. 4.2).

If TCR signalling requires inter-subunit conformational rearrangements, then drastic mutation of residues involved in formation of these interfaces would reduce normal activation levels. After correcting for background/non-specific

activation, anti-HA antibody-induced IL-2 promoter activity was expressed as a fold increase over OKT3 antibody-induced activation. IL-2 promoter activity was then plotted versus HA surface expression levels, as shown previously (see Fig. 4.2). The results obtained for CD3ε indicate that, for this subunit, cell activation is dependent on surface expression levels alone (Fig. 4.6a, b). This analysis was also extended to the TCRα and β mutants (Fig. 4.6 c, d). Similar to the results obtained for CD3ε, *i.e.* IL-2 promoter activity was found to be highly dependent on surface expression levels alone. In fact, all the mutants that were able to reach the T-cell surface with expression levels similar to those of wild-type protein, induced strong IL-2 promoter activity (*i.e.* comparable to wild-type) irrespective of the mutation introduced.

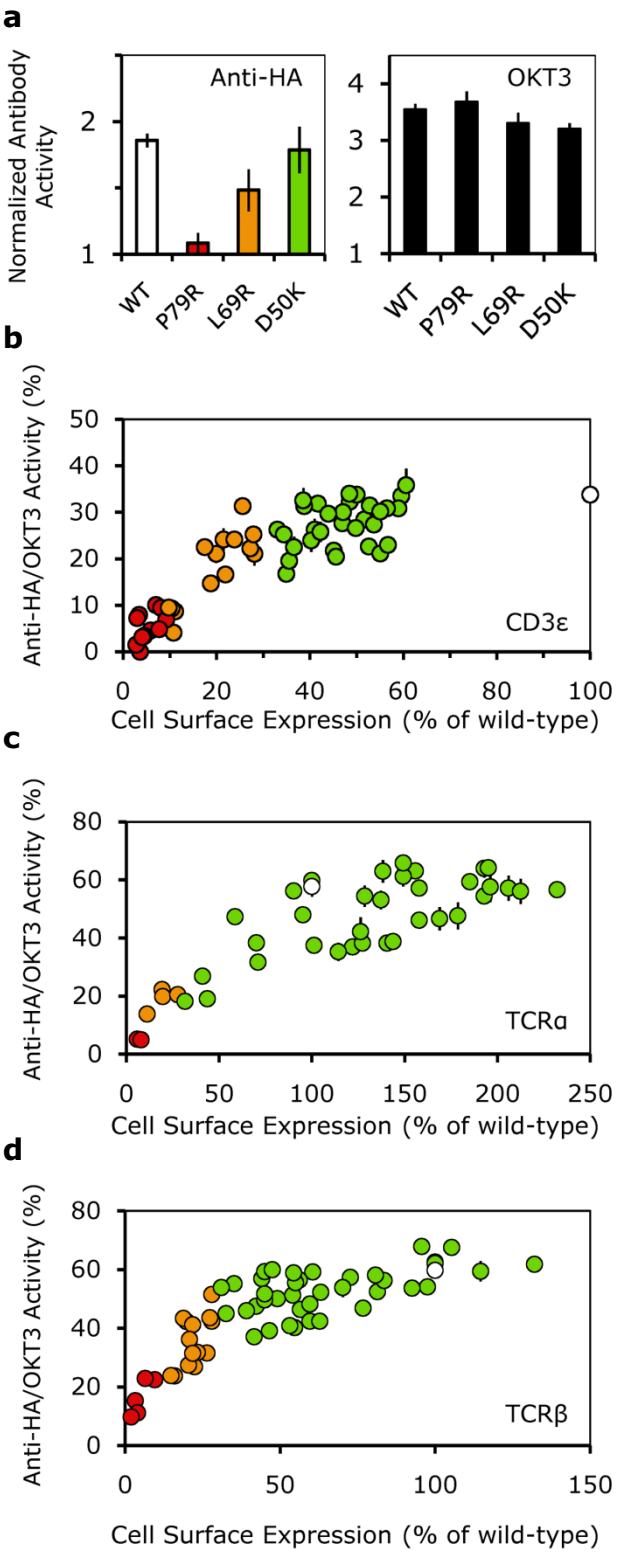

Figure 4.6: Jurkat T-cells expressing a luciferase reporter construct for NFAT/IL-2 promoter activity, and either wild-type or mutant HA-tagged CD3ε, were activated with plate bound anti-CD2 and anti-CD28 antibodies, plus either an anti-HA antibody, an anti-CD3 antibody (OKT3) or an anti-rat Thy-1 antibody (OX7). **(a)** Example of data obtained for cells expressing wild-type, P79R-, L69R- or D50K-mutated HA-tagged CD3ε. Anti-HA (*left panel*) and OKT3 (*right panel*) responses are normalized against the responses obtained with OX7. Responses for wild-type CD3ε (open bar) or the CD3ε mutants (coloured by expression level as in Fig. 4.2) are shown. **(b)** IL-2 promoter activity plotted against the surface expression level of wild-type or mutant HA-tagged CD3ε. IL-2 promoter activity is calculated as the specific response (*i.e.* following subtraction of the response to OX7) of each cell line to anti-HA antibody, divided by the specific response to OKT3, expressed as a percentage. Mutant surface expression levels were normalized to wild-type HA -tagged CD3ε. Circles corresponding to the mutant CD3ε responses are coloured by surface expression level (as in Fig. 4.2) with wild-type shown as an open circle. **(c, d)** Results obtained for wild-type and mutant forms of TCRα (**c**) and TCRβ (**d**). The data shown are representative of two independent experiments; means of triplicates ± S.E. are shown.

4.4 Discussion

4.4.1 An apparently static TCR is capable of initiating triggering

The work here described aimed to identify signatures of large structural rearrangements induced by antibody stimulation, which is a widely used surrogate of native ligand-induced signalling. If a large structural rearrangement is a requisite for initiating signalling then a subset of residues previously exposed in the folded complex would have to become buried to some extent during triggering. An extensive drastic mutagenesis approach was used to identify residues of the TCRαβ and CD3ε subunits that might be involded in these conformational changes. However, the results obtained indicate that TCR triggering does not seem to rely on burial of previously solvent-exposed surfaces and suggest instead that a largely static TCR is capable of initiating triggering.

4.4.2 Comparison to previous conformational analysis studies

The range of mutations tested included the majority of the TCR solvent-exposed residues, some of which have been proposed to play a significant role in TCR triggering. A basic patch of residues on the surface of CD3ε (βD strand) was suggested to transmit anti-CD3ε antibody binding to the rest of the complex and induce ITAM phosphorylation [60]. In the analysis here described, the charge of these residues was reversed and no difference was found on the activity of the IL-2 promoter in response to antibody stimulation, as compared to wild-type CD3ε (Fig. 4.7).

More recently, a conformational change was detected in the AB loop of TCRα upon pMHC binding [213]. Extensive mutations made on this loop were shown to abolish T-cell activation, suggesting that the conformational change observed could play an important role in TCR triggering [213]. However, drastic single-point mutation of residues that form the AB loop indicate that the ability to induce TCR triggering is mainly dependent on surface expression level (Fig. 4.8).

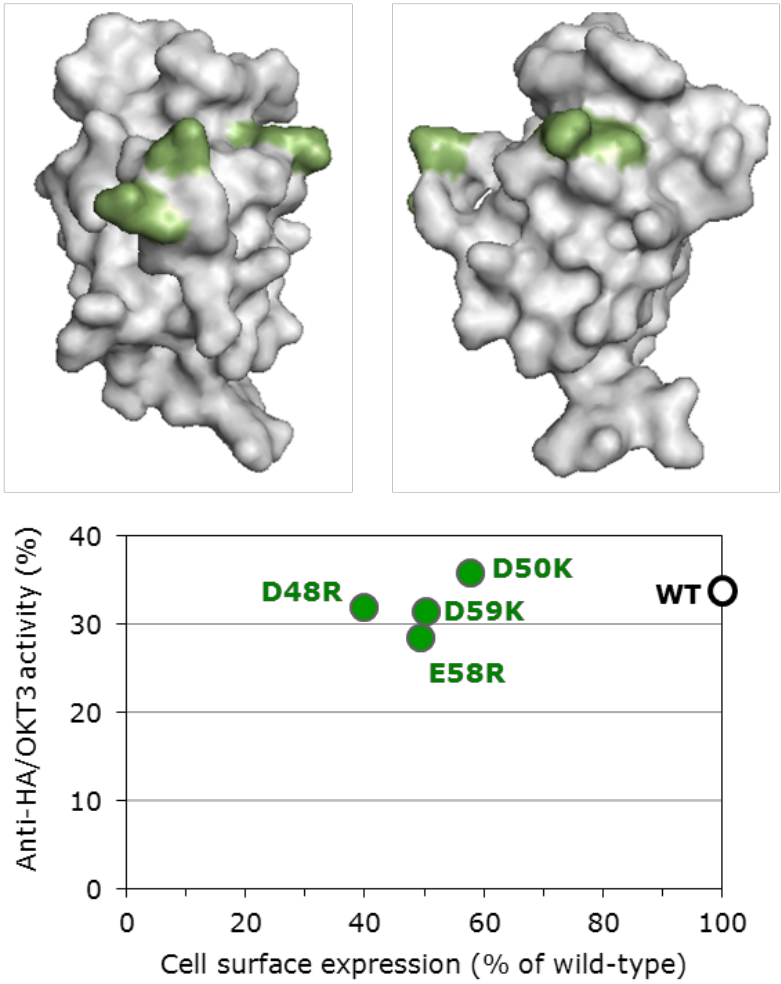

Figure 4.7: Reversing the charge of the basic residues present in CD3ε βD strand had no effect in TCR triggering. Stimulation of CD3ε mutants D48R, D50K, D59K and E58R induced an IL-2 promoter activity similar to wild-type CD3ε.

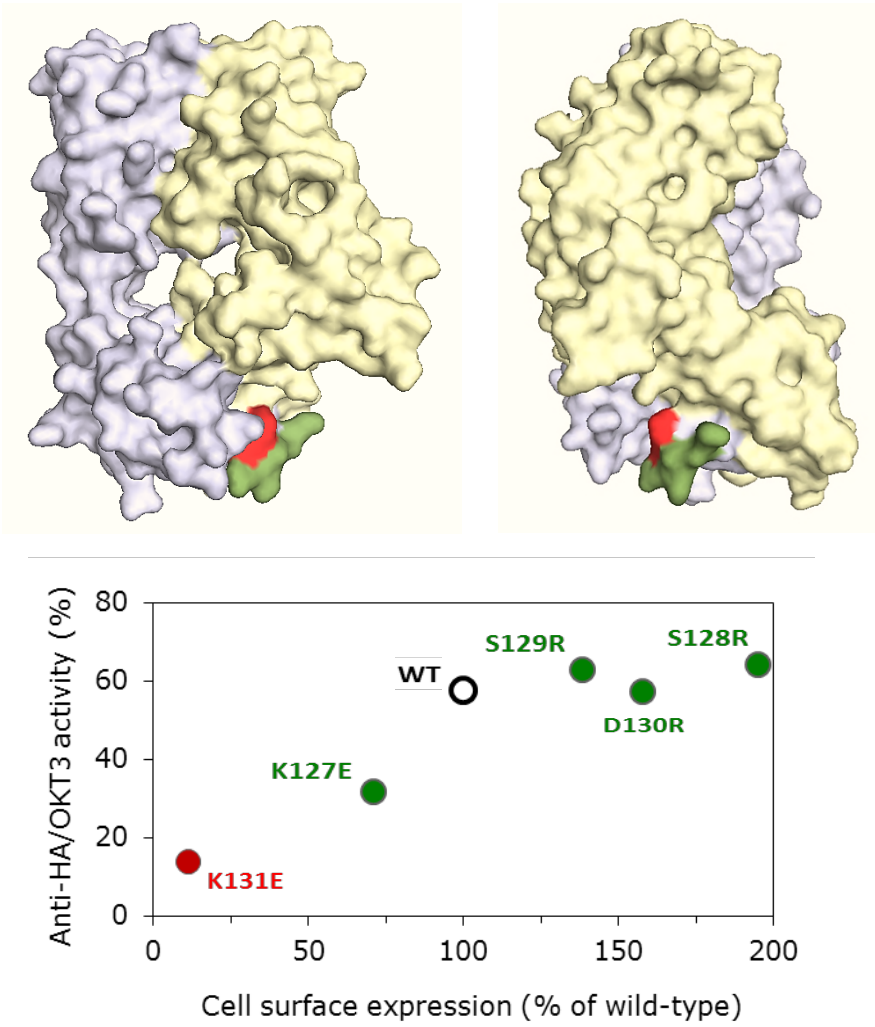

Figure 4.8: Mutations introduced in the AB loop of TCRα were able to induce an IL-2 promoter activity similar to wild-type TCRα. However, TCRα mutant K131E failed to express at the T-cell surface. Mutation K127E also reduced surface expression and thus induced lower IL-2 promoter activity, when compared to wild-type TCRα. Mutations S129R, S128R and D130R were able to induce strong IL-2 promoter activity.

Mutation of K131E decreased by more than 85% expression of the TCRα subunit, and thus compromised TCR signalling. This finding agrees well with the difficulty experienced by Beddoe *et. al.,* in expressing the LC13 TCR with the AB loop mutations (which include different K131 mutations) [213]. In that study, the surface expression of mutated TCRα was matched to that of the wild-type TCRα but only after several rounds of viral infection. Similar difficulties in expressing mutant forms of TCR/CD3 proteins at wild-type levels have also been reported in other analogous studies [52]. The outcome of saturating the ER protein-folding machinery and forcing TCR expression is difficult to determine and was not characterized.

4.4.3 Advantages and caveats of the present method

How, in general, can TCR complex stability be separated from TCR triggering? Instead of forcing TCR expression to match surface expression between mutants and wild-type proteins, two different antibodies were used to determine the effects of the mutations made in the present study: an anti-HA antibody, which triggers the TCR through a specific mutant subunit, and OKT3, which targets every TCR present at the cell surface. This approach allowed the analysis of TCR mutants in cells where endogenous subunits are always present and thus probe and compare TCR triggering efficacy without relying on constant surface expression. Introducing one mutation at a time also allowed us to understand the specific contribution of each residue during TCR triggering.

An obvious difference to the previous studies discussed above [52, 213] is the TCR-ligand used to trigger cells. In this study, antibodies instead of an agonist pMHC were used to look for the signatures of large TCR structural rearrangements. Mitogenic monoclonal antibodies (mAbs) directed against the CD3ε chain [290] have been shown by others to induce Ca^{2+} release [291], IL-2 secretion [292] and immune synapse formation [293] through the activation of the same pathways and with similar kinetics as those induced by agonist pMHC binding. It is unlikely that there is an entirely distinct triggering mechanism for

antibodies and pMHC. However, the study here described could be complemented by a similar drastic mutagenesis-based analysis of a TCR complex for which a specific agonist pMHC could be used for inducing triggering.

Systematic drastic mutations have been used previously in order to identify the ligand binding surfaces of the adhesion proteins CD2 and CD48 [294-296]. This approach has now been extended to identify surface and buried residues in the TCR complex. A single buried surface on CD3ε corresponding almost perfectly with the region buried in CD3εδ and CD3εγ heterodimers, revealed by crystallography, and a single, relatively small contiguous surface on TCRαβ that influences assembly of the TCR complex, were identified. This has suggested a new configuration for the organization of the receptor complex in which CD3ε is fully exposed in the complex, rather than contacting TCRαβ as proposed elsewhere [206].

Chapter 5

The role of phosphatases in controlling TCR phosphorylation[3]

5.1 Introduction

5.1.1 Controlling TCR ITAM phosphorylation in a resting T-cell

A fully assembled TCR complex present at the surface of a T-cell contains ten ITAM motifs. Triggering of the TCR is defined by the tyrosine phosphorylation level of these signalling motifs which is kept at surprisingly low levels by a mechanism that is not fully understood. Upon interaction with cognate pMHC the number of phosphorylated tyrosines in the cytoplasmic tails of CD3 subunits determines the T-cell response [70, 297]. Recent developments have shown the presence of active Lck at the surface of T-cells [298]. How is it, then, that TCR phosphorylation is kept at low levels in the presence of active Src kinases at the membrane?

The large number of protein tyrosine phosphatases (PTPs), their high levels of catalytic activity and a broad specificity would seem to make PTPs a good candidate to control ITAM phosphorylation [299, 300]. However, analysis of CD3ζ cytoplasmic domain ($CD3\zeta_{CD}$), and those of other ITAM-containing receptors such as the BCR, and Fc receptors, revealed a surprising interaction, at the μM range, with acidic phospholipids [227, 228, 301], which also induced

[3] The work described in this chapter was done in collaboration with Dr Chao Yu, who designed and made the plasmid constructs. This study has been published in [315].

changes in the secondary structure of $CD3\zeta_{CD}$ [302]. Importantly, it was shown that in the lipid-bound conformation, $CD3\zeta_{CD}$ was not phosphorylated by Src kinases [302]. Building on these previous results, Xu *et al.* showed, in live cells using FRET between $CD3\varepsilon_{CD}$ fused to Teal fluorescent protein and a membrane dye, that the interaction between the CD3ε cytoplasmic domain, $CD3\varepsilon_{CD}$, and the phospholipids was mediated by a cluster of positively charged amino-acids N-terminal to the proline-rich motif and the ITAM [224]. An NMR structure suggested that CD3ε ITAM tyrosine residues were also buried in a POPG/DHPC lipid bicelle [224]. The FRET-based observations have now been extended to CD3ζ [303].

Altogether, these results offered an alternative explanation to the low level of phosphorylated TCR found in resting T-cells, based on a protective "safety catch" interaction between the ITAM and the inner leaflet of the cell membrane, precluding Src phosphorylation of the tyrosine residues [229]. In this model, phosphatases were not deemed to be required or to play a significant role in controlling ITAM phosphorylation. Intrigued by the high levels of phosphorylation nevertheless induced upon phosphatase inhibition, such as in the presence of pervanadate [304], the experiments here described try to dissect the relative contribution of membrane association and phosphatase activity in controlling TCR phosphorylation in a resting T-cell.

5.2 Materials and methods

5.2.1 Construct design and cell line preparation

A cDNA fragment encoding the extracellular and transmembrane domains of human KIR2DL3 (residues 22-265) was amplified by PCR using template kindly provided by Dr. S. Brackenridge (MRC Human Immunology Unit, Oxford, UK). Fragments encoding the cytosolic domain of mouse $CD3\varepsilon_{CD}$ (residues 134-189) and mouse $CD3\varepsilon_{CD}$Emut1+2 (residues 134-189 of native $CD3\varepsilon_{CD}$, mutated at the set of clustered positively charged residues according to Xu *et al.*, [224]) were PCR amplified using mouse thymus cDNA as template. The two fragments were fused

in a second-round PCR and cloned into pHR-SIN lentiviral vector [255] encoding the secretion leader sequence from pHLsec [305] and a FLAG-tag. All the constructs were sequenced to confirm reading frame integrity.

Jurkat T cells were maintained in RPMI medium (Sigma-Aldrich, Gillingham, UK) supplemented with 10% foetal calf serum (v/v; Sigma-Aldrich), Hepes, sodium pyruvate and Penicillin-Streptomycin. Stable cell lines were made by infection with lentivirus and cell surface expression of the desired proteins was evaluated by fluorescence activated cell sorting (FACS).

5.2.2 Pervanadate treatment and cell surface immunoprecipitations

Pervanadate was freshly prepared by mixing sodium orthovanadate (Sigma-Aldrich) and H_2O_2 (Sigma-Aldrich) 10 minutes before addition to cells at a final concentration of 100 μM. Cells were treated for 20 minutes with pervanadate at 37°C. For cell surface FLAG immunoprecipitations, $5x10^7$ cells were incubated for 60 minutes on ice with 5 μg of anti-flag M2 antibody (Sigma-Aldrich), washed in phosphate buffered saline (PBS) solution and lysed for 20 minutes in 137 mM NaCl, 20 mM Tris-HCl, 2 mM EDTA, 10% glycerol, 1 mM PMSF (Sigma-Aldrich), 1 mM orthovanadate, protease inhibitor cocktails (Sigma-Aldrich, Santa Cruz Biotechnologies, Inc., Wembley, UK) and 1% NP-40 (Sigma-Aldrich). Protein complexes were immunoprecipitated with protein A/G agarose beads (Santa Cruz Biotechnologies), washed 4x with lysis buffer and eluted with reducing buffer at 95°C for 5 minutes. Equal volumes were loaded in SDS-PAGE 12% acrylamide gels and samples were transferred at 100 V for 60 minutes to nitrocellulose membrane (GE Healthcare Life Sciences, Little Chalfont, UK). After blocking with 3% BSA/0.05% Tween-20 for 60 minutes at room temperature (RT) membranes were incubated with biotinylated-anti-phospho-Tyr (p-TYR-100; Cell Signalling, Hitchin, UK), anti-Flag M2 (Sigma-Aldrich), or UCHT1 (purified from hybridoma supernatant and subsequently biotinylated) antibodies for 2 hours or overnight at 4°C. Membranes were incubated with anti-mouse horse radish peroxidase (HRP) coupled antibody (Sigma-Aldrich) or streptavidin-HRP (Cell Signalling Technology Inc) for 60 minutes at RT before

washing and adding ECL substrate (Pierce, Thermo Fisher Scientific, Cramlington, UK). For treatment with PP2, cells were incubated, with 10 μM of PP2 (Roche) at the appropriate time points.

5.2.3 Transient protein expression in HEK-293T cells

HEK-293T cells were grown in DMEM supplemented with 10% FBS, glutamine and antibiotics. Three T75 flasks were seeded with 12×10^6 293T cells to give 80% confluence on the day of transfection. Constructs, 4 μg DNA each per flask, were co-transfected using Genejuice® (Merck & Co. Inc) according to the manufacturers' instructions.

5.3 Results

5.3.1 Tyrosine phosphatases control CD3ε phosphorylation

In experiments by Xu *et al.*, the interaction of $CD3\varepsilon_{CD}$ with the cell membrane was proposed to be dependent on a group of positively-charged residues situated upstream of the proline-rich domain of the $CD3\varepsilon_{CD}$. Mutation of these residues compromised interaction with the membrane, as determined by FRET analysis (Fig. 5.1; [224]). In the context of the hypothesis proposed, *i.e.* that $CD3\varepsilon_{CD}$-cell membrane interactions prevent ITAM phosphorylation by Src kinases, it seemed relevant to determine if, *in vivo,* mutation of the residues responsible for membrane interaction would expose CD3ε to the actions of Src kinases.

In order to test these initial predictions a chimeric protein consisting of the extracellular and transmembrane domains of the human natural killer cell inhibitory receptor, KIR2DL3, was fused to wild-type $CD3\varepsilon_{CD}$ or to $CD3\varepsilon_{CD}$ mutated at the set of clustered positively charged residues, mutant Emut1+2, found to mediate membrane association, in a replicate of the constructs made by Xu *et al.* (Fig. 1; these plasmids were designed and made by Chao Yu; [224]). FLAG-tagged forms of these proteins were expressed at similar levels in Jurkat T-cells using a lentiviral expression system (Fig. 5.2; [255]) and probed for ITAM

phosphorylation by Western blotting following immunoprecipitation of cell surface FLAG-tagged proteins.

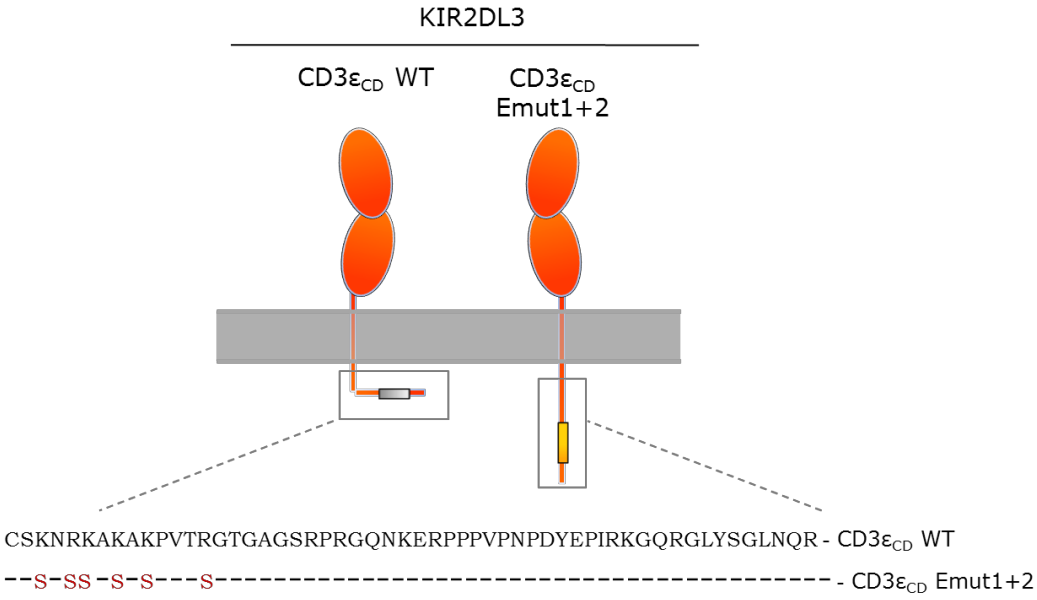

Figure 5.1: Mutation of key residues in $CD3\varepsilon_{CD}$ is abolishs ITAM interaction with the cell surface membrane. Xu *et al.* used a FRET-based assay to show that $CD3\varepsilon_{CD}$Emut1+2 does not interact with the cell membrane [224].

Neither KIR2DL3/$CD3\varepsilon_{CD}$ nor KIR2DL3/ $CD3\varepsilon_{CD}$Emut1+2, were found to be phosphorylated in resting cells (Fig. 5.2a, lanes 1, 2). Even after long exposures, ~30 minutes, no phosphorylation over background levels of cross-reactivity of the antibody, or differences in signal for the wild type versus the mutant proteins could be detected (Fig. 5.2b, lanes 1, 2). This result suggests that either membrane association is not the primary factor determining the levels of $CD3\varepsilon_{CD}$ phosphorylation *in vivo* or that the mutations introduced on $CD3\varepsilon_{CD}$, somehow, also prevent $CD3\varepsilon_{CD}$ phosphorylation.

If membrane interaction could not account for the low levels of CD3ε tyrosine phosphorylation observed, it seemed reasonable to revisit the initial

assumption that phosphatases were playing a major role in keeping CD3ε unphosphorylated [304, 306, 307]. This possibility was tested using the tyrosine phosphatase inhibitor, pervanadate [234, 308]. Upon pervanadate treatment both forms of $CD3\varepsilon_{CD}$, *i.e.* wild-type and Emut1+2, became phosphorylated (Fig. 5.2a, lane 3, 4). This suggests that $CD3\varepsilon_{CD}$ is readily accessible to kinases in resting cells, and that its phosphorylation is "quenched" by phosphatases. Levels of phosphorylation of KIR2DL3/$CD3\varepsilon_{CD}$Emut1+2 were comparable at this time point (Fig. 5.2a, lanes 3, 4), thus indicating that the Emut1+2 mutations did not enhance or prevent the phosphorylation of KIR2DL3/$CD3\varepsilon_{CD}$Emut1+2 in the untreated cells.

These experiments were then extended to $CD3\varepsilon_{CD}$ expressed in the context of the native TCR. FLAG-tagged CD3ε expressed in Jurkat T-cells (Fig. 5.3) was heavily phosphorylated in the presence, but not the absence of pervanadate (Fig. 5.3a, lanes 1, 3). As in the case of the KIR2DL3 chimera, it was found that Emut1+2 mutations did not enhance the phosphorylation of CD3ε in resting T cells (Fig. 5.3a, lanes 1, 2), or 20 minutes after the addition of pervanadate (Fig. 5.3a, lanes 3,4). It thus seems that CD3ε ITAM tyrosine residues are exposed to Src kinases and can be readily phosphorylated. In fact, examination of endogenous CD3ε phosphorylation levels upon pervanadate treatment of wild-type Jurkat T-cells reveals that, far from being sequestered or protected from the action of Src kinases, CD3ε is among the more heavily tyrosine phosphorylated proteins present in resting T-cells (Fig. 5.4a; black arrow). To confirm that CD3ε accounted for the majority of the protein present in a phosphorylated band around 17kDa that appears upon pervanadate treatment (indicated by an arrow in Fig. 5.4a), an immunodepletion assay from whole cell lysates of Jurkat cells following pervanadate treatment was made using an anti-CD3ε, UCHT1, antibody. Upon CD3ε immunoprecipitation, the phosphorylated band initially present at 17kDa was strongly diminished (Fig. 5.4b, black arrow).

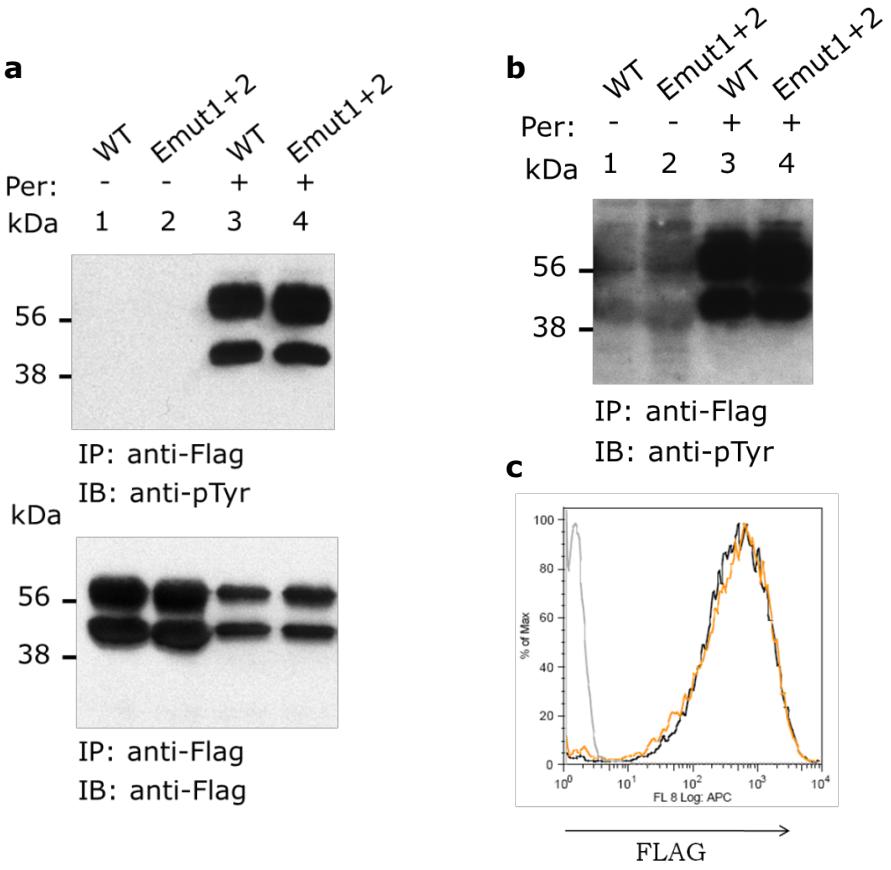

Figure 5.2: Non-membrane binding KIR2DL3/CD3ε_{CD}Emut1+2 ITAM exhibit no observable phosphorylation in resting T-cells. **(a)** Mutations introduced in CD3ε_{CD}Emut1+2 purported to disrupt the association between the ITAM and the inner leaflet of the cell membrane (Xu *et al.*; [224]) did not lead to a higher degree of phosphorylation in resting cells when compared to KIR2DL3/CD3ε_{CD}. In Jurkat T-cells treated with pervanadate (100 μM) for 20 minutes both KIR2DL3/CD3ε_{CD} and KIR2DL3/ CD3ε_{CD}Emut1+2 are phosphorylated to similar extent. Cells were immunoprecipitated with anti-FLAG M2 antibody and probed with anti-pTyr or anti-FLAG antibody. **(b)** Even after exposing film for longer periods of time no phosphorylation was detected in resting cells. **(c)** FACS analysis showed that Jurkat T-cells stably expressed equal surface levels of FLAG tagged KIR2DL3/CD3ε_{CD} (black line) and KIR2DL3/CD3ε_{CD}Emut1+2 (orange line).

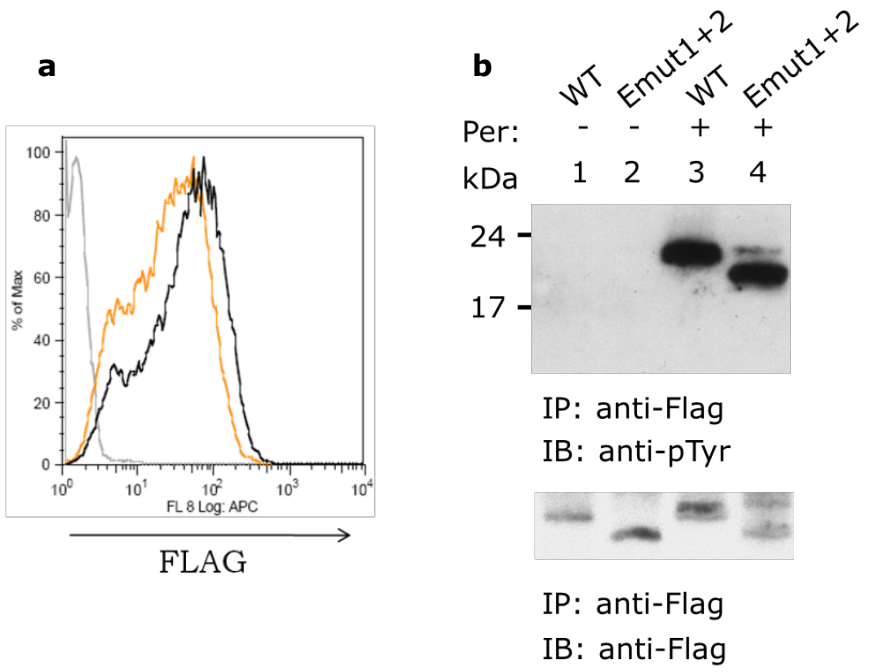

Figure 5.3: In resting T cells wild type CD3ε ITAM is readily accessible to Src kinases being kept unphosphorylated by the action of phosphatases. **(a)** Jurkat cells stably expressed similar levels of FLAG tagged wild-type (black line) and Emut1+2 CD3ε (orange line). **(b)** FLAG-tagged immunoprecipitated CD3ε shows no phosphorylation in resting cells. Moreover CD3ε Emut1+2 also lack any detectable phosphorylation. Following inhibition of phosphatases by addition of pervanadate both wild-type and Emut1+2 CD3ε show similar phosphorylation levels.

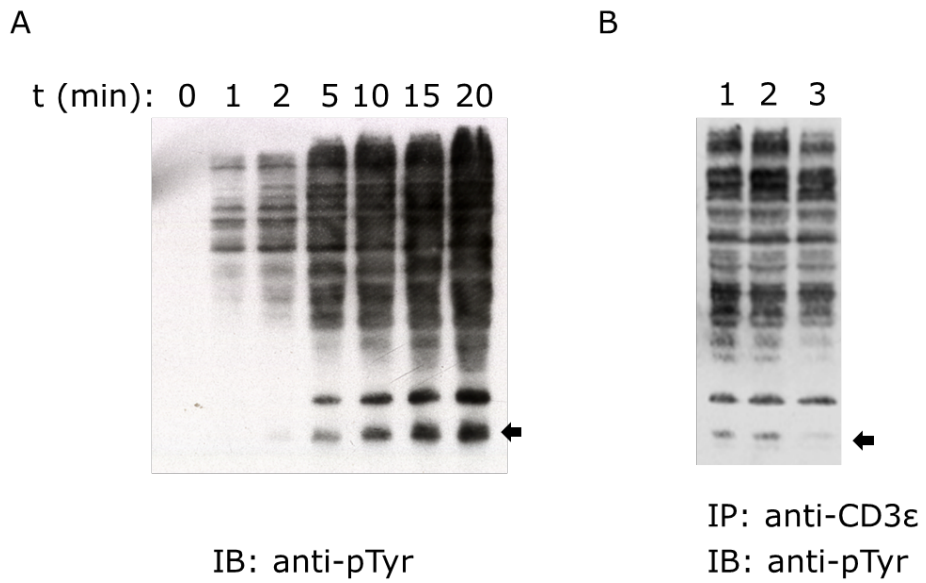

Figure 5.4: CD3ε is highly phosphorylated in Jurkat cells treated with pervanadate. **(a)** Whole cell lysates of $5x10^6$ Jurkat cells treated with pervanadate were probed with anti-pTyr antibody. The position of CD3ε is indicated with an arrow. **(b)** A depletion assay was made to determine if the lower band visible on the pTyr Western mainly consists of CD3ε. 10µg/ml of UCHT1 was used to immunoprecupitate CD3ε from whole cell lysates of cells treated with pervanadate for 15 min. After one hour of antibody binding different amounts of protein A/G beads were added to perform the immunoprecipitation. Lane 1 – 50µl of protein A/G beads were added with no antibody; lane 2 and 3, 10 and 50µl of protein A/G beads were added, respectively, together with UCHT1.

5.3.2 Positively charged residues in CD3ε promote ITAM phosphorylation and T-cell activation

Having established that the Emut1+2 mutations do not enhance the phosphorylation of CD3ε at the end of 20 minutes of pervanadate treatment in resting cells, it was then decided to examine whether the mutations had any other effects. To test whether the mutations affected the phosphorylation kinetics revealed in the presence of pervanadate, Jurkat cells expressing either FLAG-tagged forms of wild-type CD3ε or the mutated CD3εEmut1+2 were subjected to pervanadate treatment for shorter periods of time. As previously, anti-FLAG antibodies were used to immunoprecipitate cell surface proteins followed by a Western blot analysis of ITAM phosphorylation with an anti-phospho-tyrosine antibody.

Somewhat surprisingly, rather than enhancing the rate of phosphorylation, the Emut1+2 mutations reduced it (Fig. 5.5). Five minutes after starting pervandate treatment it was already possible to detect phosphorylation of wild-type CD3ε, whereas the Emut1+2 protein was only visibly phosphorylated 10 minutes later. To determine whether the effect observed on ITAM phosphorylation could also have wider implications for T-cell activation, a stimulation assay was done to compare the ability of wild-type or mutant CD3ε to trigger T-cells. The chimeric CD3εCD or the mutated Emut1+2 form fused to FLAG-tagged KIR2DL3 were stably expressed in J.RT3 T-cells. These cells were chosen for this assay because they lack TCR expression at the cell surface and have thus reduced interference arising from endogenous CD3 ITAMs. Cells were stimulated with plate-bound anti-FLAG antibodies, for 6 hours. To quantify T-cell activation an IL-2 promoter reported was used. Before stimulation, cells were transduced with a plasmid encoding three tandem copies of the IL-2/NF-AT promoter, controlling the expression of the *Renilla Luciferase* protein. This approach allowed quantification of T-cell activation, *i.e.* NF-AT translocation to the nucleus, by quantifying luminescence from *Renilla Luciferase*. Cells were also stimulated with plate bound anti-Thy-1, or donkey anti-mouse, antibodies. In

good agreement with the results obtained for the kinetic analyses of CD3ε phosphorylation, IL-2 promoter activity was higher in J.RT3 T-cells expressing wild-type $CD3\varepsilon_{CD}$ in comparison with cells expressing the Emut1+2 form of $CD3\varepsilon_{CD}$ (Fig. 5.6). These observations have recently been confirmed in similar studies of CD3ζ [303].

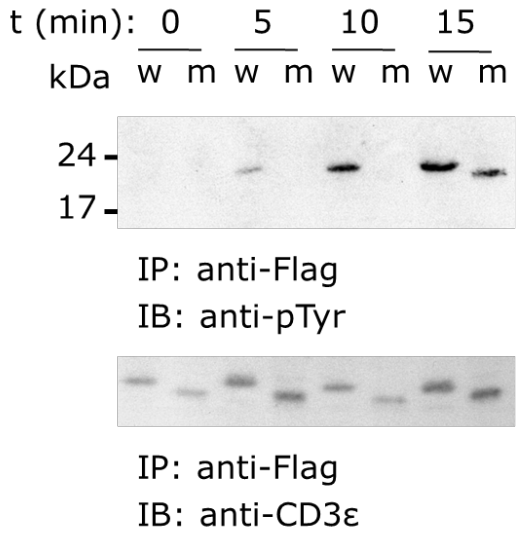

Figure 5.5: ITAM phosphorylation in wild type CD3ε is detected at higher levels and earlier time points after pervanadate addition when compared with CD3ε Emut1+2. Decreased ITAM association with the membrane (Emut 1+2) thus leads to slower phosphorylation kinetics. The membrane was stripped and re-incubated with UCHT1 after anti-FLAG immunoprecipitation.

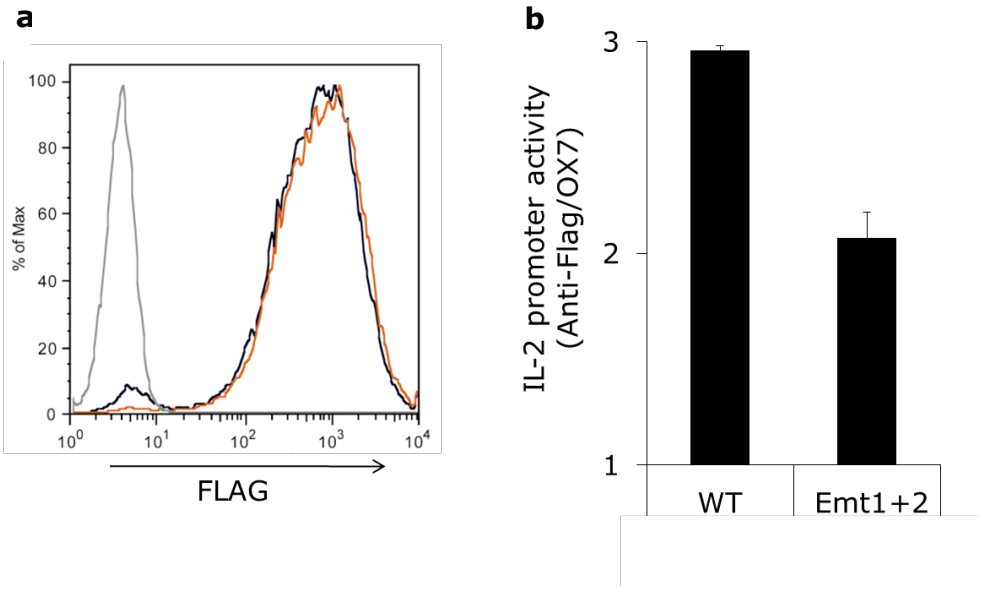

Figure 5.6: Activation of CD3ε$_{CD}$ Emut1+2 with an anti-FLAG antibody induced lower IL-2 promoter activity than wild-type CD3ε$_{CD}$. **(a)** FLAG-tagged KIR2DL3/CD3ε$_{CD}$ wild-type (black line) and KIR2DL3/CD3ε$_{CD}$ Emt1+2 (orange line) were stably expressed in J.RT3 cells, which lack expression of TCR at the cell surface. Cells were also transduced with a plasmid driving expression of *Renilla Luciferase* under control of three copies of the NF-AT promoter. **(b)** Cells expressing either KIR2DL3/CD3ε$_{CD}$ wild-type and KIR2DL3/CD3ε$_{CD}$ Emut1+2 were stimulated with anti-FLAG M2 antibody or anti-Thy1 antibody, OX7, used as a control, for 6 hours and were subsequently analysed for the luminescence output. The results shown are the average of triplicates with ± S.E.

5.3.3 Lck and CD45 control CD3ε phosphorylation

Pervanadate treatment showed that the CD3ε ITAM could be readily phosphorylated, but gave no indication as to which proteins were responsible for this effect. Given that Lck is considered to be the main Src kinase able to phosphorylate CD3 ITAMs it was decided to investigate its role in CD3ε phosphorylation during pervanadate treatment. For this, a specific inhibitor of Lck kinase activity, PP2, was added together with pervanadate to wild-type Jurkat cells. Addition of PP2 decreased the level of CD3ε tyrosine phosphorylation detected (Fig. 5.7).

It was also important to understand if specific phosphatases known to play a role in TCR triggering, like CD45, could account for the effects observed with pervanadate, *i.e.*, could CD45 actually control CD3ε ITAM phosphorylation? To test the role of CD45, the FLAG-tagged form of KIR2DL3/CD3ε_{CD} was stably expressed in HEK-293T cells. Immunoblotting with anti-pTyr antibody, following anti-FLAG immunoprecipitation of cell surface proteins, showed that there is no kinase present in HEK-293T cells that is able to phosphorylate CD3ε ITAM (Figure 5.8, lane 1). Co-expression of KIR2DL3/CD3ε_{CD} and a mutant form of LCK, Y505F, which has a higher catalytic activity than wild-type Lck [309, 310] induced phosphorylation of KIR2DL3/CD3ε_{CD} (Figure 5.8, lane 2). CD45 was then transiently expressed 24 hours after transfection of HEK-293T cells with LCK Y505F. Expression of CD45 decreased the tyrosine phosphorylation level of CD3ε ITAM (Figure 5.8, lane 3).

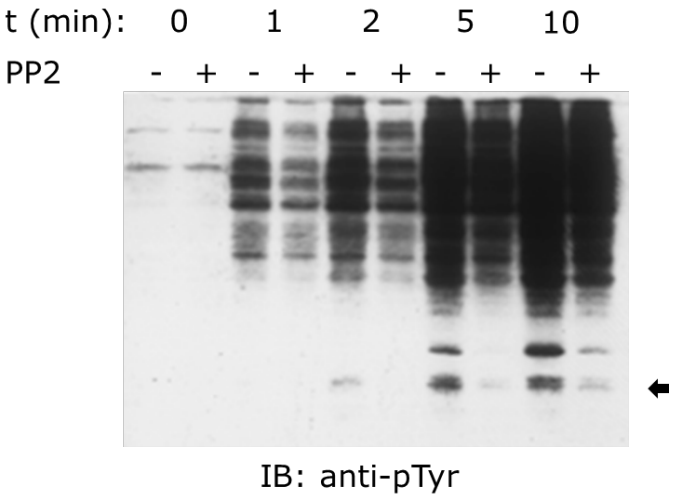

Figure 5.7: Pervanadate treatment leads to CD3ε phosphorylation by Lck. To determine the role of Lck in phosphorylating CD3ε, whole cell lysates of $5x10^6$ Jurkat cells were probed with anti-pTyr antibody following treatment with PP2 and pervanadate. The position of CD3ε is indicated with an arrow.

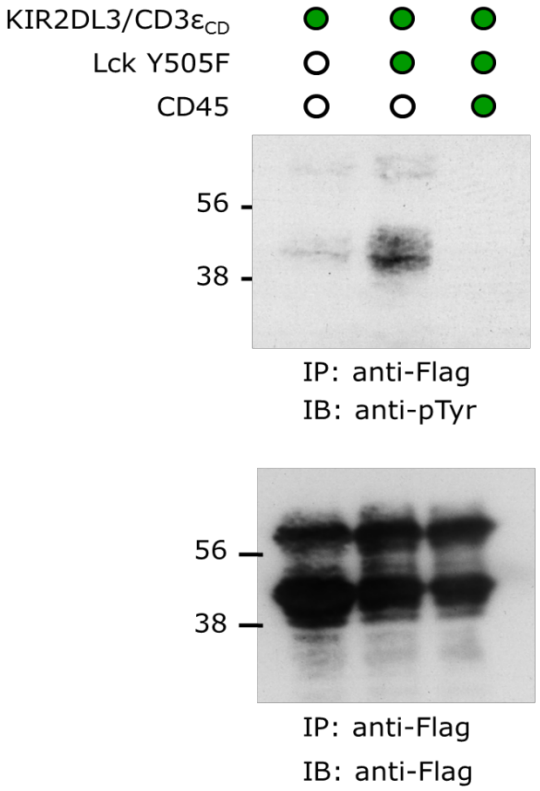

Figure 5.8: CD45 decreases the phosphorylation of CD3ε ITAM. FLAG-tagged KIR2DL3/CD3ε_{CD} was stably expressed using lentiviral transfection in HEK-293T cells. A hyper-active mutant form of Lck, Y505F, was transiently transfected (lane 2 and 3) and expressed for 48 hours. Twenty-four hours after Lck Y505F expression, CD45 was also transiently transfected and expressed for 24 hours. Forty-eight hours after Lck Y505F transfection, an anti-FLAG antibody was used for a surface immunoprecipitation of KIR2DL3/CD3ε_{CD} and samples were probed by western blotting with an anti-pTyr or anti-FLAG antibody. Green dots indicate the proteins expressed in HEK-293T cells for the corresponding assay.

5.4 Discussion

5.4.1 CD3ε ITAM-membrane interaction does not prevent phosphorylation

The results here described suggest that membrane interaction does not play the protective role in CD3ε phosphorylation that was initially proposed [224, 229, 301]. Recent work has shown that the acidic phospholipid phosphatidylserine is enriched in membrane sheets isolated from activated T cells using beads coated with anti-CD3 antibodies [311], but the extent to which this reflects the distribution of lipids in the immediate vicinity of the TCR in resting or activated cells is unclear. The density or properties of the acidic lipids adjacent to CD3ε in resting cells might be insufficient to sustain an interaction of the type demonstrated in vitro by Xu *et al*. The interaction between ITAMs and cell membranes in vivo might be too weak and/or dynamic to prevent access of the Src kinases. In fact, a mutant form of CD3ε, Emut1+2, which does not interact with the cell membrane, is not phosphorylated when expressed in Jurkat T-cells. The wild-type CD3ε and the Emut1+2 mutant were, however, readily phosphorylated upon inhibition of phosphatase activity. Although experiments with pervanadate indicate that PTPs are involved in regulating CD3 ITAM phosphorylation it does not allow us to understand what is the contribution of specific PTPs known to be involved in TCR triggering, such as CD45 [300, 312-314], in controlling CD3 ITAM phosphorylation. This matter is taken up in the next chapter.

5.4.2 What could be the functional role of CD3ε CD interaction with the cell membrane?

Mutation of the positively charged residues present in $CD3\varepsilon_{CD}$ led to a delayed phosphorylation of CD3ε ITAM when compared to wild-type CD3ε. Furthermore, activation of cells expressing KIR2DL3/$CD3\varepsilon_{CD}$ Emut 1+2 through antibody crosslinking showed almost 50% lower IL-2 promoter activity when compared with cells expressing KIR2DL3/$CD3\varepsilon_{CD}$ wild-type. Both results

suggest that contrary to initial expectations, interaction between CD3ε_{CD} and the cell membrane might promote ITAM phosphorylation. It was also found that under pervanadate treatment, Lck played a key role in ITAM phosphorylation.

A reduction in both ITAM phosphorylation levels and IL-2 promoter activity for CD3ε Emut 1+2 suggests that membrane interaction of CD3ε_{CD}, mediated through the positively charged residues favours a more efficient recognition of the tyrosines present in the ITAM motif by the Lck kinase domain. The molecular mechanism that could explain these results is not known, but some insight might be gained by a closer look at the structural information available for CD3ε_{CD}. UV circular dichroism measurements have shown that the cytoplasmic domain of CD3ε behaves as an unstructured polypeptide when present in solution [224, 226, 228, 302]. However, addition of positively charged lipids significantly alters the 3D conformation of CD3ε_{CD} [224, 226, 228, 302]. From the NMR-derived structure for CD3ε_{CD} bound to DHPC/POPG bicelles it is striking that not only the tyrosine residues from the ITAM are embedded into the hydrophobic, acyl chain, region of the lipids, but also that the majority of the positively charged residues in CD3ε_{CD} interact with the polar groups on phospholipids (Fig. 5.8). This phospholipid-induced structure of the CD3ε_{CD}, possibly driven by charge-charge interactions, could perhaps promote a secondary structural conformation that is more easily recognized by Src kinases.

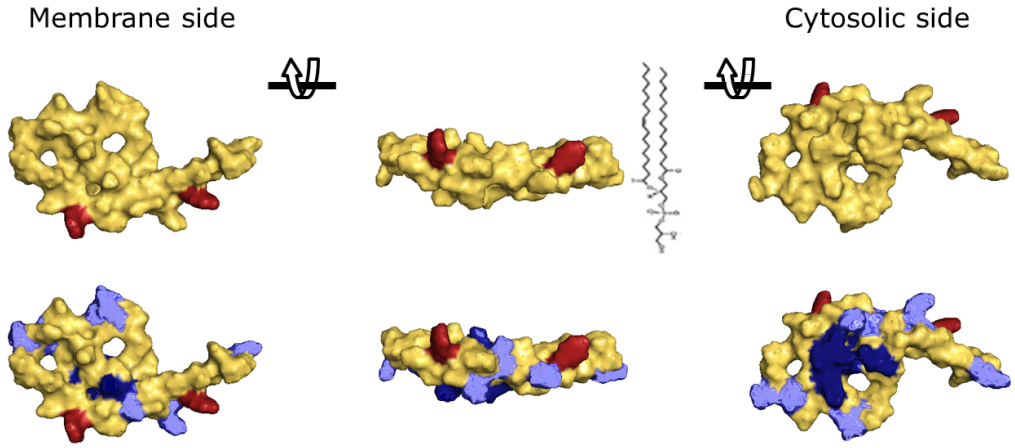

Figure 5.8: Asymmetric distribution of charged residues in CD3ε_{CD} upon interaction with lipid bicelles. NMR structure of CD3ε_{CD} interacting with DHPC/POPG bicelles shows that most of the positively charged residues (coloured blue; mutated residues in this study are coloured dark blue), face the cytosol (*left panel*), conferring a secondary structural conformation that could favour Tyr recognition by Src kinases. ITAM tyrosine residues are coloured in red.

Chapter 6

Global homeostatic control of TCR phosphorylation and local ultra-sensitive processes

6.1 Introduction

6.1.1 Understanding the role of CD45 in TCR triggering

In this study, a specific phosphatase has been tested for its role in TCR triggering. As discussed in Chapter 5, membrane association of the CD3 ITAMs does not appear to protect them from Lck phosphorylation [315]. Blocking phosphatase activity with pervanadate induced strong tyrosine phosphorylation of the CD3ε ITAM, suggesting that tyrosine phosphatases are involved in controlling overall phosphorylation levels of these signalling motifs. However, the broad specificity of pervanadate does not allow us to infer the role of specific phosphatases in controlling TCR triggering. Among the membrane tyrosine phosphatases present in T-cells, CD45 is a major candidate for involvement in TCR triggering. CD45 has been shown to influence TCR signalling and T-cell activation, but how CD45 does it is still a matter of debate [67, 175, 178, 186, 187, 304, 306, 312, 316].

Previous studies have mainly focused on the ability of CD45 to control Lck activity through dephosphorylation of its Tyr394 and Tyr505 residues [187, 188, 316-321]. The ability of CD45 to directly control tyrosine phosphorylation of CD3 ITAMs has been generally overlooked, although it has already been shown that CD45 can dephosphorylate CD3ζ, *in vitro* [191]. In Chapter 5 (§ 5.3.3) it was found that expressing CD45 in HEK-293T cells expressing Lck Y505F and a membrane bound form of CD3ε reduced ITAM phosphorylation, an indication that CD45 can also control tyrosine phosphorylation of CD3ε ITAM. The paucity

of methods available to study phosphatases in general, and in this particular case CD45, has often led to conflicting results and may have delayed a more comprehensive understanding of its role in TCR triggering [186, 187, 312]. In this study a new approach has been developed, based on the lentiviral-mediated delivery of shRNA targeting CD45 phosphatase, in order to probe the role of this tyrosine phosphatase in TCR triggering. This approach allowed us to correlate changes in protein expression and protein phosphorylation, directly related to T-cell triggering, with CD45 down-regulation.

6.2 Materials and methods

6.2.1 Plasmid construction

Cloning shRNA

The shRNA sequences targeting CD45 and TCRβ mRNA were designed after searching for the following pattern in the target mRNA:

N2[GC]N[A]N6[UT]N2[ATUC]N5[A]N2 (where N is any ucleotide)

The siRNA expression plasmid consists of a nucleotide sense sequence (identical to the target sequence in the mRNA to be down-regulated), followed by a loop, TTCAAGAGA, an antisense sequence, and a stretch of five Ts (T5) as a pol III transcriptional termination signal, downstream from a U6 promoter. Complementary overhangs from *BamHI* and *EcoRI* were included to allow insertion into plasmids digested with these enzymes. The final DNA sequence, and its complementary reverse, was ordered as a custom designed primer (Sigma-Aldrich Co.). The two DNA primers were mixed 1:1 and heated to 95°C and allowed to cool slowly to 10°C. The double-stranded DNA sequence was then cloned into the pHR-U6P lentiviral vector.

The final DNA sequences for CD45 and TCRβ were:

CD45:

5'-gatccGTACACCTCTACTCATTCATTCAAGAGATGAATGAGTAGAGG TGTACTTTTTTACGCGTg-3'

TCRβ

5'-gatccGACTGGAGTTGCTCATTTATTCAAGAGATAAATGAGCAACTCC AGTCTTTTTTACGCGTg-3'

Cloning Lck mutant Y505F

Lck was amplified with appropriate primers, including a modification of the reverse primer that encoded a mutation in the codon corresponding to Tyr 505, which was changed to Phe. After amplification, the DNA was digested with *MluI* and *BglII* and cloned into the pHR lentiviral vector. The final construct was sequenced to check reading frame and integrity.

Cloning HA-CD43-FKBP and mouse cytoCD45-FRB

The FKBP and FRB sequences were amplified from appropriate vectors, obtained from ARIAD Pharmaceuticals, Inc., Massachusetts, USA. FKBP was digested with *BamHI* and *NotI* and cloned, in frame, at the C-terminus of a sequence encoding HA-CD43 protein, immediately after the end of the transmembrane domain of CD43. FRB was amplified with appropriate primers, digested with *MluI* and *BamHI* and cloned, in frame, into a plasmid encoding the cytoplasmic domain of mouse CD45. Both constructs were sequenced to check reading frame and integrity.

6.2.2 Cell culture, isolation and lentiviral infection

Cell culture and $CD3^+CD4^+$ T-cell isolation from PBLs

Jurkat T-cells were maintained in RPMI, 10% FCS, 2% Glutamine, Hepes, Sodium Pyruvate and appropriate antibiotics. Cells were kept between 1-9x10^5

cells/ml. $CD3^+CD4^+$ cells were isolated from PBLs, using the $CD4^+$ T-cell Isolation Kit (Miltenyi Biotec), according to the manufacturer's instructions.

Lentiviral infection of Jurkats and PBL with shRNA

Following 48 hours of lentiviral production, 1 (low), 2 (intermediate) or 4 (high) ml of supernatant from HEK-293T cells in 6-well plates was collected, centrifuged at 3500 rpm for 5 min and added to $1x10^6$ Jurkat T-cells, in a total of 6 ml, adding RPMI, 10% FCS as required. Cells were tested for surface expression of determined proteins by FACS at different time points following infection. $CD3^+CD4^+$ cells were infected with the equivalent of 12 ml of lentiviral supernatant, which was concentrated at 70,000g for 2 hours at 4°C in a sucrose gradient. The lentiviral pellet was resuspended in 200 µl of PBS for 2 hours at 4°C and added to freshly isolated cells. At the time of lentiviral infection cells were stimulated with 1 µg/ml of PHA (Sigma) and IL-2. Seven days post-lentiviral infection the cells were analysed by FACS.

6.2.2 FACS analysis and kinase assay

FACS analysis

For FACS analysis $1x10^6$ cells were washed in PBS/0.05% azide, and labelled, on ice in the dark for 45 min. For surface labelling the following antibodies were used, as appropriate: anti-CD45alexa488 or alexa647, (Clone F10-89-4, AbD Serotec), anti-CD69alexa647, anti-CD69-PECy7 (clone FN50, eBioscience), anti-CD3ε-alexa488 or alexa647 (purified from hybridoma supernatant, clone UCHT1, labelled with antibody labelling kit from Molecular Probes, Invitrogen), anti-Lck (clone 73A5, Cell Signalling), anti-ZAP-70-APC (clone 1E7.2, eBioscience) and anti-LAT-APC (clone LAT.10-17, eBioscience). For intracellular staining of Lck, ZAP, and LAT, $1x10^6$ cells were washed in PBS/0.05% azide, and fixed in 500µl of 1% formaldehyde for 15 min. at room temperature. Following fixation, cells were washed in permeabilization buffer (0.5% Saponin, 3% FCS, 1% BSA, PBS)

twice. Cells were then incubated on ice, for 90 minutes with appropriate dilutions of the antibodies. After labelling, cells were washed three times in permeabilization buffer. For Lck, cells were labelled with secondary antibody, donkey anti-rabbit-APC (Molecular Probes, Invitrogen) for 45 minutes on ice, in the dark and then washed with permeabilization buffer as before. For surface and intracellular staining, the cells were washed and labelled with antibodies directed to CD45 or CD69 on ice for 45 minutes in PBS/0.05% azide, followed by a washing step with ice-cold PBS/0.05% azide and fixation with 1% formaldehyde. Intracellular staining procedure was then resumed as described.

Kinase Assay

Lck from $50x10^6$ Jurkat T-cells was immunoprecipitated with 10 µl of a rabbit anti-Lck antibody (clone 3A5, Cell Signalling Technology) following cell lysis in 500 µl of lysis buffer (140mM NaCl, 10mM Tris-HCl, 2mM EDTA, 1% NP-40, 1mM sodium orthovanadate, 1x Protease Inhibitor Cocktail, 1mM PMSF and 1x Phosphatase inhibitor cocktail, all from Sigma-Aldrich Co.), and centrifugation at 13,000 rpm for 10 minutes at 4°C. Antibody was incubated with pre-cleared lysate solution for 1 hour on ice followed by 1 hour incubation at 4°C with constant agitation with 40 µl of Protein A/G agarose Plus beads (Santa Cruz Biotech.). Beads were washed four times with lysis buffer and resuspended in 50 µl of ice-cold PBS, 1mM of PNPDYEPIRKGQRGLYSGLNQR CD3ε-peptide solution or the peptide PNPDY*EPIRKGQRGLY*SGLNQR, where Y* represents phosphorylated tyrosine for 1 hour, on ice. Following this incubation the beads were washed twice in ice-cold PBS and incubated with 2.5µg of acid-denatured rabbit enolase (Sigma-Aldrich Co.) and kinase buffer (5mM Hepes, 1mM MnCl2, 20µM Sodium orthovanadate, 10µM ATP, all from Sigma-Aldrich Co.). Beads in kinase assay buffer were incubated for 10 minutes at 37°C and the reaction was terminated with 50µM of non-reducing SDS loading buffer. Samples were aliquoted and stored at -80°C.

6.3 Results

6.3.1 Down-regulation of CD45 protein expression with shRNA

To specifically suppress CD45 activity an approach based on lentiviral-mediated delivery of a shRNA targeting CD45 mRNA (shCD45) was developed (Fig. 6.1a). In order to drive efficient expression of the shRNA the pHR-SIN plasmid was adapted by changing the SFFV promoter for an RNA polymerase III promoter, U6. The pHR-SIN-U6P was a kind gift of Professor Alain Townsend, WIMM, University of Oxford.

The design of shRNA targeting CD45 was based on a pattern derived from the Reynold algorithm which retrieves high scoring sequences corresponding to: N2[GC]N[A]N6[UT]N2[ATUC]N5[A]N2 (where N is any base-pair, and a single base-pair can be chosen from the ones present inside brackets). This pattern was then used as a selection criterion to search for candidate shRNA targets in CD45 mRNA using the Si Selection Program at the Whitehead Institute for Biomedical Research, MA, USA (http://jura.wi.mit.edu/bioc/siRNAext/ home.php). Of the possible 27 targets retrieved with this analysis, the sequence 5′ – GTACACCTCTACTCATTCA - 3′ was chosen based on: (1) the high score in both Reynold and Stockholm rules; (2) the high scoring for theoretical shRNA efficiency obtained using the algorithm developed by Matveeva *et al*, and available on http://gesteland.genetics.utah.edu/siRNA_scales/; and (3) because it targets a sequence in CD45 mRNA corresponding to the intracellular domain of the protein and is thus present in all CD45 isoforms.

Three days after lentiviral vector-mediated delivery of shRNA against CD45 into Jurkat T-cells it was possible to detect a reduction in CD45 expression at the cell surface (Fig. 6.1b). Six days after lentiviral infection, the expression level of CD45 stabilized at levels that were dependent on the amount of lentiviral supernatant used to infect cells (Fig. 6.1c,d). Jurkat cells infected with high levels of lentivirus showed a 7-10 fold reduction in CD45 expression and were stable for 10-15 days. Soon thereafter, however, the majority of cells died.

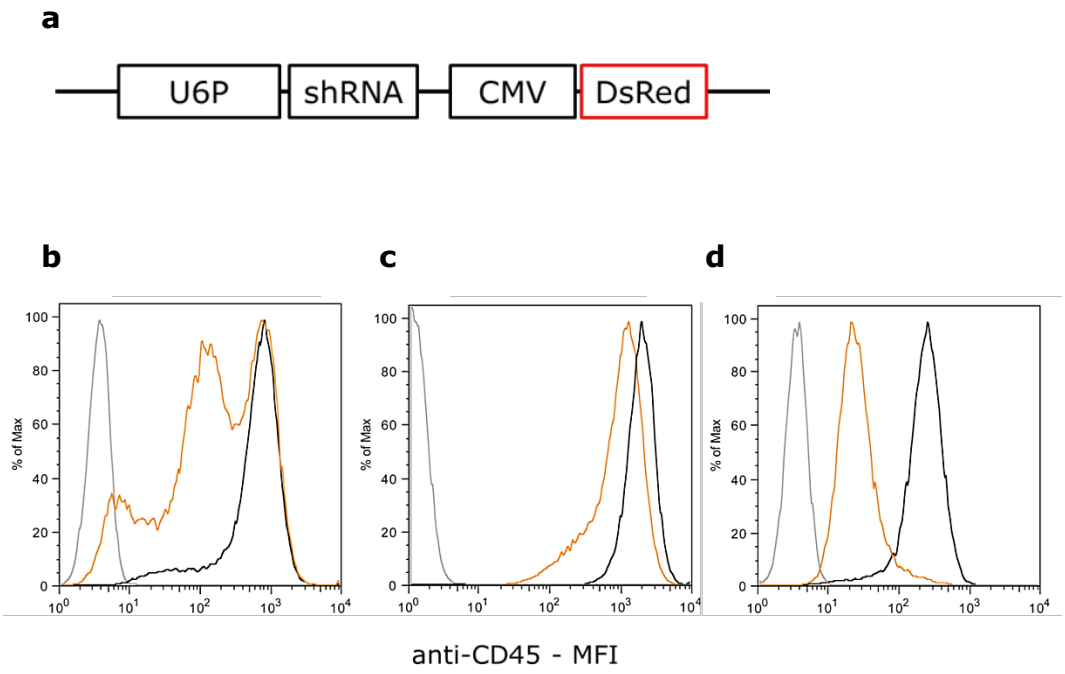

Figure 6.3: Lentiviral-mediated delivery of shRNA targeting CD45 mRNA, shCD45, downregulates CD45 expression at the surface of T cells. **(a)** To induce efficient shCD45 the SFFV promoter of pHR was changed for a polymerase III promoter, U6. **(b)** Three days following lentiviral infection of Jurkat cells with shRNA plasmid, down-regulation of CD45 could already be detected. CD45 down-regulation levels, 6 days after lentiviral infection, were dependent on the amount of lentivirus used to infect the cells. **(c)** Low levels of lentivirus induced marginal CD45 down-regulation, whereas high levels (four-fold more lentivirus) induced stronger down-regulation **(d)**. In **(b)**, **(c)** and **(d)**, isotype control is coloured in grey, wild-type Jurkats in black and Jurkats with shRNA in orange.

6.3.2 A decrease in CD45 expression is accompanied by an increase in TCR phosphorylation

In order to probe the effects of CD45 on TCR phosphorylation the shCD45 was used to create a cell line where CD45 expression was almost absent. Because Jurkats expressing shRNA against CD45 were unstable when CD45 expression fell below 20% of that of wild type cells, J45.01 cells [322], which express around 10-15% of CD45 as compared with wild-type Jurkats, were infected with shCD45. Upon infection with the shRNA, CD45 expression could not be detected by FACS on this new cell line, J45.01-shCD45 (Fig. 6.2a). Down-regulation of CD45 expression was stable and cells divided normally for long periods of time. The parental cell line, J45.01, cannot be triggered with antibody crosslinking, but is not completely signalling deficient as these cells can be stimulated by PMA and ionomycin to secrete IL-2 [322]. To test if CD45 expression levels were affecting TCR phosphorylation, CD3ε was immunoprecipitated with UCHT1 antibody from Jurkats, J45.01 and J45.01-shCD45, and probed with anti-phospho-Tyr antibody. Cells with lower levels of CD45 expression showed higher CD3ε ITAM phosphorylation (Fig. 6.2b).

6.3.3 Down-regulation of CD45 expression induces CD69 expression

In order to understand the functional consequence of an increase in TCR ITAM phosphorylation, Jurkat cells infected with shCD45 were probed for CD69 expression, an early marker for T cell activation. Cells were labelled with an anti-CD45-alexa488 antibody together with an anti-CD69-PE-Cy7 antibody and the extent of labelling was quantified by FACS, six days after lentiviral delivery of shCD45. CD69 was found to be strongly up-regulated in the cells expressing the lowest levels of CD45 (Fig. 6.3). To determine if CD69 up-regulation in response to CD45 down-regulation was a Jurkat-specific or a universal response to CD45 down-regulation, the same approach was applied to freshly isolated $CD3^+CD4^+$

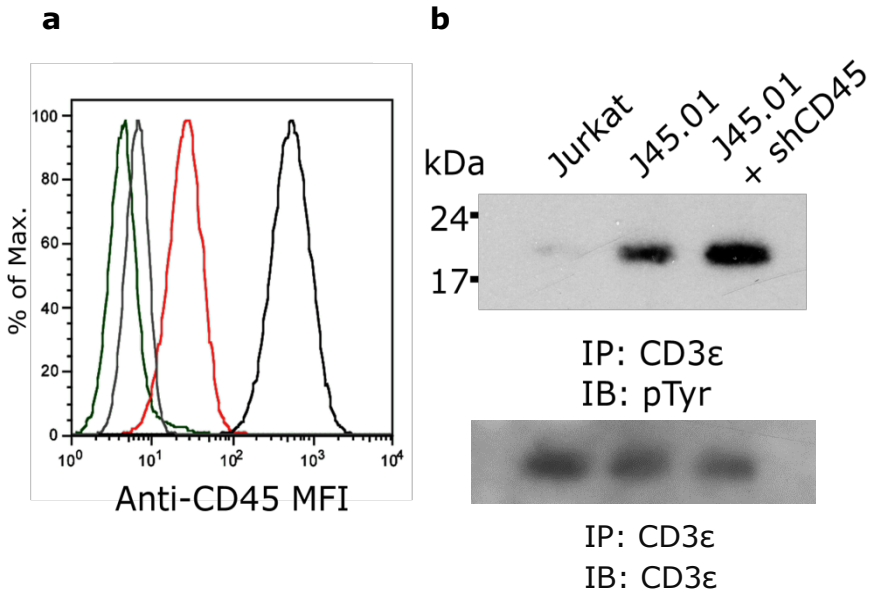

Figure 6.2: CD3ε pTyr is dependent on CD45 expression level. **(a)** Lentiviral infection of J45.01 (red line) with shCD45 generated a cell line negative for CD45 expression (green line). Jurkat T-cells express high levels of CD45 (black line; isotype control, grey line). **(b)** Immunoprecipitation of CD3ε from the cell surface shows that the decrease in CD45 expression leads to an increase in CD3ε phosphorylation.

T-cells from peripheral blood leukocytes (PBLs; Fig. 6.4a). Immediately after isolation from the PBL pool, $CD3^+CD4^+$ cells were activated with PHA (to induce cell division and promote lentiviral infection) and infected with lentivirus to deliver the shCD45 plasmid. Seven days after lentiviral infection, expression of CD45 and CD69 was quantified by FACS. Similar to the results obtained with Jurkat cells, down-regulation of CD45 led to an up-regulation of CD69 expression (Fig. 6.4b).

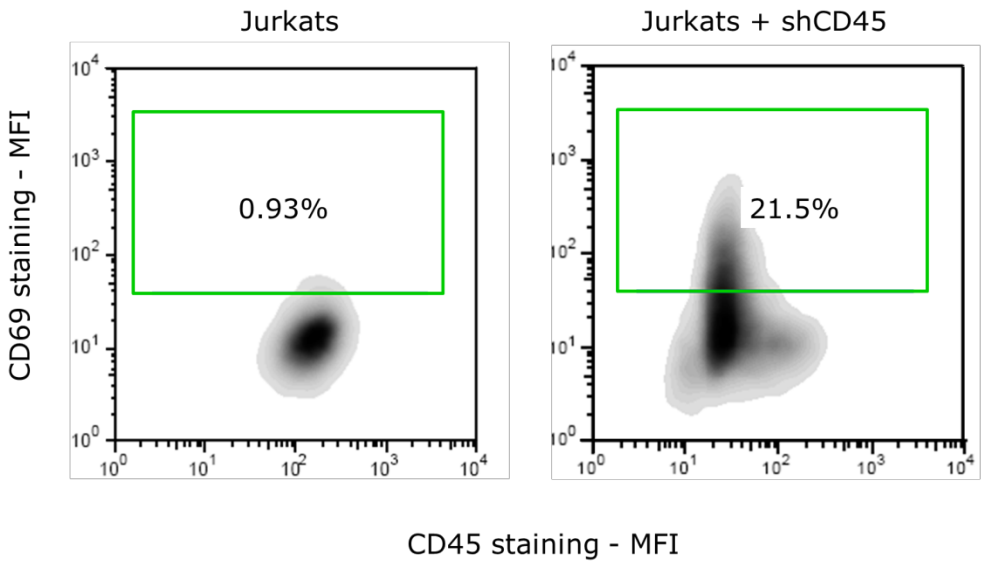

Figure 6.3: Down-regulation of CD45 induces CD69 expression. Six days following lentiviral infection of Jurkat cells with shCD45, cells were labelled with anti-CD69 and anti-CD45. Cells with reduced CD45 showed an up-regulation of CD69. Data shown is representative of six independent experiments.

6.3.4 Up-regulation of CD69 in response to CD45 down-regulation is reverted by expression of mouse CD45

The shRNA against CD45 was found to target at least 179 mRNAs in cells of human origin (determined using siRNA at Whitehead: http://jura.wi.mit.edu/bioc/database). This lack of specificity is a common problem found when using shRNA. To determine if the up-regulation of CD69 was a specific response to the down-regulation of CD45 or an off-target effect of the shRNA used, mouse CD45 (mCD45) was expressed in cells with down-regulated human CD45. Mouse and human CD45 share a high degree of similarity in the two phosphatase domains, however, the shRNA designed is specific for human CD45 and has low complementarity with the mouse CD45 mRNA sequence (Fig. 6.5a). The expression of mCD45 together with shCD45 in Jurkat cells decreased the up-

regulation of CD69 up to 85% as compared with Jurkats expressing shCD45 only (Fig. 6.5b, c). This decrease in CD69 up-regulation was dependent on the expression levels of mCD45 (Fig. 6.5c).

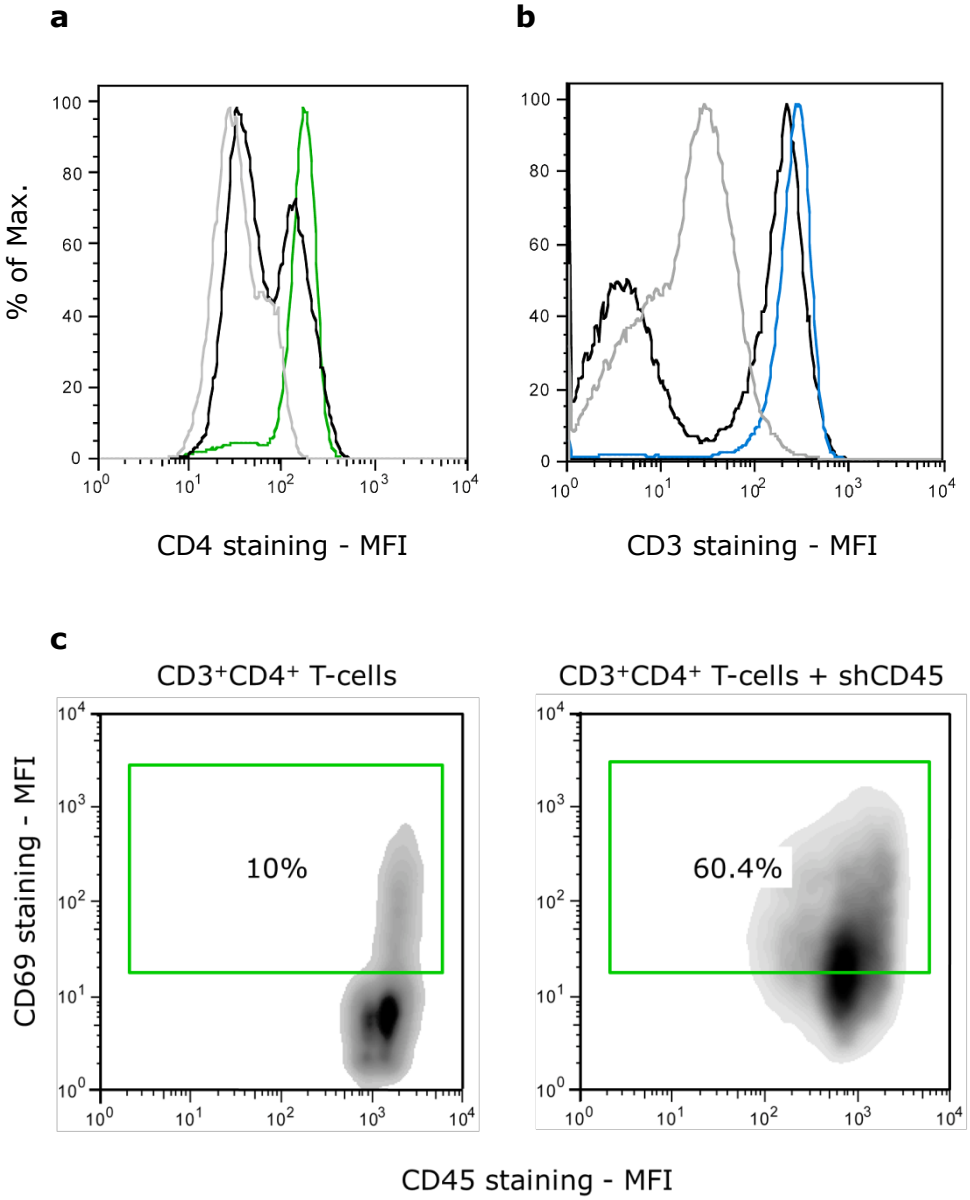

Figure 6.4: CD3+CD4+ isolated from PBL also showed an up-regulation of CD69 in response to shCD45. After isolation of CD3+CD4+, cells were labelled with anti-CD3 and anti-CD4 for FACS analysis. The isolated cells were found to be positive for CD4 (green, **(a)**; PBL, black line; isotype control, grey line) and for CD3 (blue, **(b)**). **(c)** Seven days following shCD45 expression, CD69 was found to be markedly up-regulated. Data shown is representative of three independent experiments.

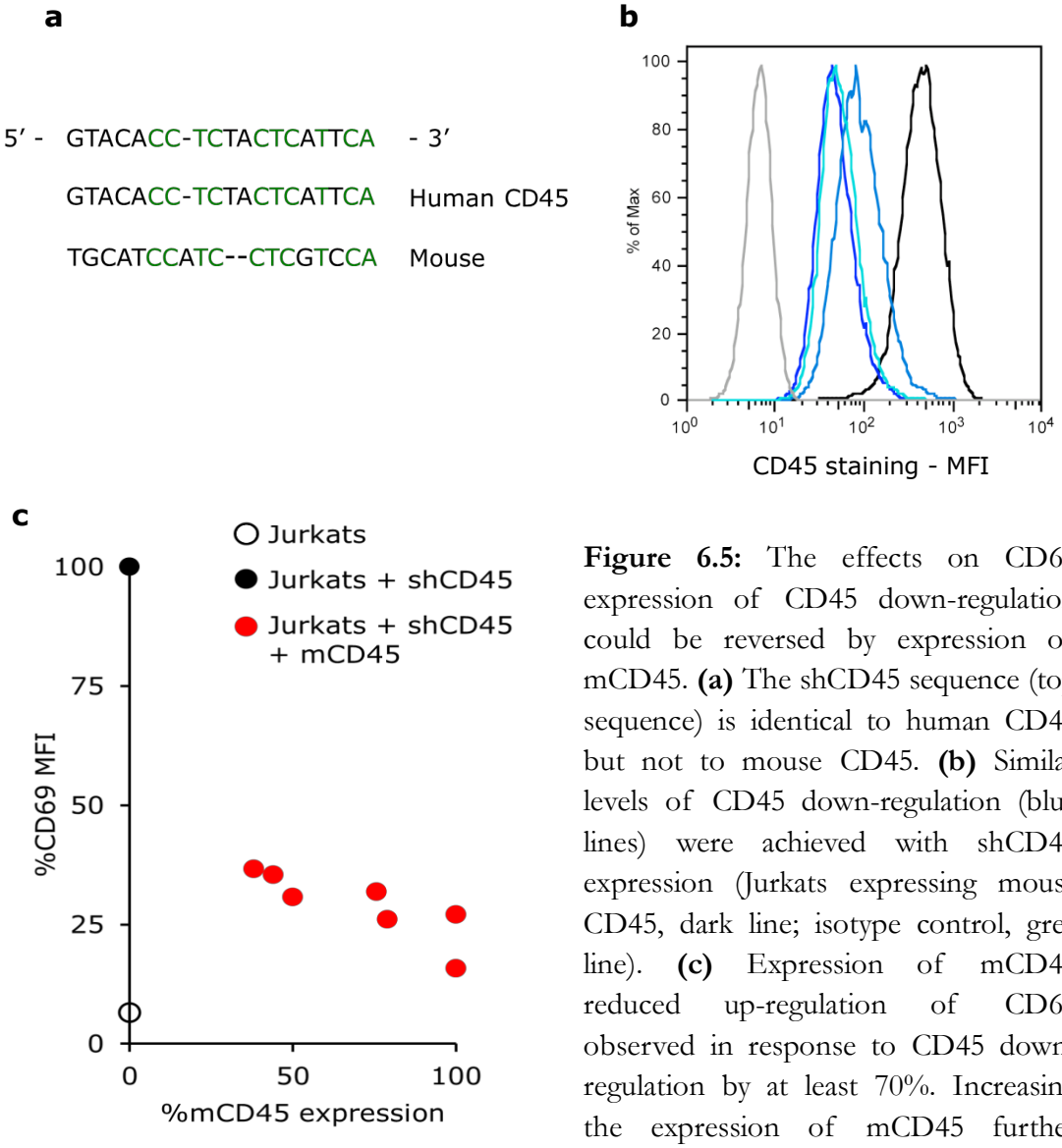

Figure 6.5: The effects on CD69 expression of CD45 down-regulation could be reversed by expression of mCD45. **(a)** The shCD45 sequence (top sequence) is identical to human CD45 but not to mouse CD45. **(b)** Similar levels of CD45 down-regulation (blue lines) were achieved with shCD45 expression (Jurkats expressing mouse CD45, dark line; isotype control, grey line). **(c)** Expression of mCD45 reduced up-regulation of CD69 observed in response to CD45 down-regulation by at least 70%. Increasing the expression of mCD45 further reduced the expression of CD69 in response to shCD45. Data from three independent experiments is shown. The percentage of CD69 expression shown is relative to wild-type Jurkats infected with shCD45.

A different approach was then developed to understand if the effect observed with expression of mCD45 was dependent on the intracellular location of the phosphatase activity, *i.e.*, if it was dependent on an increase in tyrosine phosphatase activity at the cell membrane of Jurkat T-cells. A new cell line was made expressing HA-CD43TM-FKBP and the cytoplasmic domain of mCD45 with an FRB domain at the N-terminus. FKBP and FRB domains can be dimerized upon addition of a Rapalog, such as AP-21967 [323]. Without AP-21967, FRB- mCD45 would be present in the cytoplasm. However, upon addition of the Rapalog, mCD45 would be recruited, through the FRB domain, to the membrane where it associates with the FKBP protein present in the intracellular C-terminal part of the HA-CD43TM protein (Fig. 6.6a). After establishing this cell line, human CD45 was down-regulated using shCD45, as previously described, and increasing concentrations of AP-21967 were added to the cells. As before, both CD45 and CD69 expression were quantified by FACS six days following lentiviral-mediated delivery of the shCD45 plasmid. AP-21967 is a chemically modified derivative of rapamycin and thus has immunosuppressive activity, although 1000-fold less than rapamycin [323]. Because of this immunosuppressive effect of AP-21967, wild-type Jurkat cells were also included in this experiment and treated in similar way to Jurkat cells expressing HA-CD43TM-FKBP plus FRB-mCD45. In fact, upon down-regulation of CD45, addition of AP-2196 to Jurkat cells led to a 25% decrease in CD69 expression, as compared to untreated cells (Fig. 6.6b). However, in cells expressing HA-CD43TM-FKBP and FRB-mCD45, addition of AP-2196 decreased CD69 expression up to 70% (Fig. 6.6b). The decrease in CD69 expression upon CD45 down-regulation observed with the AP-2196 treatment was also found to be dependent on the concentration used (Fig. 6.6b).

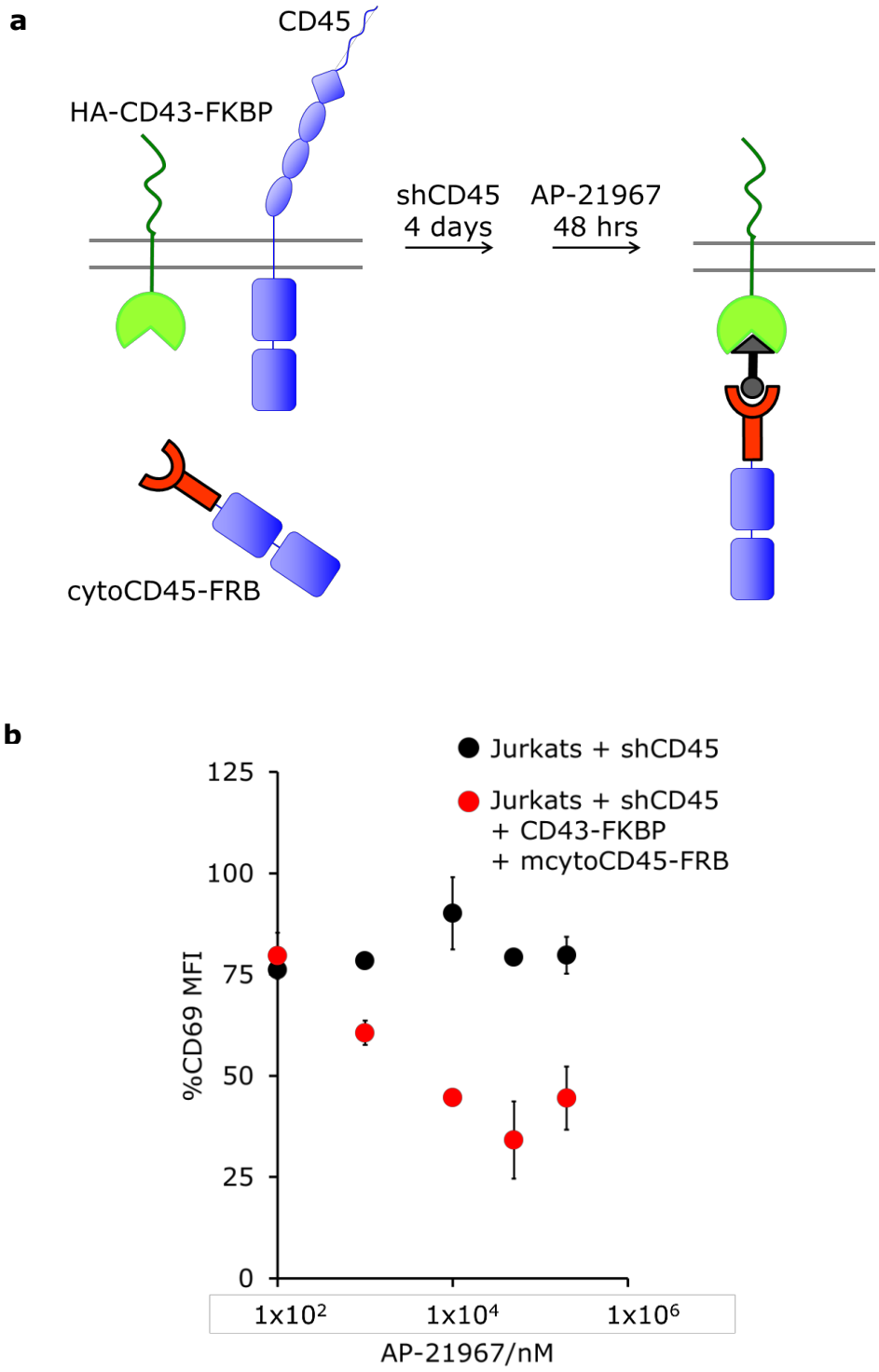

Figure 6.6: Recruitment of mCD45 to the cell membrane reduced expression of CD69 in response to shCD45. **(a)** A chimeric protein expressed at the cell membrane, HA-CD43TM-FKBP, was expressed in Jurkat T-cells together with the cytosolic domain of mCD45 fused to FRB domain. The Rapalog, AP-21967, induces dimerization between FKBP-FRB proteins, and thus addition of the Rapalog, recruits mCD45 to the cell membrane. **(b)** Recruitment of mCD45 to the membrane reduces expression of CD69 upon CD45 down-regulation. Increasing AP-21967 concentration further reduces CD69 expression. The means of two experiments ± S.E. are shown.

6.3.5 CD69 up-regulation in response to CD45 down-regulation is dependent on TCR expression

Several proteins at the cell membrane of T cells have signalling motifs that share a high degree of similarity with those present in CD3 ITAMs and can therefore be under the influence of CD45 phosphatase activity. It is therefore likely that during CD45 down-regulation other receptor proteins also undergo an increase in the half-life of their phosphorylated tyrosine signalling motifs. The contribution of these receptors to the up-regulation of CD69 is difficult to dissect, but it is important to understand if phosphorylation of CD3 ITAMs plays the main role in inducing CD69 expression. Two different experimental approaches were developed to test the contribution of TCR to the up-regulation of CD69 in response to CD45 down-regulation. Expression of CD45 in J.RT3 cells, which lack TCRβ chain and thus lack TCR expression at the cell surface, was down-regulated, as before, with shCD45. In these cells CD69 up-regulation was 25% or less of that detected in Jurkat cells (Fig. 6.7). Expressing TCRβ in these cells reconstituted TCR expression and upon down-regulation of CD45 it was now possible to detect higher levels of CD69 at the cell surface (Fig. 6.7). However, to avoid interference from possible differences between J.RT3 and Jurkats (*e.g.* J.RT3 also lack expression of CD28), a shRNA targeting 5′-GACTGGAGTTGCT CATTTA-3′ sequence of TCRβ mRNA was used to down-regulate TCR expression in wild-type Jurkat cells (Fig. 6.7). The shTCRβ was developed in the manner of shCD45 and delivered to the cells in identical fashion. Jurkat T-cells with decreasing levels of TCR expression at the cell surface were found to have increasingly lower levels of CD69 in response to CD45 down-regulation (Fig. 6.7). For both J.RT3 and Jurkats with shTCRβ, comparable levels of CD45 down-regulation were induced (Fig. 6.7).

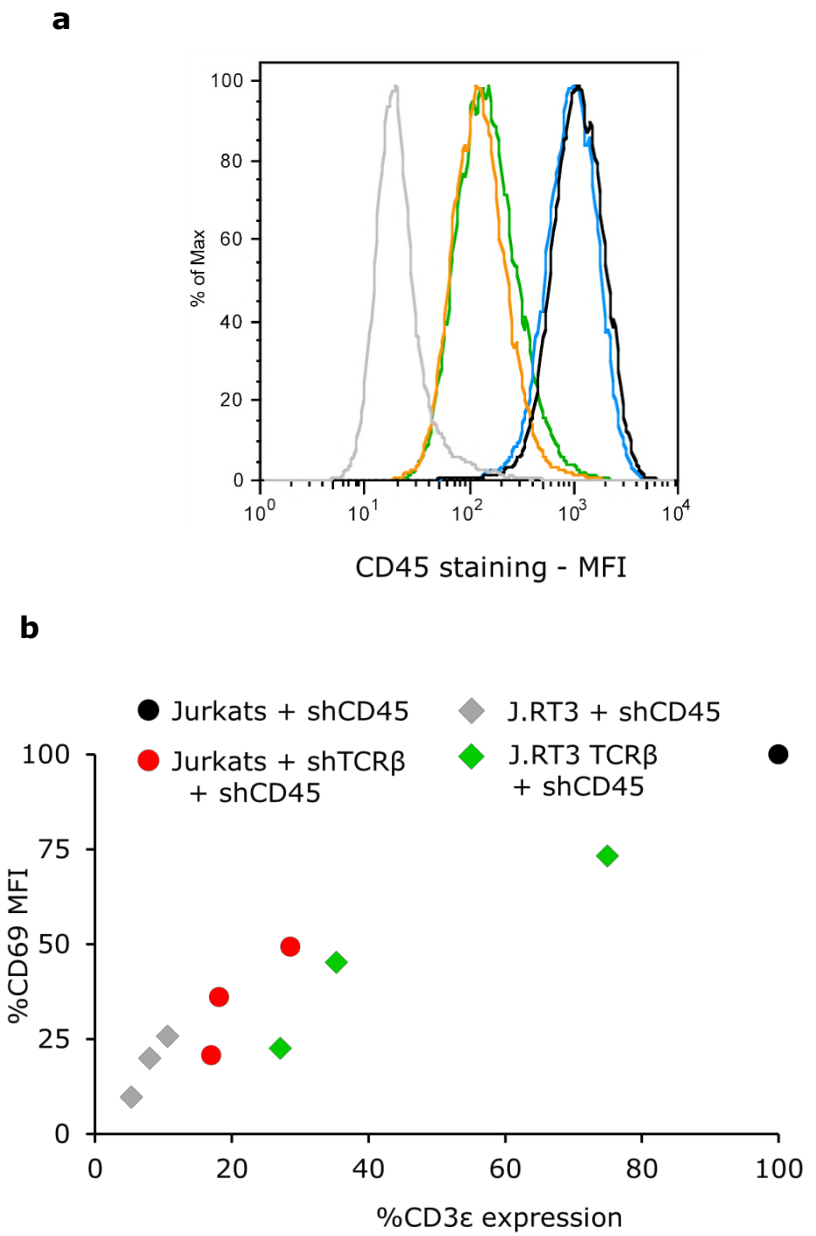

Figure 6.7: CD69 up-regulation in response to shCD45 is dependent on TCR expression. **(a)** Jurkat expressing shTCRβ (black line) and J.RT3 expressing TCRβ (light blue line) were infected with shCD45 plasmid (Jurkat+shCD45, orange line; J.RT3+shCD45, green line; isotype control, grey line). Similar levels of CD45 down-regulation were obtained between different cells. **(b)** Increasing TCR expression in J.RT3 leads to increasing CD69 expression in response to shCD45. In Jurkat T-cells, reducing TCR expression using shTCRβ reduces expression of CD69. CD69 and CD3 expression are shown relative to wild-type Jurkats+shCD45. Data from three independent experiments is shown.

6.3.6 Homeostatic control of protein expression in response to changes in kinase versus phosphatase activity in T cells

Jurkat T-cells infected with intermediate levels of shCD45 progressed to generate two well defined populations in respect to CD45 expression: one that had levels of CD45 expression close to wild-type cells and another with around 10% of CD45 expression (Fig. 6.8a). Surprisingly, both populations were found to be stable for a long period of time in culture, after an initial stage of extensive cell death following expression of shCD45. Furthermore, the levels of CD69 on these cells were low (Fig. 6.8b). The existence of stably growing cells with low levels of CD45 and CD69, was not expected since Jurkat T-cells infected with high levels of shCD45 strongly up-regulated CD69 and were never found to survive beyond 15 days after shCD45 expression. It thus seemed that, given enough time, cells could adapt to CD45 down-regulation.

Lck expression seemed a good candidate for being linked to the global levels of phosphorylation in a T cell. The rationale behind this hypothesis followed from the well-known role of Lck kinase in phosphorylating CD3 ITAMs [298] during TCR triggering [101]. To maintain overall levels of TCR triggering a reduction in CD45 could be counteracted by a reduction in Lck activity, *i.e.* expression. Jurkat cells growing in culture for 15 days following intermediate shCD45 lentiviral infection, and thus with two distinct populations expressing different CD45 levels were probed for Lck expression by intracellular FACS staining. As proposed, cells with reduced CD45 had lower levels of Lck (Fig. 6.9). Addition of PP2 overnight to these cells led to an increase in Lck expression (Fig. 6.9) Again, this result seemed to indicate that a tight balance between kinase and phosphatase activity is present in T cells.

If changes in overall kinase/phosphatase activity can be sensed by cells, and somehow be compensated for, in order to maintain a steady equilibrium, it is expected that inducing changes in kinase activity will also induce compensatory changes. To understand if this is the case, wild-type Lck, and a mutant form of this kinase, where the Tyr505 was mutated to a Phe, Lck Y505F, were expressed

in J.CaM 1.6 cells, which lack Lck expression. To confirm that the expressed forms of Lck, wild-type and Lck Y505F, were active in J.CaM 1.6 cells a stimulation assay with plate-bound OKT3 was used. Six hours following stimulation, the level of activation induced by OKT3 simulation was determined by an IL-2 reporter system, based on the quantification of luminescence from *Renilla Luciferase*, which is expressed under control of the IL-2 promoter. As expected from the literature [97, 324], Lck Y505F induced stronger T-cell activation than wild-type Lck (Fig. 6.10a). Wild-type J.CaM 1.6 cells were also found to become activated but only at higher concentrations of OKT3, likely through the action of other Src kinases present in these cells that can substitute for Lck absence, *e.g.* Fyn, which, nevertheless, seem to be less efficient than Lck, in good agreement with observations made by others [66, 68, 325]. The expression level of proteins involved in early stages of TCR triggering was then quantified by FACS for four different cell lines: Jurkats, J.CaM 1.6, J.CaM Lck and J.CaM Lck Y505F, six days after expression of the different forms of Lck. Upon expression of Lck in J.CaM 1.6 cells, and more pronouncedly for the Lck Y505F, TCR and ZAP-70 were found to be down-regulated, whereas CD45 was up-regulated. Expression of LAT did not seem to be affected by Lck.

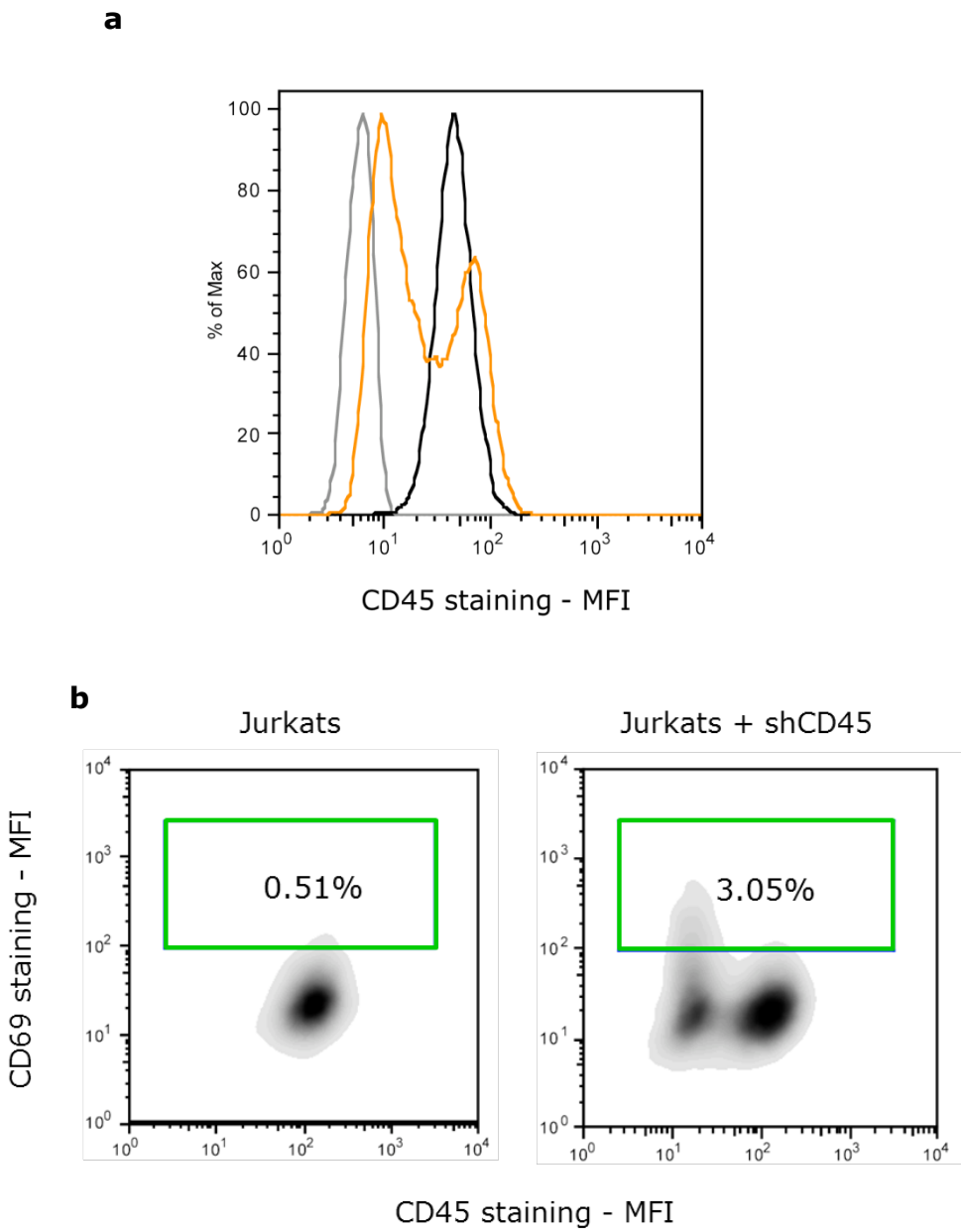

Figure 6.8: Cells infected with intermediate levels of shCD45 show the presence of two clear populations, according to CD45 expression. **(a)** Two weeks following infection of Jurkat cells (black line) with intermediate levels of shCD45 (orange line) the cells were found to have either low or high levels of CD45 (isotype control, grey line). **(b)** In cells with low levels of CD45, expression of CD69 could be detected, albeit at low levels (see Fig. 6.3 for comparison). Data shown is representative of three independent experiments.

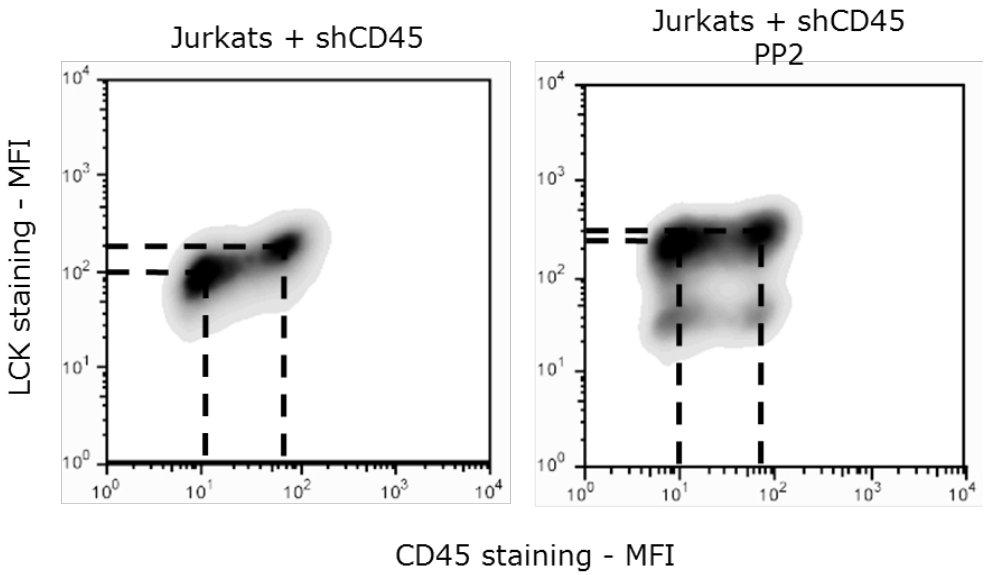

Figure 6.9: Jurkat T-cells adapted to low levels of CD45 expression were found to have low levels of Lck expression. Two weeks following infection of Jurkat T-cells with intermediate levels of shCD45 (see Fig. 6.8) the cells were probed by intracellular staining for Lck expression. The population of cells with low levels of CD45 expression also had low levels of Lck (left panel). Dotted lines are used for comparison of expression levels between the two different populations according to CD45 expression. Incubation of these cells with Lck kinase inhibitor, PP2, at 10μM, overnight, led to an up-regulation of Lck expression (right panel). Data shown is representative of three independent experiments.

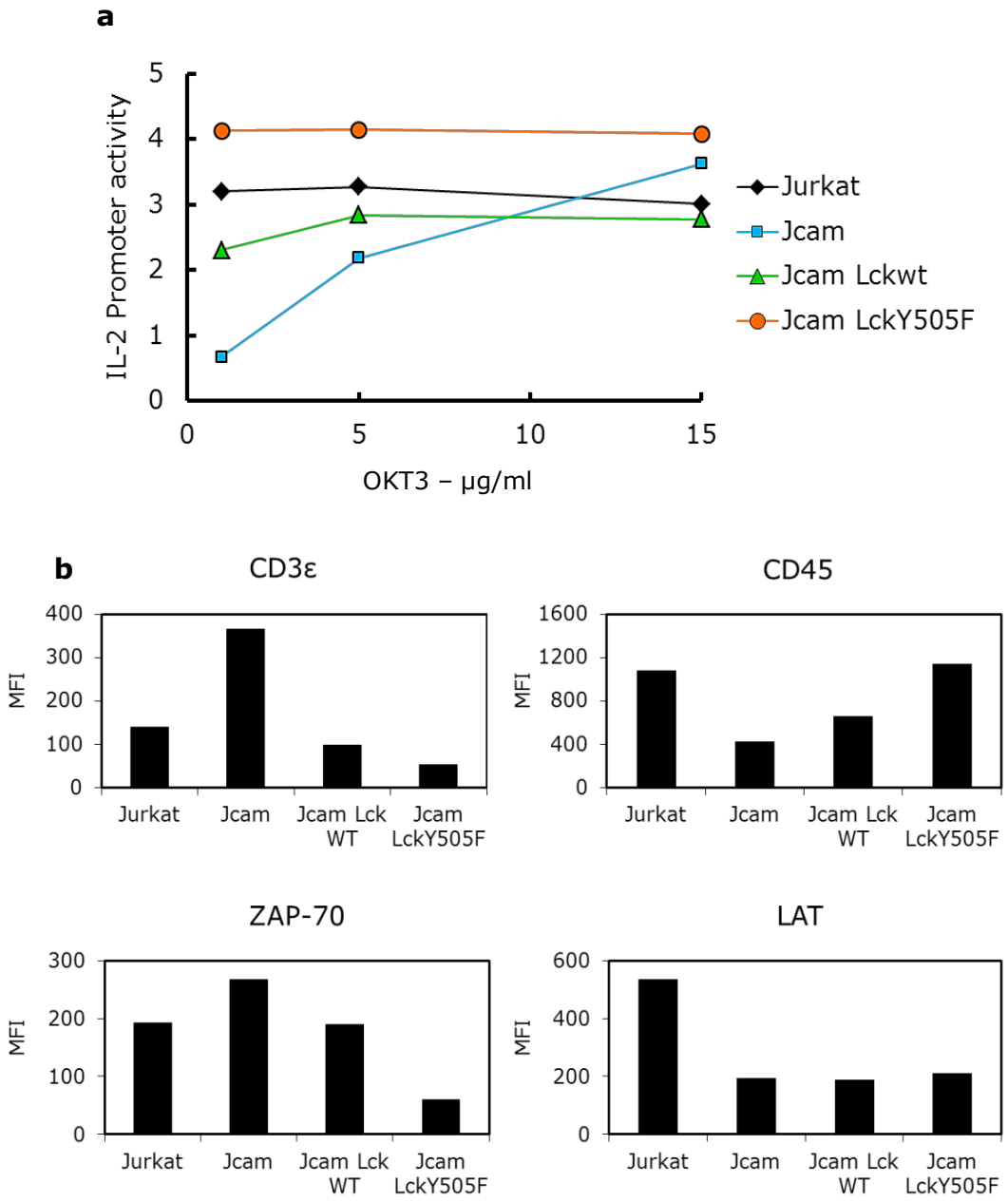

Figure 6.10: Expression of Lck in J.CaM cells induced changes in protein expression of CD45, CD3ε and ZAP-70. **(a)** The expression of wild-type Lck, and in particular, Lck Y505F, made J.CaM cells more sensitive to OKT3 stimulation, as measured by a reporter of IL-2 promoter activity. The promoter activity induced by OKT3 stimulation was normalized to that induced by an anti-rat Thy-1 antibody (OX7), used as a negative control for T-cell activation. **(b)** Expression of Lck, led to an increase in CD45 expression, and a decrease in CD3ε and ZAP-70 expression, as determined by FACS analysis with appropriate antibodies. These effects were more pronounced in J.CaM cells expressing Lck Y505F. No differences were observed for LAT. FACS analysis was undertaken six days post-Lck expression through lentiviral-mediated delivery of appropriate plasmids. A representative result from three independent assays is shown.

6.3.7 Lck kinase activity is up-regulated by phosphorylated CD3 ITAMs

The observations described in this chapter until now attempted to understand global effects, at the cellular level, of CD45 and suggested the existence of a homeostatic control of kinase and phosphatase activity. Upon close contact formation between a T cell and an APC, exclusion of large phosphatases, like CD45, will likely create a new environment that extends the half-life of phosphorylated tyrosines from CD3 ITAMs, in a small, well-defined region. Although drastic and performed at a global level, the effects of phosphatase depletion here described do seem to support this hypothesis.

Can local effects counteract global processes, which appear to suppress changes in net phosphorylation? This concept has been tested for other members of the Src family, where SH2 or SH3 binding proteins were found to control kinase activity in a mechanism that combines allosteric regulation with targeted phosphorylation activity [326-329]. To test if this was also the case for Lck, anti-Lck immunoprecipitates from resting Jurkat T-cells were incubated with a CD3ε peptide corresponding to the ITAM sequence (see §6.2.2 for peptide sequence), in its unphosphorylated or doubly phosphorylated state. After two hours incubation at 4°C, immune-precipitated Lck was incubated with acid-denatured rabbit β-enolase (47kDa), which served as readout for Lck kinase activity. Incubation of Lck with doubly phosphorylated CD3ε ITAM was found to induce a marked up-regulation in its kinase activity (Fig. 6.11).

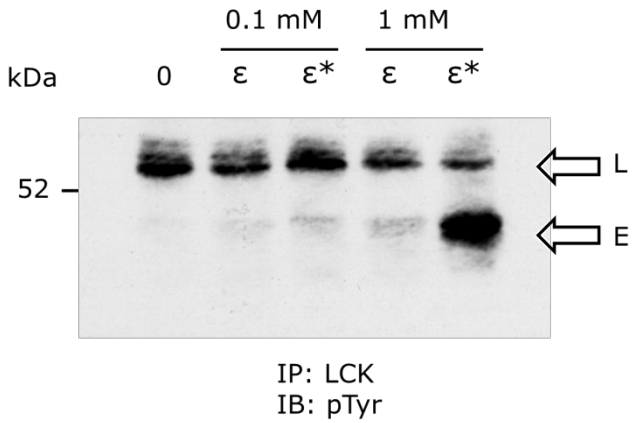

Figure 6.11: Lck kinase activity is increased upon interaction with phosphorylated CD3ε ITAM peptide. The presence of phosphorylated CD3ε ITAM peptide (ε*) led to an increase in the kinase activity of Lck. Lck kinase (L) activity was measured using denatured rabbit enolase (E) as the substrate. Non-phosphorylated CD3ε ITAM peptide (ε) had almost no effect on Lck kinase activity. Lck used in this assay was immunoprecipitated (using 73A5 antibody bound to protein A/G beads) from resting Jurkat T-cells. Representative data from three independent experiments is shown.

6.4 Discussion

6.4.1 Dissecting the functional contribution of CD45 in T-cell activation

The study here described focused on understanding the contribution of CD45 in TCR triggering. Until now, pervanadate treatment has been one of the major tools used to highlight the importance of phosphatases in TCR triggering. However, a method capable of specifically targeting the activity of relevant phosphatases in TCR triggering was lacking. The use of shRNA proved to be a successful approach for down-regulating CD45 protein in Jurkat and $CD3^+CD4^+$ T cells isolated from PBLs.

In the literature, different reports ascribe to CD45 a positive, a negative or even a dual effect on T-cell activation [186, 312]. Most of these investigations

have, however, focused on the role of CD45 in controlling Lck activity [188, 320, 330]. Because CD45 can dephosphorylate both Tyr394 and Tyr505 with different efficacies [321], it becomes challenging to comprehend its effect on Lck and in T-cell activation in general. Here, the main focus was placed not on the CD45 contribution to Lck activity but on CD45 role in controlling TCR phosphorylation, at a global, cellular level. It might seem somewhat surprising that down-regulation of a single protein can have such pronounced effects. However, this phenotype was only detected upon a drastic down-regulation of CD45, around 80-90%, and in a relatively short period of time. Given that CD45 accounts for almost 90% of the phosphatase activity present in T cells these observations stress the importance of phosphatases in controlling TCR triggering. But, several cell lines have been generated with decreased levels, or even lacking CD45, without showing signs of being in an activated state [316, 331-333]. The homeostatic balance found between CD45 and Lck, and between Lck, TCR and ZAP-70, seems to suggest that cells actively adapt to different conditions and have mechanisms to counteract changes in kinase versus phosphatase activity in particular. These compensatory mechanisms likely explain the resting phenotype of cell lines with down-regulated CD45, like J45.01 [319, 322, 334].

The use of shCD45 allowed monitoring the evolution of the cellular response to decreased phosphatase activity. The phenotype induced after expression of shCD45 was shown to be specific to the depletion of CD45 and dependent on a decrease in phosphatase activity at the cell membrane. Furthermore, it was dependent on TCR expression.

6.4.2 Local regulatory mechanisms to control kinase activity

The extended half-life of CD3ε phosphorylated ITAM observed upon CD45 depletion agrees well with previously proposed models for initiation of TCR triggering [232, 335]. This result, however, must be interpreted with some caution given the large global reduction in CD45 induced by shCD45, which is much greater than what is proposed to occur at the initial stage of TCR triggering [232].

Nevertheless, it seems plausible that smaller, local, decreases in phosphatase activity resulting from close contact formation between a T-cell and an APC, might also extend half-life of phosphorylated CD3 ITAMs.

Gathering observations made for other members of Src kinase family, raised the possibility that in these close contact zones, the presence of phosphorylated ITAMs could control Lck activity. The crystal structure of Src family proteins in active and inactive states revealed how binding of the SH2 to the C-terminal phosphorylated tyrosine, coupled with the binding of SH3 to a PxxP domain, "locked" the kinase in an inactive state [171, 173, 336-338]. These results also provided mechanistic support for previous work showing that inducing the release from the intra-molecular binding of SH2 or the SH3 by a competing protein leads to up-regulation of Src kinase activity [328, 329]. An experiment to test if Lck activity could be controlled by phosphorylated ITAMs thus seemed to be of significant importance. The outcome from this experiment suggests that, at least for CD3ε ITAM, Lck activity can be up-regulated by phosphorylated ITAMs. From previous reports, this effect could be explained by (1) a stabilization of Lck in its open state and (2) a competition between the C-terminal Tyr505 and ITAM for binding to the SH2 domain of Lck, which again could increase the presence of the stable "open" and active form of Lck. This hypothesis, however, requires further studies for confirmation. For instance, repeating the experiment with a form of Lck where the residue responsible for recognition of the phosphorylated tyrosine on the SH2 domain has been mutated.

Chapter 7

Extraction and purification of the TCR complex

7.1 Introduction

7.1.1 Quaternary structure of the TCR complex

Since the discovery of the TCR complex significant advances have been made in understanding receptor assembly, stoichiometry and valency [48, 50, 53, 276]. Despite these advances, the molecular mechanism behind TCR triggering remains to be understood. Obtaining structural information is often the key step in understanding function and modes of action of enzymes and receptors. In the case of the TCR, the overall quaternary structure of the entire complex is still unknown. The structure of the TCRαβ, CD3γε and CD3δε heterodimer ectodomains have been determined by X-ray crystallography and/or NMR [42, 43, 55, 57, 61, 339], but the structure of the entire TCR complex has not been revealed.

Inter-subunit interactions have been proposed to play an important role in TCR triggering. For example, anti-CD3ε antibodies, which have been used as immunomodulating agents in the treatment of autoimmune diseases and in preventing transplant rejection, have been proposed to induce triggering by "dislodging" CD3ε from the TCRαβ [60]. However, these interactions have not been directly confirmed on intact complexes. The same is true of other TCR triggering models based on changes between inter-subunit contacts [53, 206, 213, 218, 340].

Solving the molecular structure of myoglobin/haemoglobin [341, 342], DNA [343] and, more recently, of β_2AR in an active conformation [344] and bound to G-proteins [345], led to significant advances in understanding the mode of action of these molecules. Likewise, solving the overall structure of the TCR complex will set a new framework for a possible mechanism of action. Following results from Chapter 4, a more detailed knowledge on the overall quaternary structure of the complex could also reveal subtle changes upon pMHC cognate binding.

The work described in this chapter aims to define and optimize the first step required to solve the structure of the TCR complex, namely: extraction and purification of the receptor from the cell surface. Once a protocol has been established, it will be possible to probe TCR complex structure by single-particle cryo-electron microscopy (cryo-EM) in the first instance. cryo-EM has been successfully used to determine low-resolution three-dimensional (3D) reconstructions of a number of protein complexes [346-350]. The size and the structural information already available for TCRαβ, CD3γε and CD3δε heterodimers, which could be docked into a low-resolution structure, make the TCR complex suitable for a cryo-EM analysis. Recently, this approach has been used by Arechaga *et al.*, [351]. However, the final 3D reconstruction structure obtained for the TCR complex, at 35Å resolution, was found to be much larger than expected and hindered a conclusive insight into the TCR/CD3 inter-subunit interactions forming the complex. The protocol here described for TCR extraction and purification is significantly different from the one used by Arechaga *et al.*.

7.2 Materials and methods

7.2.1 Expression of TCRgp100

Cloning of TCRgp100 and CD3 subunits

The full length sequences of TCRαβ, with variable region recognizing gp100-MHC were PCR amplified from a plasmid kindly provided by Bent Jakobsen (Immunocore, UK). TCRα and TCRβ were amplified with primers incorporating a 5' *BglI* and a 3' *HindIII*, and were ligated to a modified version of pHR-SIN which had multiple 2A viral sequences [352], all differing from each other by introduction of different silent mutations. CD3γ, residue 1-144, was PCR amplified from Jurkat cDNA with primers containing 5' *MluI* and 3' *KpnI*, and sub-cloned, in frame, after TCRα, with a 2A sequence at the N-terminus of CD3γ signal peptide. CD3ε, residue 1-162, 5' primer containing a *BamHI* and 3' *XhoI*, and CD3ζ, residue 1-58, with primers containing 5' *Xba*I and 3' *AgeI,* were amplified by PCR from Jurkat cDNA and subcloned into plasmid containing TCRα-2A-CD3γ and into another plasmid containing TCRβ-2A. 2A sequences were cloned between TCR subunit DNA sequences. For expression of CD3δ, the pHR-IRES-GFP was modified to include a signal peptide (derived from human RPTP), followed by an HA tag (as defined by Sigma-Aldrich Co.) *via BglII* (5') and *BamHI* (3'). DNA encoding CD3δ, residues 22-134, was amplified from plasmid templates and cloned into this vector using the *BamHI* (5') and *XhoI* (3') restriction sites. The 2A sequences introduced the following residues at the corresponding C-termini of the TCRα, TCRβ, and CD3ε proteins: GSGVKQTLNFDLLKLAGDVESNPG and a Pro residue at the N-terminus of CD3ε and CD3ζ. All of the final constructs were sequenced to confirm sequence integrity and reading frame.

Expression of TCRgp100 complex

HEK-293T cells were transiently transfected with pHR-SIN vector constructs, together with pMD.G and p8.91 lentiviral vectors [255] in 6-well plates using Genejuice (Merck, Darmstadt, Germany) according to the manufacturer's instructions. Supernatant from two 6-well plates, *i.e.* a total of 4 ml, for each of the TRCgp100 expression cassettes, was harvested at 48-72 hours after transfection and centrifuged at 3000 rpm for 5 minutes at RT to remove cell

debris. 1x10^6 CHO cells were transduced using this supernatant overnight. The cells were transduced with one of the three plasmids made to drive complete TCR complex expression, every 5 days.

FACS analysis

Samples were stained on ice in the dark in PBS, 0.05% sodium azide, using monoclonal antibodies specific for HA (HA-7, Sigma-Aldrich Co., Gillingham, UK), hTCRαβ (Caltag, Burlingame, CA; directly conjugated to R-Phycoerythrin), peptide-MHC, directly conjugated with alexa647 dye (according to the manufacturers' protocol, Molecular Probes, Invitrogen), and UCHT1, for 45 minutes. After washing, cells were then stained with anti-mouse Alexa 647 (Invitrogen, Paisley, UK), or anti-mouse PE-Cy7 (eBioscience, CA, USA) for 30 mins. The cells were fixed in 2% PFA 0.05% sodium azide in PBS for 10 minutes 20,000 live cells were collected on a CyAn FACS machine (Dakocytomation, Glostrup, Denmark) and the data was analyzed using FlowJo software version 8.7.3 (Treestar, Ashland, OR).

7.2.2 Extraction and Purification of TCR complex from cell surface of CHO cells

Protocol I: 5-10x10^8 cells

CHO cells expressing TCRgp100 were washed in ice-cold PBS and labelled with excess pMHC-biotin, *i.e.* 40 μg, for 45 minutes on ice. Cells were washed twice in ice cold PBS and lysed in digitonin (Sigma-Aldrich Co., UK) or DDM (Generon, UK), with different % w/v of these detergents, plus 20 mM Hepes, pH 7.4, 120 mM NaCl, 10 mM iodocetamide, 2 mM EDTA, 1 mM PMSF and 1x protease inhibitor cocktail, all reagents from Sigma-Aldrich Co., UK, for 1 hour, on ice, with agitation. 1 ml of lysis buffer was used for 50x10^6 CHO cells. The lysate was centrifuged at 1300 rpm, for 10 minutes at 4°C. The soluble fraction was incubated with Soft-link Avidin resin beads (Promega, UK) for 2 hours with constant agitation at 4°C. Beads were washed 5 times, in lysis buffer, and then

resuspended in SDS-loading buffer and heated to 95°C, for 5 minutes Samples were aliquoted and stored at -80°C for western blotting analysis.

Protocol II: >1x10^9 cells

CHO cells were washed in ice cold PBS and labelled on ice for 45 minutes with excess pMHC-biot. Cells were washed twice in ice cold PBS and then resuspended in hypotonic lysis buffer, 10 mM Tris-HCl, pH 7.4, 1 mM PMSF, 1x protease inhibitor cocktail. 1 ml of hypotonic lysis buffer was used for 50x10^6 CHO cells. The suspension was centrifuged at 40,000*g* for 20 min. Following centrifugation the supernatant was discarded and the membrane pellet was weighed and resuspended in solubilization buffer, 0.5% DDM, 140 mM NaCl, 20 mM Tris-HCl, pH 7.4, 1 mM PMSF, 1x protease inhibitor cocktail, 2 mM EDTA, 10 mM iodocetamide by 20 strokes in a dounce homogenizer and then agitating continuously at 4°C for 1 hour. Ten millilitres of solubilization buffer were used for each gram of crude membranes. After stirring, the solution was centrifuged at 40,000*g* at 4°C for 20 min. The supernatant was incubated with previously regenerated Soft-link Avidin resin beads (according to the manufacturers' protocol; Promega, UK) for 2 hours with constant agitation, at 4°C. Beads were washed 6 x 1 ml, in solubilization buffer and then incubated with 10 mM biotin (Sigma-Aldrich Co., UK), 120 mM NaCl, 10 mM Tris-HCl, pH 7.4, 0.1% DDM, at 4°C, for 15', 45', 60' or overnight. Elution fractions were used immediately for FPLC analysis or kept aliquoted at -80°C for future analysis. For FPLC analysis, 15' and 45' biotin-eluted samples were concentrated using centricon centrifugal filter units (Millipore) with 100,000 kDa molecular weight cut-off, by centrifugation at 4000*g* for 5-10 minutes 4°C.

FPLC analysis

Gel filtration of eluted samples (15′ and 45′) from Soft-link Avidin resin was undertaken using the Äkta FPLC system (GE Healthcare), coupled with a Superose 6 HR 10/30 column kept at 4°C. The column was equilibrated and

eluted with 120 mM NaCl, 10 mM Tris-HCl, pH 7.4, 0.1% DDM. Before FPLC analysis protein concentration was determined spectrophotometrically at 280 nm. The loaded sample was then eluted through the column using one column volume of buffer, with 500 µl fractions collected after the void volume (8 ml). The protein concentration of each fraction was determined as above and desired fractions were pooled where necessary.

Quantitative Western blot

Quantitative Western blotting of appropriate samples probed with anti-HA or UCHT1 antibodies was done using a LI-COR Odyssey® Imager. Briefly, following SDS-PAGE using 10-12% acrylamide gels, proteins were blotted to a PVDF membrane and blocked with Odyssey Blocking Buffer for 45 minutes at RT. Membranes were incubated with appropriate dilutions of anti-HA or UCHT1 antibodies, washed 3x in TBS-Tween (0.05%) and then incubated with anti-mouse IRDye® 700 or 800 (LI-COR Bioscience). Membranes were dried for two hours to overnight and then analyzed on a LI-COR Odyssey® Imager following the manufacturers' instructions.

7.3 Results

7.3.1 Overall strategy for TCR extraction and purification

In order to extract fully assembled TCR complexes it was reasoned to be important to specifically isolate complexes expressed at the cell surface. Extraction and purification of proteins from the cell membranes of eukaryotic cells requires large working volumes (100-1000 ml and is a lengthy process (24-48 hours). Efficient capture of the target protein thus requires a high affinity ligand, and particularly one with a low dissociation rate, ensuring that it remains bound to the target protein throughout the different stages of the isolation and purification procedure. Expression of the TCR at the cell surface is dependent on efficient assembly of its composing 8 subunits [48-50]. Targeting the TCR present at the

cell surface ensures that only fully assembled complexes are captured and avoids misfolded or incomplete complexes present, for example, in the ER [353].

It was thus decided to immunoprecipitate a TCR complex, TCRgp100, which binds with extremely with high-affinity, 11 nM, and with a K_{off} of 33 hours, to a gp100 peptide covalently bound to an MHC molecule that was in turn biotinylated at the C-terminus (pMHC-biot.) [354]. TCR-pMHC interaction is usually characterized by a weak affinity (1-10μM) [355, 356],. However, using bacteriophage display and directed molecular evolution of the TCR CDR3 and CDR2 loops it has been possible to generate a TCRαβ with much higher affinities for pMHC [354, 357]. The DNA sequence for the variable region of the TCRαβgp100, and biotinylated gp100 peptide-MHC were kindly provided by Bent Jakobsen (Immunocore, Abingdon, UK) and Andrew Sewell (Cardiff University).

7.3.2 Establishing a cell line expressing TCRgp100

Lentiviral-mediated delivery of the required plasmids was used to stably express the TCRgp100 complex in different eukaryotic cell lines. However, the previously used pHR-SIN or the pHR-SIN-IRES plasmid could not be used to efficiently express the six proteins that compose the TCR in a single cell. Multiple protein expression from a single plasmid can be achieved by taking advantage of 2A viral peptide sequences [352, 358]. These sequences are used by viruses such as picornaviruses and tetraviruses to co-express multiple proteins from a single mRNA. 2A sequences are usually of 18-22 residues in length and have a highly conserved motif at the c-terminus: Asp-Val/Ile-Glu-X-Asn-Pro-Gly-↓-Pro (↓ is used to indicate absence of covalent amino-acid pairing; [358]). The N-terminal part of the 2A sequence impairs bond formation between Gly and Pro, possibly though a ribosome skip mechanism, which results in expression of two independent proteins [358]. Insertion of the 2A sequence can therefore generate multiple proteins from a single mRNA transcript, and it has been used previously to drive the expression of a full TCR complex from two plasmids [70, 352].

The pHR-SIN was therefore engineered to incorporate three 2A sequences allowing expression of up to four proteins. Three plasmids were created to express the TCR complex (Fig. 7.1). One plasmid contained DNA sequences to enable expression of TCRα, CD3γ, CD3ε and CD3ζ; a second plasmid contained DNA sequences to express TCRβ, CD3ε and CD3ζ; and a third plasmid was used to express a chimeric CD3δ fused with an HA-tag at the N-terminus of the protein, and also a GFP protein, expressed independently of HA- CD3δ through the use of an IRES sequence (Fig. 7.1). In total, two copies of CD3ε and CD3ζ were introduced into the plasmids, in order to compensate for the stoichiometry of these proteins in the TCR complex [49, 142, 145]. For all proteins, only the DNA sequence corresponding to the extracellular and transmembrane domains was cloned into the plasmids. The cytoplasmic domains were excluded in order to avoid any interaction between these domains and other proteins.

Four different cell lines were infected with the described plasmids: HEK-293T, CHO, J.CaM 1.6 (Jurkat derived cell line, negative for Lck expression) and C1R (B-cell line). Infections were carried out sequentially, with the plasmid driving expression of TCRα, CD3γ, CD3ε, CD3ζ first, followed by TCRβ, CD3ε, CD3ζ and HA-CD3δ-IRES-GFP. Surface expression of the TCR complex was detected by pMHC, UCHT1 and anti-HA staining of the cells using FACS analysis (Fig. 7.2). TCRgp100 could not be detected at the surface of J.CaM 1.6 and C1R (Fig. 7.2). However, both HEK-293T and CHO cells expressed high levels of TCRgp100 at the cell surface when probed with pMHC-biotin (Fig. 7.2). Furthermore, in CHO cells, high levels of TCRαβ expression were found in cells expressing high levels of GFP (Fig. 7.2). This correlation was reasoned to be an indication of efficient assembly and surface expression of TCR complexes in these cells, since very few cells expressed GFP but not TCR. The correlation between TCRαβ and GFP expression was weaker in transduced HEK-293T cells (Fig. 7.2).

CHO cells expressing TCRαβ and GFP were sorted by MoFlo® cytometry to obtain a stable cell line with high expression of the TCRgp100 complex (Fig. 7.3a). After cell sorting, probing the cell surface with an anti-CD3ε and pMHC showed that cells with high levels of CD3ε also expressed high levels

of TCRαβ, which was another indication that correctly assembled TCR complexes were present at the surface of these cells (Fig. 7.3b).

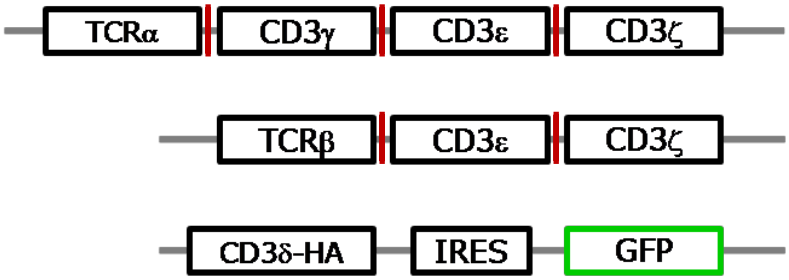

Figure 7.1: Constructs for expression of the TCRgp100 complex. The DNA sequences for TCRαβ and CD3 proteins were cloned into three lentiviral vectors that were used to stably infect different cell lines. Viral 2A sequences (shown in red) allowed expression of multiple proteins from a single plasmid.

7.3.3 Immunoprecipitation of TCRgp100 with pMHC

Cell surface TCRαβ was immunoprecipitated after labelling live cells on ice with pMHC-biotin. The cell membrane was lysed with the mild non-ionic detergent digitonin (0.5% w/v) to maintain the charge-charge transmembrane interactions established between TCR complex subunits ([48]; (Protocol I, see §7.2.2 for details). Under these conditions, HA-CD3δ was found to co-precipitate with the TCRαβ (Fig. 7.4).

Surface immunoprecipitation was then compared with a whole cell lysate immunoprecipitation of TCR complexes with pMHC-biot. Probing the immunoprecipitated samples with anti-HA and anti-CD3ε (UCHT1 antibody) by Western blotting revealed that in both surface and whole cell immunoprecipitations, HA-CD3δ and CD3ε co-precipitated with TCRαβ. However, whereas in cell surface immunoprecipitation samples, HA-CD3δ and CD3ε were found to migrate at the correct size expected for these proteins, in whole cell lysates multiple bands could be detected (Fig. 7.5a, b). This result is in

agreement with reports indicating that a significant amount of intracellular CD3 proteins are misfolded and establish disulphide bonds that are not present in correctly assembled TCR complexes [359, 360]. Addition of β-mercaptoethanol to the immunoprecipitation samples showed that under reducing conditions only one band for HA-CD3δ could be detected (Fig. 7.5c).

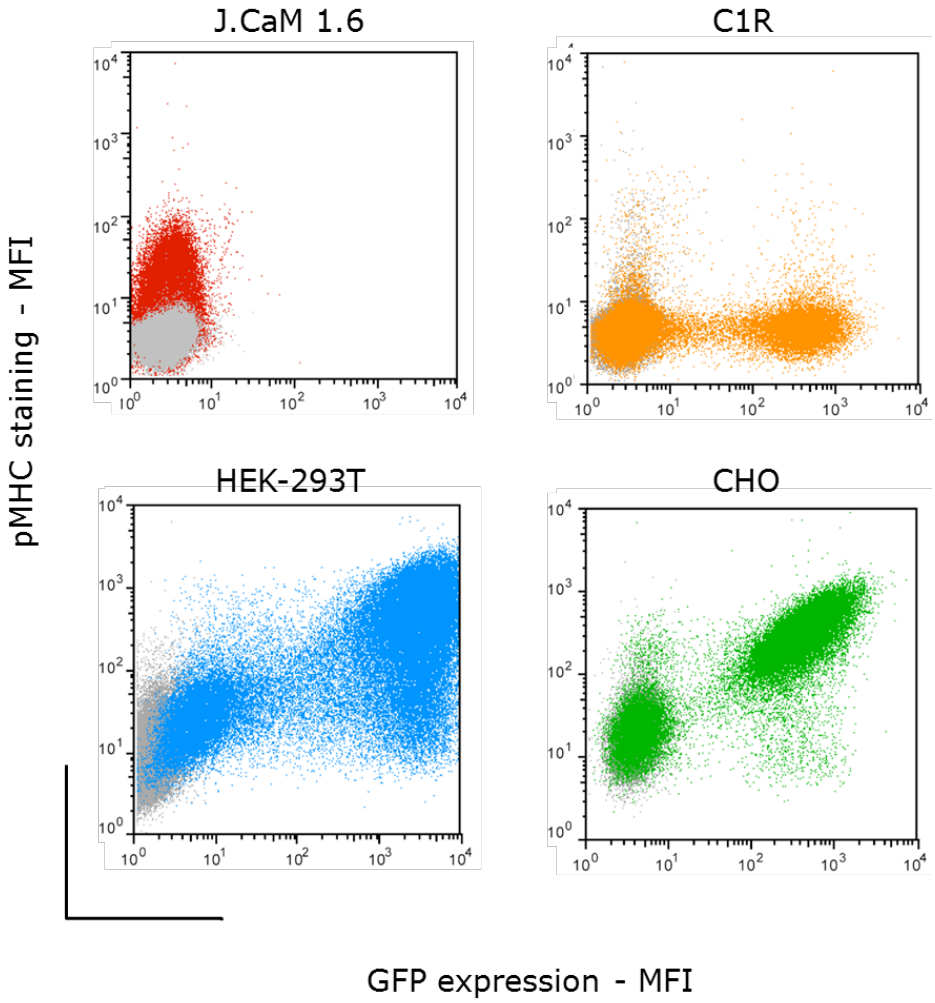

Figure 7.2: Establishing a cell line expressing the TCRgp100 complex. Lentiviral-mediated delivery of the plasmids shown in Fig. 7.1 led to surface expression of TCRαβ, as detected by pMHC-alexa647 FACS staining, in HEK-293T and CHO cells. Expression was low in J.CaM 1.6 and could not be detected in C1R cells. CHO cells expressing high levels of GFP (present in the pHR-HA-CD3δ-IRES-GFP plasmid) also expressed high levels of TCRαβ. Staining of wild-type cell lines is shown in grey.

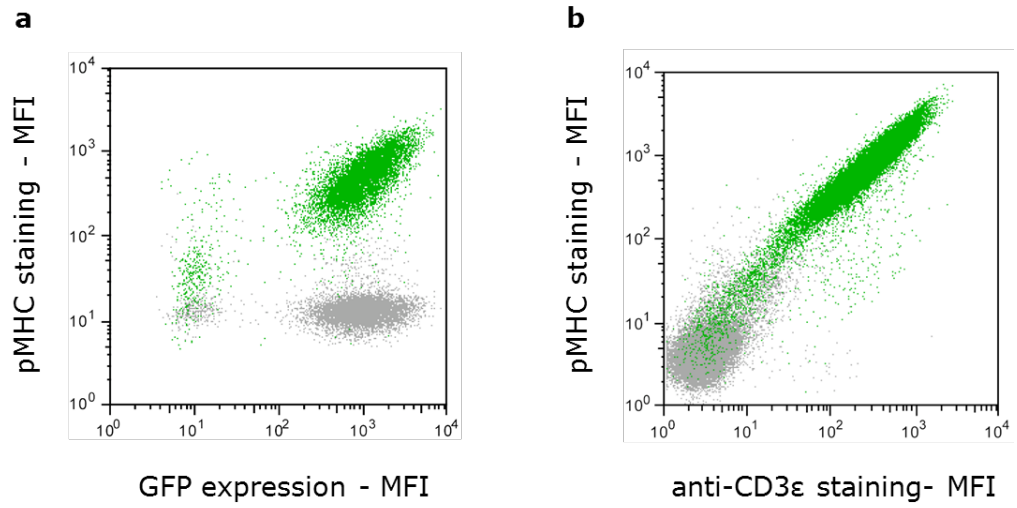

Figure 7.3: Cells expressing high levels of TCRαβ were FACS sorted. **(a)** After FACS sorting, a homogenous population of CHO cells expressing TCRαβ was obtained. Data for cells stained with pMHC-biotin-alexa647 are coloured in green, and data for cells stained with donkey anti-mouse-alexa647 are coloured in grey. **(b)** A positive correlation was also found between expression levels of TCRαβ and CD3ε. Wild-type CHO cells are coloured in grey.

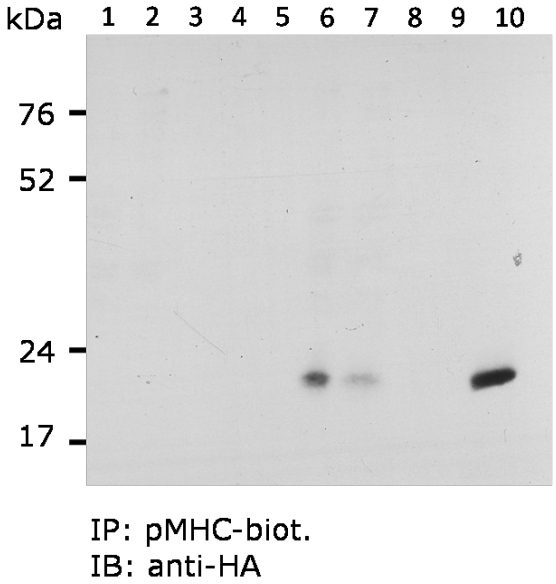

Figure 7.4: Immunoprecipitation of TCRαβ with pMHC co-precipitates non-covalently bound HA-CD3δ. Following cell surface labelling with gp100 pMHC, cells were lysed in digitonin and streptavidin agarose beads were then used to pull down biotinylated pMHC. Lane 1-5, wild-type CHO cells; Lane 6-10: CHO-TCR cell line. Lane 1, 6: whole cell lysate; lane 2, 7: TCR depleted lysate; lane 3,4 and 8,9: streptavidin-bead wash; Lane 5, 10: pMHC elution from streptavidin beads with 1% SDS buffer for 5 minutes at 95ºC.

7.3.4 Optimizing TCRgp100 complex extraction from the cell membrane

Co-precipitation of HA-CD3δ and CD3ε with pMHC-biotin indicated that under these extraction conditions the TCR complex is kept intact, and that presumably weak interactions established between TCRαβ and the CD3 subunits are not disrupted by digitonin, in agreement with results found by others [208, 245, 351, 361]. However, digitonin is not ideal to perform cryo-EM analysis [362] and it was therefore necessary to test if another non-ionic detergent, n-dodecyl-β-D-maltoside (DDM), a widely used detergent for both cryo-EM and crystallization studies, could be used to extract the TCR complex from the cell membrane. Comparison with digitonin revealed that DDM was more effective in maintaining non-covalent interactions between TCRαβ and the CD3 dimers, as more HA-CD3δ and CD3ε could be detected in TCRαβ immunoprecipitation samples (Fig. 7.6a, b).

Measurement of TCRgp100 surface expression in CHO cells by FACS showed there are approximately 52,500 TCR complexes/CHO cell (corresponding to a UCHT1 MFI, measured by FACS, that is 4.5-fold higher than wild type Jurkat cells; see Fig. 3.4, §3.3.4) and therefore 10 μg of TCR complex are present in $8.8x10^8$ cells (assuming a 133 kDa complex). By immunoblotting a purified HA-tagged protein of known concentration, HA-CD5, together with samples from the pMHC-biotin immunoprecipitation with an anti-HA antibody it was possible to estimate the amount of HA-CD3δ present in TCRαβ immunoprecipitates (Fig. 7.6a). It was estimated that from $8.8x10^8$ cells, 1.6 μg of TCR complex had been recovered, assuming that for every HA-CD3δ a fully assembled complex was present.

Cryo-EM analysis requires around 10μg of purified protein. However, to confirm that fully assembled, and homogeneous, complexes are being extracted it will be necessary to perform size-exclusion chromatography on the purified samples, followed by an SDS-PAGE analysis to confirm the presence of all of the TCR subunits, in the appropriate stoichiometry. To perform this analysis ~100μg of TCR complex are expected to be required.

To extract 100 µg of TCR complex, the protocol being used had to be optimized and adapted to work with a larger number of cells, in the range of 5-20x10^9. For this number of cells, direct solubilization of cell membrane in DDM is not feasible. The protocol (Protocol II, see §7.2.2 for details) was therefore adapted to include a cell membrane enrichment step, which relied on cell lysis with a hypotonic, detergent-free buffer, followed by ultracentrifugation for recovery of cell membrane and exclusion of cytosolic organelles. Before lysis, cells were labelled with pMHC-biotin in order to immunoprecipitate only well-folded TCRgp100 present at the cell surface. After pMHC-biotin labelling, the cells were lysed and membrane pellets were resuspended in 0.5% DDM buffer added to a final volume defined by the pellet weight. pMHC-biotin was captured by Softlink-avidin resin beads (Promega, UK) and eluted with biotin. This new protocol allowed recovery of around 100µg of TCR complex, as determined by quantitative HA-CD3δ Western blotting, from 1.5x10^{10} cells, which corresponds to a maximum theoretical yield of 35% (Fig. 7.7).

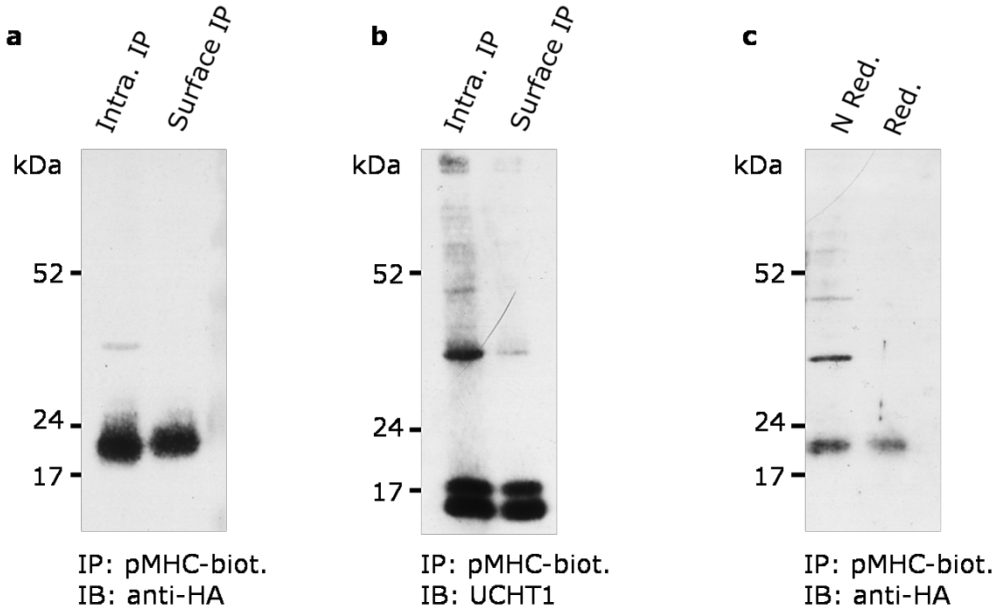

Figure 7.5: Only cell surface TCR complex is correctly folded and assembled. The TCR complex was immunoprecipitated with gp100 pMHC from either the cell surface (Surface IP) or whole cell lysates (Intra. IP). Both CD3δ **(a)** and CD3ε **(b)** are detected in multiple bands upon Western-blotting with appropriate antibodies under non-reducing conditions. **(c)** Anti-HA western-blotting of a whole cell lysate TCR immunoprecipitation in the presence of a reducing agent (Red.) detects a single band of the size expected for CD3δ.

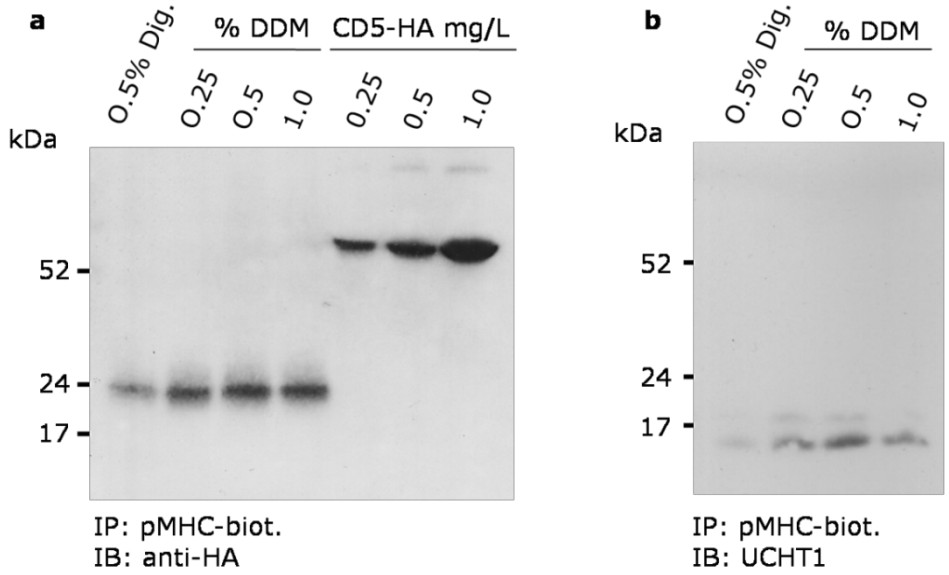

Figure 7.6: DDM is a suitable detergent to solubilize TCR complex from the cell surface of CHO cells. Different concentrations of DDM were used to solubilize the TCR complex following cell labelling with pMHC-biotin. Western-blotting with anti-HA **(a)** or anti-CD3ε **(b)** showed that these proteins co-precipitated with the TCRαβ.

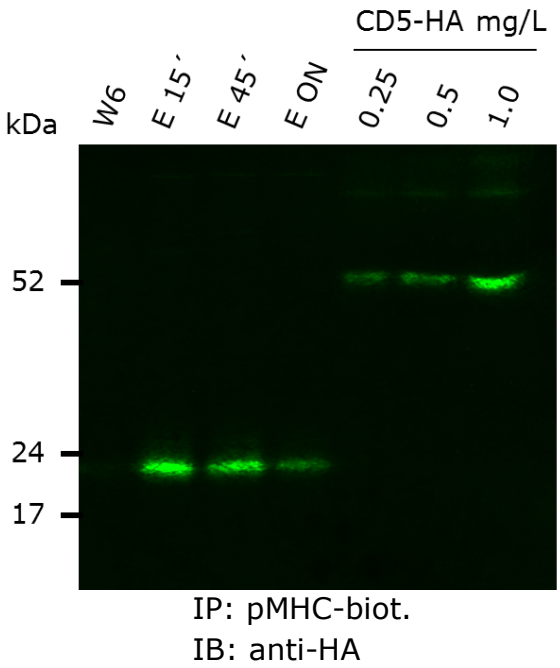

Figure 7.7: Immunoprecipitation of TCRαβ with gp100 pMHC followed by biotin elution from Softlink-Avidin purifies non-covalently bound HA-CD3δ. Purified CD5-HA of known concentration was used to determine the amount of isolated HA-CD3δ: 0.83 µg in 15' elution (E 15) with biotin at 4°C, 1.07 µg in 45' elution (E 45) and 0.21 µg following overnight (ON) elution, corresponding, respectively, to 5.4 µg, 6.9 µg and 1.3 µg of TCR purified from $1.5x10^9$ cells, and a

7.3.5 FPLC analysis of purified TCRgp100 complex

The 15 and 45 minute biotin elution from the pMHC-biotin Soft-link Avidin immunoprecipitations were pooled, concentrated and analysed by FPLC, using a Superose 6 HR 10/30 column kept at 4°C (Fig. 7.8a). Fractions of 0.5 ml were collected and probed by Western blotting with anti-HA, anti-CD3ε and streptavidin-HRP. HA-CD3δ, CD3ε and pMHC-biotin were found to be present in the same fractions (7.8b).

To determine if these proteins were associated in a single complex, samples corresponding to the 13-16 ml elution were pooled, concentrated, and labelled with a saturating amount of anti-CD3ε (UCHT1) antibody, for 1 hour on ice. After UCHT1 binding, protein samples were analysed again by FPLC, using the same column and settings as before. Western blotting with an anti-HA antibody revealed that upon addition of UCHT1 whole antibody, HA-CD3δ elution had shifted by 1 ml, corresponding to an increase in protein size, indicating that both HA-CD3δ and CD3ε were co-associated (Fig. 7.9b). However, at the end of the first FPLC run, only 5-10μg of protein could be recovered, and after the second FPLC analysis, proteins could only be detected by Western blotting.

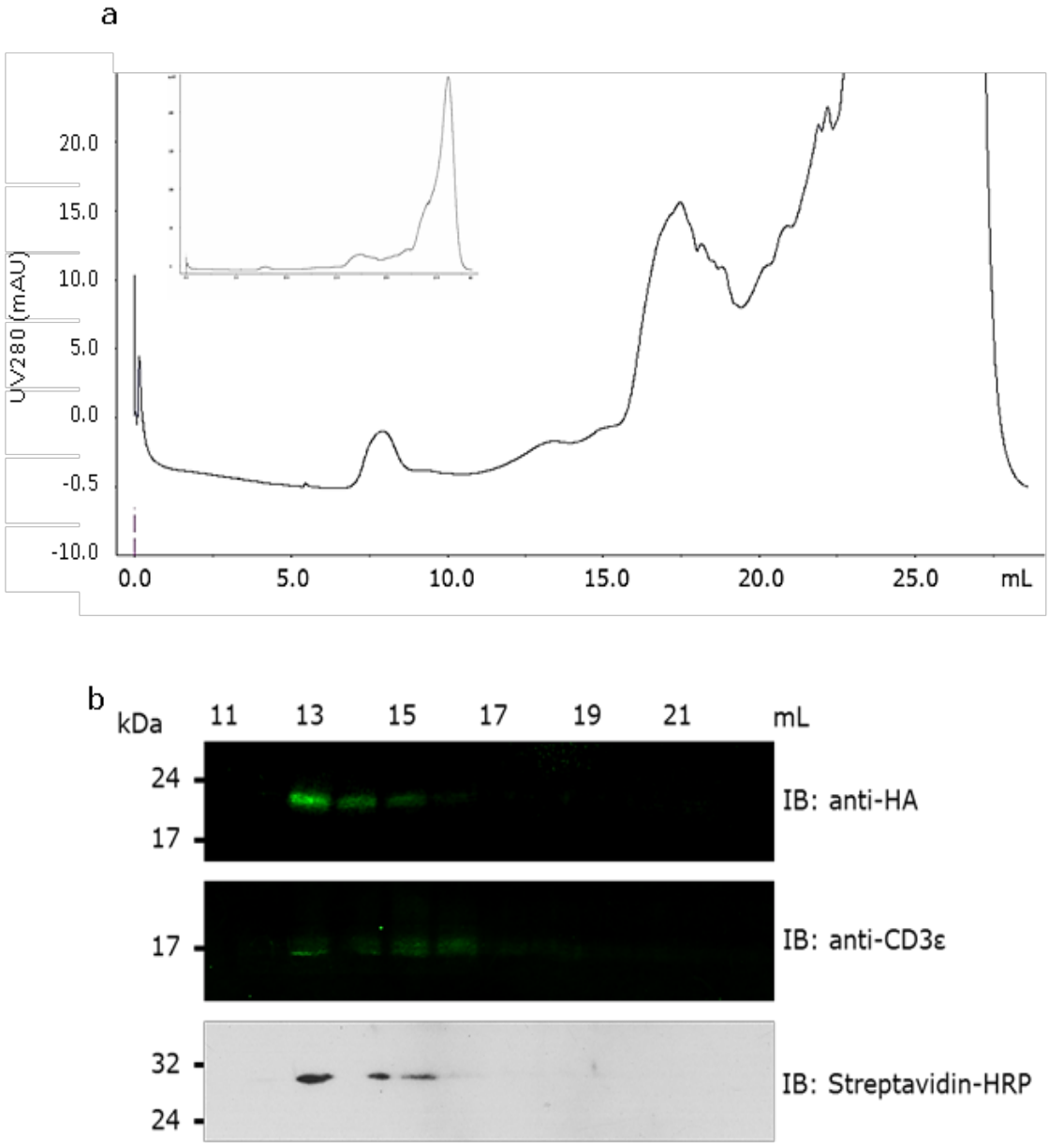

Figure 7.8: Co-elution of TCR subunits analysed by gel-filtration chromatography. **(a)** Gel-filtration of pooled 15' and 45' eluted with 10 mM biotin from Softlink-Avidin following immunoprecipitation of TCRαβ with gp100 pMHC ($1.2x10^{10}$ cells were used). Gel-filtration was done using a Superose 6 HR column at 4°C, with 150 mM NaCl, 10 mM Tris-HCl, pH 7.4 and 0.5% DDM. The entire chromatogram is shown in the inset. **(b)** Fractions of 0.5 ml were collected and probed by Western blotting with anti-HA and anti-CD3ε antibodies and with streptavidin-HRP.

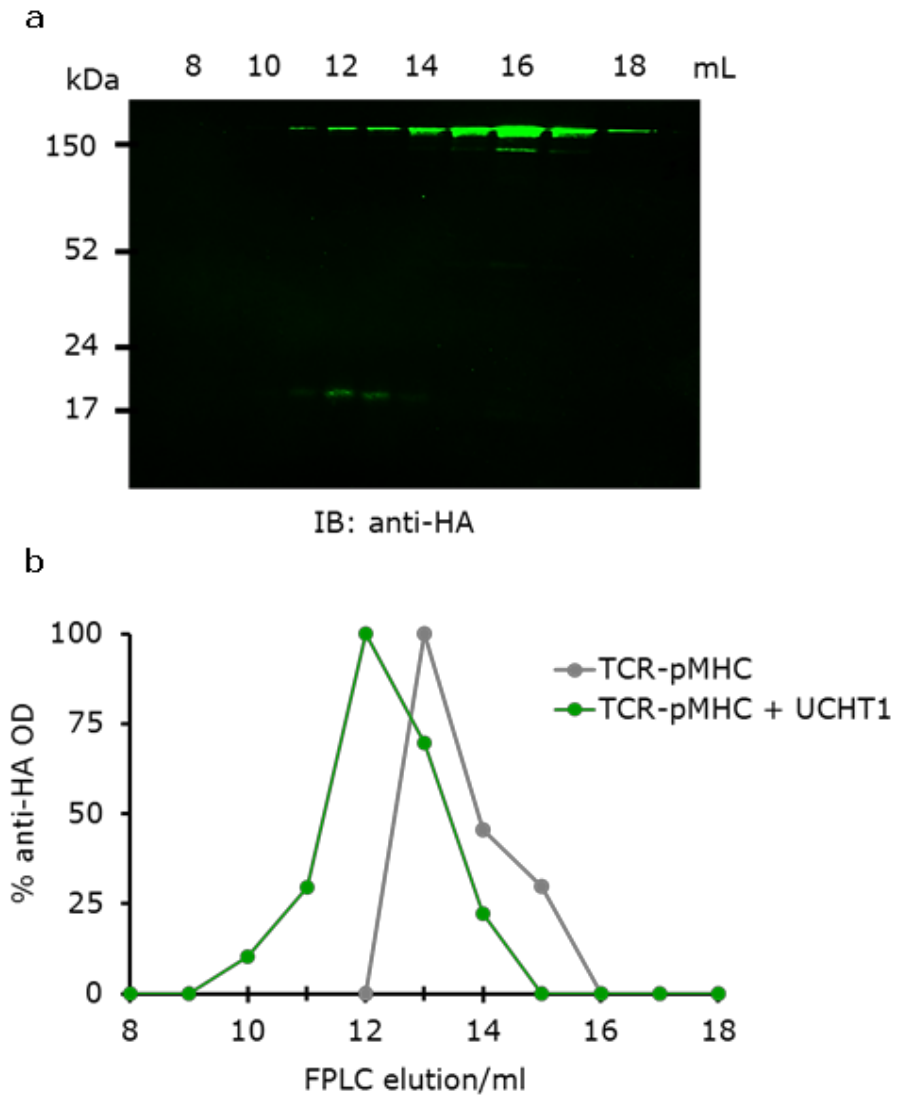

Figure 7.9: Addition of anti-CD3ε antibody to gel-filtration-isolated TCR-pMHC shifts the peak elution volume of HA-CD3δ from 13 ml to 12 ml. **(a)** Pooled samples from 13 ml to 15 ml (see Fig. 7.8) were incubated with 100 µg of anti-CD3ε antibody, concentrated, and subjected to gel-filtration as done previously. Fractions were collected and probed by Western blotting with an anti-HA antibody to detect presence of HA-CD3δ. **(b)** Elution peak, as detected by Western blotting, of HA-CD3δ had shifted from 13 ml to 12 ml, indicating an increase in size of the complex containing HA-CD3δ upon addition of whole anti-CD3ε antibody.

7.4 Discussion

7.4.1 Purification of the TCR complex

The work described in this chapter aimed to establish a protocol for extraction and purification of the intact TCR complex from the cell membrane. The use of a very high affinity pMHC allowed targeting and immunoprecipitation of the cell surface TCRgp100, expressed at high levels in a CHO cell line. Analysis of the proteins co-precipitated with TCRαβ revealed the presence of HA-CD3δ and CD3ε, an indication that fully assembled complexes were extracted from the cell membrane. Furthermore, FPLC analysis of the biotin eluate from Soft-link Avidin beads showed that pMHC-biot., HA-CD3δ and CD3ε were migrating together, and eluted at the same column elution volume. Addition of an anti-CD3ε antibody to the samples containing pMHC-biotin, HA-CD3δ and CD3ε, caused a shift in the elution of HA-CD3δ, which is not covalently bound to other TCR subunits, indicating that at least HA-CD3δ and CD3ε interactions are kept during the extraction protocol.

The maximum theoretical yield obtained for TCR complex recovery, based on quantification of HA-CD3δ and assuming a direct proportion between this protein and a fully assembled complex, was estimated to be around 35%. However, between elution from Soft-link Avidin resin and the FPLC analysis the majority (>90%) of the protein was lost. The volume necessary for efficient elution from avidin beads is 3 ml, which needs to be concentrated to 0.5-1 ml before loading onto the FPLC column. The protein was concentrated with a centricon Ultracel YM-100 membrane, 100,000 kDa molecular weight cut-off, by centrifugation at 4000*g*, for 5-10 minutes, at 4°C. One possibility is that during centrifugation DDM micelles might accumulate close to the filter membrane (the average DDM micelle size is 77 kDa), locally increasing detergent concentration and disrupting and aggregating TCR complexes. If this is the case, the centrifugation step could be done for a shorter period of time (30 seconds to 1 minute) followed by a re-suspension of the protein sample, repeating these steps

until the sample volume is reduced to 0.5 ml. Another possibility could be the use of stirred-cell concentrators, which rely on pressure filtering, with constant agitation of the sample.

The stability of TCR complex proteins/DDM micelles could also benefit from addition of a new class of detergents, *i.e.* amphiphiles derived from neopentyl glycol structure with hydrophilic groups derived from maltose, which show enhanced stability relative to DDM of the protein-micelle structure [363]. This new class of detergents has been successfully used recently for both protein crystallization and single-particle cryo-EM analysis of β_2AR [344, 345].

Chapter 8

General discussion

TCR triggering comprises a key step in the initiation of antigen-specific T cell responses. Nevertheless, some of the basic properties of the TCR complex, such as its valency and quaternary structure, are uncertain and the molecular mechanism that controls TCR phosphorylation, before and after cognate pMHC interaction, is also a matter of debate. This thesis has taken different approaches to extend our understanding of TCR complex structure and of the molecular processes that regulate its levels of phosphorylation.

8.1 Results from this thesis

8.1.1 The TCR complex is monomeric at the cell surface – functional implications for receptor triggering

In Chapter 3, a new method, called DySCo, was developed to quantify the degree of association of molecules diffusing at the surface of live cells, based on single-molecule video microscopy. The degree of association determined for the TCR complex was lower than that found for the monomeric protein CD86 (now published in ref. [143]). This result is in agreement with other studies probing TCR complex stoichiometry at the cell membrane *in situ* [142, 145], but contrasts with reports using different single-molecule imaging techniques such as electron microscopy and super-resolution microscopy [207, 208, 247, 364], where oligomers or "clusters" of TCR complexes have been found. How to reconcile these results is not a straightforward task. It seems, however, reasonable to argue that the use of bivalent antibody-coupled beads to identify the TCR in electron

microscopy studies might have induced some degree of receptor clustering [208, 247, 364]. Moreover, the membrane fixation protocols of the type used in these studies do not necessarily prevent protein movement [250]. In the case of super-resolution experiments by Lillemeier and co-workers, the TCR was found to be present in small clusters of 5-20 complexes when the TCR was imaged during contacts of T-cells with glass surfaces [207], but it now seems that T cells can signal upon interaction with surfaces, such as glass, that lack TCR ligands [145, 365]. In an elegant study Huse *et al.* used an antigenic peptide (bound to an MHC molecule) that is biologically inert until exposed to ultraviolet light (UV) to probe the kinetics of TCR triggering and the sensitivity of this receptor [365]. Unexpectedly, without exposure to UV it was possible to detect the adaptor protein Grb2 at the cell membrane. Grb2 (discussed in §1.3.2) is recruited to the plasma membrane by phospo-LAT. The presence of Grb2 at the membrane is thus indicating that some form of signalling is present in T cells prior to cognate TCR-pMHC interaction. More recently, James *et al.* used fluorescence recovery after photobleaching (FRAP) to probe the effects of an interaction with a glass surface on TCR mobility [145]. Jurkat T-cells and J45.01, a cell line with reduced expression of CD45 that is unable to trigger in response to TCR stimulation, were used to probe the TCR mobility in distinct regions of the cell. At the "top" of the cell, that is, "away" from a glass-surface contact, no differences could be found between signalling competent Jurkat T-cells and signalling compromised J45.01 cells whereas, at the surface contacting the glass, the results were significantly different. In J45.01 78% of the TCR molecules diffused back into the photobleached region whereas only 58% of the TCR returned in Jurkat T-cells. These findings raise the possibility that the reduction in mobility at the glass-interacting surface of the cell measured in the FRAP experiments is due to the clustering observed by Lillemeier *et al.* [207]. The nature of the signalling induced by the mere contact with a surface is not known, but it could arise from focal adhesion-mediated signalling. These structures sense mechanical force, such as that induced by a resistant surface like glass and, importantly, signalling through

focal adhesions is also compromised in J45.01 cells. Alternatively, contact with the glass surface could induce CD45 segregation, inducing weak local signalling.

In the single-molecule DySCo experiments, the cell surface contacting the glass was also imaged and the association level found for the TCR complex was around 5% (in comparison with ~10% for CD86). For these experiments, it was necessary to reduce the TCR levels by >90% in order to work in the single-molecule regime, in which case it is possible that there was insufficient receptor signalling to induce clustering artefacts. Nevertheless, even under these conditions, the behaviour of the TCR (and CD86) is not totally random, since there is at least 5% association of the proteins above background. Actin is likely to contribute to these effects as latrunculin treatment reduced this low level of association by almost 50%.

In a previous study, James *et al.* used a single-molecule spectroscopic technique, two-colour coincidence detection (TCCD) to probe the dynamics of protein-protein interactions [142]. Importantly, this analysis was done at the top surface of the cell and even here non-random behaviour of the membrane proteins was observed for the TCR complex and for other monomeric proteins analysed. It seems likely that a combination of the effects described by Kusumi and co-workers [144, 146, 366], wherein the actin meshwork underlying the cell membrane restricts and "corrals" protein diffusion, and also the behaviour of proteins in crowded environments [160] could account for the non-random behaviour of these proteins. Single-molecule studies show that many plasma membrane proteins do not obey simple Brownian motion but rather exhibit fast switching between different diffusing states [366]. Altogether, these effects indicate that conclusions regarding the valency of membrane molecules taken from measurements of protein association must be made with great caution and must be made in the context of comparisons with known dimeric and monomeric proteins, which is rarely done. Comparing the degree of association obtained for the TCR complex with that determined for CD28 and CD86 suggests that the TCR is no more an obligate dimer than CD86. It could be argued that the lower levels of expression used might have affected possible dynamic interactions [367],

but CD28 was also expressed at similar levels and exhibited fivefold higher levels of association than CD86.

A functionally monovalent TCR imposes important constraints on the triggering mechanism of this receptor. With the present results it seems likely that triggering relies on signalling through single TCR complexes rather than through the re-organization of complex bi- or multivalent receptors. Perhaps more importantly, a functionally monovalent TCR signalling unit, *i.e.* with one TCRαβ per unit, also ensures that the T cell response is only dependent on the intrinsic antigenicity of a given pMHC molecule. A bivalent interaction would offer the advantage of up to 100x lower dissociation rates when compared with a monovalent interaction [368], strongly biasing responses towards peptides expressed at very high levels on antigen presenting cells versus more weakly expressed peptides. In these circumstances, the efficiency of presentation rather than its inherent immunogenicity would likely determine the outcome of the response to a given antigen.

8.1.2 TCR triggering is not dependent on conformational changes

With results from Chapter 3 indicating that the TCR is a monovalent complex the question then arises of how a monovalent TCR/pMHC complex might initiate signalling. The valency of G-protein coupled receptors (GPCRs), one of the best-studied families of triggering receptors, has also been controversial [143, 369] but there is clear experimental evidence that a single, monovalent, purified GPCR is fully functional [370]. In the case of these receptors signalling is transduced across the cell membrane through a clear-cut conformational rearrangement upon ligand binding [371-373].

Although there are obvious structural differences between the TCR and GPCRs it is possible that some conformational rearrangement of TCR subunits, involving either the extracellular or intracellular domains, could contribute to receptor triggering. Rearrangements of each of these parts of the receptor were addressed in this thesis.

No large-scale extracellular subunit rearrangements accompany TCR triggering

A number of triggering models proposed for the TCR complex are based on rearrangements of TCR-CD3 subunits upon pMHC interaction [53]. Given the lack of even an overall TCR complex structure for the "resting" complex, testing these models is extremely challenging. However, all of these models rely on a common feature, *i.e.* that large inter-subunit rearrangements would lead to the burial of solvent-exposed surfaces. In Chapter 4 an extensive mutagenesis-based approach was used to determine the dependence of TCR triggering on large inter-subunit rearrangements. The mutations of CD3ε, TCRα and TCRβ implied that the TCR complex is able to signal as a largely static object, that is, without relying on the formation of new subunit interactions.

The idea that native ligands might induce triggering *via* a mechanism involving relatively minor or no structural rearrangements in the receptor is not a new one. Following detailed comparisons of a number of complexes, Garcia *et al.* concluded that "no large-scale conformational changes are obvious in the complex structures that might have an impact on signal transduction" [42]. Similarly, for pMHC antigens that induce qualitatively distinct signals, and focusing particularly on the well-ordered variable regions of the TCR, Ding and Wiley *et al.* proposed that "the lack of correlation between structural changes and the type of T cell signals induced provides direct evidence that different signals are not generated by different ligand-induced conformational changes in the αβ TCR" [57]. The early structural work thus implied that ligand recognition by TCRαβ involves rigid-body interactions with pMHC. Furthermore, Shore *et al.* (submitted for publication) have recently solved the crystal structure of mouse CD3ε bound to an Fab fragment of the mitogenic antibody 2C11. This structure can now be directly compared with an equivalent, unliganded, CD3ε molecule from the same species for the first time. In solution at least, binding of the mitogenic Fab did not induce any major intra-subunit conformational change. The ability to trigger *via* rigid-body interactions would not be unique to the TCR as the

extracellular structure of CTLA-4, which shares with TCR the lack of cytoplasmic associated kinases, also remains unchanged upon ligand binding, at least in solution [374].

What else can be inferred from the triggering assay for CD3ε, TCRα and TCRβ mutants? To start with, there is a striking correlation between surface expression and triggering capacity. For all the mutants tested, increasing expression levels led to stronger T-cell activation, until a plateau was eventually reached. Surface expression similar or close to that of wild-type protein led to "high" activation levels. Not surprisingly, mutants that failed to be detected at the cell surface did not induce triggering above background levels. More interestingly, intermediate expression levels also induced intermediate T-cell activation. In the light of these results it would be interesting to determine why the mutations have decreased protein expression. It is possible that the mutations simply affected the rate of folding of more-or-less normal complexes, or that slightly misfolded complexes reached the surface. In the second case, this would strengthen the argument that the TCR is less dependent on its correct folding/structure, than it is on just reaching the cell surface. Irrespective of all this, the complex was still able to trigger, to an extent that was proportional to its expression level. For all the three proteins studied, no single mutation was found to significantly impair T-cell activation, taking into account its expression level. This is an indication that TCR triggering is not dependent on the formation of new protein-protein interfaces, and thus that it does not rely on large inter-subunit conformational rearrangements.

The mutagenesis approach also provided a better understanding of possible subunit interactions within the complex, offering two important new insights. First, apart from the interface that it forms with CD3δ and CD3γ, CD3ε is apparently completely exposed in the complex. This observation explains the greater antigenicity of CD3ε versus CD3δ and CD3γ, but is inconsistent with early [375, 376] and more recent [54] studies. The expectation that CD3ε interacts directly with TCRαβ came from early studies in which CD3ε was chemically cross-linked to both TCRα and TCRβ [375, 377] and from the apparent ability of CD3ε

to rescue TCRβ expression in co-transfections [376, 378]. However, other cross-linking studies suggest closer association of TCRβ with CD3γ than with the other CD3 chains [44] and the expression of chimeric proteins suggests preferential association of TCRα with CD3εδ [379, 380]. Preferential associations must involve CD3δ and CD3γ chains directly, as CD3ε is present in both heterodimers. Owing to their extreme sensitivity to mutation, it was not possible to assign docking sites for TCRαβ on CD3δ and CD3γ. It seems clear, however, that similar regions at the "top" of both CD3δ and γ, where all four of the conserved glycosylation sites are found in primates (at the start of the C and G strands in CD3γ and in the BC and FG loops of CD3δ), are exposed in the complex. A second conclusion is that TCRαβ contacts the CD3 chains at a single site formed by the Cβ CD and EF loops plus several Cα DE loop residues, in agreement with results found by others [48, 52, 53, 206]. Although the patch on TCRαβ is relatively small, it protrudes from the structure in such a way that both CD3γ and CD3δ could form small contacts with TCRαβ.

The challenge now is to determine how such a monomeric complex could initiate signalling without substantial changes in the overall structure and disposition of the component subunits. For example, it is possible that much more subtle conformational rearrangements induce signalling by the receptor. Conscious of the uncertainties created by the lack of a quaternary structure it seemed important to design an approach to purify the entire TCR complex for structural studies. The first steps towards the extraction and purification of the TCR complex for cryo-EM studies were described in Chapter 7. The approach developed, *i.e.* involving surface capture of TCR complexes expressed at high levels in a CHO cell line, offers significant advantages over other methods where complexes are extracted from whole cell lysates. Previous approaches have tried to capture the TCR complex using affinity tags placed at the cytoplasmic tail of different subunits [245, 351]. This, however, has a major disadvantage: targeting an intracellular region of the complex requires protein targeting and isolation from cell lysates. The assembly of the TCR complex is not a faultless mechanism. For example, in the present study (§7.3.3) misfolding of CD3 chains was observed to

lead to the formation of unusual disulphide-bonded CD3 dimers, as observed by others. The reason for this is that, at any point in time, a number of TCR complexes is being formed at the ER and degraded at specific lysosome compartments. Upon cell lysis all these incomplete or abnormal TCR complexes become accessible for purification procedures.

In the strategy described in Chapter 7, targeting functional cell surface TCRαβ with a high-affinity pMHC ensures that only correctly expressed proteins and most likely fully assembled complexes, defined as those reaching the cell surface, are captured and used for purification. Successful cryo-EM structural reconstruction is highly dependent on isolating biochemically homogeneous samples. Incomplete or incorrectly assembled complexes present inside the cell would drastically reduce the ability to obtain high resolution images. Combining the crystal structures already available for TCR and CD3 dimers, together with the information obtained by the mutagenesis analysis of the inter-subunit contacts and, in the future, the cryo-EM study of the entire complex it will be possible to confidently establish an overall structure for this receptor and ascertain if smaller conformational changes occur upon pMHC ligation.

CD3εcytoplasmic domain interactions with the plasma membrane do not protect it from Tyr phosphorylation

In biochemical analyses of CD3ζ cytoplasmic domain interactions with the acidic lipid dimyristoylphosphatidylglycerol (DMPG; which is abundant in the inner leaflet of the plasma membrane) Stern and co-workers observed an unexpected affinity between these molecules [223, 228]. More surprising was the finding that this interaction was accompanied by a lipid-dependent structural change in the CD3ζ cytoplasmic domain [223]. In light of these results it was proposed that binding of CD3ζ to the inner leaflet of the cell membrane could somehow affect Src phosphorylation of the CD3 ITAMs [223]. Building on these observations Xu *et al.,* asked if a similar interaction between CD3ε and the plasma membrane could occur *in vivo* [224]. The outcome of their FRET experiments suggested that this could indeed be the case and an NMR structure of CD3ε cytoplasmic domain

with an acidic-phospholipid mixture revealed that the two Tyr residues from the ITAM present in CD3ε were buried in the acyl region of the phospholipids [224]. With these results Xu *et al.* went on to propose that this association could control TCR triggering by sequestering ITAMs from Src kinase phosphorylation. The importance of these findings for TCR triggering led to several review articles suggesting a new framework for the mechanism of TCR triggering [101, 229, 230, 381]. Importantly, Xu *et al.* were able to identify the residues responsible to mediate the interaction between the CD3ε cytoplasmic domain and the plasma membrane [224]; mutation of these residues was shown to abolish membrane interaction of CD3ε. However, the original study failed to probe the biological consequences of these mutations. This seemed to be a vital experiment given the potential impact of their results.

The work described in Chapter 5 aimed to understand what is the functional role of CD3ε cytoplasmic domain interaction with the plasma membrane. If the membrane interaction prevents Src accessibility to the ITAM then mutation of the residues responsible for the interaction (CD3εEmut1+2; §5.3.1) should expose the Tyr residues and lead to ITAM phosphorylation. This was not found to be the case. No Tyr phosphorylation could be detected in either wild-type or mutant CD3ε expressed in Jurkat T-cells. This result indicated that membrane interaction cannot be the mechanism responsible for the absence of CD3 ITAM phosphorylation in resting T cells. What is the mechanism controlling ITAM phosphorylation, then? Phosphatases, discussed in detail in §1.4.3, seemed an obvious candidate. Blocking phosphatase activity with pervanadate readily induced the strong Tyr phosphorylation of both wild-type and mutant CD3ε. In fact, and completely opposite to what was proposed in the initial studies by Stern *et al.,* and Xu *et al.,* mutation of the residues responsible for CD3ε interaction with the plasma membrane slowed down ITAM phosphorylation upon pervanadate treatment and also decreased T-cell activation in response to anti-TCR antibody stimulation. Similar observations have just been recently extended to CD3ζ in a similar study [225].

The outstanding conclusion from the experiments described in Chapter 5 is that membrane interaction is unlikely to be the molecular mechanism responsible for controlling CD3ε phosphorylation, in fact, if it has any functional role, this seems to favour phosphorylation. Crucially these results left an important question unanswered: what is the mechanism controlling CD3 phosphorylation? Pervanadate treatment suggested that phosphatases could be the answer. In their published response to the results described in Chapter 5 and discussed above, Gagnon *et al.*, speculated about the real effect of pervanadate [382]. In their report, it was found by a FRET analysis that pervanadate apparently induced the dissociation of $CD3\varepsilon_{CD}$, possibly by reducing the negative charge of the inner leaflet of the cell membrane, *i.e.*, that pervanadate led to a re-distribution of the cell membrane phospholipids. This result led Gagnon *et al.* to suggest that pervanadate acted directly on the CD3ε cytoplasmic domain forcing its exposure to Src kinases. The molecular mechanism behind this effect of pervanadate was not discussed. It seems however, more likely that the observed dissociation of CD3ε cytoplasmic domain from the cell membrane upon pervanadate treatment is a consequence of tyrosine phosphorylation. Phosphorylation of CD3ε would change the charge balance of its cytoplasmic domain through the addition of the negatively charged phosphates to the Tyr residues. This change in size and charge of Tyr could explain, based on the previous NMR data and the charge-mediated interaction between the CD3ε cytoplasmic domain and the cell membrane, the dissociation of the CD3ε cytoplasmic domain from the membrane. In any case, the important point is that even in the absence of a CD3ε interaction with the plasma membrane there is no observable phosphorylation and therefore some other mechanism must be responsible for controlling this crucial step in TCR triggering.

8.1.3 CD45: a local, direct regulator of TCR phosphorylation?

These considerations made it important to study in detail the role of phosphatases and, in particular, the role of abundant membrane tyrosine phosphatases such as CD45, in controlling the levels of TCR phosphorylation.

The role of PTPs in TCR triggering has been difficult to dissect and, as a consequence, remains very controversial [178, 186-188]. In fact, recent studies have tended to completely overlook any contribution of PTPs in TCR triggering and suggest instead triggering models where receptor clustering/aggregation or different conformational rearrangements are the sole mediators of signalling [208, 216-218, 243, 340, 364, 383, 384]. PTPs might not act alone in the initial TCR triggering events but their potential contribution certainly needs to be considered. Some reports have focused on the role of CD45 in different stages of T-cell development and activation. The mouse knockout for CD45 leads to a severe compromise of thymus development, limiting most studies of TCR triggering [316]. However, in an elegant study McNeill *et al.* reconstituted CD45 knockout mice with T-cells with different levels of CD45 and found that only 3% of wild-type CD45 activity restored T cell numbers and normal cytotoxic T cell responses [321]. These observations have also been confirmed to some extent in studies made by Weiss and co-workers more recently. Jurkat-derived cell lines with low levels of CD45 were generated and, surprisingly, these cells fail to become activated [322]. What can be concluded from these reports showing a positive, a negative or even a dual role for CD45 in controlling TCR triggering? There are likely two factors that contribute to these somewhat contradictory results. The first arises from the fact that Lck activity is also controlled by this PTP [187]. The second key point is that TCR triggering is an extremely fast process. Ideally, in disentangling these effects, TCR triggering ought to be analysed immediately after specific CD45 inhibition, but this has not been possible. One approach, developed in Chapter 6, is to down-regulate CD45, and thus decrease phosphatase activity at the cell membrane, using lentiviral-mediated delivery of shRNA targeting CD45. The caveat of this approach is that it still does not allow any conclusions to be inferred about the effects of acute blockade of CD45 activity, *i.e.* on the order of seconds. Instead, responses to down-regulation of CD45 were followed on a time-scale of days. This approach nevertheless revealed that in cells completely lacking CD45, enhanced constitutive tyrosine phosphorylation of CD3ε could be detected. Whether this is the result of changes induced in Lck

activity or some other mechanism is not yet known. Furthermore, a drastic reduction of CD45 (seven to nine fold) led to the surface expression of CD69, an early marker of T-cell activation, in both Jurkat T-cells and freshly isolated $CD3^+CD4^+$ T cells from PBLs. CD69 up-regulation in response to CD45 down-regulation was also dependent on TCR expression: reduction of cell surface TCR expression led to lower levels of CD69 up-regulation. These results therefore seem to suggest that T-cell activation is directly affected by CD45. The broad specificity and high levels of activity of CD45 [385, 386] most likely favour the direct control of TCR triggering through the dephosphorylation of CD3 ITAM tyrosine residues. One report has already shown *in vitro* the ability of CD45 to dephosphorylate CD3ζ [191] and in Chapter 5, it was found that co-expression Lck Y505F and the CD3ε in HEK-293T cells induced the strong phosphorylation of ITAM tyrosine which was almost completely absent when CD45 was also included in the transfection. It is conceivable that the interplay of Lck (with smaller contributions from other Src kinases such as Fyn) and CD45 directly determines TCR phosphorylation. Perturbations of this balance, such as those induced by CD45 down-regulation, would be expected to affect T-cell activation, as observed in the experiments presented in Chapter 6.

Is tonic control of receptor triggering unique to the TCR? The epidermal growth factor receptor (EGFR) provides one of the most important paradigms for receptor triggering and was for a long time assumed to rely only on ligand-induced dimerization to induce kinase activation [195]. Recent work, however, suggests that monomers and dimers of the EGFR exist in equilibrium and, importantly, receptors from the EGFR family cycle between a phosphorylated and unphosphorylated state on the time scale of seconds [200, 387, 388]. EGFR phosphorylation thus seems to be under tonic control by membrane PTP with ligand-binding to the receptor overcoming this steady state by inducing kinase activity and/or PTP inhibition [389]. In lymphocytes, CD45 has been shown to directly dephosphorylate and inactivate JAK-family kinases, in response to several cytokines [390, 391], suggesting that even these classical, dimerizing, JAK/STAT dependent receptors are under global tonic control by PTPs. Control of cellular

metabolic processes by phosphorylation-dephosphorylation cycles is also a well-established mechanism for cytosolic proteins, like ERK, Akt, Jnk, p38 and cell-cycle cyclins [387, 392]. If a similar mechanism is indeed controlling TCR phosphorylation it clearly would not be very unique.

8.1.4 Lck and CD45: global homeostatic control of TCR phosphorylation

Down-regulating CD45 in experiments described in Chapter 6 induced strong T-cell activation but then revealed how cells can slowly adapt to this new condition and return to a resting phenotype. Strong down-regulation of CD45 induced T-cell activation followed by extensive cell death. However, cells infected with a lower dose of lentiviral plasmids carrying shRNA were able to proliferate normally after an initial period of cell death. Probing CD45 expression in these cells revealed the presence of two populations, one with almost wild-type levels of CD45 and another with markedly reduced (7-8 fold) expression of this PTP. Surprisingly, the CD69 levels in cells with low CD45 expression were extremely low compared with Jurkat T-cells infected with high doses of lentiviruses even though the reduced, new levels of CD45 were very similar. Several possibilities could explain the discrepancy in CD69 up-regulation following similar levels of CD45 down-regulation. One possibility, taking into consideration the time-scale of these responses, is that cellular adaptation is occurring in the cultures in which there is no CD69 upregulation. Indeed, cells expressing lower levels of CD45 also had lower levels of Lck, and treatment of the cells with the Lck inhibitor PP2 led to an up-regulation of Lck expression for all cells. This suggests that cells can adapt to CD45 down-regulation and return to a basal phenotype by reducing Lck expression.

It therefore seems as if an active, apparently homeostatic process is adjusting Lck expression in response to changes in CD45 activity. If this were true, then it would be expected that expression of Lck in an Lck deficient cell line would in turn induce changes in CD45 expression. Taking advantage of J.Cam 1.6 T-cells, a cell line derived from Jurkat T-cells where expression of Lck is absent, it

was possible to test this hypothesis. Expression of wild-type Lck not only induced CD45 upregulation but even led to a reduction in TCR and ZAP-70 expression. These observations suggest that there is homeostatic control of CD45, Lck, TCR and ZAP-70 that is sensitive to global changes in CD45 and Lck enzymatic activity. Expression of a mutant form of Lck, Y505F, which has a higher overall kinase activity [309, 310], induced even more pronounced up-regulation of CD45 and down-regulation of TCR and ZAP-70.

Homeostatic, or retrograde, signalling is a common mechanism for fine-tune and adapting signalling responses to diverse stimuli. In eukaryotes at least two fundamental processes rely on homeostatic responses at the protein expression level to allow cell survival: control of ATP production and a response to sudden accumulations of unfolded proteins in the ER. ATP levels change abruptly in response to diverse stimuli. A sudden decrease in ATP triggers several mitochondrial signalling pathways leading to up-regulation of proteins involved in ATP production [393-395]. A similar type of regulatory mechanism is observed when accumulation of unfolded proteins in the lumen of the ER triggers an increase in gene expression of chaperones [396]. In both examples, feedback loops sense and adapt to new conditions by modifying gene expression in order to sustain cellular viability.

In the case of the effects observed in Jurkat T-cells, what could be the mechanism of the homeostatic equilibrium observed? It is tempting to speculate that similar mechanisms involved in the desensitization of the TCR signalling pathways following strong T-cell activation could be involved in the adaptive responses to changes in the CD45/Lck equilibrium. TCR activation is followed by a stage of desensitization where, for example, surface expression of the TCR is down-regulated through a mechanism that, although it is not fully understood, seems to involve Lck activity [397]. However, the correlation found between Lck and CD45 expression dependent on global enzymatic activity of these proteins inside the cells does not appear to have been described before.

The homeostatic control of protein expression might explain why low levels of CD45 have not been linked to TCR triggering before. In previous studies it is

possible that, during the selection or maturation of cells in which CD45 has been knocked down, feedback mechanisms have led the cell to adapt to the new condition and maintain a "resting" phenotype [178, 186]. The new CD45 down-regulation approach described in this thesis allowed close monitoring of the expression level of proteins involved in T-cell activation unmasking a previously overlooked role of CD45 in controlling TCR phosphorylation levels [178, 300, 312].

8.1.5 Local ultra-sensitive processes controlling Lck activity

Crystal structures of Src kinases offer snapshots of the "closed"-inactive and "open"-active states but are generally uninformative with regard to the dynamics of their formation. Small-angle X-ray solution scattering combined with molecular dynamics simulations revealed the equilibrium between the different conformational states of Src and Hck in solution [398, 399]. The results indicated that in the unphosphorylated form these kinases mainly adopt two distinct states: around 84% of Src or Hck assuming a closed, inactive conformation and 16% an open, active state. Phosphorylated Tyr505 Src forms a single, closed conformation [399].

Given the high degree of conservation of Src family kinases it seemed very likely that Lck is also distributed between multiple states *in vivo* and Acuto and co-workers [298] were among the first to approach this quantitatively. Using the levels of phosphorylation of Tyr505 and Tyr394 to draw inferences about the distribution of Lck between active and inactive states, they concluded that up to 40% of Lck is constitutively active. An additional striking outcome of their global analysis of Lck phosphorylation was that upon T-cell activation there was no apparent increase in the levels of activated, *i.e.* Tyr394 phosphorylated Lck. An important caveat is that local changes in Lck phosphorylation might not be detectable following whole-cell lysis prior to Western blotting or might not be resolved by confocal immunofluorescence microscopy, the main approaches used by Acuto *et al.*

Among local processes that might have been missed it is possible that the interaction of kinase SH2 domains with their substrates, which would itself be phosphorylation dependent, would stabilize the kinase in the active or "primed" state, favouring multi-site phosphorylation of receptors with more than one tyrosine [166]. This has been confirmed for peptides that displace the SH2 or SH3 domains of c-Src, Hck, and closely related Fes and Abl kinases [326, 328, 329, 336, 400]. In fact, the arrangement of an N-terminal SH2 linked to a TyrK domain is highly conserved and probably evolved as an invariant signalling unit early in evolution [401]. The SH2-TyrK unit has been found in the unicellular choanoflagellate *Monosiga brevicollis* [402] and probably evolved to efficiently target tyrosine kinase activity to specific sites in the cell. Observations involving c-Src, Hck, Fes and other kinases suggest that during the course of evolution the initial role of SH2 domains in delivering TyrK to specific targets evolved to incorporate another function: an allosteric control of the kinase activity. The up-regulation in Lck kinase activity observed in response to phosphorylated CD3ε ITAM, described in Chapter 6, suggests this kinase activity is also under some form of allosteric regulation with important consequences for the local control of TCR triggering.

8.2 Final remarks

The solution to the TCR "triggering problem" remains elusive, but there is also a great deal still to be learned about the "resting" state of the triggering apparatus of the T cell. An important challenge is to identify the feedback control mechanisms underpinning the homeostatic control of TCR phosphorylation in resting cells, if it occurs. Similarly, a much better understanding of the intrinsic and extrinsic factors driving the inter-conversion of the active and inactive states of the Src kinases is required, both in resting cells and under conditions of receptor triggering. It will also be important to know the actual levels of activity of the various states of Lck so that a better understanding of how much activity needs to be constrained in resting cells can be derived. It will also be helpful to

know the effective affinities of the SH2 domain of Lck for phosphorylated Tyr505 versus membrane anchored, tyrosine phosphorylated substrates, so that the extent to which, if at all, local substrate interactions impose "switch-like" behaviour on Lck can be estimated.

Bibliography

1. MORRIS, S.C., *Early Metazoan Evolution: Reconciling Paleontology and Molecular Biology*. American Zoologist, 1998. **38**(6): p. 867-877.
2. Beutler, B., *Innate immunity: an overview*. Molecular immunology, 2004. **40**(12): p. 845-59.
3. Muller, W.E., *The origin of metazoan complexity: porifera as integrated animals*. Integrative and comparative biology, 2003. **43**(1): p. 3-10.
4. Dewel, R.A., *New perspectives on the origin of metazoan complexity: an introduction to the symposium*. Integrative and comparative biology, 2003. **43**(1): p. 1-2.
5. Janeway, C.A., Jr. and R. Medzhitov, *Innate immune recognition*. Annual review of immunology, 2002. **20**: p. 197-216.
6. Cooper, M.D. and M.N. Alder, *The evolution of adaptive immune systems*. Cell, 2006. **124**(4): p. 815-22.
7. Burnet, M., *Auto-immune disease. I. Modern immunological concepts*. British medical journal, 1959. **2**(5153): p. 645-50.
8. Fearon, D.T. and R.M. Locksley, *The instructive role of innate immunity in the acquired immune response*. Science, 1996. **272**(5258): p. 50-3.
9. Medzhitov, R., *Recognition of microorganisms and activation of the immune response*. Nature, 2007. **449**(7164): p. 819-26.
10. Iwasaki, A. and R. Medzhitov, *Regulation of adaptive immunity by the innate immune system*. Science, 2010. **327**(5963): p. 291-5.
11. Hemmi, H., et al., *A Toll-like receptor recognizes bacterial DNA*. Nature, 2000. **408**(6813): p. 740-5.
12. Akira, S. and K. Takeda, *Toll-like receptor signalling*. Nature reviews. Immunology, 2004. **4**(7): p. 499-511.
13. Martinon, F., A. Mayor, and J. Tschopp, *The inflammasomes: guardians of the body*. Annual review of immunology, 2009. **27**: p. 229-65.
14. Rifkin, I.R., et al., *Toll-like receptors, endogenous ligands, and systemic autoimmune disease*. Immunological reviews, 2005. **204**: p. 27-42.
15. Medzhitov, R. and C.A. Janeway, Jr., *Decoding the patterns of self and nonself by the innate immune system*. Science, 2002. **296**(5566): p. 298-300.
16. Medzhitov, R. and C.A. Janeway, Jr., *Innate immunity: impact on the adaptive immune response*. Current opinion in immunology, 1997. **9**(1): p. 4-9.
17. Nossal, G.J., *Negative selection of lymphocytes*. Cell, 1994. **76**(2): p. 229-39.
18. Oettinger, M.A., et al., *RAG-1 and RAG-2, adjacent genes that synergistically activate V(D)J recombination*. Science, 1990. **248**(4962): p. 1517-23.
19. Schatz, D.G., M.A. Oettinger, and D. Baltimore, *The V(D)J recombination activating gene, RAG-1*. Cell, 1989. **59**(6): p. 1035-48.
20. Harwood, N.E. and F.D. Batista, *Early events in B cell activation*. Annual review of immunology, 2010. **28**: p. 185-210.
21. Nossal, G.J., *Antibody production by single cells*. British journal of experimental pathology, 1958. **39**(5): p. 544-51.
22. Nossal, G.J., *Antibody production by single cells. III. The histology of antibody production*. British journal of experimental pathology, 1959. **40**: p. 301-11.

23. Harwood, N.E. and F.D. Batista, *New insights into the early molecular events underlying B cell activation.* Immunity, 2008. **28**(5): p. 609-19.
24. Depoil, D., et al., *Early events of B cell activation by antigen.* Science signaling, 2009. **2**(63): p. pt1.
25. Kelsoe, G., *Life and death in germinal centers (redux).* Immunity, 1996. **4**(2): p. 107-11.
26. Rajewsky, K., *Clonal selection and learning in the antibody system.* Nature, 1996. **381**(6585): p. 751-8.
27. Woof, J.M. and D.R. Burton, *Human antibody-Fc receptor interactions illuminated by crystal structures.* Nature reviews. Immunology, 2004. **4**(2): p. 89-99.
28. Medzhitov, R. and C.A. Janeway, Jr., *Innate immune recognition and control of adaptive immune responses.* Seminars in immunology, 1998. **10**(5): p. 351-3.
29. Medzhitov, R. and C.A. Janeway, Jr., *Innate immune induction of the adaptive immune response.* Cold Spring Harbor symposia on quantitative biology, 1999. **64**: p. 429-35.
30. Moretta, A., *Natural killer cells and dendritic cells: rendezvous in abused tissues.* Nature reviews. Immunology, 2002. **2**(12): p. 957-64.
31. Born, W.K., C.L. Reardon, and R.L. O'Brien, *The function of gammadelta T cells in innate immunity.* Current opinion in immunology, 2006. **18**(1): p. 31-8.
32. Boismenu, R. and W.L. Havran, *An innate view of gamma delta T cells.* Current opinion in immunology, 1997. **9**(1): p. 57-63.
33. Allison, J.P., B.W. McIntyre, and D. Bloch, *Tumor-specific antigen of murine T-lymphoma defined with monoclonal antibody.* Journal of immunology, 1982. **129**(5): p. 2293-300.
34. Haskins, K., et al., *The major histocompatibility complex-restricted antigen receptor on T cells. I. Isolation with a monoclonal antibody.* The Journal of experimental medicine, 1983. **157**(4): p. 1149-69.
35. Meuer, S.C., et al., *Clonotypic structures involved in antigen-specific human T cell function. Relationship to the T3 molecular complex.* The Journal of experimental medicine, 1983. **157**(2): p. 705-19.
36. Stehelin, D., et al., *DNA related to the transforming gene(s) of avian sarcoma viruses is present in normal avian DNA.* Nature, 1976. **260**(5547): p. 170-3.
37. Spector, D.H., H.E. Varmus, and J.M. Bishop, *Nucleotide sequences related to the transforming gene of avian sarcoma virus are present in DNA of uninfected vertebrates.* Proceedings of the National Academy of Sciences of the United States of America, 1978. **75**(9): p. 4102-6.
38. Hedrick, S.M., et al., *Isolation of cDNA clones encoding T cell-specific membrane-associated proteins.* Nature, 1984. **308**(5955): p. 149-53.
39. Hedrick, S.M., et al., *Sequence relationships between putative T-cell receptor polypeptides and immunoglobulins.* Nature, 1984. **308**(5955): p. 153-8.
40. Chien, Y.H., et al., *Somatic Recombination in a Murine T-Cell Receptor Gene.* Nature, 1984. **309**(5966): p. 322-326.
41. Yanagi, Y., et al., *A Human T-Cell-Specific Cdna Clone Encodes a Protein Having Extensive Homology to Immunoglobulin-Chains.* Nature, 1984. **308**(5955): p. 145-149.

42. Garcia, K.C., et al., *An alphabeta T cell receptor structure at 2.5 A and its orientation in the TCR-MHC complex*. Science, 1996. **274**(5285): p. 209-19.
43. Garboczi, D.N., et al., *Structure of the complex between human T-cell receptor, viral peptide and HLA-A2*. Nature, 1996. **384**(6605): p. 134-41.
44. Brenner, M.B., I.S. Trowbridge, and J.L. Strominger, *Cross-linking of human T cell receptor proteins: association between the T cell idiotype beta subunit and the T3 glycoprotein heavy subunit*. Cell, 1985. **40**(1): p. 183-90.
45. Samelson, L.E., J.B. Harford, and R.D. Klausner, *Identification of the components of the murine T cell antigen receptor complex*. Cell, 1985. **43**(1): p. 223-31.
46. Sussman, J.J., et al., *Failure to synthesize the T cell CD3-zeta chain: structure and function of a partial T cell receptor complex*. Cell, 1988. **52**(1): p. 85-95.
47. Wegener, A.M., et al., *Distinct domains of the CD3-gamma chain are involved in surface expression and function of the T cell antigen receptor*. The Journal of biological chemistry, 1995. **270**(9): p. 4675-80.
48. Call, M.E., et al., *The organizing principle in the formation of the T cell receptor-CD3 complex*. Cell, 2002. **111**(7): p. 967-79.
49. Call, M.E., J. Pyrdol, and K.W. Wucherpfennig, *Stoichiometry of the T-cell receptor-CD3 complex and key intermediates assembled in the endoplasmic reticulum*. EMBO J, 2004. **23**(12): p. 2348-57.
50. Call, M.E. and K.W. Wucherpfennig, *Common themes in the assembly and architecture of activating immune receptors*. Nat Rev Immunol, 2007. **7**(11): p. 841-50.
51. Xu, C., M.E. Call, and K.W. Wucherpfennig, *A membrane-proximal tetracysteine motif contributes to assembly of CD3deltaepsilon and CD3gammaepsilon dimers with the T cell receptor*. The Journal of biological chemistry, 2006. **281**(48): p. 36977-84.
52. Kuhns, M.S. and M.M. Davis, *Disruption of extracellular interactions impairs T cell receptor-CD3 complex stability and signaling*. Immunity, 2007. **26**(3): p. 357-69.
53. Kuhns, M.S., M.M. Davis, and K.C. Garcia, *Deconstructing the form and function of the TCR/CD3 complex*. Immunity, 2006. **24**(2): p. 133-9.
54. Kuhns, M.S., et al., *Evidence for a functional sidedness to the alphabetaTCR*. Proceedings of the National Academy of Sciences of the United States of America, 2010. **107**(11): p. 5094-9.
55. Sun, Z.J., et al., *Mechanisms contributing to T cell receptor signaling and assembly revealed by the solution structure of an ectodomain fragment of the CD3 epsilon gamma heterodimer*. Cell, 2001. **105**(7): p. 913-23.
56. Sun, Z.-Y.J., et al., *Solution structure of the CD3epsilondelta ectodomain and comparison with CD3epsilongamma as a basis for modeling T cell receptor topology and signaling*. Proceedings of the National Academy of Sciences of the United States of America, 2004. **101**(48): p. 16867-72.
57. Ding, Y.H., et al., *Four A6-TCR/peptide/HLA-A2 structures that generate very different T cell signals are nearly identical*. Immunity, 1999. **11**(1): p. 45-56.
58. Stewart-Jones, G.B., et al., *A structural basis for immunodominant human T cell receptor recognition*. Nature immunology, 2003. **4**(7): p. 657-63.

59. Stewart-Jones, G.B., et al., *Structures of three HIV-1 HLA-B*5703-peptide complexes and identification of related HLAs potentially associated with long-term nonprogression.* Journal of immunology, 2005. **175**(4): p. 2459-68.
60. Kjer-Nielsen, L., et al., *Crystal structure of the human T cell receptor CD3 epsilon gamma heterodimer complexed to the therapeutic mAb OKT3.* Proc Natl Acad Sci U S A, 2004. **101**(20): p. 7675-80.
61. Sun, Z.Y., et al., *Solution structure of the CD3epsilondelta ectodomain and comparison with CD3epsilongamma as a basis for modeling T cell receptor topology and signaling.* Proc Natl Acad Sci U S A, 2004. **101**(48): p. 16867-72.
62. Call, M.E., et al., *The structure of the zetazeta transmembrane dimer reveals features essential for its assembly with the T cell receptor.* Cell, 2006. **127**(2): p. 355-68.
63. Rudolph, M.G., R.L. Stanfield, and I.A. Wilson, *How TCRs bind MHCs, peptides, and coreceptors.* Annu Rev Immunol, 2006. **24**: p. 419-66.
64. Reth, M., *Antigen receptor tail clue.* Nature, 1989. **338**(6214): p. 383-4.
65. Chan, A.C., et al., *ZAP-70: a 70 kd protein-tyrosine kinase that associates with the TCR zeta chain.* Cell, 1992. **71**(4): p. 649-62.
66. Chan, A.C., D.M. Desai, and A. Weiss, *The role of protein tyrosine kinases and protein tyrosine phosphatases in T cell antigen receptor signal transduction.* Annual review of immunology, 1994. **12**: p. 555-92.
67. Weiss, A. and D.R. Littman, *Signal transduction by lymphocyte antigen receptors.* Cell, 1994. **76**(2): p. 263-74.
68. van Oers, N.S., N. Killeen, and A. Weiss, *Lck regulates the tyrosine phosphorylation of the T cell receptor subunits and ZAP-70 in murine thymocytes.* The Journal of experimental medicine, 1996. **183**(3): p. 1053-62.
69. Weissenhorn, W., et al., *Phosphorylated T cell receptor zeta-chain and ZAP70 tandem SH2 domains form a 1:3 complex in vitro.* European journal of biochemistry / FEBS, 1996. **238**(2): p. 440-5.
70. Holst, J., et al., *Scalable signaling mediated by T cell antigen receptor-CD3 ITAMs ensures effective negative selection and prevents autoimmunity.* Nature immunology, 2008. **9**(6): p. 658-66.
71. Blanden, R.V., et al., *Genes required for cytotoxicity against virus-infected target cells in K and D regions of H-2 complex.* Nature, 1975. **254**(5497): p. 269-70.
72. Zinkernagel, R.M. and P.C. Doherty, *Restriction of in vitro T cell-mediated cytotoxicity in lymphocytic choriomeningitis within a syngeneic or semiallogeneic system.* Nature, 1974. **248**(450): p. 701-2.
73. Mazza, C. and B. Malissen, *What guides MHC-restricted TCR recognition?* Seminars in immunology, 2007. **19**(4): p. 225-35.
74. Van Laethem, F., et al., *Deletion of CD4 and CD8 coreceptors permits generation of alphabetaT cells that recognize antigens independently of the MHC.* Immunity, 2007. **27**(5): p. 735-50.
75. Madden, D.R., *The three-dimensional structure of peptide-MHC complexes.* Annual review of immunology, 1995. **13**: p. 587-622.
76. Stern, L.J., et al., *Crystal structure of the human class II MHC protein HLA-DR1 complexed with an influenza virus peptide.* Nature, 1994. **368**(6468): p. 215-21.

77. Madden, D.R., et al., *The three-dimensional structure of HLA-B27 at 2.1 A resolution suggests a general mechanism for tight peptide binding to MHC.* Cell, 1992. **70**(6): p. 1035-48.
78. Bjorkman, P.J., et al., *Structure of the human class I histocompatibility antigen, HLA-A2.* Nature, 1987. **329**(6139): p. 506-12.
79. Bjorkman, P.J., et al., *The foreign antigen binding site and T cell recognition regions of class I histocompatibility antigens.* Nature, 1987. **329**(6139): p. 512-8.
80. Townsend, A. and J. Trowsdale, *The transporters associated with antigen presentation.* Seminars in cell biology, 1993. **4**(1): p. 53-61.
81. Townsend, A. and H. Bodmer, *Antigen recognition by class I-restricted T lymphocytes.* Annual review of immunology, 1989. **7**: p. 601-24.
82. Heemels, M.T. and H. Ploegh, *Generation, translocation, and presentation of MHC class I-restricted peptides.* Annual review of biochemistry, 1995. **64**: p. 463-91.
83. Townsend, A.R., et al., *Cytotoxic T lymphocytes recognize influenza haemagglutinin that lacks a signal sequence.* Nature, 1986. **324**(6097): p. 575-7.
84. Townsend, A.R., et al., *The epitopes of influenza nucleoprotein recognized by cytotoxic T lymphocytes can be defined with short synthetic peptides.* Cell, 1986. **44**(6): p. 959-68.
85. Unanue, E.R., *Antigen-presenting function of the macrophage.* Annual review of immunology, 1984. **2**: p. 395-428.
86. Babbitt, B.P., et al., *Binding of immunogenic peptides to Ia histocompatibility molecules.* Nature, 1985. **317**(6035): p. 359-61.
87. Shi, G.P., et al., *Cathepsin S required for normal MHC class II peptide loading and germinal center development.* Immunity, 1999. **10**(2): p. 197-206.
88. Lotteau, V., et al., *Intracellular transport of class II MHC molecules directed by invariant chain.* Nature, 1990. **348**(6302): p. 600-5.
89. Ghosh, P., et al., *The structure of an intermediate in class II MHC maturation: CLIP bound to HLA-DR3.* Nature, 1995. **378**(6556): p. 457-62.
90. Allison, T.J., et al., *Structure of a human gammadelta T-cell antigen receptor.* Nature, 2001. **411**(6839): p. 820-4.
91. Hayday, A. and R. Tigelaar, *Immunoregulation in the tissues by gammadelta T cells.* Nature reviews. Immunology, 2003. **3**(3): p. 233-42.
92. Das, H., et al., *MICA engagement by human V gamma 2V delta 2 T cells enhances their antigen-dependent effector function.* Immunity, 2001. **15**(1): p. 83-93.
93. Parrott, D.M. and M.A. de Sousa, *Changes in the thymus-dependent areas of lymph nodes after immunological stimulation.* Nature, 1966. **212**(5068): p. 1316-7.
94. Jenkins, M.K., et al., *CD28 delivers a costimulatory signal involved in antigen-specific IL-2 production by human T cells.* Journal of immunology, 1991. **147**(8): p. 2461-6.
95. Michel, F., et al., *CD28 as a molecular amplifier extending TCR ligation and signaling capabilities.* Immunity, 2001. **15**(6): p. 935-45.
96. Irving, B.A., A.C. Chan, and A. Weiss, *Functional characterization of a signal transducing motif present in the T cell antigen receptor zeta chain.* J Exp Med, 1993. **177**(4): p. 1093-103.

97. Straus, D.B. and A. Weiss, *Genetic evidence for the involvement of the lck tyrosine kinase in signal transduction through the T cell antigen receptor.* Cell, 1992. **70**(4): p. 585-93.
98. Wange, R.L., et al., *Tandem SH2 domains of ZAP-70 bind to T cell antigen receptor zeta and CD3 epsilon from activated Jurkat T cells.* J Biol Chem, 1993. **268**(26): p. 19797-801.
99. Zhang, W., et al., *LAT: the ZAP-70 tyrosine kinase substrate that links T cell receptor to cellular activation.* Cell, 1998. **92**(1): p. 83-92.
100. Sommers, C.L., L.E. Samelson, and P.E. Love, *LAT: a T lymphocyte adapter protein that couples the antigen receptor to downstream signaling pathways.* Bioessays, 2004. **26**(1): p. 61-67.
101. Smith-Garvin, J.E., G.A. Koretzky, and M.S. Jordan, *T cell activation.* Annu Rev Immunol, 2009. **27**: p. 591-619.
102. Acuto, O., V. Di Bartolo, and F. Michel, *Tailoring T-cell receptor signals by proximal negative feedback mechanisms.* Nature reviews. Immunology, 2008. **8**(9): p. 699-712.
103. Das, J., et al., *Digital signaling and hysteresis characterize ras activation in lymphoid cells.* Cell, 2009. **136**(2): p. 337-51.
104. Feinerman, O., et al., *Variability and robustness in T cell activation from regulated heterogeneity in protein levels.* Science, 2008. **321**(5892): p. 1081-4.
105. Stefanova, I., et al., *TCR ligand discrimination is enforced by competing ERK positive and SHP-1 negative feedback pathways.* Nat Immunol, 2003. **4**(3): p. 248-54.
106. Grakoui, A., et al., *The immunological synapse: a molecular machine controlling T cell activation.* Science, 1999. **285**(5425): p. 221-7.
107. Monks, C.R., et al., *Three-dimensional segregation of supramolecular activation clusters in T cells.* Nature, 1998. **395**(6697): p. 82-6.
108. Lee, K.H., et al., *T cell receptor signaling precedes immunological synapse formation.* Science, 2002. **295**(5559): p. 1539-42.
109. Krummel, M.F. and M.M. Davis, *Dynamics of the immunological synapse: finding, establishing and solidifying a connection.* Curr Opin Immunol, 2002. **14**(1): p. 66-74.
110. Campi, G., R. Varma, and M.L. Dustin, *Actin and agonist MHC-peptide complex-dependent T cell receptor microclusters as scaffolds for signaling.* J Exp Med, 2005. **202**(8): p. 1031-6.
111. Yokosuka, T., et al., *Newly generated T cell receptor microclusters initiate and sustain T cell activation by recruitment of Zap70 and SLP-76.* Nat Immunol, 2005. **6**(12): p. 1253-62.
112. Varma, R., et al., *T cell receptor-proximal signals are sustained in peripheral microclusters and terminated in the central supramolecular activation cluster.* Immunity, 2006. **25**(1): p. 117-27.
113. van Der Merwe, P.A. and S.J. Davis, *Immunology. The immunological synapse--a multitasking system.* Science, 2002. **295**(5559): p. 1479-80.
114. Prasad, K.V., et al., *T-cell antigen CD28 interacts with the lipid kinase phosphatidylinositol 3-kinase by a cytoplasmic Tyr(P)-Met-Xaa-Met motif.*

Proceedings of the National Academy of Sciences of the United States of America, 1994. **91**(7): p. 2834-8.
115. Rudd, C.E., et al., *Two-step TCR zeta/CD3-CD4 and CD28 signaling in T cells: SH2/SH3 domains, protein-tyrosine and lipid kinases.* Immunology today, 1994. **15**(5): p. 225-34.
116. Cai, Y.C., et al., *Selective CD28pYMNM mutations implicate phosphatidylinositol 3-kinase in CD86-CD28-mediated costimulation.* Immunity, 1995. **3**(4): p. 417-26.
117. Schneider, H., et al., *Mechanisms of CD28 signalling.* Research in immunology, 1995. **146**(3): p. 149-54.
118. Brunet, J.F., et al., *A new member of the immunoglobulin superfamily--CTLA-4.* Nature, 1987. **328**(6127): p. 267-70.
119. Sharpe, A.H., *Mechanisms of costimulation.* Immunological reviews, 2009. **229**(1): p. 5-11.
120. Fife, B.T. and J.A. Bluestone, *Control of peripheral T-cell tolerance and autoimmunity via the CTLA-4 and PD-1 pathways.* Immunological reviews, 2008. **224**: p. 166-82.
121. Krummel, M.F. and J.P. Allison, *CD28 and CTLA-4 have opposing effects on the response of T cells to stimulation.* The Journal of experimental medicine, 1995. **182**(2): p. 459-65.
122. Valk, E., C.E. Rudd, and H. Schneider, *CTLA-4 trafficking and surface expression.* Trends in immunology, 2008. **29**(6): p. 272-9.
123. Downey, J., et al., *TCR/CD3 mediated stop-signal is decoupled in T-cells from Ctla4 deficient mice.* Immunology letters, 2008. **115**(1): p. 70-2.
124. Schneider, H., et al., *CTLA-4 disrupts ZAP70 microcluster formation with reduced T cell/APC dwell times and calcium mobilization.* European journal of immunology, 2008. **38**(1): p. 40-7.
125. Qureshi, O.S., et al., *Trans-endocytosis of CD80 and CD86: a molecular basis for the cell-extrinsic function of CTLA-4.* Science, 2011. **332**(6029): p. 600-3.
126. Harding, C.V. and E.R. Unanue, *Quantitation of antigen-presenting cell MHC class II/peptide complexes necessary for T-cell stimulation.* Nature, 1990. **346**(6284): p. 574-6.
127. Demotz, S., H.M. Grey, and A. Sette, *The minimal number of class II MHC-antigen complexes needed for T cell activation.* Science, 1990. **249**(4972): p. 1028-30.
128. Davis, S.J., et al., *The nature of molecular recognition by T cells.* Nat Immunol, 2003. **4**(3): p. 217-24.
129. Davis, M.M., et al., *Ligand recognition by alpha beta T cell receptors.* Annu Rev Immunol, 1998. **16**: p. 523-44.
130. van der Merwe, P.A. and A.N. Barclay, *Transient intercellular adhesion: the importance of weak protein-protein interactions.* Trends Biochem Sci, 1994. **19**(9): p. 354-8.
131. Davis, S.J., et al., *CD2 and the nature of protein interactions mediating cell-cell recognition.* Immunol Rev, 1998. **163**: p. 217-36.
132. van der Merwe, P.A. and S.J. Davis, *Molecular interactions mediating T cell antigen recognition.* Annu Rev Immunol, 2003. **21**: p. 659-84.

133. Irvine, D.J., et al., *Direct observation of ligand recognition by T cells.* Nature, 2002. **419**(6909): p. 845-9.
134. Delon, J., et al., *CD8 expression allows T cell signaling by monomeric peptide-MHC complexes.* Immunity, 1998. **9**(4): p. 467-73.
135. Ma, Z., et al., *Surface-anchored monomeric agonist pMHCs alone trigger TCR with high sensitivity.* PLoS biology, 2008. **6**(2): p. e43.
136. Garcia, K.C., L. Teyton, and I.A. Wilson, *Structural basis of T cell recognition.* Annu Rev Immunol, 1999. **17**: p. 369-97.
137. Dustin, M.L., et al., *Visualization of CD2 interaction with LFA-3 and determination of the two-dimensional dissociation constant for adhesion receptors in a contact area.* J Cell Biol, 1996. **132**(3): p. 465-74.
138. Huppa, J.B., et al., *TCR-peptide-MHC interactions in situ show accelerated kinetics and increased affinity.* Nature, 2010. **463**(7283): p. 963-U143.
139. Berg, L.J., *Strength of T cell receptor signaling strikes again.* Immunity, 2009. **31**(4): p. 529-31.
140. Springer, T.A., *Adhesion receptors of the immune system.* Nature, 1990. **346**(6283): p. 425-34.
141. van Kooyk, Y. and C.G. Figdor, *Avidity regulation of integrins: the driving force in leukocyte adhesion.* Curr Opin Cell Biol, 2000. **12**(5): p. 542-7.
142. James, J.R., et al., *Single-molecule level analysis of the subunit composition of the T cell receptor on live T cells.* Proc Natl Acad Sci U S A, 2007. **104**(45): p. 17662-7.
143. James, J.R., et al., *A rigorous experimental framework for detecting protein oligomerization using bioluminescence resonance energy transfer.* Nat Methods, 2006. **3**(12): p. 1001-6.
144. Kusumi, A., et al., *Paradigm shift of the plasma membrane concept from the two-dimensional continuum fluid to the partitioned fluid: high-speed single-molecule tracking of membrane molecules.* Annual review of biophysics and biomolecular structure, 2005. **34**: p. 351-78.
145. James, J.R., et al., *The T cell receptor triggering apparatus is composed of monovalent or monomeric proteins.* The Journal of biological chemistry, 2011. **286**(37): p. 31993-2001.
146. Kusumi, A. and Y. Sako, *Cell surface organization by the membrane skeleton.* Current opinion in cell biology, 1996. **8**(4): p. 566-74.
147. Ritchie, K. and A. Kusumi, *Role of the membrane skeleton in creation of microdomains.* Sub-cellular biochemistry, 2004. **37**: p. 233-45.
148. Fujiwara, T., et al., *Phospholipids undergo hop diffusion in compartmentalized cell membrane.* The Journal of cell biology, 2002. **157**(6): p. 1071-81.
149. Murase, K., et al., *Ultrafine membrane compartments for molecular diffusion as revealed by single molecule techniques.* Biophysical journal, 2004. **86**(6): p. 4075-93.
150. Simons, K. and G. van Meer, *Lipid sorting in epithelial cells.* Biochemistry, 1988. **27**(17): p. 6197-202.
151. van Meer, G. and K. Simons, *Lipid polarity and sorting in epithelial cells.* Journal of cellular biochemistry, 1988. **36**(1): p. 51-8.
152. Munro, S., *Lipid rafts: elusive or illusive?* Cell, 2003. **115**(4): p. 377-88.

153. Eggeling, C., et al., *Direct observation of the nanoscale dynamics of membrane lipids in a living cell.* Nature, 2009. **457**(7233): p. 1159-62.
154. Shaw, A.S., *Lipid rafts: now you see them, now you don't.* Nature immunology, 2006. **7**(11): p. 1139-42.
155. Harder, T., et al., *Lipid domain structure of the plasma membrane revealed by patching of membrane components.* The Journal of cell biology, 1998. **141**(4): p. 929-42.
156. Viola, A., et al., *T lymphocyte costimulation mediated by reorganization of membrane microdomains.* Science, 1999. **283**(5402): p. 680-2.
157. Janes, P.W., S.C. Ley, and A.I. Magee, *Aggregation of lipid rafts accompanies signaling via the T cell antigen receptor.* The Journal of cell biology, 1999. **147**(2): p. 447-61.
158. Kenworthy, A.K., N. Petranova, and M. Edidin, *High-resolution FRET microscopy of cholera toxin B-subunit and GPI-anchored proteins in cell plasma membranes.* Molecular biology of the cell, 2000. **11**(5): p. 1645-55.
159. Glebov, O.O. and B.J. Nichols, *Lipid raft proteins have a random distribution during localized activation of the T-cell receptor.* Nature cell biology, 2004. **6**(3): p. 238-43.
160. Douglass, A.D. and R.D. Vale, *Single-molecule microscopy reveals plasma membrane microdomains created by protein-protein networks that exclude or trap signaling molecules in T cells.* Cell, 2005. **121**(6): p. 937-50.
161. Dengl, S., et al., *Structure and in vivo requirement of the yeast Spt6 SH2 domain.* Journal of molecular biology, 2009. **389**(1): p. 211-25.
162. King, N., et al., *The genome of the choanoflagellate Monosiga brevicollis and the origin of metazoans.* Nature, 2008. **451**(7180): p. 783-8.
163. Schieven, G., J. Thorner, and G.S. Martin, *Protein-tyrosine kinase activity in Saccharomyces cerevisiae.* Science, 1986. **231**(4736): p. 390-3.
164. Kennelly, P.J., *Protein kinases and protein phosphatases in prokaryotes: a genomic perspective.* FEMS microbiology letters, 2002. **206**(1): p. 1-8.
165. Alonso, A., et al., *Protein tyrosine phosphatases in the human genome.* Cell, 2004. **117**(6): p. 699-711.
166. Davis, S.J. and P.A. van der Merwe, *Lck and the nature of the T cell receptor trigger.* Trends in immunology, 2011. **32**(1): p. 1-5.
167. Veillette, A., et al., *The CD4 and CD8 T cell surface antigens are associated with the internal membrane tyrosine-protein kinase p56lck.* Cell, 1988. **55**(2): p. 301-8.
168. Barber, E.K., et al., *The CD4 and CD8 antigens are coupled to a protein-tyrosine kinase (p56lck) that phosphorylates the CD3 complex.* Proceedings of the National Academy of Sciences of the United States of America, 1989. **86**(9): p. 3277-81.
169. Kim, P.W., et al., *A zinc clasp structure tethers Lck to T cell coreceptors CD4 and CD8.* Science, 2003. **301**(5640): p. 1725-8.
170. Boggon, T.J. and M.J. Eck, *Structure and regulation of Src family kinases.* Oncogene, 2004. **23**(48): p. 7918-27.
171. Sicheri, F., I. Moarefi, and J. Kuriyan, *Crystal structure of the Src family tyrosine kinase Hck.* Nature, 1997. **385**(6617): p. 602-9.

172. Xu, W., et al., *Crystal structures of c-Src reveal features of its autoinhibitory mechanism.* Molecular cell, 1999. **3**(5): p. 629-38.
173. Xu, W., S.C. Harrison, and M.J. Eck, *Three-dimensional structure of the tyrosine kinase c-Src.* Nature, 1997. **385**(6617): p. 595-602.
174. Yamaguchi, H. and W.A. Hendrickson, *Structural basis for activation of human lymphocyte kinase Lck upon tyrosine phosphorylation.* Nature, 1996. **384**(6608): p. 484-9.
175. Trowbridge, I.S. and M.L. Thomas, *CD45: an emerging role as a protein tyrosine phosphatase required for lymphocyte activation and development.* Annual review of immunology, 1994. **12**: p. 85-116.
176. Thomas, M.L., *The leukocyte common antigen family.* Annual review of immunology, 1989. **7**: p. 339-69.
177. Barclay, A.N., et al., *The leukocyte-common antigen (L-CA) family.* Advances in experimental medicine and biology, 1988. **237**: p. 3-7.
178. Hermiston, M.L., Z. Xu, and A. Weiss, *CD45: a critical regulator of signaling thresholds in immune cells.* Annual review of immunology, 2003. **21**: p. 107-37.
179. Desai, D.M., et al., *Ligand-mediated negative regulation of a chimeric transmembrane receptor tyrosine phosphatase.* Cell, 1993. **73**(3): p. 541-54.
180. Trowbridge, I.S. and M.L. Thomas, *Cd45 - an Emerging Role as a Protein-Tyrosine-Phosphatase Required for Lymphocyte-Activation and Development.* Annual Review of Immunology, 1994. **12**: p. 85-116.
181. Oberdoerffer, S., et al., *Regulation of CD45 alternative splicing by heterogeneous ribonucleoprotein, hnRNPLL.* Science, 2008. **321**(5889): p. 686-691.
182. Kung, C., et al., *Mutations in the tyrosine phosphatase CD45 gene in a child with severe combined immunodeficiency disease.* Nature medicine, 2000. **6**(3): p. 343-5.
183. Kishihara, K., et al., *Normal B lymphocyte development but impaired T cell maturation in CD45-exon6 protein tyrosine phosphatase-deficient mice.* Cell, 1993. **74**(1): p. 143-56.
184. Mee, P.J., et al., *Greatly reduced efficiency of both positive and negative selection of thymocytes in CD45 tyrosine phosphatase-deficient mice.* European Journal of Immunology, 1999. **29**(9): p. 2923-2933.
185. Byth, K.F., et al., *CD45-null transgenic mice reveal a positive regulatory role for CD45 in early thymocyte development, in the selection of CD4(+)CD8(+) thymocytes, and in B cell maturation.* Journal of Experimental Medicine, 1996. **183**(4): p. 1707-1718.
186. Hermiston, M.L., J. Zikherman, and J.W. Zhu, *CD45, CD148, and Lyp/Pep: critical phosphatases regulating Src family kinase signaling networks in immune cells.* Immunological reviews, 2009. **228**(1): p. 288-311.
187. Ashwell, J.D. and U. D'Oro, *CD45 and Src-family kinases: and now for something completely different.* Immunology today, 1999. **20**(9): p. 412-6.
188. D'Oro, U. and J.D. Ashwell, *Cutting edge: the CD45 tyrosine phosphatase is an inhibitor of Lck activity in thymocytes.* Journal of immunology, 1999. **162**(4): p. 1879-83.
189. Zikherman, J., et al., *CD45-Csk phosphatase-kinase titration uncouples basal and inducible T cell receptor signaling during thymic development.* Immunity, 2010. **32**(3): p. 342-54.

190. Janeway, C.A., Jr., *The T cell receptor as a multicomponent signalling machine: CD4/CD8 coreceptors and CD45 in T cell activation.* Annual review of immunology, 1992. **10**: p. 645-74.
191. Furukawa, T., et al., *Specific interaction of the CD45 protein-tyrosine phosphatase with tyrosine-phosphorylated CD3 zeta chain.* Proceedings of the National Academy of Sciences of the United States of America, 1994. **91**(23): p. 10928-32.
192. Alarcon, B., et al., *T-cell antigen-receptor stoichiometry: pre-clustering for sensitivity.* EMBO Rep, 2006. **7**(5): p. 490-5.
193. Yarden, Y. and J. Schlessinger, *Epidermal growth factor induces rapid, reversible aggregation of the purified epidermal growth factor receptor.* Biochemistry, 1987. **26**(5): p. 1443-51.
194. Kato, H., et al., *Role of tyrosine kinase activity in signal transduction by the insulin-like growth factor-I (IGF-I) receptor. Characterization of kinase-deficient IGF-I receptors and the action of an IGF-I-mimetic antibody (alpha IR-3).* The Journal of biological chemistry, 1993. **268**(4): p. 2655-61.
195. Ullrich, A. and J. Schlessinger, *Signal transduction by receptors with tyrosine kinase activity.* Cell, 1990. **61**(2): p. 203-12.
196. Cunningham, B.C., et al., *Dimerization of the extracellular domain of the human growth hormone receptor by a single hormone molecule.* Science, 1991. **254**(5033): p. 821-5.
197. Weiss, A. and J. Schlessinger, *Switching signals on or off by receptor dimerization.* Cell, 1998. **94**(3): p. 277-80.
198. Remy, I., I.A. Wilson, and S.W. Michnick, *Erythropoietin receptor activation by a ligand-induced conformation change.* Science, 1999. **283**(5404): p. 990-3.
199. Garrett, T.P., et al., *Crystal structure of a truncated epidermal growth factor receptor extracellular domain bound to transforming growth factor alpha.* Cell, 2002. **110**(6): p. 763-73.
200. Chung, I., et al., *Spatial control of EGF receptor activation by reversible dimerization on living cells.* Nature, 2010. **464**(7289): p. 783-7.
201. Godfrey, D.I., J. Rossjohn, and J. McCluskey, *The fidelity, occasional promiscuity, and versatility of T cell receptor recognition.* Immunity, 2008. **28**(3): p. 304-14.
202. Yamasaki, S., et al., *Mechanistic basis of pre-T cell receptor-mediated autonomous signaling critical for thymocyte development.* Nature immunology, 2006. **7**(1): p. 67-75.
203. Pang, S.S., et al., *The structural basis for autonomous dimerization of the pre-T-cell antigen receptor.* Nature, 2010. **467**(7317): p. 844-8.
204. Mahtani-Patching, J., et al., *PreTCR and TCRgammadelta signal initiation in thymocyte progenitors does not require domains implicated in receptor oligomerization.* Science signaling, 2011. **4**(182): p. ra47.
205. Irving, B.A., F.W. Alt, and N. Killeen, *Thymocyte development in the absence of pre-T cell receptor extracellular immunoglobulin domains.* Science, 1998. **280**(5365): p. 905-8.

206. Kuhns, M.S., et al., *Evidence for a functional sidedness to the alphabetaTCR.* Proceedings of the National Academy of Sciences of the United States of America, 2010. **107**(11): p. 5094-9.
207. Lillemeier, B.F., et al., *TCR and Lat are expressed on separate protein islands on T cell membranes and concatenate during activation.* Nature immunology, 2010. **11**(1): p. 90-6.
208. Schamel, W.W., et al., *Coexistence of multivalent and monovalent TCRs explains high sensitivity and wide range of response.* J Exp Med, 2005. **202**(4): p. 493-503.
209. Dunne, P.D., et al., *DySCo: quantitating associations of membrane proteins using two-color single-molecule tracking.* Biophys J, 2009. **97**(4): p. L5-7.
210. Schilham, M.W., et al., *Alloreactive cytotoxic T cells can develop and function in mice lacking both CD4 and CD8.* European journal of immunology, 1993. **23**(6): p. 1299-304.
211. Jiang, N., et al., *Two-stage cooperative T cell receptor-peptide major histocompatibility complex-CD8 trimolecular interactions amplify antigen discrimination.* Immunity, 2011. **34**(1): p. 13-23.
212. Xu, H. and D.R. Littman, *A Kinase-Independent Function of Lck in Potentiating Antigen-Specific T-Cell Activation.* Cell, 1993. **74**(4): p. 633-643.
213. Beddoe, T., et al., *Antigen ligation triggers a conformational change within the constant domain of the alphabeta T cell receptor.* Immunity, 2009. **30**(6): p. 777-88.
214. Alam, S.M., et al., *Qualitative and quantitative differences in T cell receptor binding of agonist and antagonist ligands.* Immunity, 1999. **10**(2): p. 227-37.
215. Reich, Z., et al., *Ligand-specific oligomerization of T-cell receptor molecules.* Nature, 1997. **387**(6633): p. 617-20.
216. Gil, D., et al., *Recruitment of Nck by CD3 epsilon reveals a ligand-induced conformational change essential for T cell receptor signaling and synapse formation.* Cell, 2002. **109**(7): p. 901-12.
217. Gil, D., et al., *T cell receptor engagement by peptide-MHC ligands induces a conformational change in the CD3 complex of thymocytes.* J Exp Med, 2005. **201**(4): p. 517-22.
218. Martinez-Martin, N., et al., *Cooperativity between T cell receptor complexes revealed by conformational mutants of CD3epsilon.* Sci Signal, 2009. **2**(83): p. ra43.
219. Szymczak, A.L., et al., *The CD3epsilon proline-rich sequence, and its interaction with Nck, is not required for T cell development and function.* J Immunol, 2005. **175**(1): p. 270-5.
220. Tailor, P., et al., *The proline-rich sequence of CD3epsilon as an amplifier of low-avidity TCR signaling.* J Immunol, 2008. **181**(1): p. 243-55.
221. Mingueneau, M., et al., *The proline-rich sequence of CD3epsilon controls T cell antigen receptor expression on and signaling potency in preselection CD4+CD8+ thymocytes.* Nat Immunol, 2008. **9**(5): p. 522-32.
222. Laczko, I., et al., *Conformational effect of phosphorylation on T cell receptor/CD3 zeta-chain sequences.* Biochem Biophys Res Commun, 1998. **242**(3): p. 474-9.
223. Aivazian, D. and L.J. Stern, *Phosphorylation of T cell receptor zeta is regulated by a lipid dependent folding transition.* Nat Struct Biol, 2000. **7**(11): p. 1023-6.

224. Xu, C., et al., *Regulation of T cell receptor activation by dynamic membrane binding of the CD3epsilon cytoplasmic tyrosine-based motif.* Cell, 2008. **135**(4): p. 702-13.
225. Zhang, H., et al., *Basic residues in the T-cell receptor zeta cytoplasmic domain mediate membrane association and modulate signaling.* Proceedings of the National Academy of Sciences of the United States of America, 2011.
226. Sigalov, A.B. and G.M. Hendricks, *Membrane binding mode of intrinsically disordered cytoplasmic domains of T cell receptor signaling subunits depends on lipid composition.* Biochem Biophys Res Commun, 2009. **389**(2): p. 388-93.
227. Sigalov, A., D. Aivazian, and L. Stern, *Homooligomerization of the cytoplasmic domain of the T cell receptor zeta chain and of other proteins containing the immunoreceptor tyrosine-based activation motif.* Biochemistry, 2004. **43**(7): p. 2049-61.
228. Sigalov, A.B., et al., *Lipid-binding activity of intrinsically unstructured cytoplasmic domains of multichain immune recognition receptor signaling subunits.* Biochemistry, 2006. **45**(51): p. 15731-9.
229. Kuhns, M.S. and M.M. Davis, *The safety on the TCR trigger.* Cell, 2008. **135**(4): p. 594-6.
230. Dustin, M.L., *The cellular context of T cell signaling.* Immunity, 2009. **30**(4): p. 482-92.
231. Davis, S.J. and P.A. van der Merwe, *The structure and ligand interactions of CD2: implications for T-cell function.* Immunol Today, 1996. **17**(4): p. 177-87.
232. Davis, S.J. and P.A. van der Merwe, *The kinetic-segregation model: TCR triggering and beyond.* Nat Immunol, 2006. **7**(8): p. 803-9.
233. Barr, A.J., et al., *Large-scale structural analysis of the classical human protein tyrosine phosphatome.* Cell, 2009. **136**(2): p. 352-63.
234. O'Shea, J.J., et al., *Activation of human peripheral blood T lymphocytes by pharmacological induction of protein-tyrosine phosphorylation.* Proc Natl Acad Sci U S A, 1992. **89**(21): p. 10306-10.
235. Choudhuri, K., et al., *T-cell receptor triggering is critically dependent on the dimensions of its peptide-MHC ligand.* Nature, 2005. **436**(7050): p. 578-82.
236. Choudhuri, K., et al., *Peptide-major histocompatibility complex dimensions control proximal kinase-phosphatase balance during T cell activation.* J Biol Chem, 2009. **284**(38): p. 26096-105.
237. Lin, J. and A. Weiss, *The tyrosine phosphatase CD148 is excluded from the immunologic synapse and down-regulates prolonged T cell signaling.* J Cell Biol, 2003. **162**(4): p. 673-82.
238. Geppert, T.D. and P.E. Lipsky, *Accessory cell independent proliferation of human T4 cells stimulated by immobilized monoclonal antibodies to CD3.* Journal of immunology, 1987. **138**(6): p. 1660-6.
239. James, S.E., et al., *Antigen sensitivity of CD22-specific chimeric TCR is modulated by target epitope distance from the cell membrane.* Journal of immunology, 2008. **180**(10): p. 7028-38.
240. Leupin, O., et al., *Exclusion of CD45 from the T-cell receptor signaling area in antigen-stimulated T lymphocytes.* Curr Biol, 2000. **10**(5): p. 277-80.
241. Freiberg, B.A., et al., *Staging and resetting T cell activation in SMACs.* Nat Immunol, 2002. **3**(10): p. 911-7.

242. Chakraborty, A.K. and J. Das, *Pairing computation with experimentation: a powerful coupling for understanding T cell signalling.* Nature reviews. Immunology, 2010. **10**(1): p. 59-71.
243. Minguet, S., et al., *Full activation of the T cell receptor requires both clustering and conformational changes at CD3.* Immunity, 2007. **26**(1): p. 43-54.
244. San Jose, E., et al., *Assembly of the TCR/CD3 complex: CD3 epsilon/delta and CD3 epsilon/gamma dimers associate indistinctly with both TCR alpha and TCR beta chains. Evidence for a double TCR heterodimer model.* European journal of immunology, 1998. **28**(1): p. 12-21.
245. Swamy, M., et al., *The 450 kDa TCR Complex has a Stoichiometry of alphabetagammaepsilondeltaepsilonzetazeta.* Scandinavian journal of immunology, 2008. **67**(4): p. 418-20; author reply 421.
246. Fernandez-Miguel, G., et al., *Multivalent structure of an alphabetaT cell receptor.* Proceedings of the National Academy of Sciences of the United States of America, 1999. **96**(4): p. 1547-52.
247. Lillemeier, B.F., et al., *Plasma membrane-associated proteins are clustered into islands attached to the cytoskeleton.* Proc Natl Acad Sci U S A, 2006. **103**(50): p. 18992-7.
248. Sanan, D.A. and R.G. Anderson, *Simultaneous visualization of LDL receptor distribution and clathrin lattices on membranes torn from the upper surface of cultured cells.* The journal of histochemistry and cytochemistry : official journal of the Histochemistry Society, 1991. **39**(8): p. 1017-24.
249. Kumar, R., et al., *Increased sensitivity of antigen-experienced T cells through the enrichment of oligomeric T cell receptor complexes.* Immunity, 2011. **35**(3): p. 375-87.
250. Tanaka, K.A., et al., *Membrane molecules mobile even after chemical fixation.* Nature methods, 2010. **7**(11): p. 865-6.
251. Joo, C., et al., *Advances in single-molecule fluorescence methods for molecular biology.* Annual review of biochemistry, 2008. **77**: p. 51-76.
252. Leake, M.C., et al., *Stoichiometry and turnover in single, functioning membrane protein complexes.* Nature, 2006. **443**(7109): p. 355-8.
253. Hern, J.A., et al., *Formation and dissociation of M1 muscarinic receptor dimers seen by total internal reflection fluorescence imaging of single molecules.* Proceedings of the National Academy of Sciences of the United States of America, 2010. **107**(6): p. 2693-8.
254. Koyama-Honda, I., et al., *Fluorescence imaging for monitoring the colocalization of two single molecules in living cells.* Biophysical journal, 2005. **88**(3): p. 2126-36.
255. Naldini, L., et al., *In vivo gene delivery and stable transduction of nondividing cells by a lentiviral vector.* Science, 1996. **272**(5259): p. 263-7.
256. Axelrod, D., *Total Internal Reflection Fluorescence Microscopy*, in *Biophysical Tools for Biologists, Vol 2: in Vivo Techniques*2008, Elsevier Academic Press Inc: San Diego. p. 169-221.
257. Oh, S., et al., *Tracking and coordination of multiple agents using sensor networks: System design, algorithms and experiments.* Proceedings of the Ieee, 2007. **95**(1): p. 234-254.

258. Yoon, J.W., et al., *Bayesian inference for improved single molecule fluorescence tracking.* Biophysical journal, 2008. **94**(12): p. 4932-47.
259. Crocker, J.C. and D.G. Grier, *Methods of digital video microscopy for colloidal studies.* Journal of Colloid and Interface Science, 1996. **179**(1): p. 298-310.
260. Bruckbauer, A., et al., *Nanopipette delivery of individual molecules to cellular compartments for single-molecule fluorescence tracking.* Biophysical Journal, 2007. **93**(9): p. 3120-3131.
261. Lachmanovich, E., et al., *Co-localization analysis of complex formation among membrane proteins by computerized fluorescence microscopy: application to immunofluorescence co-patching studies.* Journal of Microscopy-Oxford, 2003. **212**: p. 122-131.
262. Zhang, X., et al., *Crystal structure of the receptor-binding domain of human B7-2: insights into organization and signaling.* Proceedings of the National Academy of Sciences of the United States of America, 2003. **100**(5): p. 2586-91.
263. Galimi, F., et al., *Development of ecdysone-regulated lentiviral vectors.* Molecular therapy : the journal of the American Society of Gene Therapy, 2005. **11**(1): p. 142-8.
264. Favier, B., et al., *TCR dynamics on the surface of living T cells.* International immunology, 2001. **13**(12): p. 1525-32.
265. Andrews, N.L., et al., *Actin restricts Fc epsilon RI diffusion and facilitates antigen-induced receptor immobilization.* Nature Cell Biology, 2008. **10**(8): p. 955-963.
266. Labrecque, N., et al., *How much TCR does a T cell need?* Immunity, 2001. **15**(1): p. 71-82.
267. Burbach, B.J., et al., *T-cell receptor signaling to integrins.* Immunological reviews, 2007. **218**: p. 65-81.
268. Dustin, M.L., *Cell adhesion molecules and actin cytoskeleton at immune synapses and kinapses.* Current opinion in cell biology, 2007. **19**(5): p. 529-33.
269. Dorsch, S., et al., *Analysis of receptor oligomerization by FRAP microscopy.* Nature methods, 2009. **6**(3): p. 225-30.
270. Patterson, G., et al., *Superresolution imaging using single-molecule localization.* Annual review of physical chemistry, 2010. **61**: p. 345-67.
271. Betzig, E., et al., *Imaging intracellular fluorescent proteins at nanometer resolution.* Science, 2006. **313**(5793): p. 1642-5.
272. Rust, M.J., M. Bates, and X. Zhuang, *Sub-diffraction-limit imaging by stochastic optical reconstruction microscopy (STORM).* Nature methods, 2006. **3**(10): p. 793-5.
273. Boniface, J.J., et al., *Thermodynamics of T cell receptor binding to peptide-MHC: evidence for a general mechanism of molecular scanning.* Proc Natl Acad Sci U S A, 1999. **96**(20): p. 11446-51.
274. Krogsgaard, M., et al., *Evidence that structural rearrangements and/or flexibility during TCR binding can contribute to T cell activation.* Mol Cell, 2003. **12**(6): p. 1367-78.
275. Hennecke, J. and D.C. Wiley, *T cell receptor-MHC interactions up close.* Cell, 2001. **104**(1): p. 1-4.
276. Rudolph, M.G., R.L. Stanfield, and I.A. Wilson, *How TCRs bind MHCs, peptides, and coreceptors.* Annual review of immunology, 2006. **24**: p. 419-66.

277. Frank, S.J., et al., *Structural mutations of the T cell receptor zeta chain and its role in T cell activation.* Science, 1990. **249**(4965): p. 174-7.
278. Ohashi, P.S., et al., *Reconstitution of an active surface T3/T-cell antigen receptor by DNA transfer.* Nature, 1985. **316**(6029): p. 606-9.
279. Cunningham, B.C. and J.A. Wells, *High-resolution epitope mapping of hGH-receptor interactions by alanine-scanning mutagenesis.* Science, 1989. **244**(4908): p. 1081-5.
280. Evans, E.J., et al., *Crystal structure and binding properties of the CD2 and CD244 (2B4)-binding protein, CD48.* The Journal of biological chemistry, 2006. **281**(39): p. 29309-20.
281. Davis, S.J., et al., *The role of charged residues mediating low affinity protein-protein recognition at the cell surface by CD2.* Proceedings of the National Academy of Sciences of the United States of America, 1998. **95**(10): p. 5490-4.
282. Bainbridge, J.W., et al., *In vivo gene transfer to the mouse eye using an HIV-based lentiviral vector; efficient long-term transduction of corneal endothelium and retinal pigment epithelium.* Gene therapy, 2001. **8**(21): p. 1665-8.
283. Hubbard, S.J., Thornton, J.M. , *'NACCESS', Computer Program.* Department of Biochemistry and Molecular Biology, University College London, 1993.
284. Arnett, K.L., S.C. Harrison, and D.C. Wiley, *Crystal structure of a human CD3-epsilon/delta dimer in complex with a UCHT1 single-chain antibody fragment.* Proceedings of the National Academy of Sciences of the United States of America, 2004. **101**(46): p. 16268-73.
285. Kjer-Nielsen, L., et al., *Crystal structure of the human T cell receptor CD3 epsilon gamma heterodimer complexed to the therapeutic mAb OKT3.* Proceedings of the National Academy of Sciences of the United States of America, 2004. **101**(20): p. 7675-80.
286. Van Wauwe, J.P., J.R. De Mey, and J.G. Goossens, *OKT3: a monoclonal anti-human T lymphocyte antibody with potent mitogenic properties.* J Immunol, 1980. **124**(6): p. 2708-13.
287. Weiss, A., et al., *Role of T3 surface molecules in human T-cell activation: T3-dependent activation results in an increase in cytoplasmic free calcium.* Proc Natl Acad Sci U S A, 1984. **81**(13): p. 4169-73.
288. Crabtree, G.R. and E.N. Olson, *NFAT signaling: choreographing the social lives of cells.* Cell, 2002. **109 Suppl**: p. S67-79.
289. Northrop, J.P., K.S. Ullman, and G.R. Crabtree, *Characterization of the nuclear and cytoplasmic components of the lymphoid-specific nuclear factor of activated T cells (NF-AT) complex.* J Biol Chem, 1993. **268**(4): p. 2917-23.
290. Burns, G.F., A.W. Boyd, and P.C. Beverley, *Two monoclonal anti-human T lymphocyte antibodies have similar biologic effects and recognize the same cell surface antigen.* Journal of immunology, 1982. **129**(4): p. 1451-7.
291. Weiss, A., et al., *Role of T3 surface molecules in human T-cell activation: T3-dependent activation results in an increase in cytoplasmic free calcium.* Proceedings of the National Academy of Sciences of the United States of America, 1984. **81**(13): p. 4169-73.

292. Weiss, A., R.L. Wiskocil, and J.D. Stobo, *The role of T3 surface molecules in the activation of human T cells: a two-stimulus requirement for IL 2 production reflects events occurring at a pre-translational level.* Journal of immunology, 1984. **133**(1): p. 123-8.
293. Ilani, T., et al., *T cell antigen receptor signaling and immunological synapse stability require myosin IIA.* Nat Immunol, 2009. **10**(5): p. 531-9.
294. Davis, S.J., et al., *The role of charged residues mediating low affinity protein-protein recognition at the cell surface by CD2.* Proc Natl Acad Sci U S A, 1998. **95**(10): p. 5490-4.
295. Evans, E.J., et al., *Crystal structure and binding properties of the CD2 and CD244 (2B4)-binding protein, CD48.* J Biol Chem, 2006. **281**(39): p. 29309-20.
296. van der Merwe, P.A., et al., *Topology of the CD2-CD48 cell-adhesion molecule complex: implications for antigen recognition by T cells.* Curr Biol, 1995. **5**(1): p. 74-84.
297. Malissen, B., *CD3 ITAMs count!* Nature immunology, 2008. **9**(6): p. 583-4.
298. Nika, K., et al., *Constitutively active Lck kinase in T cells drives antigen receptor signal transduction.* Immunity, 2010. **32**(6): p. 766-77.
299. Mustelin, T., et al., *Protein tyrosine phosphorylation in T cell signaling.* Frontiers in bioscience : a journal and virtual library, 2002. **7**: p. d918-69.
300. Mustelin, T., et al., *Role of protein tyrosine phosphatases in T cell activation.* Immunological reviews, 2003. **191**: p. 139-47.
301. Aivazian, D. and L.J. Stern, *Phosphorylation of T cell receptor zeta is regulated by a lipid dependent folding transition.* Nature structural biology, 2000. **7**(11): p. 1023-6.
302. Duchardt, E., et al., *Structure induction of the T-cell receptor zeta-chain upon lipid binding investigated by NMR spectroscopy.* Chembiochem : a European journal of chemical biology, 2007. **8**(7): p. 820-7.
303. Zhang, H., et al., *Basic residues in the T-cell receptor zeta cytoplasmic domain mediate membrane association and modulate signaling.* Proceedings of the National Academy of Sciences of the United States of America, 2011. **108**(48): p. 19323-8.
304. Secrist, J.P., et al., *Stimulatory effects of the protein tyrosine phosphatase inhibitor, pervanadate, on T-cell activation events.* The Journal of biological chemistry, 1993. **268**(8): p. 5886-93.
305. Aricescu, A.R., W. Lu, and E.Y. Jones, *A time- and cost-efficient system for high-level protein production in mammalian cells.* Acta crystallographica. Section D, Biological crystallography, 2006. **62**(Pt 10): p. 1243-50.
306. Chan, A.C., D.M. Desai, and A. Weiss, *The role of protein tyrosine kinases and protein tyrosine phosphatases in T cell antigen receptor signal transduction.* Annu Rev Immunol, 1994. **12**: p. 555-92.
307. Schade, A.E. and A.D. Levine, *Signal transduction through the T cell receptor is dynamically regulated by balancing kinase and phosphatase activities.* Biochem Biophys Res Commun, 2002. **296**(3): p. 637-43.
308. Swarup, G., S. Cohen, and D.L. Garbers, *Inhibition of membrane phosphotyrosyl-protein phosphatase activity by vanadate.* Biochem Biophys Res Commun, 1982. **107**(3): p. 1104-9.

309. Abraham, N. and A. Veillette, *Activation of P56lck through Mutation of a Regulatory Carboxy-Terminal Tyrosine Residue Requires Intact Sites of Autophosphorylation and Myristylation.* Molecular and Cellular Biology, 1990. **10**(10): p. 5197-5206.
310. Amrein, K.E. and B.M. Sefton, *Mutation of a Site of Tyrosine Phosphorylation in the Lymphocyte-Specific Tyrosine Protein-Kinase, P56lck, Reveals Its Oncogenic Potential in Fibroblasts.* Proceedings of the National Academy of Sciences of the United States of America, 1988. **85**(12): p. 4247-4251.
311. Zech, T., et al., *Accumulation of raft lipids in T-cell plasma membrane domains engaged in TCR signalling.* The EMBO journal, 2009. **28**(5): p. 466-76.
312. Alexander, D.R., *The CD45 tyrosine phosphatase: a positive and negative regulator of immune cell function.* Seminars in immunology, 2000. **12**(4): p. 349-59.
313. Johnson, K.G., et al., *A supramolecular basis for CD45 tyrosine phosphatase regulation in sustained T cell activation.* Proc Natl Acad Sci U S A, 2000. **97**(18): p. 10138-43.
314. Irles, C., et al., *CD45 ectodomain controls interaction with GEMs and Lck activity for optimal TCR signaling.* Nature Immunology, 2003. **4**(2): p. 189-197.
315. Fernandes, R.A., et al., *What controls T cell receptor phosphorylation?* Cell, 2010. **142**(5): p. 668-9.
316. Stone, J.D., et al., *Aberrant TCR-mediated signaling in CD45-null thymocytes involves dysfunctional regulation of Lck, Fyn, TCR-ζeta, and ZAP-70.* Journal of immunology, 1997. **158**(12): p. 5773-82.
317. Ostergaard, H.L., et al., *Expression of CD45 alters phosphorylation of the lck-encoded tyrosine protein kinase in murine lymphoma T-cell lines.* Proceedings of the National Academy of Sciences of the United States of America, 1989. **86**(22): p. 8959-63.
318. Hurley, T.R., R. Hyman, and B.M. Sefton, *Differential effects of expression of the CD45 tyrosine protein phosphatase on the tyrosine phosphorylation of the lck, fyn, and c-src tyrosine protein kinases.* Molecular and cellular biology, 1993. **13**(3): p. 1651-6.
319. Koretzky, G.A., M. Kohmetscher, and S. Ross, *CD45-associated kinase activity requires lck but not T cell receptor expression in the Jurkat T cell line.* The Journal of biological chemistry, 1993. **268**(12): p. 8958-64.
320. D'Oro, U., et al., *Mutational analysis of Lck in CD45-negative T cells: dominant role of tyrosine 394 phosphorylation in kinase activity.* Molecular and cellular biology, 1996. **16**(9): p. 4996-5003.
321. McNeill, L., et al., *The differential regulation of Lck kinase phosphorylation sites by CD45 is critical for T cell receptor signaling responses.* Immunity, 2007. **27**(3): p. 425-37.
322. Koretzky, G.A., et al., *Tyrosine phosphatase CD45 is required for T-cell antigen receptor and CD2-mediated activation of a protein tyrosine kinase and interleukin 2 production.* Proc Natl Acad Sci U S A, 1991. **88**(6): p. 2037-41.
323. Bayle, J.H., et al., *Rapamycin analogs with differential binding specificity permit orthogonal control of protein activity.* Chemistry & biology, 2006. **13**(1): p. 99-107.

324. D'Oro, U., et al., *Activation of the Lck tyrosine kinase targets cell surface T cell antigen receptors for lysosomal degradation.* Immunity, 1997. **7**(5): p. 619-28.
325. Palacios, E.H. and A. Weiss, *Function of the Src-family kinases, Lck and Fyn, in T-cell development and activation.* Oncogene, 2004. **23**(48): p. 7990-8000.
326. Alexandropoulos, K. and D. Baltimore, *Coordinate activation of c-Src by SH3- and SH2-binding sites on a novel, p130(Cas)-related protein, Sin.* Genes & Development, 1996. **10**(11): p. 1341-1355.
327. Moarefi, I., et al., *Activation of the Src-family tyrosine kinase Hck by SH3 domain displacement.* Nature, 1997. **385**(6617): p. 650-3.
328. Young, M.A., et al., *Dynamic coupling between the SH2 and SH3 domains of c-Src and hck underlies their inactivation by C-terminal tyrosine phosphorylation.* Cell, 2001. **105**(1): p. 115-126.
329. Liu, X., et al., *Regulation of c-Src tyrosine kinase activity by the Src SH2 domain.* Oncogene, 1993. **8**(5): p. 1119-26.
330. Sieh, M., J.B. Bolen, and A. Weiss, *CD45 specifically modulates binding of Lck to a phosphopeptide encompassing the negative regulatory tyrosine of Lck.* The EMBO journal, 1993. **12**(1): p. 315-21.
331. Volarevic, S., et al., *Regulation of TCR signaling by CD45 lacking transmembrane and extracellular domains.* Science, 1993. **260**(5107): p. 541-4.
332. Falahati, R. and D. Leitenberg, *Selective regulation of TCR signaling pathways by the CD45 protein tyrosine phosphatase during thymocyte development.* Journal of immunology, 2008. **181**(9): p. 6082-91.
333. Hovis, R.R., et al., *Rescue of signaling by a chimeric protein containing the cytoplasmic domain of CD45.* Science, 1993. **260**(5107): p. 544-6.
334. Koretzky, G.A., et al., *Tyrosine phosphatase CD45 is essential for coupling T-cell antigen receptor to the phosphatidyl inositol pathway.* Nature, 1990. **346**(6279): p. 66-8.
335. Choudhuri, K. and P.A. van der Merwe, *Molecular mechanisms involved in T cell receptor triggering.* Seminars in immunology, 2007. **19**(4): p. 255-61.
336. Moarefi, I., et al., *Activation of the Src-family tyrosine kinase Hck by SH3 domain displacement.* Nature, 1997. **385**(6617): p. 650-653.
337. Schindler, T., et al., *Crystal structure of Hck in complex with a Src family-selective tyrosine kinase inhibitor.* Molecular cell, 1999. **3**(5): p. 639-48.
338. Alvarado, J.J., et al., *Crystal Structure of the Src Family Kinase Hck SH3-SH2 Linker Regulatory Region Supports an SH3-dominant Activation Mechanism.* Journal of Biological Chemistry, 2010. **285**(46): p. 35455-35461.
339. Arnett, K.L., S.C. Harrison, and D.C. Wiley, *Crystal structure of a human CD3-epsilon/delta dimer in complex with a UCHT1 single-chain antibody fragment.* Proc Natl Acad Sci U S A, 2004. **101**(46): p. 16268-73.
340. Alarcon, B., et al., *Initiation of TCR signaling: regulation within CD3 dimers.* Immunological Reviews, 2003. **191**(1): p. 38-46.
341. Perutz, M.F., et al., *Structure of haemoglobin: a three-dimensional Fourier synthesis at 5.5-A. resolution, obtained by X-ray analysis.* Nature, 1960. **185**(4711): p. 416-22.
342. Kendrew, J.C., et al., *A three-dimensional model of the myoglobin molecule obtained by x-ray analysis.* Nature, 1958. **181**(4610): p. 662-6.

343. Watson, J.D. and F.H. Crick, *Molecular structure of nucleic acids; a structure for deoxyribose nucleic acid.* Nature, 1953. **171**(4356): p. 737-8.
344. Rasmussen, S.G., et al., *Structure of a nanobody-stabilized active state of the beta(2) adrenoceptor.* Nature, 2011. **469**(7329): p. 175-80.
345. Rasmussen, S.G., et al., *Crystal structure of the beta2 adrenergic receptor-Gs protein complex.* Nature, 2011. **477**(7366): p. 549-55.
346. Frauenfeld, J., et al., *Cryo-EM structure of the ribosome-SecYE complex in the membrane environment.* Nature structural & molecular biology, 2011. **18**(5): p. 614-21.
347. Samso, M., T. Wagenknecht, and P.D. Allen, *Internal structure and visualization of transmembrane domains of the RyR1 calcium release channel by cryo-EM.* Nature structural & molecular biology, 2005. **12**(6): p. 539-44.
348. Henderson, R., et al., *Tilt-pair analysis of images from a range of different specimens in single-particle electron cryomicroscopy.* Journal of molecular biology, 2011. **413**(5): p. 1028-46.
349. Frank, J., *Single-particle imaging of macromolecules by cryo-electron microscopy.* Annual review of biophysics and biomolecular structure, 2002. **31**: p. 303-19.
350. Allen, G.S., et al., *The cryo-EM structure of a translation initiation complex from Escherichia coli.* Cell, 2005. **121**(5): p. 703-12.
351. Arechaga, I., et al., *Structural characterization of the TCR complex by electron microscopy.* International immunology, 2010. **22**(11): p. 897-903.
352. Szymczak, A.L., et al., *Correction of multi-gene deficiency in vivo using a single 'self-cleaving' 2A peptide-based retroviral vector.* Nature biotechnology, 2004. **22**(5): p. 589-94.
353. Call, M.E., J. Pyrdol, and K.W. Wucherpfennig, *Stoichiometry of the T-cell receptor-CD3 complex and key intermediates assembled in the endoplasmic reticulum.* The EMBO journal, 2004. **23**(12): p. 2348-57.
354. Zhao, Y., et al., *High-affinity TCRs generated by phage display provide CD4+ T cells with the ability to recognize and kill tumor cell lines.* Journal of immunology, 2007. **179**(9): p. 5845-54.
355. van der Merwe, P.A. and S.J. Davis, *Molecular interactions mediating T cell antigen recognition.* Annual Review of Immunology, 2003. **21**: p. 659-684.
356. Davis, S.J., et al., *The nature of molecular recognition by T cells.* Nature Immunology, 2003. **4**(3): p. 217-224.
357. Boulter, J.M. and B.K. Jakobsen, *Stable, soluble, high-affinity, engineered T cell receptors: novel antibody-like proteins for specific targeting of peptide antigens.* Clinical and experimental immunology, 2005. **142**(3): p. 454-60.
358. Donnelly, M.L., et al., *The 'cleavage' activities of foot-and-mouth disease virus 2A site-directed mutants and naturally occurring '2A-like' sequences.* The Journal of general virology, 2001. **82**(Pt 5): p. 1027-41.
359. Alcover, A. and B. Alarcon, *Internalization and intracellular fate of TCR-CD3 complexes.* Critical reviews in immunology, 2000. **20**(4): p. 325-46.
360. Huppa, J.B. and H.L. Ploegh, *The alpha chain of the T cell antigen receptor is degraded in the cytosol.* Immunity, 1997. **7**(1): p. 113-122.

361. Swamy, M., et al., *A native antibody-based mobility-shift technique (NAMOS-assay) to determine the stoichiometry of multiprotein complexes.* Journal of immunological methods, 2007. **324**(1-2): p. 74-83.
362. Rubinstein, J.L., *Structural analysis of membrane protein complexes by single particle electron microscopy.* Methods, 2007. **41**(4): p. 409-16.
363. Chae, P.S., et al., *Maltose-neopentyl glycol (MNG) amphiphiles for solubilization, stabilization and crystallization of membrane proteins.* Nature methods, 2010. **7**(12): p. 1003-8.
364. Kumar, R., et al., *Increased Sensitivity of Antigen-Experienced T Cells through the Enrichment of Oligomeric T Cell Receptor Complexes.* Immunity, 2011. **35**(3): p. 375-387.
365. Huse, M., et al., *Spatial and temporal dynamics of T cell receptor signaling with a photoactivatable agonist.* Immunity, 2007. **27**(1): p. 76-88.
366. Ritchie, K., et al., *Detection of non-Brownian diffusion in the cell membrane in single molecule tracking.* Biophysical journal, 2005. **88**(3): p. 2266-77.
367. Molnar, E., S. Deswal, and W.W. Schamel, *Pre-clustered TCR complexes.* FEBS letters, 2010. **584**(24): p. 4832-7.
368. Jacobs, H., *Pre-TCR/CD3 and TCR/CD3 complexes: decamers with differential signalling properties?* Immunology today, 1997. **18**(12): p. 565-9.
369. Gurevich, V.V. and E.V. Gurevich, *GPCR monomers and oligomers: it takes all kinds.* Trends in Neurosciences, 2008. **31**(2): p. 74-81.
370. Whorton, M.R., et al., *A monomeric G protein-coupled receptor isolated in a high-density lipoprotein particle efficiently activates its G protein.* Proceedings of the National Academy of Sciences of the United States of America, 2007. **104**(18): p. 7682-7687.
371. Kobilka, B.K., *Agonist-induced conformational changes in the beta(2) adrenergic receptor.* Journal of Peptide Research, 2002. **60**(6): p. 317-321.
372. Ghanouni, P., et al., *Agonist-induced conformational changes in the G-protein-coupling domain of the beta(2) adrenergic receptor.* Proceedings of the National Academy of Sciences of the United States of America, 2001. **98**(11): p. 5997-6002.
373. Jensen, A.D., et al., *Agonist-induced conformational changes at the cytoplasmic side of transmembrane segment 6 in the beta(2) adrenergic receptor mapped by site-selective fluorescent labeling.* Journal of Biological Chemistry, 2001. **276**(12): p. 9279-9290.
374. Yu, C., et al., *Rigid-body ligand recognition drives cytotoxic T-lymphocyte antigen 4 (CTLA-4) receptor triggering.* The Journal of biological chemistry, 2011. **286**(8): p. 6685-96.
375. Koning, F., W.L. Maloy, and J.E. Coligan, *The implications of subunit interactions for the structure of the T cell receptor-CD3 complex.* European journal of immunology, 1990. **20**(2): p. 299-305.
376. Manolios, N., et al., *Pairwise, cooperative and inhibitory interactions describe the assembly and probable structure of the T-cell antigen receptor.* The EMBO journal, 1991. **10**(7): p. 1643-51.
377. Koning, F., et al., *The biosynthesis and assembly of T cell receptor alpha- and beta-chains with the CD3 complex.* J Immunol, 1988. **140**(9): p. 3126-34.

378. Manolios, N., O. Kemp, and Z.G. Li, *The T cell antigen receptor alpha and beta chains interact via distinct regions with CD3 chains.* European journal of immunology, 1994. **24**(1): p. 84-92.
379. Backstrom, B.T., et al., *Positive selection through a motif in the alphabeta T cell receptor.* Science, 1998. **281**(5378): p. 835-8.
380. Gouaillard, C., et al., *Evolution of T cell receptor (TCR) alpha beta heterodimer assembly with the CD3 complex.* European journal of immunology, 2001. **31**(12): p. 3798-805.
381. Dustin, M.L., *Visualizing immune system complexity.* Sci Signal, 2009. **2**(66): p. mr4.
382. Gagnon, E., et al., *Response multilayered control of T cell receptor phosphorylation.* Cell, 2010. **142**(5): p. 669-71.
383. Takeuchi, K., et al., *Structural and functional evidence that Nck interaction with CD3 epsilon regulates T-cell receptor activity.* Journal of Molecular Biology, 2008. **380**(4): p. 704-716.
384. Kim, S.T., et al., *The alpha beta T Cell Receptor Is an Anisotropic Mechanosensor.* Journal of Biological Chemistry, 2009. **284**(45): p. 31028-31037.
385. Fischer, E.H., H. Charbonneau, and N.K. Tonks, *Protein tyrosine phosphatases: a diverse family of intracellular and transmembrane enzymes.* Science, 1991. **253**(5018): p. 401-6.
386. Barr, A.J., et al., *Large-Scale Structural Analysis of the Classical Human Protein Tyrosine Phosphatome.* Cell, 2009. **136**(2): p. 352-363.
387. Kleiman, L.B., et al., *Rapid phospho-turnover by receptor tyrosine kinases impacts downstream signaling and drug binding.* Molecular cell, 2011. **43**(5): p. 723-37.
388. Zhang, X., et al., *An allosteric mechanism for activation of the kinase domain of epidermal growth factor receptor.* Cell, 2006. **125**(6): p. 1137-49.
389. Reynolds, A.R., et al., *EGFR activation coupled to inhibition of tyrosine phosphatases causes lateral signal propagation.* Nature cell biology, 2003. **5**(5): p. 447-53.
390. Irie-Sasaki, J., et al., *CD45 is a JAK phosphatase and negatively regulates cytokine receptor signalling.* Nature, 2001. **409**(6818): p. 349-54.
391. Yamada, T., et al., *CD45 controls interleukin-4-mediated IgE class switch recombination in human B cells through its function as a Janus kinase phosphatase.* The Journal of biological chemistry, 2002. **277**(32): p. 28830-5.
392. Domingo-Sananes, M.R., et al., *Switches and latches: a biochemical tug-of-war between the kinases and phosphatases that control mitosis.* Philosophical transactions of the Royal Society of London. Series B, Biological sciences, 2011. **366**(1584): p. 3584-94.
393. Rohas, L.M., et al., *A fundamental system of cellular energy homeostasis regulated by PGC-1 alpha.* Proceedings of the National Academy of Sciences of the United States of America, 2007. **104**(19): p. 7933-7938.
394. Liu, Z.C. and R.A. Butow, *Mitochondrial retrograde signaling.* Annual Review of Genetics, 2006. **40**: p. 159-185.
395. Butow, R.A. and N.G. Avadhani, *Mitochondrial signaling: The retrograde response.* Molecular Cell, 2004. **14**(1): p. 1-15.

396. Walter, P. and D. Ron, *The Unfolded Protein Response: From Stress Pathway to Homeostatic Regulation.* Science, 2011. **334**(6059): p. 1081-1086.
397. Jose, E.S., et al., *Triggering the TCR complex causes the downregulation of nonengaged receptors by a signal transduction-dependent mechanism.* Immunity, 2000. **12**(2): p. 161-170.
398. Yang, S., et al., *Multidomain assembled states of Hck tyrosine kinase in solution.* Proceedings of the National Academy of Sciences of the United States of America, 2010. **107**(36): p. 15757-62.
399. Bernado, P., et al., *Structural characterization of the active and inactive states of Src kinase in solution by small-angle X-ray scattering.* Journal of molecular biology, 2008. **376**(2): p. 492-505.
400. Filippakopoulos, P., et al., *Structural coupling of SH2-kinase domains links Fes and Abl substrate recognition and kinase activation.* Cell, 2008. **134**(5): p. 793-803.
401. Filippakopoulos, P., S. Muller, and S. Knapp, *SH2 domains: modulators of nonreceptor tyrosine kinase activity.* Current opinion in structural biology, 2009. **19**(6): p. 643-9.
402. Li, W., et al., *Signaling properties of a non-metazoan Src kinase and the evolutionary history of Src negative regulation.* The Journal of biological chemistry, 2008. **283**(22): p. 15491-501.